

**Luminescence Applications**  
**in Biological, Chemical, Environmental,**  
**and Hydrological Sciences**



ACS SYMPOSIUM SERIES **383**

# **Luminescence Applications** **in Biological, Chemical, Environmental,** **and Hydrological Sciences**

**Marvin C. Goldberg, EDITOR**  
*U.S. Geological Survey*

Developed from a symposium sponsored  
by the Division of Environmental Chemistry  
at the 193rd Meeting  
of the American Chemical Society,  
Denver, Colorado  
April 5-10, 1987



American Chemical Society, Washington, DC 1989



### Library of Congress Cataloging-in-Publication Data

Luminescence applications in biological, chemical, environmental, and hydrological sciences.

Marvin C. Goldberg, editor

“Developed from a symposium sponsored by the Division of Environmental Chemistry at the 193rd Meeting of the American Chemical Society, Denver, Colorado, April 5–10, 1987.”

p. cm.—(ACS Symposium Series, 0097–6156; 383).

Includes index.

ISBN 0–8412–1560–X

1. Luminescence spectroscopy—Congresses.
2. Biochemistry—Technique—Congresses.
3. Environmental chemistry—Technique—Congresses.

I. Goldberg, Marvin C., 1933– . II. American Chemical Society. Division of Environmental Chemistry. III. Series

QP519.9.L84L86 1989  
543\*.0858—dc19

88–39131  
CIP

Copyright © 1989

American Chemical Society

All Rights Reserved. The appearance of the code at the bottom of the first page of each chapter in this volume indicates the copyright owner's consent that reprographic copies of the chapter may be made for personal or internal use or for the personal or internal use of specific clients. This consent is given on the condition, however, that the copier pay the stated per-copy fee through the Copyright Clearance Center, Inc., 27 Congress Street, Salem, MA 01970, for copying beyond that permitted by Sections 107 or 108 of the U.S. Copyright Law. This consent does not extend to copying or transmission by any means—graphic or electronic—for any other purpose, such as for general distribution, for advertising or promotional purposes, for creating a new collective work, for resale, or for information storage and retrieval systems. The copying fee for each chapter is indicated in the code at the bottom of the first page of the chapter.

The citation of trade names and/or names of manufacturers in this publication is not to be construed as an endorsement or as approval by ACS of the commercial products or services referenced herein; nor should the mere reference herein to any drawing, specification, chemical process, or other data be regarded as a license or as a conveyance of any right or permission to the holder, reader, or any other person or corporation, to manufacture, reproduce, use, or sell any patented invention or copyrighted work that may in any way be related thereto. Registered names, trademarks, etc., used in this publication, even without specific indication thereof, are not to be considered unprotected by law.

PRINTED IN THE UNITED STATES OF AMERICA

**American Chemical Society  
Library**

1155 16th St., N.W.

In Luminescence Applications—Goldberg, M.; ACS Symposium Series, 4th ed.; American Chemical Society: Washington, DC, 1989.

Washington, D.C. 20036

# ACS Symposium Series

**M. Joan Comstock, *Series Editor***

## *1988 ACS Books Advisory Board*

**Paul S. Anderson**  
Merck Sharp & Dohme Research  
Laboratories

**Harvey W. Blanch**  
University of California—Berkeley

**Malcolm H. Chisholm**  
Indiana University

**Alan Elzerman**  
Clemson University

**John W. Finley**  
Nabisco Brands, Inc.

**Natalie Foster**  
Lehigh University

**Marye Anne Fox**  
The University of Texas—Austin

**Roland F. Hirsch**  
U.S. Department of Energy

**G. Wayne Ivie**  
USDA, Agricultural Research Service

**Michael R. Ladisch**  
Purdue University

**Vincent D. McGinniss**  
Battelle Columbus Laboratories

**Daniel M. Quinn**  
University of Iowa

**James C. Randall**  
Exxon Chemical Company

**E. Reichmanis**  
AT&T Bell Laboratories

**C. M. Roland**  
U.S. Naval Research Laboratory

**W. D. Shults**  
Oak Ridge National Laboratory

**Geoffrey K. Smith**  
Rohm & Haas Co.

**Douglas B. Walters**  
National Institute of  
Environmental Health

**Wendy A. Warr**  
Imperial Chemical Industries

## Foreword

The ACS SYMPOSIUM SERIES was founded in 1974 to provide a medium for publishing symposia quickly in book form. The format of the Series parallels that of the continuing ADVANCES IN CHEMISTRY SERIES except that, in order to save time, the papers are not typeset but are reproduced as they are submitted by the authors in camera-ready form. Papers are reviewed under the supervision of the Editors with the assistance of the Series Advisory Board and are selected to maintain the integrity of the symposia; however, verbatim reproductions of previously published papers are not accepted. Both reviews and reports of research are acceptable, because symposia may embrace both types of presentation.

# Preface

LUMINESCENCE YIELDS DATA that often cannot be provided by any other methodology. This book is a compilation of a wide variety of original research contributions. Substantial information is given on the use of luminescence techniques to understand specific cell responses and the chemical mechanisms of cell action. An examination of natural environments is presented in the form of specific studies that characterize materials in both solid and liquid form and give information on the respective reactions of these materials in soil and water systems. Advanced research on standardization and standards developed for luminescence studies, as well as both active and passive use of luminescence, is included.

Developments in laser design, microelectronics, and computers over the past 20 years have resulted in a renaissance for fundamental and analytical applications of molecular luminescence. Twenty years ago the conventional wisdom was that, although luminescence is inherently very sensitive for detection of emitters, the generally broad, featureless emission band and the frequent interferences from trace contaminants made interpretation of luminescence spectra difficult. It became necessary to isolate samples of unknown materials to such a high degree that luminescence measurements did not contribute much additional material. Today, new techniques have made luminescence spectroscopy indispensable as a sensor of chemical species in environments as diverse and complex as biochemical fluids, chromatographic columns, the Earth's atmosphere and waters. Furthermore, luminescence allows the determination of internal energy states and follows how they change with time on a scale that can be as short as one picosecond. Such measurements are crucial for fundamental investigations of the dynamics of chemical processes.

For analytical applications, many techniques have greatly improved our ability to analyze multicomponent systems. These include the coupling of luminescent detectors with chromatographic columns and other separation devices; combining lifetime and polarization data with spectral measurement; three-dimensional plotting of the total excitation-emission intensity matrix; synchronous scanning of the excitation and emission wavelengths, tagging specific molecules in a mixture with unique fluorescent labels; and using tunable lasers to induce emission from electronic states that are characteristic of

particular molecules. Chemi-excitation of luminescent molecules is another versatile way to impart additional sensitivity and specificity to the analysis of multicomponent systems. Compounds such as amines and amino acids have been derivatized and made to react with oxalates and hydrogen peroxide after high-performance liquid chromatography separations. The chemiluminescent reactions permit detection at femtomole levels.

Fluorescence analysis has been extended to many nonfluorescent species by the development of a wide range of derivatizing agents that form a fluorescent product. This approach has been especially useful with biochemical molecules, many of which are not natural fluorophores.

Luminescence lifetimes are measured by analyzing the rate of emission decay after pulsed excitation or by analyzing the phase shift and demodulation of emission from chromophores excited by an amplitude-modulated light source. Improvements in this type of instrumentation now allow luminescence lifetimes to be routinely measured accurately to nanosecond resolution, and there are increasing reports of picosecond resolution. In addition, several individual lifetimes can be resolved from a mixture of chromophores, allowing identification of different components that might have almost identical absorption and emission features.

In studies of molecular dynamics, lasers of very short pulse lengths allow investigation by laser-induced fluorescence of chemical processes that occur in a picosecond time frame. This time period is much less than the lifetimes of any transient species that could last long enough to yield a measurable vibrational spectrum. Such measurements go beyond simple detection and characterization of transient species. They yield details never before available of the time behavior of species in fast reactions, such as temporal and spatial redistribution of initially localized energy in excited molecules. Laser-induced fluorescence characterizes the molecular species that have formed, their internal energy distributions, and their lifetimes.

Biological applications of luminescence make use of resonance energy transfer as a microscopic ruler to measure distances between chemical groups in complicated biological structures. Electronic excitation of a fluorophore can be dissipated either by fluorescent emission or by nonradiative resonant energy transfer to an acceptor molecule. The transfer rate depends on the distance between donor and acceptor groups. Fluorescence lifetimes are shortened as the fraction of energy dissipated nonradiatively increases. Resonant energy transfer is particularly significant over the distance range of 2 to 5 nm, which is also the range of typical protein diameters and membrane thicknesses. As a result, fluorescent lifetime measurements of natural and derivative fluorophores are used to determine distances between binding sites on



proteins and chromophore distances in biological aggregates. Such measurements have produced important results regarding the conformation and structures of several proteins and geometric details of protein-membrane interactions. Particularly valuable is the fact that luminescence measurements of molecular conformation can often be made in situ, yielding unique information not possible from X-ray diffraction about molecules that change shape when crystallizing or do not form crystals at all.

Many biologically important processes are related to changes in activity caused by environmental changes at metal binding sites on proteins. The normally bound ions  $\text{Ca}^{2+}$  and  $\text{Mg}^{2+}$  can be replaced by the transition metal ion fluorescent probes  $\text{Tb}^{3+}$  and  $\text{Eu}^{3+}$ , whose luminescent lifetimes are very sensitive to their chemical environment, especially the degree of hydration. Their emission lifetimes can be used to track environmental changes at binding sites while a protein is reacting or responding to external influences. There are many other instances where the sensitivity of chromophore lifetimes to their chemical surroundings has been used to probe the details of environmental conditions around a chromophore, such as solvation, micelle structures, and the structures of dissolved complexes.

The reactivity of large and complex molecules is often closely related to their size and shape. Luminescence polarization sometimes offers a way to determine these properties. Electronic excitation of a chromophore with polarized light will produce polarized emission. However, any rotation of the molecule after excitation but before emission will cause some depolarization of the emission. Depolarization and lifetime measurements can be used together to determine rates of rotation of chromophoric molecules that can be related to a molecule's rotational diameter. Studying the temperature behavior of depolarization can yield additional information about a molecule's shape. Observing how rotational rates change under different conditions can indicate corresponding changes in the shape of a molecule, such as denaturation of proteins at high temperatures or complex formation at high concentrations.

Luminescence science has developed into a powerful tool for studying nature in macro- and microenvironments. At present, there are many scientific advances being reported that incorporate fluorescence technology into the research regimen. I expect this trend to continue as the scientific community becomes more cognizant of the knowledge to be gained by use of luminescence techniques.

The purpose of the symposium on which this book is based was to report original research advances that use luminescence as a basic investigative tool. Because these applications transcend the field of chemistry, a multidisciplinary group of prominent scientists contributed

to the symposium to enrich it with a variety of applications. Researchers in the biological, chemical, and physical sciences have been in the forefront of those employing luminescence methodology and have brought some innovative uses of luminescence to bear on their research. This book presents excellent research results in the biological, chemical, environmental, and hydrological sciences. Each chapter addresses an important application of luminescence and advances its particular subject discipline.

### **Acknowledgments**

I wish to acknowledge the assistance of the many people who contributed to this publication. Patricia M. Negomir's help in organizing this book was greatly appreciated. John B. Weeks gave material assistance to the compilation of the book. Peter L. Martin did an excellent job of editing the chapters. Patricia A. Griffiths, Linda S. Britton, and their staff supplied typing assistance that was invaluable. Rance Velopoldi contributed to the design of the dust jacket. Finally, I wish to thank all of the contributing authors for being patient while awaiting publication of their material and for doing such an outstanding job in their respective fields.

MARVIN C. GOLDBERG  
U.S. Geological Survey  
Box 25046, MS 424  
Lakewood, CO 80225

September 26, 1988

## Chapter 1

# The Science of Luminescence

Marvin C. Goldberg and Eugene R. Weiner

U.S. Geological Survey, Box 25046, MS 424, Lakewood, CO 80225

The use of luminescence methods to measure the properties of chemical and biochemical systems has expanded so greatly in recent years that technical reviews and bibliographies no longer attempt to encompass the entire field, dealing instead with some restricted portion of the major subdivisions that have evolved. In the 1986 *Fundamental Reviews of Analytical Chemistry*, Wehry (1) lists 639 references in a biannual review titled "Molecular Fluorescence, Phosphorescence, and Chemiluminescence" which is focused mainly on analytical applications, and totally excludes the major topics of atomic fluorescence; molecular luminescence in flames, plasmas, and discharges; infrared fluorescence; solid state phosphor and semiconductor luminescence; radioluminescence; liquid scintillation counting; X-ray induced luminescence; and luminescence probing of biochemical, macromolecular, and micellar systems. Activity in each of the excluded areas is at least comparable to that in analytical applications of luminescence and the literature dealing with applications to biochemical, macromolecular, and micellar systems is by far the largest. Luminescence measurements have become an essential tool in nearly every aspect of molecular research. In contrast, the comparable biannual review in the 1956 *Analytical Reviews of Analytical Chemistry* (2) is titled simply "Fluorometric Analysis" and contains just 93 references, with no apologies for omission of any important topics.

The immense growth in the luminescence literature during the period between these two reviews had little to do with developments in fundamental theory. It was mainly due to the availability of new instrumentation, such as the photomultiplier (around 1950), the laser (around 1960), transistor and microcircuit electronics (around 1970), and ready access to laboratory computers (around 1975). All aspects of luminescence theory now being used to interpret luminescence measurements have been known since the early 1900's and nearly all of the types of measurements now being made had been initiated with cruder techniques by 1930. We discuss here many of the latest techniques in luminescence analysis with selected highlights from the historical development of luminescence and a look at several recent developments in luminescence applications that appear likely to be important to future research.

### *A Short History of Molecular Luminescence*

*The Early Period.* Luminescent phenomena such as the aurora borealis, phosphorescence of the sea, luminous animals and insects, and phosphorescent wood were the earliest of spectral observations because they require nothing more than the

This chapter not subject to U.S. copyright  
Published 1989 American Chemical Society

unaided eye as a detector. Harvey (3) reports that one of the earliest written references to luminescence appeared in the Chinese literature of around 1500-1000 B.C., describing glowworms and fireflies. Harvey gives a fascinating account of the many early attempts to explain luminescence, which took a definitely modern scientific approach by the seventeenth century, after experimental research had become a respectable activity for philosophers. Francis Bacon, the great advocate of observation over speculation, already had noted by 1605 that different kinds of luminescence seemed to have different origins, writing (3), "...it is not the property of fire alone to give light", and pointing out that "...sugar shineth only while it is in scraping; and salt water while it is in dashing; glowworms have their shining while they live, or a little after; only scales of fish putrefied seem to be of the same nature with shining wood: and it is true, that all putrefaction hath with it an inward motion, as well as fire or light". This last comment has in it the seeds of the much later description of light and heat as generated by internal vibrations and propagated according to wave theory.

The Bolognian stone, the first artificial inorganic phosphor, was discovered accidentally in 1603 by Vincenzo Cascariolo, an Italian bootmaker and amateur alchemist (3). He had found some heavy stones near his home and tried to extract precious metals from them. After being heated in his furnace, the stones had the ability to emit a reddish light for a lengthy time after being placed in the dark. We now know that the Bolognian stone was mainly barium sulfate with probable traces of bismuth or manganese, and was converted to the sulfides by strong heating. This important discovery attracted the attention of Galileo and his contemporaries who recognized that the phosphor would not luminesce until after it had been exposed to natural light. Since light had to be absorbed into the stone, as a sponge absorbs water, before the stone would emit light, the behavior of the phosphor implied at the time that light was a material substance. This led Galileo to speculate that light must travel with a finite velocity, which he tried unsuccessfully to measure. The Italian mathematician Zucchi wrote in 1652 (3) that the Bolognian stone emitted more intensely if it was exposed to brighter light and that the color of the emitted light did not change when the stone was exposed to white light, or to light passed through green, yellow, or red colored glass (a primitive spectroscopic experiment). He concluded that the light is not simply absorbed and reemitted unchanged, as is water from a sponge, but, "rather it excites and unites with a spirituous substance contained in the stone, and when the illumination has ceased, this substance gradually dissipates..."

The first recorded observation of fluorescence from a solution (prompt emission, in contrast to the delayed emission called phosphorescence of the Bolognian stone, see Table I) appears to be by Nicolas Monardes (3) in 1565, who reported that when a cup made of a certain wood called *lignum nephriticum* was filled with water, a blue tinge could be observed. The luminescent properties of aqueous extracts of this wood intrigued many seventeenth century scientists. Athanasius Kircher, the first prominent scientist of this period to specialize in studies of luminescence (3), examined aqueous extracts of the wood in 1646, stating that the colors observed depended on the ambient light intensity in which the observations were made. Robert Boyle in 1664, Isaac Newton in 1672, and Robert Hooke in 1678 all discerned that Kircher was wrong and that the color of the wood extract depended on the angle of viewing, being yellow by transmitted light and blue by "reflected" light, meaning when viewed off the angle of transmission where a faint emission could be detected. Harvey (3) points out that although Kircher is generally regarded as the discoverer of fluorescence in solutions, Boyle was the first to describe some of the important chemical characteristics of fluorescing organic solutions. Boyle found that after many extractions, the wood lost its power to make a fluorescent solution and concluded that there must be an "essential salt" in the wood that was responsible for the luminescence. He also reported that the light was generated without heat, that air (oxygen) was necessary and that extinguishing the light by evacuation was reversible, that the fluorescence was more visible in dilute solutions, and that adding an acid destroyed the effect, which returned

with the further addition of a base. All of these scientists believed they were observing a reflection phenomenon, not distinguishing clearly between emission and reflection.

Frictional and impact heating of objects had led many scientists to the conclusion that heat was related to some sort of internal motion. Because light and heat often accompany one another, it was logical to look for similarities in origin. Descartes, who advocated that matter was made up of small particles in constant motion and that fire was violent motion of these particles around their common center, believed that friction between the internal particles of matter generated the light. He developed an amazingly perceptive theory of light around 1637. Quoting Harvey (3), "...Descartes regarded light as rapid motion in a subtle (elastic) fluid (the æther), made up of particles (the first element) invading all space, even the pores of solid bodies like glass. Its particles moved in vortices, not in straight lines. Space was a plenum, with no vacuum anywhere. Light was not a transmission of particles but was communicated by the push or pressure of one particle to another, as the motion of one end of a stick is felt at the other. The sun's particles were in agitation and transmitted this agitation instantaneously throughout the Universe." A similar theory was proposed around 1665 by Robert Hooke (3-4), who wrote that light consists of rapid vibrations propagated instantaneously, or very nearly so, over any distance and that hot bodies emit light because of internal vibrations. He argued that luminescence without heat also arose from the same kind of internal motions. By 1700, observations of all the various types of luminescence (Table I), except for crystalloluminescence, had been recorded and several were recognized as being of different origins. In 1718, Newton (6) wrote in favor of Hooke's hypothesis, that the incandescence of all luminous bodies, whether hot or cold, originated from "vibratory motions of their parts". Confirmation of this speculation had to await the developments of the spectroscope and quantum theory. Harvey (3) recounts how Newton's pinhole and prism arrangement were used by Zanotti (1748) and Dessaignes (1811) to study inorganic phosphors, by Melvill (1752) to examine the bright yellow sodium color in an alcohol flame containing sea salt, by Priestley (1767) to look at electroluminescence, and by Herschel (1822) for studying colored flames. None of these investigators were able to obtain an accurate spectrum with Newton's apparatus, although Herschel suggested that the dispersed light patterns might be useful for detection of small quantities of compounds.

In 1802, Humphry Davy observed that this ultraviolet region could excite luminescence from a phosphor. A major instrumental improvement, necessary for the development of a practical spectroscope, was Wollaston's (7) introduction in 1802 of a slit in place of Newton's pinhole, with which he saw the dark lines in the solar spectrum later known as Fraunhofer lines. Wollaston did not recognize the significance of the dark lines and believed they simply separated the colors. These lines were rediscovered in 1814 by Fraunhofer (3-4) who had turned Wollaston's device into a practical spectroscope by adding a collimating tube and a telescopic eyepiece for viewing the image of the slit. Spectroscopic experiments by Bunsen and Kirchoff (8) in 1861 led to the interpretation of the Fraunhofer lines as being due to absorption of solar light by atoms and molecules in the atmospheres of the earth and the sun. These studies laid the foundation for spectral analysis based on the fact that every gaseous chemical element has a unique line spectrum.

The study of bioluminescence turned in the right direction in 1821 when Isaac François Macaire (3) suggested that the source of light in the glowworm might be some organic compound rather than an inorganic phosphor, as was commonly assumed. Macaire had observed that all chemical reagents that cause albumin to coagulate also extinguish the glowworm's light and concluded that the luminous substance might be some form of albumin.

Louis Pasteur (3) described in 1864 the spectrum of the light from the tropical luminous beetle *Pyrophorous* as continuous, without dark or light bands. In 1885, Raphael Dubois (3) obtained a cold water extract and a hot water extract from *Pyrophorous* which, when mixed together, reacted to produce light. Dubois named the

hot water extract *luciferin* and the cold water extract *luciferase*. He was able to demonstrate that luciferase and luciferin comprised an enzyme-substrate system. Dubois' work stimulated a resurgence of interest in bioluminescence. By 1889, M. W. Beijerinck (3) had used luminescent bacteria analytically to detect small amounts of oxygen.

Stokes (10), who coined the word "fluorescence" from fluor spar, made a thorough scientific investigation of photoluminescence in 1852. He was the first to state clearly that fluorescence was an emission process. He showed that emission intensity depends on sample concentration and proposed the principle, now known as Stokes' law, which states that fluorescent emission is always of longer wavelength than the excitation. He reported that emission from certain crystals was polarized but emission from solutions was not polarized, whether or not the exciting light was polarized. He also described how a tube of quinine solution glowed brightly with a blue color when placed in the ultraviolet portion of the solar spectrum. Stokes commented on the high sensitivity of fluorescent emission and predicted that fluorescence analysis was "...likely to prove a great value in the separation of organic compounds".

Edmund Becquerel (11) continued along the line of Stokes' studies, measuring the excitation and emission spectra of several phosphors, the influence of temperature, and many other parameters. Numerous scientists had observed that luminescence lifetimes appeared to vary considerably from compound to compound. Among the properties that Becquerel measured was the duration of luminescence after excitation ceased. For this purpose, he built the first phosphoroscope in 1858, with which he could measure emission lifetimes as short as  $10^{-4}$  seconds. With his phosphoroscope, Becquerel identified two different types of decay kinetics, exponential and hyperbolic, which he attributed to monomolecular and bimolecular decay mechanisms. Becquerel's son Henri also was a distinguished luminescence investigator. Henri Becquerel has a special place in the history of science for accidentally discovering radioactivity in 1896 while studying the luminescence of some uranium salts (9). He found that the salts could expose photographic plates through their black paper wrapping. The first specific suggestion to use fluorescence in an analytical application appears to have been in 1867 by Goppelsröder (12), who proposed the analysis of Al(III) by the fluorescence of its morin chelate. Luminescence excited by cathode rays was described by Goldstein (13) in 1876 and by Crooks (14) in 1881.

The term "luminescence" (the Greek translation of *lucifer*, meaning *light bearer*) was introduced by Eilhardt Wiedemann (15) in 1888, in order to distinguish between light emission from thermally excited substances and light emission from molecules that have been excited by other means without increasing their average kinetic energy. Emission having an intensity that exceeds emission of the same frequency from a black body at the same temperature, was termed luminescence by Wiedemann. In other words, Wiedemann characterized luminescence by the fact that it does not obey Kirchoff's law of thermal emission and absorption from a black body. He also reported that the double salts of platinum emitted polarized light when excited by cathode rays, illustrating that luminescence can originate from different kinds of excitation. Wiedemann classified six different kinds of luminescence according to their method of excitation. Although excitation mechanisms are much better understood today, contemporary classifications of luminescence are essentially the same as Wiedemann's as is illustrated in Table I.

The very first spectroscopic instruments, from Newton's prism and pinhole to Fraunhofer's simple spectroscope, were constructed to observe luminescence. Even though the great sensitivity of luminescence detection seemed to promise that luminescence would become an important tool for chemical analysis, the fact is that absorption spectroscopy was the first spectroscopic technique to be widely used. At first glance, this may seem surprising since absorption spectroscopy is inherently less sensitive and had to await the development of more complex instrumentation, especially, electronically amplified detection.

Table I. Types of Luminescence

Effect	Cause
<i>Fluorescence</i>	Emission of light due to an "allowed" electronic transition between excited and ground states having the same spin multiplicity, usually singlet. Lifetimes for such transitions are typically around $10^{-8}$ s. Originally it was believed that the onset of fluorescence was instantaneous (within $10^{-11}$ to $10^{-7}$ s) with the onset of radiation but the discovery of delayed fluorescence (16), which arises from thermal excitation from the lowest triplet state to the first excited singlet state and has a lifetime comparable to that for phosphorescence, makes this an invalid criterion. Specialized terms such as <i>photoluminescence</i> , <i>cathodoluminescence</i> , <i>anodoluminescence</i> , <i>radioluminescence</i> , and <i>Xray fluorescence</i> sometimes are used to indicate the type of exciting radiation.
<i>Phosphorescence</i>	Emission of light due to a "forbidden" electronic transition between excited and ground states having different spin multiplicities, usually triplet to singlet. Lifetimes for such transitions typically range from milliseconds to minutes.
<i>Thermoluminescence</i>	Emission of light accompanying mild heating of substances and arising from thermally activated ion recombination. The sample has been previously excited by exposure to light or particle radiation and the energy "frozen in", to be released (not produced) by heating. It actually is a delayed phosphorescence.
<i>Electroluminescence</i>	Emission of light accompanying the introduction of an electric field and arising from electronic excitation due to the presence of the electric field.
<i>Galvanoluminescence</i>	Emission of light accompanying the passage of an electric current through aqueous solutions and arising from chemical reactions of chemiluminescent species produced during electrolysis.
<i>Sonoluminescence</i>	Emission of light accompanying the passage of intense sound waves through a liquid and arising from electrical discharges in the residual gas of cavities formed by the acoustic energy in the liquid.
<i>Triboluminescence</i>	Emission of light accompanying the rubbing or crushing of certain crystals and arising from frictional charge separation at the crystal surfaces. Also called <i>piezoluminescence</i> .
<i>Crystalloluminescence</i>	Emission of light accompanying the crystallization of certain crystals from solution and probably arising from cleavages occurring during the growth of individual crystals. Thus, it is a form of triboluminescence. Luminescence which appears when crystals dissolve is termed <i>lyoluminescence</i> .
<i>Chemiluminescence</i>	Emission of light from electronically excited species produced in a chemical reaction.
<i>Bioluminescence</i>	Chemiluminescence from a biological system.

The high sensitivity of luminescence detection results from the fact that emitted photons are observed directly and many detectors, including the eye, will respond to small numbers of photons. Spectral absorption in a dilute sample, on the other hand, which compares the light intensity transmitted through an absorbing sample with the intensity of light incident on the sample, requires the detection of a small difference between large signals and can only be observed with electronic instrumentation. Furthermore, many luminescent phenomena emit in the high energy blue and ultraviolet regions of the spectrum, where numerous sensitive detectors are available, whereas absorption spectra of interest are frequently in the infrared spectral region where detectors are relatively inefficient. Nevertheless, even though absorption measurements are inherently less sensitive than luminescence measurements, the first extensively used analytical applications of molecular spectroscopy developed around absorption spectrometers. For an analytical technique to be widely useful, it must be selective as well as sensitive and this was the "Achilles heel" of luminescence spectroscopy. Room temperature luminescent emission is generally broad and featureless, attributes which, in earlier times, usually negated its high sensitivity because band overlapping made multicomponent analyses impossible. The sensitivity of the method could not be fully utilized until its selectivity was improved. In fact, under conditions of low selectivity, the high sensitivity often was as much of a problem as a benefit because there were frequent interferences from trace impurities. Even though Jean Becquerel (17) discovered in 1907 that cooling samples to liquid air temperatures narrowed the spectral features considerably and increased the information content of luminescent spectra, this approach was not practical for routine use and attracted little interest for chemical analysis.

It was spectral absorption spectroscopy that became the earliest spectroscopic method widely used for molecular chemical analysis, and the prediction of Stokes (10) concerning the potential usefulness of fluorescence analysis was long delayed in its attainment. Even though absorption spectroscopy is less sensitive than luminescence spectroscopy it was found more useful because of its broader applicability. Many molecules that are not luminescent will absorb light and are subject to measurement whereas only those molecules that undergo a transition process when at an energy level above the ground state, will luminesce and are subject to luminescent measurements. The high degree of selectivity inherent in luminescence analysis could not be realized until the fresh insights of quantum theory revealed new, potentially measurable luminescence parameters and stimulated the improvements in instrumentation necessary to measure them.

*The Modern Period.* Luminescence experiments after 1900, in what might be called the modern period of experimentation, were based on the ideas emerging from quantum mechanics. The development of quantum theory in the early 1900's gave a solid theoretical foundation to the vast accumulation of spectral data reported during the previous 200 years. Quantum theory led to a very complete understanding of luminescent emission, readily explaining prior observations and allowing predictions of new phenomena. As a result, luminescence was well understood theoretically by 1920-1930, at which time it was recognized that luminescence spectroscopy is inherently more selective than absorption spectroscopy because at least five independent luminescence variables can be measured which are characteristic of a given sample component:

- emission intensity as a function of excitation wavelength.
- excitation intensity as a function of emission wavelength.
- excited state lifetime.
- emission polarization.
- quantum yield.

By comparison, the only variable measured in absorption spectroscopy is transmission as a function of incident wavelength. Once quantum theory had revealed the potential



of luminescence spectroscopy for studying molecular systems, the development of instruments for measuring the luminescence variables followed closely.

It becomes difficult at this point to follow a central thread of historical development. As the insights of quantum theory continued to stimulate new approaches to all the sciences, discoveries and applications related to luminescence appeared rapidly in many diverse fields. As a result, the remaining history necessarily becomes highly selective and many interesting and important aspects of recent luminescence history have surely been omitted.

Resonance radiation was demonstrated by Robert Wood (18) in 1905 when he showed that when a bulb filled with sodium vapor at low pressure was irradiated with light from an intense sodium flame, the bulb emitted only the sodium D lines, with very narrow widths that corresponded to thermal Doppler broadening only, even though the D lines in the higher temperature exciting source were much broader. By 1911, Selenyi (19) had shown experimentally that emission from fluorescein has a spatial intensity distribution that is characteristic of an electric dipole oscillator, confirming the theoretical explanation of the origin of polarized emission. Although Stokes (10) had not detected polarized fluorescence from solutions, Weigert (20) observed in 1920, while studying fluorescent dye solutions, that such fluorescence is quite common. He found that the amount of polarization changes with solution viscosity and temperature, indicating that Brownian motion influences the polarization. Then between 1926-1929, Perrin (21-22) developed a theory for Weigert's Brownian depolarization and showed that differences in the polarization of fluorescein in solutions of various viscosities were determined by the rotational rate and fluorescence lifetime of the molecules, a finding that foreshadowed today's extensive use of luminescence measurements to study the motions and the physical, chemical, and electronic environments of the emitting species.

In 1922, Cario and Franck (23) demonstrated sensitized fluorescence in gaseous systems. A gas molecule that does not absorb energy from an illuminating light can be made to fluoresce by introducing another sensitizing molecule that does absorb from the light source. Cario and Franck illuminated a mixture of thallium and mercury vapors with the mercury resonance line, photoexciting only the mercury atoms. Emission of the characteristic thallium lines results when excited mercury atoms transfer their electronic energy to unexcited thallium atoms by collision. The first analysis of atomic fluorescence from metal atoms in flames was reported by Nichols and Howes (24) in 1924. Today, atomic fluorescence flame spectrometry is one of the most important techniques for elemental analysis of metals.

Perrin observed in 1925 that increases in solution concentration were accompanied by increased depolarization and attributed this to energy transfer between like molecules (25), a far reaching concept that anticipated the discovery by Gaviola and Pringsheim (26) in 1927 that sensitized fluorescence occurs in liquid as well as in gaseous systems. Gaviola and Pringsheim found, that electronic energy can be transferred over longer distances than exist in a collisional encounter, in accordance with the quantum theory of nonradiative resonant electronic energy transfer (27). By measuring the depolarization of fluorescein, immobilized in a glycerol solution to eliminate the rotational depolarization observed by Perrin (21-22), they proved that depolarization also arises by electronic energy transfer from photoexcited molecules to unexcited molecules which then emit with a net loss of polarization, confirming Perrin's (25) conjecture about concentration depolarization. An important result of their experiments was the finding that electronic energy can be transferred over distances nearly the order of the emission wavelength (50-100 nm). Then in 1928, Warburg and Negelein (28) used the new technique of energy transfer depolarization to show that electronic energy could be transferred from the aromatic amino acids to the heme in a heme protein. Perrin's treatment of energy transfer depolarization was later modernized by Förster (29) in 1948 in terms of modern quantum theory, and Förster's treatment has been valuable for clarifying the behavior

of many photochemical processes where energy migration is important, as in photosynthesis (30). Methods based on Förster's theory have since developed into an elegant technique for using energy transfer phenomena as a molecular ruler, accurately measuring the distances between fluorophore positions, particularly in biochemical systems (31).

Gaviola (32) reported the construction of the first phase fluorometer in 1927, with which he measured the fluorescence lifetime of aqueous rhodamine B as 2 nanoseconds and that of fluorescein as 4.5 nanoseconds, in close agreement with the accepted values of today. In a phase fluorometer, the intensity of the excitation light source is sinusoidally modulated. The time lag between energy absorption and emission by sample molecules introduces a phase delay and demodulation, relative to the exciting waveform, into the emission from excited fluorophores. The phase delay and demodulation each can be used separately to calculate fluorescence lifetime. The resolution of Gaviola's device was about one nanosecond, a great improvement over Bequerel's (11) phosphoroscope. Teale (33) describes how visual detection was used for the phase measurement in Gaviola's instrument; a polarizer was rotated to visually match a double image. The more obvious pulse excitation method for measuring fluorescence lifetimes, where the time decay of emission intensity is measured directly, was not to appear until around 1950, following the commercial availability of photomultipliers.

Between 1923 and 1927, the concepts of *quantum efficiency* (number of photons emitted divided by number of photons absorbed by a sample) and *quantum yield* (fraction of excited molecules that emit) had been defined and values determined for many compounds by Vavilov (34). The quantum yield indicates the extent that other energy loss mechanisms compete with emission in an excited molecule. Although the quantum yield is influenced by the molecular environment of the emitter, for a given environment it depends on the nature of the emitting compound and is independent of concentration and excitation wavelength, at least at low concentrations (35). Thus, it serves as another measurable parameter that can be used to identify the compounds in a sample and also, because of its sensitivity to the surroundings of the luminophore, to probe the environment of the emitter.

The short period 1926-1927 was remarkably productive with regard to its impact on present day research. Techniques that are based on Gaviola's phase fluorometer, Perrin's theory of rotational depolarization, Vavilov's clarification of the concept of quantum yield, and the demonstration by Gaviola and Pringsheim of resonant energy transfer in solutions, have become indispensable tools in all areas of molecular research. It is interesting to note that Gregorio Weber (36), in 1983, picked just these four discoveries as his choices for the four most important advances in the field of fluorescence spectroscopy of solutions and biochemical systems.

In 1931, K. Weber (37) showed that the fluorescence spectrum of 1-naphthylamine-4-sulfonate was affected differently by pH changes than was the absorption spectrum, illustrating that the different electron configurations of the ground and excited states may cause them to exhibit very different chemical behaviors. This finding initiated a continuing series of studies using luminescence to examine the unique chemistry of electronically excited species. Information about the chemical properties of excited species is essential to an understanding of chemical reactions initiated by the absorption of high energy quanta, as occur in photochemistry and radiation chemistry. Förster and Kasper (38) in 1954 observed red-shifted emission from concentrated pyrene solutions that they attributed to the formation of a molecular dimer formed from two pyrene molecules, one excited and one in its ground state, later to be called an excimer by Stevens and Hutton (39). By 1955, Förster (40) and Weller (41) had measured excited state ionization constants of organic acids and determined that many have excited state values that differ by several orders of magnitude from the ground state values. In 1963 Leonhardt and Weller (42) detected emission from excited state complexes of unlike molecules, which later became known as exciplexes. Förster

and Selinger (43) in 1964 studied the kinetics of excimer formation in micelles, which they were able to relate to diffusion rates and microviscosities within a micelle. Luminescence studies of excited state chemistry have evolved into a line of research that is helping to bring order into the study of excited state reactions by providing essential data for many species, such as excited state ionization constants (44), excited state proton transfer rates (45), kinetic mechanisms and rate constants for excimer and exciplex reactions (46), and relaxation characteristics of polar solvents (47).

Jablonski (48-49) developed a theory in 1935 in which he presented the now standard "Jablonski diagram" of singlet and triplet state energy levels that is used to explain excitation and emission processes in luminescence. He also related the fluorescence lifetimes of the perpendicular and parallel polarization components of emission to the fluorophore emission lifetime and rate of rotation. In the same year, Szymanowski (50) measured apparent lifetimes for the perpendicular and parallel polarization components of fluorescein in viscous solutions with a phase fluorometer. It was shown later by Spencer and Weber (51) that phase shift methods do not give correct values for polarized lifetimes because the theory does not include the dependence on modulation frequency.

In 1944, Lewis and Kasha (52) identified phosphorescence as a "forbidden" transition from an excited triplet state to the ground singlet state and suggested the use of phosphorescence spectra to identify molecules. Since then, phosphorimetry has developed into a popular method of analysis that, when compared with fluorometry, is more sensitive for some organic molecules and often provides complimentary information about structure, reactivity, and environmental conditions (53).

Pulse fluorometry for directly measuring fluorescence and polarization decay times was developed during the 1950's, immediately following the commercial availability of photomultipliers (the RCA 1P28 photomultiplier introduced around 1950 quickly became ubiquitous in spectroscopy laboratories). Ware (54) placed in the introductory part of his paper on the current technique of pulse fluorometry, a brief outline of the early history of pulse methods, from the nanosecond measurements of Brody in 1957, who connected the output of his photomultiplier directly to the deflection plates of a Tektronix oscilloscope because pulse amplifiers at that time could not handle transient signals in the nanosecond range, to the picosecond measurements that first appeared in the 1970's using single-photon time-correlation methods with pulsed lasers and synchrotron radiation light sources. Single-photon counting time-correlation techniques evolved around 1960 (55-58) and has been crucial for the development of instruments that measure the time dependence of depolarization by pulse methods. Synchrotron radiation was first used to measure fluorescence lifetimes in 1973 (59). The cavity-dumped mode-locked CW laser was developed as a source for the single photon technique in the 1970's (60-61).

The fluorescent lifetime of chlorophyll *in vivo* was first measured in 1957, independently by Brody and Rabinowitch (62) using pulse methods, and by Dmitrievsky and co-workers (63) using phase modulation methods. Because the measured quantum yield was lower than that predicted from the measured lifetime, it was concluded that much of the chlorophyll molecule was non-fluorescent, suggesting that energy transfer mechanisms were the means of moving absorbed energy to reactive parts of the molecule.

Luminescence measurements on proteins occupy a large part of the biochemical literature. In what surely was one of the earliest scientific reports of protein photoluminescence uncomplicated by concurrent insect or microorganism luminescence, Beccari (64), in 1746, detected a visible blue phosphorescence from chilled hands when they were brought into a dark room after exposure to sunlight. Stokes (10) remarked that the "dark" (ultraviolet) portion of the solar spectrum was most efficient in generating fluorescent emission and identified fluorescence from animal matter in 1852. In general, intrinsic protein fluorescence predominantly occurs between 300 nm and 400 nm and is very difficult to detect visually. The first

quantitative study of protein fluorescence, by Shore and Pardee (65) in 1956, had to await the development of high-pressure quartz xenon lamps, blazed diffraction gratings, large throughput spectrometers with quartz optics and sample holders, and UV-sensitive photomultipliers, all of which became available during the period 1950-1960.

In 1952, Shpol'skii observed (66) that the fluorescence spectra of many aromatic molecules changed from broad bands to relatively sharp ( $\sim 10\text{ cm}^{-1}$ ) fine structure when the aromatic molecules were dissolved in an n-alkane solvent and frozen to liquid nitrogen or liquid helium temperatures. The best results are obtained when the length of the solvent molecule closely matches the long axis length of the aromatic solute molecule. Under these conditions, the solute molecule can replace a solute molecule in the crystalline lattice without significant strain so that there is a reduction (relative to vitreous solvents) of the number of solvent cage orientations that are possible. This method of spectral line narrowing has become an important standard technique in luminescence spectroscopy. Also in 1952, Weber (67-68) introduced the idea of adding an extrinsic fluorescent probe to proteins, to facilitate measuring the steady state rotational depolarization of proteins and obtaining information about their size, conformation, and flexibility. With this work, Weber showed how the fluorescence polarization technique could be used to measure the Brownian motion of proteins. Proteins had been thought to adhere to a rather rigid "lock and key" mechanism in their reactions but the earliest fluorescence polarization measurements showed that many proteins were very flexible. The concept has since been highly developed by Weber and his co-workers (36, 51, 67-68) by combining steady state methods with phase modulation methods for measuring fluorescence lifetimes, depolarization, and differential phase polarization.

An indication of two or more lifetimes can arise when a single fluorophore is found in two or more very different surroundings, as long as the characteristics of the different surroundings remain distinct for a time of the order of the lifetime of the fluorescence. Much information can be learned about the in situ behavior of proteins by studying the causes for heterogeneity of lifetime measurements. Polarization and emission lifetime measurements of tryptophan or probe residues on proteins often show heterogeneous decay behavior that can be linked to dynamic exchange interactions between residues on different sites. Changes in quantum yields and emission maxima of intrinsic fluorescence also can be used to monitor conformational changes of proteins and their interaction with ligands (71).

In 1947, William McElroy (72) discovered that adenosine triphosphate (ATP) and magnesium were essential for the bioluminescence reactions by which fireflies produce light. During the period 1956-69, McElroy and associates isolated the light producing substances luciferin and luciferase from fireflies and, along with other workers, described the reaction mechanism and kinetics (73). Because of the importance of ATP in the mechanism, firefly luciferase is used in a standard analytical procedure that is specific and extremely sensitive for ATP. The detection limit for the firefly assay method is about  $10^{-11}\text{ mol/L}$  ATP, allowing the detection of single cells in certain cases (74). Since ATP is present in all organisms with a fairly constant intercellular concentration, ATP concentration is a useful index of total biomass and has been applied as such to monitor bacteria in food, biomass in environmental waters and soils, bacterial screening in urine, and biomass in wastewater and sewage sludge (75). The probable universality of ATP as a metabolite and the high sensitivity of its analysis suggest the use of the firefly assay technique as a tool for the detection of life on other planets.

The use of phase sensitive detection with the phase fluorometer to analyze multicomponent systems was first described in 1970 by Veselova and coworkers (76). By using phase sensitive detection, the detector phase angle can be adjusted to be exactly out of phase with the phase-delayed emission from any single fluorophore, suppressing its contribution to the total emission signal. Phase sensitive detection, coupled with

measurements at several different modulation frequencies can be used to separate the individual emission spectra and fluorescent lifetimes of the different components in a mixture of fluorophores, providing the lifetimes are different enough to allow the required detector phase angles to be resolved. An improved method using a cross-correlation technique was developed about the same time (77), in which the gain of the photomultiplier detector is modulated at a frequency slightly different from that of the excitation energy. This generates directly in the detector a low frequency cross-correlation signal around 10 Hz that carries the same phase and modulation information as the original high frequency. The phase and modulation of the low frequency cross-correlation signal can be measured with a better signal-to-noise ratio and permits much greater precision than direct measurements on the high frequency signal.

At present, lifetime differences around 1–10 ps are measurable with phase modulation and pulse methods. This allows a clear experimental separation of phenomena that occur in a time scale where molecular motions and interactions are important, around 1 ns to 1  $\mu$ s or longer, from those occurring within 0.1 ns to 1 ps, which arise from phenomena that reflect only internal energy changes unaffected by molecular motions. Weber (36) has referred to events occurring in the time domain shorter than 0.1 ns as belonging to the "private life" of molecules, while those occurring in a time interval around 1 ns or longer belong to their "public life".

The story of luminescence advances since 1970 is best found in the current literature. It is too large and diversified to be readily summarized in a single article and too recent to edit for the most important events. Luminescence studies are so pervasive throughout all the fields of science that each special sphere of inquiry could have its own recent history of luminescence. Many of the most important developments of today will necessarily remain hidden to most scientists until later discoveries reveal their significance. For these reasons, this report continues with a personal selection of topics, chosen to guide the reader to a potpourri of interesting recent reports.

#### *A Look at Some Important Recent Developments in Luminescence*

The active state of luminescence spectrometry today may be judged by an examination of the 1988 issue of *Fundamental Reviews of Analytical Chemistry* (78), which divides its report titled "Molecular Fluorescence, Phosphorescence, and Chemiluminescence Spectrometry" into about 27 specialized topical areas, depending on how you choose to count all the subdivisions. This profusion of luminescence topics in *Fundamental Reviews* is just the tip of the iceberg, because it omits all publications not primarily concerned with analytical applications. *Fundamental Reviews* does, however, represent a good cross-section of the available techniques because nearly every method for using luminescence in scientific studies eventually finds a use in some form of chemical analysis. Since it would be impossible to mention here all of the current important applications and developments in the entire universe of luminescence, this report continues with a look at progress in a few current areas that seem significant to the author for their potential impact on future work.

**Multidimensional measurements.** A major use of luminescence measurements is to probe the environment of the emitting species. Many luminescence parameters are sensitive to the surroundings as well as the nature of the luminophore. The high sensitivity of luminescence measurements allows small changes in measured parameters caused by environmental differences to be quantitatively measured. (See the paragraph below on lanthanide ion probes for an example.) Excitation and emission maxima, quantum yield, depolarization, temperature coefficient, and lifetimes all can be affected by environmental changes such as pH, ionic strength, temperature, viscosity, chemical binding, and unpaired electron spin density, making luminescence measurements inherently information-rich about the species emitting

and their environment. Luminescence is especially well suited for monitoring chemical processes that are sensitive to the immediate environment, as in living cells.

Multidimensional measurements combine two or more luminescence parameters, either simultaneously or in sequence, into a single measurement in order to make possible a more complete utilization of the information present in the luminescent signal, permitting a more complete characterization of the luminescent material and increasing analytical selectivity. The combination of luminescence measurements with other techniques, such as chromatographic separation and chemical derivatization, also enhance analytical selectivity and could properly be included in the category of multidimensional measurements. Miller (79) regards HPLC coupled with fluorescence detectors as one of the most important current applications of fluorescence. In chapter 12 of this book, Nelson *et al.*, describe the development of derivitizing agents useful for making fluorophores from nonfluorescent compounds so they can be analyzed by HPLC with fluorescent detection.

Even the fact that some species do not fluoresce may be used as a selectivity tool. Computers and modern electronics have made multidimensional measurements possible on a hitherto unprecedented scale and this approach has been one of the most effective ways to achieve high selectivity in luminescence measurements. Many ingenious techniques have recently become available for utilizing the multiple luminescence variables and these have made luminescence measurements a routine and valuable tool in almost all areas of experimental science.

Many current multidimensional methods are based on instruments that combine measurements of several luminescence variables and present a multiparameter data set. The challenge of analyzing such complex data has stimulated the application of special mathematical methods (80-85) that are made practical only with the aid of computers. It is to be expected that future analytical strategies will rely heavily on computerized pattern recognition methods (79, 86) applied to libraries of standardized multidimensional spectra, a development that will require that published luminescence spectra be routinely corrected for instrumental artifacts. Warner *et al.*, (84) have discussed the multiparameter nature of luminescence measurements in detail and list fourteen different parameters that can be combined in various combinations for simultaneous measurement, thereby maximizing luminescence selectivity with multidimensional measurements. Table II is adapted from their paper with the inclusion of a few additional parameters. Several of the entries: excitation-emission matrix, synchronous spectra, and time-resolved depolarization, are themselves widely used multidimensional measurements that may be combined further with other parameters.

Table II. Luminescence Parameters that can be Combined for Selectivity Enhancement

<u>Spectral measurements</u>	<u>Lifetime measurements</u>	<u>Polarization measurements</u>	<u>Miscellaneous measurements</u>
Excitation spectra	Fluorescence	Static depolarization	Quenchometry
Emission spectra	Phosphorescence	Differential phase	Surfactant enhancement (micelles, etc.)
Low-temperature spectra	(both time and phase resolved)	Depolarization	
Excitation-emission matrix		Time-resolved depolarization	Sensitized measurements
Synchronous spectra			Chemical derivatization
Quantum yield		Circular polarization	Chromatographic detection
<u>Two-photon excitation</u>		<u>Circular dichroism</u>	

New ways to combine the various parameters of Table II are continually appearing in the literature. One of the most popular methods of multidimensional analysis is to measure the excitation-emission matrix (EEM), which allows plotting the emission intensity at all combinations of excitation and emission wavelengths in a single three-dimensional graph (81, 84-85, 87). Synchronous scanning (85, 88-89) is a simplification of the EEM technique in which both the excitation and emission wavelengths are scanned simultaneously with a typical offset of 50-100 nm. This approach generates a single two-dimensional slice through an EEM surface (90) and is especially useful for rapid screening analyses of complex mixtures. Synchronous scan luminescence spectrometry has recently been used in combination with a supersonic jet expansion (91). By setting the wavelength difference to zero, a characteristic single very sharp emission line was obtained for each component in a mixture of seven polyaromatic hydrocarbons.

Paski and Blades (92) recently have found lifetime-wavelength resolved spectra useful for separating mixtures of inorganic powders which have been otherwise difficult to analyze. Lifetimes by the pulse method were determined as a function of emission wavelength and computer analysis of the data allowed separation of individual components from synthetic three-component mixtures. Wild (93) has compared EEM spectra of pyrene frozen in a single crystal of n-heptane, in a n-heptane Shpol'skii matrix, and in ethanol glass to study the effects of different kinds of sites on the spectrum. EEM spectra are utilized in chapters 8 and 13 of this book. Hurtubise *et al.* show that an EEM spectra of a mixture of benzo(a)pyrene and benzo(e)pyrene adsorbed on an  $\alpha$ -cyclodextrin-NaCl matrix allows the identification of nanogram levels of either compound in the presence of an excess of the other. Theisen reports on the development of a catalog of EEM "signatures" for materials having luminescence stimulated by solar radiation, referenced to the solar Fraunhofer lines.

*Spectral line narrowing techniques.* The usefulness of spectral measurements often depends on the wavelength resolution that can be attained. The broadness of spectral features in many luminescence spectra limit the application of optical spectroscopy for fundamental measurements such as energy level structure, radiative decay behavior, and energy transfer mechanisms as well as for analytical identification. The main causes of line broadening are thermal Doppler broadening, instrumental distortions, and inhomogeneous broadening. The thermal broadening contribution to line width can be reduced by cryogenic cooling and supersonic jet cooling. Instrumental limitations on line sharpness are minimized by using the best available optical components and laser light sources. Inhomogeneous broadening arises from emitters that are in slightly different microenvironments, causing small differences in the energy levels of otherwise identical emitters. In solids, microenvironments are not uniform because of crystal strains and defects; in solutions, because of inhomogeneities of the solvent cages. After thermal broadening is minimized, the residual line widths are mainly due to inhomogeneous broadening and are still about  $0.1\text{-}10\text{ cm}^{-1}$  in many solid materials, and around  $300\text{ cm}^{-1}$  for an organic compound in a vitreous solvent. Each emitter has a characteristic instrumentally limited homogeneous line width centered around the environmentally shifted energy level. The amount of improvement possible is indicated by the fact that the homogeneous line width at low temperatures ( $<77\text{ K}$ ), which would be the sample line width if inhomogeneous broadening did not contribute, may be only  $10^{-3}\text{ cm}^{-1}$  or less wide.

Two line narrowing techniques, matrix isolation and resonant laser excitation, are being used separately and in combination to eliminate inhomogeneous broadening (94). Microenvironmental inhomogeneities are reduced by freezing the sample into uniform site locations in isolation or Shpol'skii matrices (95). Alternatively, with highly monochromatic and tunable lasers, it is possible to photoexcite only the subset of emitter sites in a low temperature matrix which have

excitation energies in resonance with the laser energy, effectively observing only those emitters having a high degree of energy level uniformity (95).

"Hole burning" (94) is another laser technique for increasing spectral information content that is closely related to line narrowing. Hole burning is the marking of a narrow population distribution in a broad inhomogeneously broadened line. It is accomplished by exposing the sample to narrow width laser excitation that promotes a small portion of the band emitters to another excited level, decreasing the population emitting in a small range of the broad band and creating a well defined intensity notch in the band. The notch may be interpreted as a sharp spectral line and offers a spectroscopic technique capable of revealing nuclear hyperfine structure (97). In a review of the 1988 International Conference on Luminescence, McClure (97) commented that "No longer can one tolerate the loss of information in an inhomogeneously broadened line".

**Rare Earth Ion Probes.** The use of rare earth ion fluorescent tags offers a different approach to attaining the high resolution fluorescence spectra necessary to probe environmental changes (98). Lanthanide and actinide ions have long excited state lifetimes (1 ms-10 ms) and correspondingly sharp emission lines. Small changes in their crystal field environment can cause easily measured changes in their fluorescence spectra. An especially fruitful application has been the substitution of lanthanide trivalent ions (designated Ln(III)) for Ca(II) at calcium binding sites in proteins (99), allowing many different measurements of the physical environment of the proteins under physiologically significant changes. For example, Canada (100-101) has found that the quenching of Tb(III) luminescence by two particular anticancer drugs in tumorigenic indicates that both drugs associate with same Ca(II) binding protein in the cell membrane. From the temperature dependence of the lifetime of Tb(III) in the protein calmodulin, Austin *et al.* (102) have concluded that there is a phase change from a rubberlike structure to a glass structure around 200 K. Other novel studies of protein dynamics and microenvironments with lanthanide probes were made by O'Hara *et al.* (103), who measured protein motions in various environments from the temperature dependence of Förster energy transfer, and Wensel *et al.* (104) who determined the characteristics of the electrostatic field around DNA by studying collisional energy transfer from Tb(III) chelates.

The long lifetimes of rare earth ion probes can be useful in another way for increasing analytical selectivity. In many cases, the single beam nature of fluorescence instruments means that the sensitivity of a fluorescence measurement is blank limited (105) from scattered radiation and impurity emission from the sample matrix. Increasing the measurement selectivity by adding a temporal dimension to the measurement will not always work because most molecules have fluorescence lifetimes in the nanosecond range and the background lifetime may not be sufficiently different from the sample lifetime for easy separation. This is a particular problem in immunoassays (see below) of blood samples, where there is appreciable background emission from proteins and other fluorophores in the blood (106). If a lanthanide ion label can be attached to the sample molecule, a fluorophore is produced with an emission lifetime in the microsecond range, which can easily be selectively analyzed after the background emission has died out.

**Luminescence Immunoassay.** Immunoassay techniques based on fluorescence and chemiluminescence instead of radioactive tags are becoming important alternatives to radioimmunoassay because of less stringent safety and disposal problems, longer reagent shelf life, and more conventional instrumentation (79, 107-110). The analysis must distinguish between the portion of the antigen that is bound to antibodies and the portion remaining unbound. In the most common type of fluoroimmunoassay, this is accomplished by using polarized exciting light and detecting the degree of polarization of the emission. Fluorescent tagged antigens of low molecular mass rotate so rapidly with Brownian motion that between the times of absorption and emission they lose all



traces of their original position and the emitted light is essentially non-polarized. However, tagged antigens bound to macromolecular antibodies rotate much more slowly and their fluorescent emission is partially polarized, allowing an experimental distinction between the amounts of bound and unbound antigens. In chapter 4, Sklar *et al.*, apply this approach very effectively to a study of the interaction dynamics between proteins and ligands.

Several other techniques have evolved for biochemical assays. In chapter 2 of this book, Omann and Sklar report on a method of fluoroimmunoassay where the bound and unbound antigen are separated by the quenching of fluorescence that accompanies antibody binding. Then, in chapter 3, Holl and Webb show how they achieved a sensitive measurement of nucleic acids by the enhancement in fluorescence that accompanies the binding of fluorescent dyes to nucleic acids. Chandler *et al.*, also used fluorescence enhancement to monitor calcium mobility in neutrophil cells.

With simple fluorometers, the sensitivity of fluoroimmunoassay is one or two orders of magnitude below that of radioimmunoassay, but with the high source intensities possible with laser excitation, the sensitivity of fluoroimmunoassay is comparable to that of radioimmunoassay (107). Kato *et al.*, (111) reported a sensitivity of 1 attomol/L for the fluorometric assay of  $\beta$ -galactosidase conjugates. Many immunoassays have been developed around chemiluminescent and bioluminescent reactions, allowing high sensitivity with relatively simple equipment (79, 106, 110, 112, 113). The sensitivities of chemi- and bioluminescence assays are somewhat lower in general than for fluoroimmunoassays but the procedures are experimentally simpler. Note however, that Givens *et al.*, in chapter 8 of this book present a careful comparison of chemiluminescent and fluorescent methods for assaying amino acids monomers and oligomers and find that, for their systems, chemiluminescence is 50 times more sensitive than fluorescence. They also describe a chemiluminescent detector for HPLC.

*Environmental Studies.* Many analyses of environmentally important substances suffer from the same difficulties commonly encountered in biochemical assays: the sample often is in very low concentration; it may be inhomogeneous; it may be in an environment that contributes a large background signal. The luminescent methods useful in biochemistry are increasingly being used in environmental studies. Seitz (114) studied the binding of metal ions to humic substances in natural waters by the quenching of the natural fluorescence of fulvic acid by bound heavy metal ions and the binding of organic fluorophores to fulvic acid by rotational depolarization (115). He also obtained conformational information about a soil fulvic acid by rotational depolarization, concluding that the soil fulvic acid has a flat extended shape. In this book, Goldberg and Negomir report on rotational depolarization measurements of both fulvic and humic acids obtained from natural waters, finding equivalent sphere volumes for fulvic acids that are smaller than that of Seitz. They used dynamic depolarization techniques to obtain conformational information, finding that the water fulvic acid was spherical in the pH range 3 to 11, changing shape at higher and lower pH values. Using phase modulated fluorometry, Goldberg and Negomir found that there are two or more fluorophores present in their fulvic acid.

In their report on derivatizing reagents useful for HPLC analysis, chapter 12 of this book, Nelson *et al.*, thoroughly discuss the value of HPLC with fluorescent detection for analyzing low levels of fluorescent compounds introduced into groundwaters for tracing water movement. Kenny *et al.*, chapter 14, report on ground water pollution monitoring, where they used laser induced fluorescence in a fiber-optic probe designed to be lowered into a well.

*Thermoluminescence.* Thermoluminescence is a property of some solids in which excitation by light or particle radiation is frozen in as trapped electrons and holes or a crystal defect. Subsequent heating allows relaxation of the excited state and emission

of the energy. Thermoluminescence of minerals is routinely used as an indication of the past irradiation dose. Thermoluminescence from mineral artifacts such as pottery, which have been heated in their fabrication, is a measure of the radiation dose since the time of manufacture and is commonly used to determine the age of the artifact. The usual procedure is to heat the sample at temperatures up to 500 °C while observing blue and ultraviolet emission from the sample through filters that block the long wavelength thermal emission. Recently, spectral analysis of the emitted light has been shown to improve the accuracy of dating for some minerals and also to yield fundamental information about the nature of the emitting species and their structural defects (116).

In a more general application, thermoluminescence is used to study mechanisms of defect annealing in crystals. Electron holes and traps, crystal defects, and color-centers are generated in crystals by isotope or X-ray irradiation at low temperatures. Thermoluminescent emission during the warmup can be interpreted in terms of the microenvironments around the various radiation induced defects and the dynamics of the annealing process (117-118).

*Fiber Optic Fluorescent Sensors.* A versatile remote analytical probe can be made by attaching a fluorophore to the end of an optical fiber. The excitation light travels down the fiber to the fluorophore and the emission travels back to a detector. The tiny fiber can be inserted into locations difficult to sample by other methods, as, for example, a catheter into a blood vessel for *in vivo* measurement of dissolved oxygen (119) or anesthesia gas (120). Analysis is based on the modification of the emission characteristics of a fluorophore fastened to the probe tip by the chemical environment around the tip of the fiber and can be based on fluorescent quenching, enhancement, or wavelength shift. The small size of the fibers allows excellent spatial resolution and fiber optic detection has been used to localize lung (121) and mammary (122) tumors made fluorescent with a hematoporphyrin derivative. One advantage of fiber optic detection of laser induced fluorescence is its ability to minimize background radiation. The fiber optic terminus has a limited field of view so that by placing the fiber tip close to the laser focus region, light scattering in the background is largely outside of the cone of acceptance of the fiber tip. Sepaniak and Yeung (123) measured low picogram quantities of antitumor drugs in a flow cell equipped with fiber optic detection that virtually eliminated background signal due to specular scatter and flow cell fluorescence. Fiber optic techniques can also utilize chemi- and bioluminescent reactions as probes.

*Luminescence lifetime spectroscopy.* In addition to the nanosecond lifetime measurements that are now rather routine, lifetime measurements on a femtosecond time scale are being attained with the intensity correlation method (124), which is an indirect technique for investigating the dynamics of excited states in the time frame of the laser pulse itself. The sample is excited with two laser pulse trains of equal amplitude and frequencies  $\nu_1$  and  $\nu_2$  and the time-integrated luminescence at the difference frequency ( $\nu_1 - \nu_2$ ) is measured as a function of the relative pulse delay. Hochstrasser (125) has measured inertial motions of rotating molecules in condensed phases on time scales shorter than the collision time, allowing insight into relaxation processes following molecular collisions.

### Summary

An historical outline has been presented of some of the important developments in the study of luminescence, which reveals that most of the theory and practice used today were already in place by 1930. This is followed by a selection of recent developments in applications of luminescence intended to suggest to the reader possible uses of this versatile research tool in his own research.

*Literature Cited*

1. Wehry, E.L. *Anal. Chem.* 1986, *58*, 13R-33R.
2. White, C. E. *Anal. Chem.* 1956, *28*, 621-25.
3. Harvey, E.N. *A History of Luminescence From the Earliest Times Until 1900* ; American Philosophical Society: Philadelphia, 1957; p 692.
4. Born, M. *Principles of Optics* ; Pergamon: London, 1959.
5. Newton, I. *Phil. Trans.* 1672, *6*, 3075-87.
6. Newton, I. *Opticks*, 2nd edition; London, 1718; p 190.
7. Wollaston, W.H. *Phil. Trans.* 1802, *92*, 378.
8. Bunsen, R.; Kirchoff, G. *Abh. kgl. Akad. Wiss.*, Berlin, 1861.
9. Richtmeyer, F. K.; Kennard, E. H.; Lauritsen, T. *Introduction to Modern Physics*, 5th ed.; McGraw-Hill: New York, 1955.
10. Stokes, Sir G.G. *Philos. Trans. R. Soc. London A* 1852, *142*, 463.
11. Becquerel, E. *Com. Rend. Acad. Sci.*. 1858, *46*, 969-75.
12. Goppelsröder, F. *J. Prakt. Chem.*, 1867, *101*, 408.
13. Goldstein, E. *Sitzber. d. Ac. d. Wiss. Wein.* 1879, *80*, II, 151.
14. Crooks, W. *Proc. Roy. Soc.* 1881, *32*, 206.
15. Wiedemann, E. *Ann. der Physik* 1888, *34*, 446-49.
16. Lewis, G.N.; Lipkin, D.; Magel, T.T. *J. Am. Chem. Soc* 1941, *63*, 3005.
17. Becquerel, J. *Le Radium* 1907, *4*, 329.
18. Wood, R.W. *Phil. Mag.* 1905, *10*, 513-25.
19. Selenyi, P. *Ann. Physik* 1911, *35*, 444.
20. Weigert, F. *Verhandel. Deut. Ges. Phys.* 1920, *23*, 100.
21. Perrin, F. *J. Phys. Rad.* 1926, *1*, 390.
22. Perrin, F. *Ann. Phys. (Paris)* 1929, *12*, 169.
23. Cario, G.; Franck, J. *Z. Physik* 1922, *11*, 161.
24. Nichols, E.L.; Howes, H.L. *Phys. Rev.* 1924, *23*, 472.
25. Perrin, J. *Duexieme Conseil de Chemie Solvay, Gauthier Villars, Paris*, 1925, p 322.

26. Gaviola, G.; Pringsheim, P. *Z. Physik* 1927, 43, 384.
27. Kallman, H.; London, F. *Z. Physik. Chem.* 1929, B2, 207.
28. Warburg, O.; Negelein, E. *Biochem. Z.* 1928, 193, 339-46.
29. Förster, T. *Ann. Physik* 1948, 2, 55.
30. Moya, I. *NATO ASI Ser., Ser.A Time-Resolved Fluorescence Spectroscopy in Biochemistry and Biology*; Plenum Press: New York, 1983; pp 741-54.
31. Stryer, L. *Annu. Rev. Biochem.* 1978, 47, 819-46.
32. Gaviola, E. *Z. Physik* 1927, 42, 853-61.
33. Teale, F.W. J. *NATO ASI Ser., Ser.A Time-Resolved Fluorescence Spectroscopy in Biochemistry and Biology*; Plenum Press: New York, 1983; pp 59-80.
34. Vavilov, S. I. *Z. Physik* 1927, 42, 311.
35. Pringsheim, P.; Vogel, M. *Luminescence of Liquids and Solids*; Interscience: New York, 1943; p 25.
36. Weber, G. *NATO ASI Ser., Ser.A Time-Resolved Fluorescence Spectroscopy in Biochemistry and Biology*; Plenum: New York; 1983, pp 1-20.
37. Weber, K. *Z. Phys. Chem. (Leipzig)* 1931, B15, 18.
38. Förster, T.; Kasper, K. *Z. Phys. Chem. N. F.* 1954, 1, 275.
39. Stevens, B.; Hutton, E. *Nature* 1960, 186, 1045.
40. Förster, T. *Z. Electrochem.*, 1950, 54, 42.
41. Weller, A. *Z. Phys. Chem.* 1955, 3, 238.
42. Leonhardt, H.; Weller, A. *Ber. Bunsenges Phys. Chem.* 1963, 67, 79.
43. Förster, T.; Selinger, B. K. *Z. Naturforsch. A*, 1964, 19, 38.
44. Ireland, J.F.; Wyatt, P. A. H. *Adv. Phys. Org. Chem.*, 1976, 12, 131.
45. Brand, L.; Laws, W.R. *NATO ASI Ser., Ser.A Time-Resolved Fluorescence Spectroscopy in Biochemistry and Biology*; Plenum Press: New York, 1983; pp 319-40.
46. Ware, W.R. *NATO ASI Ser., Ser.A Time-Resolved Fluorescence Spectroscopy in Biochemistry and Biology*; ; Plenum Press: New York, 1983; pp 341-62.
47. DeToma, R.P. *NATO ASI Ser., Ser.A Time-Resolved Fluorescence Spectroscopy in Biochemistry and Biology*; Plenum Press: New York, 1983; pp 393-410.
48. Jablonski, A. *Z. Physik* 1935, 94, 38-46.
49. Jablonski, A. *Z. Physik* 1935, 95, 53-65.

50. Szymanowski, W. *Z. Phys.* 1935, *95*, 466-473.
51. Spencer, R.D.; Weber, G. *J. Chem. Phys.* 1970, *52*, 1654.
52. Lewis, G.N.; Kasha, M. J. *J. Am. Chem. Soc.* 1944, *66*, 2100.
53. McCarthy, W.J.; Winefordner, J.D. In *Fluorescence: Theory, Instrumentation, and Practice*; Guilbault, G.G., Ed.; Marcel Dekker: New York, 1967; pp 371-442.
54. Ware, W.R. *NATO ASI Ser., Ser.A Time-Resolved Fluorescence Spectroscopy in Biochemistry and Biology*; Plenum Press: New York, 1983; pp 23-57.
55. Bennett, W.R.; Jaran, A.; Ballik, E.A. *Bull. Amer. Phys. Soc.* 1960, *5*, 496.
56. Bennett, W.R. In *Advanced Quantum Electronics*; Singer, J. Ed.; Columbia University Press: New York, 1961.
57. Bollinger, L.M.; Thomas, G E. *Rev. Sci. Instrum.* 1961, *32*, 1044.
58. Koehlin, Y. *Acad. Sci. Paris Compt. Rend.* 1961, *252*, 391.
59. Lindqvist, L.; Lopez-Delgado, R.; Martin, M.; Tramer, A. *Proc. Intern. Symp. Synchrotron Rad. Users*, 1974.
60. Lytle, F.E.; Kelsey, M.S. *Anal. Chem.* 1974, *46*, 855.
61. Harris, J.M.; Gray, L.M.; Pelletier, M.J.; Lytle, F.E. *Mol. Photochem.* 1977, *8*, 161.
62. Brody, S.S.; Rabinowitch, E. *Science* 1957, *125*, 555.
63. Dmitrievsky, O.D.; Ermolaev, V.L.; Terenin, A.N. *Dokl. Akad. Nauk. SSSR* 1957, *114*, 468.
64. Beccari, J.B. *Phil. Trans. Roy. Soc.* 1746, *44*, 81.
65. Shore, V.G.; Pardee, A.B. *Arch. Biochem. Biophys.* 1956, *60*, 100.
66. Shpol'skii, E.V.; Illina, A.A.; Klimova, L.A. *Dokl. Akad. Nauk SSSR* 1952, *87*, 935.
67. Weber, G. *Biochem. J.* 1952, *51*, 145-155.
68. Weber, G. In *Advances in Protein Chemistry*; Anson, M.L.; Bailey K.; Edsall, J.T., Ed.; Academic Press: New York, 1953; pp 415-59.
69. Weber, G. *J. Chem. Phys.* 1977, *66*, 4081-4091.
70. Weber, G. *Acta Phys. Pol.* 1978, *A54*, 859-965.
71. Beecham, J.M. Brand, L. *Ann. Rev. Biochem.*; Richardson, C.C.; Boyer, P.D.; Dawid, I.B.; Meister, A., Ed.; Annual Reviews, Inc.: Palo Alto, 1985; p 44.
72. McElroy, W.D. *Proc. Nat. Acad. Sci., U.S.A* 1947, *33*, 342.

73. DeLuca, M.; McElroy, W.D. In *Methods in Enzymology, LVII*; DeLuca, M., Ed.; Academic Press: New York, 1978; p 3.
74. Wettermark, G.; Stymne, H.; Brodin, S.E.; Petersson, B. *Anal. Biochem.* 1975, **63**, 293.
75. Lundin, A. In *Clinical and Biochemical Luminescence*; Kricka, L.J.; Carter, T.J. N., Ed.; Marcel Dekker: New York, 1982; pp 43-74.
76. Veselova, T.V.; Cherkasov, A.S.; Shirokov, V.I. *Opt. Spectrosc.* 1970, **29**, 617-18.
77. Spencer, R. D.; Weber G. *Ann. N. Y. Acad. Sci.* 1969, **158**, 361-76.
78. Warner, I.M.; McGown, L.B. *Anal. Chem.* 1988, **60**, 162R-74R.
79. Miller, James, N. *Analyst* 1984, **109**, 191-198.
80. Warner, I.M. In *Contemporary Topics in Analytical and Clinical Chemistry*, Vol. 4; Hercules, D.M.; Hieftje, G.M.; Snyder, L.R.; Evenson, M.A., Eds.; Plenum: New York, 1982.
81. McGown, L.B.; Bright, F.V. *Anal. Chem.* 1984, **56**, 1400A.
82. Weber, G. *J. Phys. Chem.* 1981, **85**, 949.
83. Warner, I.M.; Christian, G.D.; Davidson, E.R.; Callis, J.B. *Anal. Chem.* 1977, **49**, 564-73.
84. Warner, Isiah M.; Patonay, Gabor; Thomas, Mark P. *Anal. Chem.* 1985, **57** (3), 463A-83A.
85. Warner, I.M.; McGown, L.B. *CRC Critical Reviews in Analytical Chemistry* 1982, **13** (3), 155-221.
86. Varmuza, K. *Pattern Recognition in Chemistry*, Springer-Verlag: Berlin, 1980.
87. Weiner, E.R.; Goldberg, M.C. *Am. Lab.*, 1982, **14**, 91-103.
88. Vo-Dinh, T. In *New Directions in Molecular Luminescence*; Eastwood, D., Ed.; ASTM Subcommittee E13.06 on Molecular Luminescence: Philadelphia, 1982; pp 5-16.
89. Rubio, S.; Gomez-Hens, A.; Valcarcel, M. *Talanta*, 1986, **33**, 633-40.
90. Weiner, E.R. *Anal. Chem.*, 1978, **50**, 1583.
91. Imasaka, T.; Tsukamoto, A.; Ishibashi, N. *Anal. Chem.* 1988, **60**, 1362.
92. Paski, E.F.; Blades, M.W. *Anal. Chem.* 1988, **60**, 1224.
93. Wild, U.P. *Proc. of the Int.Conf. on Lumin.*, 1987.
94. Weber, M.J. *Amer. Cer. Soc. Bull.*, 1985, **64**, 1439-43.

95. Conrad, V.B.; Gore, R.R.; Hammons, J.L.; Maple, J.R.; Perry, M.B.; Wehry, E. L. In *New Directions in Molecular Luminescence*; Eastwood, D., Ed.; ASTM Tech. Pub. 822, ASTM: Philadelphia, 1982; p 32.
96. MacFarlane, R.M. *Proc. Int. Conf. on Lumin.*, 1987.
97. McClure, D.S. *Proc. Int. Conf. on Lumin.*, 1987.
98. Wright, J.C. In *Modern Fluorescence Spectroscopy, vol. 4*; Wehry, E.L., Ed.; Plenum: New York, 1981; p 51.
99. Horrocks, W, DeW. In *Advances in Inorganic Biochemistry, vol. 4*; Eichorn, G. L.; Marizilli, L G., Ed.; Elsevier: Amsterdam, 1982; pp 201-61.
100. Canada, R.G. *Biochim. Biophys. Acta* 1986, *887*, 29-34.
101. Canada, R G. *Biophys. J.* 1987, *51*, 521a.
102. Austin, R.B.; Stein, D.L.; Wang *J. Proc. Nat. Acad. Sci., U.S.A.* 1987, *84*, 1541-45.
103. O'Hara, P.B.; Gorski, K.; Rosen, M. *Fed. Proc.* 1986, *45*, 160.
104. Wensel, T.G.; Meares, C.F.; Vlachy, V.; Matthew, J.B. *Proc. Nat. Acad. Sci., U.S.A* 1986, *83*, 3267-71.
105. Lytle, F.E. *J. Chem. Educ.* 1982, *59*, 915-20.
106. Townshend, A. In *Advances in Standards and Methodology in Spectrophotometry*; Burgess, C.; Mielenz, Eds.; Elsevier: Amsterdam, 1987; pp 21-37.
107. Sepaniak, M. *J.Clin. Chem.* 1985, *31*, 671-678.
108. Chait, E.M.; Ebersole, R.C. *Anal. Chem.* 1981, *53*, 682A-692A.
109. Visor, G.C.; Schulman, S.G. *J. Pharm. Sci.* 1981, *70*, 469.
110. Kricka, L.J.; Carter, T.J.N. In *Clinical and Biochemical Luminescence*; Kricka, L.J.; Carter, T.J.N., Eds.; Marcel Dekker: New York, 1982; pp 153-78.
111. Kato, K.; Hamaguchi, Y.; Okawa, S.; Ishikawa, E.; Kobayashi, K.; Katunuma, N. *Lancet*, 1977, *1*, 40.
112. *Bioluminescence and Chemiluminescence, Basic Chemistry and Analytical Applications*; DeLuca, M. A.; McElroy, W. D. Eds.; Academic: New York, 1981; p 782.
113. *Bioluminescence and Chemiluminescence, New Perspectives*; Schölmerich, J.; Andreason, R.; Kapp, A.; Ernst, M.; Woods, W.G., Eds.; John Wiley and Sons: New York, 1987, p 600.
114. Seitz, W.R., *Trends in Anal. Chem.* 1981, *1*, 79-83.
115. Roemelt, P.M.; Seitz, W.R. *Environ. Sci. Technol.* 1982, *16*, 613-616.

116. Huntley, D. J.; Godfrey-Smith, D. I.; Thewalt, M. L.W.; Berger, G.W. *J. Lumin.*, 1988, *39*, 123-36.
117. *Luminescence of Inorganic Solids*; Goldberg, P., Ed.; Academic: New York, 1966; p 765.
118. *Proc. Int. Conf. on Lumin.*, Williams, Ed.; Plenum: New York, 1973; p 723.
119. Peterson, J.I.; Fitzgerald, R.V. *Anal. Chem.* 1984, *56*, 62-7.
120. Wolfbeis, O.S.; Posch, H.E. *Anal. Chem.* 1984, *57*, 2556-61.
121. Profio, A.E.; Doinan, D.R.; Balchum, O.J.; Huth, G.C. *Med. Phys.* 1984, *10*, 35-39.
122. Van der Putten, W.J.; van Gemert, M.J. *Phys. Med. Bio.*, 1983, *28*, 633-38.
123. Sepaniak, M.J.; Yeung, E.S. *J. Chromotogr.* 1980, *190*, 377-83.
124. von der Linde, D.; Kuhl, J.; Rosengart, E. *J. Lumin.* 1981, *24-25*, 675.
125. Hochstrasser, R.M. *Proc. Int. Conf. on Lumin.*, 1987.

RECEIVED September 12, 1988



## Chapter 2

# Spectrofluorometric Analyses of Cell Responses

## Activation of Neutrophils by Chemoattractants and Hexachlorocyclohexanes

Geneva M. Omann<sup>1</sup> and Larry A. Sklar

Department of Immunology, Scripps Clinic and Research Foundation,  
10666 North Torrey Pines Road, La Jolla, CA 92037

Stimulation of cells elicits a complex series of responses within the cells. We have been particularly interested in the activation of human neutrophils by chemoattractants and the molecular basis of this activation. Several spectrofluorometric assays have recently been developed for studying these responses: Quin-2, Indo-1, and Fura-2 have been introduced as calcium chelators; light-scattering parameters have been shown to indicate degranulation, actin polymerization, and aggregation; *para*-hydroxyphenylacetic acid serves as an indicator for oxidant production; elastase substrates that release fluorescent cleavage products are available. Fluorescence methods for ligand-receptor dynamics have also been introduced. Spectrofluorometers with simultaneous, multichannel data acquisition capabilities are available for doing high-resolution kinetic analysis of these responses. Moreover, by combining kinetic analyses of function and receptor binding, detailed quantitative information about amplification in the activation pathways has been obtained. Recent experiments indicate that the  $\gamma$  isomer of 1,2,3,4,5,6-hexachlorocyclohexane (an insecticide) also stimulates neutrophils. Thus these types of analyses are relevant for analyzing the effect of environmental chemicals on normal cell function.

In this paper we review the fluorescence and spectroscopic assays commonly used in our lab to study neutrophil activation. The advantages of these assays are threefold. (1) These assays are very sensitive. (2) These are kinetic assays which can be measured with a time resolution of 1 s or less. This is important since many of these responses occur within seconds of stimulation and are

<sup>1</sup>Current address: Research Service (151), VA Medical Center, University of Michigan, 2215 Fuller Road, Ann Arbor, MI 48105

transient. (3) Several different responses can be measured simultaneously. Thus correlation or lack thereof between signals and responses can be assessed.

The neutrophil is an interesting system in which to study signal transduction and response generation for a number of reasons:

1. The neutrophil is a primary cell type which interacts with and is influenced by the environment. Neutrophils are important in host defense and play a role in the phagocytosis of particulate material. We obtain these cells in highly purified form from human blood (1,2).

2. These cells respond to a number of different chemoattractants which have specific and distinct receptors on the membrane surface (for recent reviews see Refs. 3 and 4). Such chemoattractants include *N*-formylpeptides, which are bacterial peptides, and mediators of inflammation such as leukotriene B<sub>4</sub>, C5a, and platelet activating factor.

3. These stimuli elicit a complex series of responses that result in cell functions such as chemotaxis and release of inflammatory compounds, oxidants, and proteases. Probably related to chemotaxis is a rapid, transient actin polymerization response. Inflammation results in part from the release of proteases and myeloperoxidase normally stored in granules inside the cell (5) and from oxidants produced by an NADPH-oxidase system (6) located primarily in the plasma membrane.

4. The signal pathway is at least partially known (Figure 1; for reviews see Refs. 3, 4, and 6). Ligand binding to receptor causes activation of a guanine-nucleotide-binding protein (G protein), which activates phospholipase C. This enzyme releases inositol trisphosphate (IP<sub>3</sub>) and diacylglycerol (DAG) from phosphatidylinositol 4,5-bisphosphate. IP<sub>3</sub> causes the release of Ca<sup>2+</sup> from intracellular stores. Ca<sup>2+</sup> activates calmodulin-dependent protein kinases, and Ca<sup>2+</sup> and DAG activate protein kinase C. Phosphorylation events are thought to be involved in initiation of oxidant production and degranulation.

Ca<sup>2+</sup> may activate phospholipase A<sub>2</sub> and cause production of lysolipids and fatty acids. In addition, ionic fluxes across the membrane occur, leading to pH changes and membrane depolarization. It is not clear how these other responses are initiated, but there may be direct G-protein links to effector systems such as phospholipase A<sub>2</sub> or ionic channels.

We will first summarize the fluorescence and spectroscopic assays that have been developed for the fluorometer and then describe their applications using flow cytometry. We will summarize research which exemplifies the utility of simultaneous measurement of responses and shows how these methods have provided information about the signal transduction pathways and activation in neutrophils. Lastly, we will describe how these methods have been used to characterize the effects of hexachlorocyclohexanes on neutrophil functions. Although we are limiting this to a discussion of neutrophils, these approaches are completely generalizable to other cell types and have already been applied to some. We hope this summary will be useful to workers who wish to extend these techniques to the cell systems of interest to them.

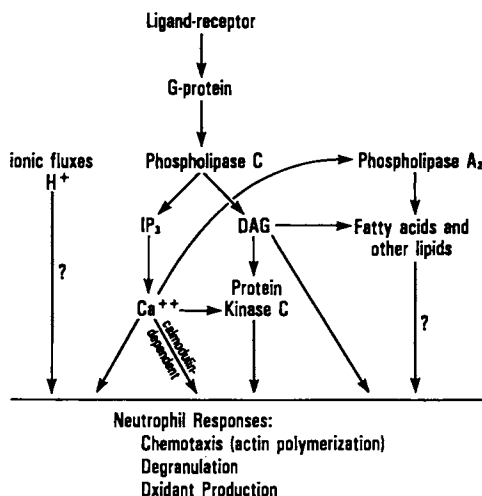


Figure 1. Simplified schematic of receptor-mediated signal transduction in neutrophils. Binding of ligand to the receptor activates a guanine-nucleotide-binding protein (G protein), which then stimulates phospholipase C. Phosphatidylinositol 4,5-bisphosphate is cleaved to produce diacylglycerol (DAG) and inositol 1,4,5-trisphosphate (IP<sub>3</sub>). DAG stimulates protein kinase C. IP<sub>3</sub> causes the release of Ca<sup>2+</sup> from intracellular stores, which results in an increase in the cytosolic Ca<sup>2+</sup> concentration. This increase in Ca<sup>2+</sup> may stimulate protein kinase C, calmodulin-dependent protein kinases, and phospholipase A<sub>2</sub>. Protein phosphorylation events are thought to be important in stimulating degranulation and oxidant production. In addition, ionic fluxes occur across the plasma membrane. It is possible that phospholipase A<sub>2</sub> and ionic channels may be governed by G protein interactions.

### Spectrofluorometric Assays

Table I describes several of the fluorescent assays that have been used in our lab to study neutrophil activation. Fluorescein-labeled *N*-formylhexapeptide (FLPEP) has been used to characterize the kinetics of ligand binding, dissociation, and internalization at 37°C (7,8). FLPEP is added to a suspension of cells, then receptor-bound and free FLPEP in solution are distinguished by adding antibody to fluorescein. This is a high-affinity antibody which binds free FLPEP within 1 s but does not bind cell-bound FLPEP. When it binds the FLPEP, it quenches the fluorescein fluorescence. Hence the residual fluorescence after antibody addition represents FLPEP that is bound to the cell. Nonspecific binding is determined in cell suspensions that contain an excess of nonfluorescent peptide. Kinetic data for total and nonspecific binding are subtracted to give the specific amount bound at the time of antibody addition, and the slow decline in fluorescence intensity thereafter reflects dissociation of bound peptide (also see Ref. 8 for more details).

Oxidant production is measured with the fluorogenic substrate *para*-hydroxyphenylacetic acid (PHPA) in the presence of superoxide dismutase and peroxidase (9). Under these conditions, superoxide is converted to H<sub>2</sub>O<sub>2</sub> by the superoxide dismutase, and two molecules of PHPA are converted to a fluorescent diadduct by H<sub>2</sub>O<sub>2</sub> and peroxidase. Similar assays have been devised using homovanillic acid (16) or scopoletin (17) instead of PHPA.

Membrane depolarization can be measured by members of a class of fluorophores (commonly referred to as the carbocyanine dyes) which have been designed to partition into the membrane, where their orientation and spectral properties change with changes in the electrochemical gradient across the membrane (18). 3,3'-dipropylthiodicarbocyanine [diS-C<sub>3</sub>-(5)] (Refs. 10, 11) and 3,3'-dipentylloxycarbocyanine [di-O-C<sub>5</sub>-(3)] (Refs. 19,20) have been useful in studying membrane potential changes in neutrophils.

Elastase release from dense granules is monitored with a non-fluorescent substrate containing a coumarin derivative. When the substrate is cleaved, fluorescent aminomethylcoumarin is released. The rate of aminomethylcoumarin production is proportional to the amount of elastase released (12).

Fluorescein absorbance is sensitive to pH. This property is utilized to measure cytosolic pH changes. Fluorescein derivatives that contain esters on the carboxyl groups have been constructed. These compounds partition through the cell membrane and, once inside the cell, the esters are cleaved by nonspecific esterases in the cytosol, leaving free carboxyl groups; thus the probe cannot diffuse out of the cell (or at least does so slowly). Commonly used derivatives are 6-carboxyfluorescein (21-23) and the more recently developed probe 2',7'-bis(2-carboxyethyl)-5-(and-6)-carboxyfluorescein (13, 24,25).

Intracellular calcium elevation is monitored by fluorescent chelators developed by Tsien and coworkers. These indicators are loaded into cells the same way the pH indicators are. With Quin-2 (14), one of the first such probes developed, the quantum yield increases about fourfold when Ca<sup>2+</sup> binds to it. The second generation of Ca<sup>2+</sup> probes, Indo-1 and Fura-2 (15), are now being widely used in a variety of cell types. These probes are in most cases

Table I. Fluorescence Assays of Neutrophil Functions

Function	Fluorophore	Wavelength (nm)		Filters	Ref.
		Excitation	Emission		
Binding of formylpeptide.	Fluorescein-labeled <i>N</i> -formylhexapeptide.	490	520	Corion 5200 bandpass, Corning 3-70.	(7)
Oxidant production.	2,2'-Dihydroxybiphenyl-5,5'-diacetate.	340	400	Corning 3-73	(9)
Membrane depolarization.	3,3'-Dipropylthiodicarbocyanine.	610	>620	Corning 2-59	(10, 11)
Elastase release	Aminomethylcoumarin	380	460	Corion 4900 bandpass	(12)
Intracellular pH	2',7'-bis-(2-carboxyethyl)-5-(and-6)-carboxyfluorescein.	490	520	Corion 5200 bandpass, Corning 3-70.	(13)
Intracellular calcium.	Quin 2	340	490	Corion 4900 bandpass	(14)
	Indo-1	340	400, 490	Corion 4900 bandpass	(15)

preferable to Quin-2, since they have lower  $\text{Ca}^{2+}$  buffering capacities and higher quantum yields. Indo-1 shows spectral shifts when  $\text{Ca}^{2+}$  binds to it.  $\text{Ca}^{2+}$ -bound Indo-1 has an emission peak at  $\sim 400$  nm, and free Indo-1 has a peak at  $\sim 490$  nm. This assay is benefited by the ability to measure emission at two different wavelengths. Intracellular free  $\text{Ca}^{2+}$  can be quantified by taking the ratio of intensities ( $F_{400}/F_{490}$ ) and comparing it with a standard curve of Indo-1 in solution that has been titrated with known amounts of  $\text{Ca}^{2+}$ . Fura-2 can also be used as a calcium indicator, but it requires dual excitation. Several instruments that have been designed for dual excitation and emission to use with these probes are now commercially available.

### Spectroscopic Assays

In addition to the fluorescence assays there are light-scattering and transmittance assays which are typically performed on the fluorometer (Table II). A transient right-angle light-scatter response in the absence of cytochalasins was initially reported by Yuli and Snyderman (26). We have shown that this right-angle light-scatter response correlates with actin polymerization in the neutrophils and hence is correlated with cytoskeletal activation (27).

In the presence of cytochalasins (cytoskeletal disruptors) the actin polymerization is inhibited, but degranulation is enhanced. Under these conditions, the right-angle light scatter reflects this degranulation (28). This has been demonstrated by simultaneous measurements of right-angle light scatter and elastase release using the aminomethylcoumarin assay (in the presence of cytochalasin B) (28).

Transmittance can be used to monitor aggregation. As the cells aggregate, there are fewer total particles to scatter light and, hence, more light is transmitted. This is the same principle behind aggregometers. We monitor this transmittance change on the SLM fluorometer (28).

In the presence of cytochrome C, changes in transmittance at 550 nm reflect oxidant production as superoxide reduces the cytochrome C. This is usually done as an absorbance assay in a spectrophotometer, but it can be performed as a transmittance assay on the SLM fluorometer (10).

Table II. Spectroscopic Assays of Neutrophil Functions

Function	Parameter Measured	Wave-length <sup>a</sup>	Ref.
Actin polymerization (without cytochalasin B present).	Right-angle light scatter.	Any	(26-28)
Degranulation (in presence of cytochalasin B).	Right-angle light scatter.	Any	(28)
Aggregation -----	Transmittance <sup>b</sup> ---	Any	(28,29)
Oxidant production -----	Transmittance <sup>b</sup> --	550 nm	(10)

<sup>a</sup>Emission is read at same wavelength as excitation in all tests.

<sup>b</sup>Transmittance through cytochrome C decreases as released superoxide reduces the cytochrome C.

### *Fluorometer Configuration*

Figure 2 shows a schematic of the SLM 8000 fluorometer. This is essentially a first-generation multiphototube fluorometer which we have adapted for use in these measurements. A number of second-generation instruments that are now commercially available were developed specifically for the purpose of providing dual excitation and/or emission for use with the calcium probes. On our instrument, excitation is through a single monochromator. Light coming from the sample or through it is detected by photomultiplier tubes (PMTs) in as many as four different positions. Transmittance measurements detect the light that comes straight through the sample to position D. At a right angle to the excitation light is position A, which detects light through the emission monochromator on the left side of the instrument. On the right side is a custom-made beam splitter box, which allows light to pass through filters to PMT B and shunts light through different filters to PMT C. We frequently use PMT A and PMT B for monitoring fluorescence and PMT C for right-angle light scatter. The SLM microprocessor can monitor three channels at once. So, we can monitor as many as three different responses at the same time on a single sample.

### *Assays by Flow Cytometry*

Many of these assays have a counterpart in flow cytometry. Figure 3 is a schematic showing the basic principles of flow cytometry. Cells flow in single file from a nozzle, and a laser excitation beam is focused on that stream. PMTs are placed to measure forward light scatter, fluorescence, and side scatter. The intensity is measured for each cell as it comes through the beam. Of the assays listed in Table I, those in which the cell is labeled directly with a fluorophore can be used in flow cytometric assays: FLPEP binding (7), membrane depolarization and intracellular  $\text{Ca}^{2+}$  (30), and intracellular pH. Actin polymerization and degranulation can be measured by right-angle light scatter (28). Oxidant production cannot be measured by the PHPA assay, but methods for measuring oxidants produced inside the cell have been developed for flow cytometry. For example, Bass et al. (31) measured oxidant production using intracellularly trapped nonfluorescent 2',7'-dichlorofluorescein, which becomes oxidized to form fluorescent 2',7'-dichlorofluorescein. Aggregation can be measured in flow because the forward- and side-scatter parameters also distinguish singlets from doublets and triplets and so on.

Another very useful flow cytometric assay is an actin polymerization assay (32). Cells are stimulated, and aliquots of the cells are removed, fixed, and stained with a fluorescent phalloidin or phalloidin- $\alpha$  mushroom toxin which binds specifically to filamentous actin (F-actin). Fluorescence of the bound probe is then quantified in the flow cytometer. The histograms in Figure 4 show that three parameters are measured simultaneously. The cytometer measures rhodamine fluorescence (in this case rhodamine-phalloidin was used), forward light scatter, and side scatter (or right-angle light scatter). Forward scatter is sensitive to particle size and side scatter is sensitive to particle granularity. Thus, cell aggregates can be detected because their forward- and side-scatter intensities

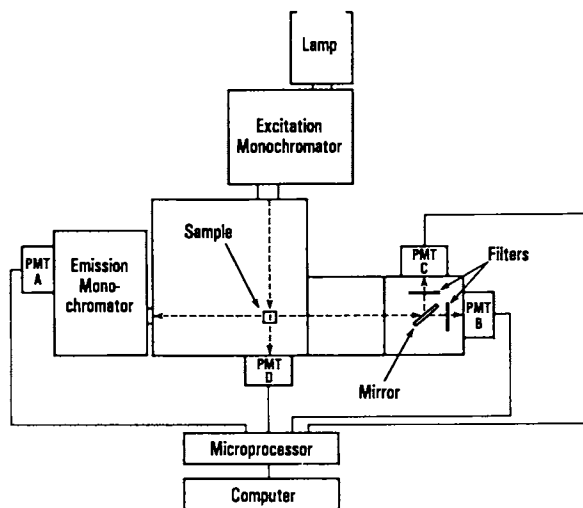


Figure 2. Schematic of the SLM 8000 fluorometer. Excitation occurs through the excitation monochromator, and light emitted from the sample is observed in as many as four different positions. Photomultiplier tubes (PMTs) A, B, and C can be used to monitor fluorescence or right-angle light scatter through the monochromator (PMT A) or through filters (PMT B and C), and position D measures transmittance. Three channels can be monitored simultaneously with measurements being acquired at intervals of 1 s or less. The data are stored by the computer for subsequent manipulation.



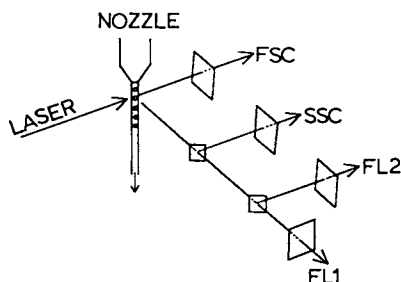


Figure 3. Schematic of cell analysis by flow cytometry. Cells flow in a stream from a nozzle in single file and are illuminated as they pass through a laser beam which is focused on the stream. Fluorescence and side-scatter light is detected at right angles to the excitation beam using dichroic mirrors to shunt light through side filters which select fluorescence emission (FL1 and FL2) and side-scattered (SSC) wavelengths. Forward light scatter (FSC) is also detected. All parameters are collected and correlated for each particle as it passes through the beam.

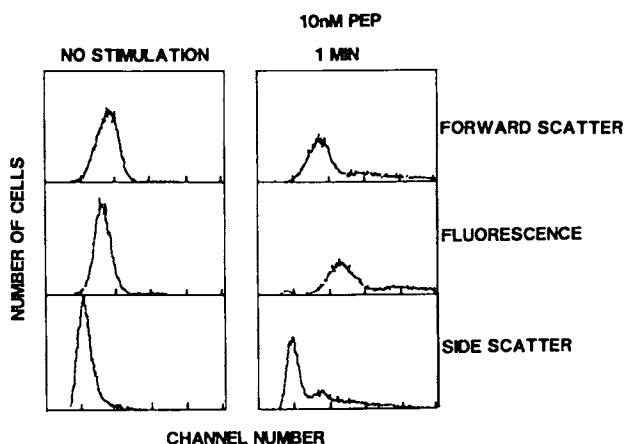


Figure 4. Flow-cytometric histograms for fixed, rhodamine-phalloidin stained neutrophils that are unstimulated or stimulated with 10 nM *N*-formylhexapeptide for 1 min. 10,000 particles were observed and forward scatter, rhodamine fluorescence, and side scatter measured for each particle. The light intensity scale is divided into 256 channels (channel number) on the  $x$ -axis, and the number of particles within a given channel are plotted on the  $y$ -axis. Measurement of a homogeneous (singlet) population of cells (left panel, unstimulated cells) results in a Gaussian distribution, and the average intensity for a large number of cells is calculated as the mean channel number of the histograms. After 1 min of stimulation (right panel), aggregation has occurred, the number of cells that appear as singlets has decreased, and the distribution has been skewed to greater intensities due to doublets, triplets, etc.

are greater than those of singlets. This can be seen in Figure 4, where stimulated cells show a significant number of particles with side-scatter and forward-scatter intensities that are 2-3 times greater than for the singlet population. The average intensity of a large number of cells (in this case, 10,000 particles) is calculated as the mean channel number of each histogram after gating out the aggregates.

We perform spectrofluorometric and cytometric assays in a pseudosimultaneous manner: The live cells are stirred in a cuvette in the fluorometer, and right-angle light scatter is observed during stimulation; aliquots for the F-actin assay are removed and rapidly fixed at various intervals during the time course of stimulation. Using 340-nm excitation, we can leave the cover off the sample chamber of the fluorometer since ambient light contains relatively little light at 340 nm. Measurements performed in this manner gave an excellent inverse correspondence: the increase in concentration of polymerized actin was matched in relative magnitude and in time by the decrease in right-angle light scatter measured on the fluorometer (Figure 5A; Refs. 3,27). To verify that the fixing procedure was indeed rapid, right-angle light scatter on the fluorometer (live cells) was compared with the side scatter measured on the fixed cells by flow cytometry (27), and, as is seen in Figure 5B, the two measurements were in excellent agreement.

In addition, one can quantify the relative number of particles that exist as singlets (Figure 4). A drop in the percentage of singlets means an increase in the aggregation. Figure 6 shows the pseudosimultaneous measurement of right-angle light scatter on the fluorometer, F-actin, and the percentage of singlets. We note that when binding of formylpeptide to new receptors is blocked by adding a receptor antagonist, the right-angle light scatter and actin polymerization rapidly recover. In addition, disaggregation occurs, but only begins after the actin has depolymerized nearly to resting levels. This suggests that actin polymerization may be related to aggregation, perhaps by exposing or reorganizing adhesion molecules at the membrane surface. We are continuing to study this phenomenon.

#### *Examples of Simultaneous Measurements*

Figure 7 shows simultaneous measurement of degranulation by right-angle light scatter and  $\text{Ca}^{2+}$  detected by Indo-1, which requires two fluorescence channels. The right-angle light-scatter assay for degranulation (in the presence of cytochalasin B) is essential because it would be impossible to combine the fluorescent amino-methylcoumarine assay and the Indo-1 assay. There is relatively good correlation between the maximum  $\text{Ca}^{2+}$  elevation and the final amount of degranulation. But it is interesting to note that there is not a direct correlation in time, i.e., the maximum  $\text{Ca}^{2+}$  level is reached well before maximum degranulation.

Figure 8 shows the simultaneous measurement of  $\text{Ca}^{2+}$  as determined by Quin-2 and oxidant production measured by PHPA (33). Quin-2 and PHPA are the only combination we have found that allows us to look at  $\text{Ca}^{2+}$  and oxidant production simultaneously. For this experiment, Quin-2 is detected at 490 nm through a bandpass filter and PHPA is monitored at 400 nm through the monochromator. Under

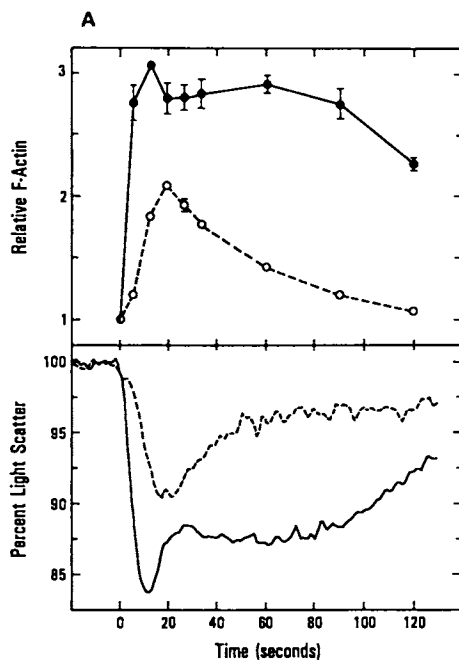


Figure 5A. Correlation of right-angle light scatter with actin polymerization. The top panel shows flow-cytometric data for relative F-actin polymerization measured as rhodamine-phalloidin binding to fixed, stained cells during the time course of stimulation by 1-nM (solid line, solid circles) or 0.01-nM (dashed line, open circle) FLPEP. The bottom panel shows the corresponding right-angle light-scatter data acquired pseudosimultaneously on live cells in the fluorometer. The data are averaged for duplicate determinations from one donor. Reproduced with permission from Ref. 3. Copyright 1987 American Physiological Society.

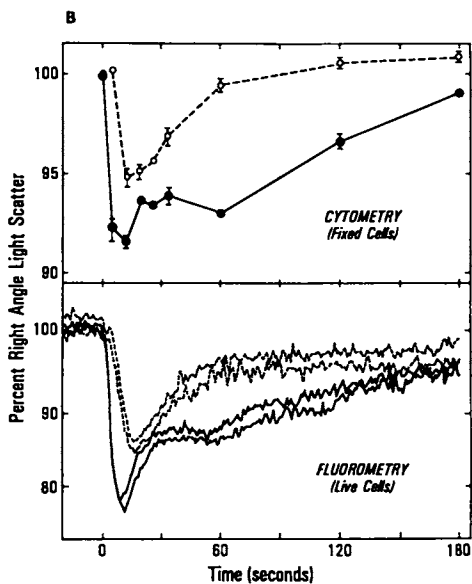


Figure 5B. Correlation of right-angle light scatter measured by fluorometry and flow cytometry. The top panel shows flow-cytometric data of side scatter of fixed, stained cells during the time course of stimulation by 1-nM (solid line, solid circles) or 0.01-nM (dashed line, open circle) FLPEP. The bottom panel shows the corresponding right-angle light-scatter data acquired pseudo-simultaneously on live cells in the fluorometer. The flow-cytometric data have been averaged, but the fluorometry data are plotted for both duplicates from one donor. Reproduced with permission from Ref. 27. Copyright 1985 Rockefeller University Press.

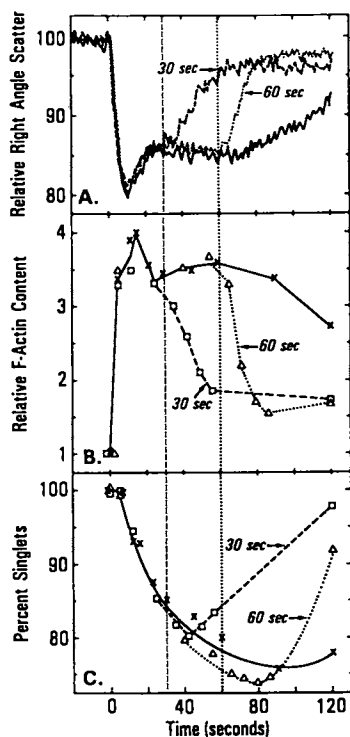


Figure 6. Pseudosimultaneous measurement of right-angle light scatter, relative F-actin, and aggregation. A. Right-angle light scatter measured on live cells in the fluorometer. B. Relative F-actin content measured as rhodamine-phalloidin binding to fixed stained cells. C. Aggregation measured (for fixed stained cells) as a decrease in the percent of particles that are singlets. Cells were stimulated with 1-nM FLPEP (solid line, X) or stimulated with 1-nM FLPEP followed by addition of  $10^{-5}$  M receptor antagonist tert-butoxycarbonyl-phenylalanyl-leucyl-phenylalanyl-leucylphenylalanine (tBOC) at 30 s (dashed line,  $\square$ ) or at 60 s (dotted line,  $\Delta$ ). The vertical dashed and dotted lines indicate 30 and 60 s after stimulus addition. Revised and reproduced with permission from Ref. 27. Copyright 1985 Rockefeller University Press.

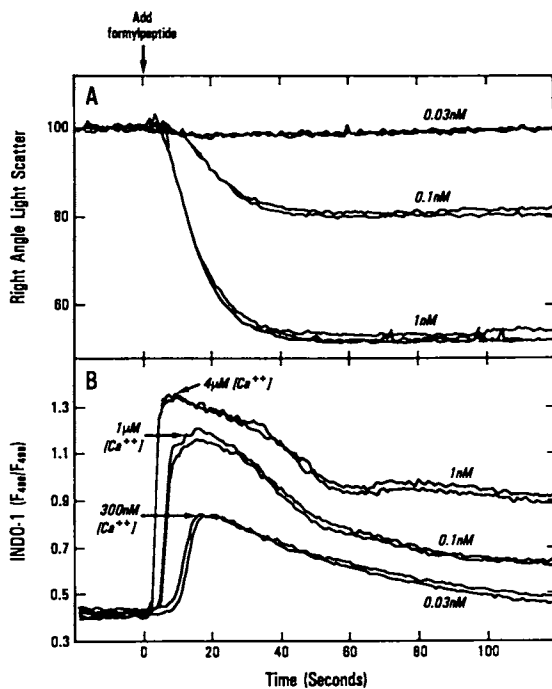


Figure 7. Neutrophil degranulation (A) and Indo-1-detected cytosolic  $\text{Ca}^{2+}$  responses (B) in the presence of cytochalasin B. Cells were labeled with Indo-1, degranulation was measured as right-angle light scatter, and the Indo-1-detected  $\text{Ca}^{2+}$  response was measured as the ratio of fluorescence at 400 nm to that at 490 nm. FLPEP concentrations were 1, 0.1, and 0.03 nM as indicated. Maximal cytosolic calcium concentrations were approximately 4  $\mu\text{M}$  (for 1-nM FLPEP), 1  $\mu\text{M}$  (for 0.1-nM FLPEP), and 300 nM (for 0.03-nM FLPEP). Resting cytosolic  $\text{Ca}^{2+}$  was approximately 60 nM.

these conditions, there is some crossover of PHPA fluorescence into the Quin-2 channel, but this can be subtracted out by computer (9). In this experiment FLPEP is the stimulus. When occupancy of new receptors is blocked by the addition of a formylpeptide receptor antagonist 30 s after stimulation (dashed line, Figure 8), the intracellular  $\text{Ca}^{2+}$  remains elevated for  $\sim 10$  s, but then decays rapidly. The oxidant production rapidly plateaus. The first derivative of these data represent the time course of activation then turn-off of the NADPH oxidase system. The fact that  $\text{Ca}^{2+}$  and oxidant production decay in concert may indicate that these events are linked in formylpeptide-stimulated cells.

Hence, pseudosimultaneous spectroscopic and flow-cytometric measurements suggest that actin polymerization may be functionally related to aggregation, possibly by reorganization of adhesive molecules on the cell surface. Simultaneous spectroscopic and fluorometric measurements suggest that the signal  $\text{Ca}^{2+}$  may be related to oxidant production and degranulation.

#### *Binding Data and Functional Data*

FLPEP binding data and functional assays have been combined to relate function to receptor occupancy. Using the fluorometric binding assays listed in Table I and flow-cytometric methods (34), the apparent on and off rate constants for FLPEP binding at  $37^\circ\text{C}$  have been determined (7). Using these constants, we can estimate the number of receptors bound for any ligand concentration at any time during the course of binding. In addition, binding can be stopped at any time after addition of FLPEP by adding antiluorescein antibody or antagonist.

Knowledge of the receptor binding characteristics has been combined with functional data to determine how many receptors are required to initiate responses (29). A study of oxidant production in which the number of receptors occupied was limited by adding antiluorescein antibody at various times after adding FLPEP showed that  $\sim 30\%$  receptor occupancy was required to elicit half-maximal oxidant production (29). However, when actin-associated right-angle light scatter was studied, it was shown that half-maximal response requires less than 0.1% receptor occupancy; approximately 10-20 receptors out of a total 60,000 were required to initiate half-maximal response (29). Thus combining receptor occupancy and functional data shows that distinct responses have distinct receptor occupancy requirements. Since receptors are coupled to cell responses via branching pathways (Figure 1), it may be that the biochemical events along the branching paths that lead to distinct cell responses are saturated by different numbers of occupied receptors.

#### *Effects of Hexachlorocyclohexanes on Neutrophil Function*

There are several isomers of 1,2,3,4,5,6-hexachlorocyclohexane (HCH). The  $\gamma$  isomer is insecticidally active, whereas most of the others are relatively inactive. These compounds have been shown to activate inflammatory functions of neutrophils (35,36). Using Indo-1, we have characterized intracellular  $\text{Ca}^{2+}$  mobilization in response to these compounds. Figure 9 shows the responses of cells labeled with Indo-1 to stimulation by  $\gamma$ -,  $\alpha$ -,  $\beta$ -, and  $\delta$ -HCH at a concentration of  $260 \mu\text{M}$ .

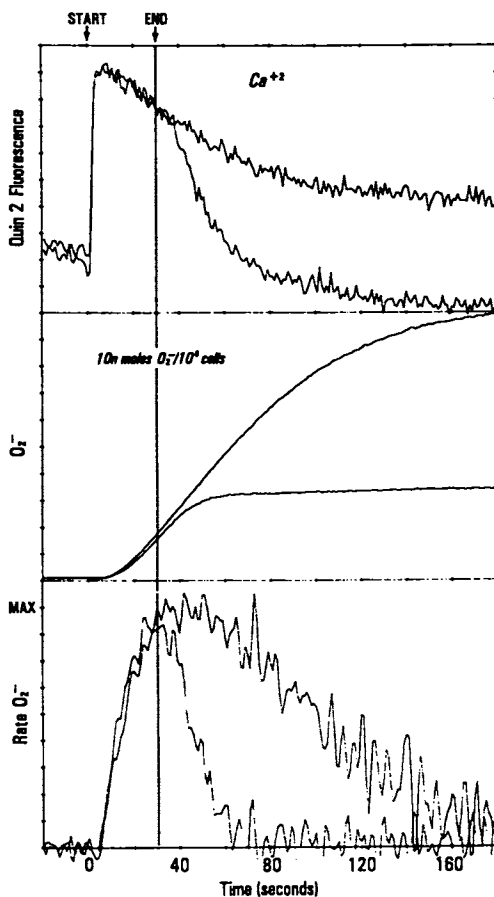


Figure 8. Simultaneous measurement of intracellular  $\text{Ca}^{2+}$  and oxidant production in neutrophils. Cells were labeled with Quin-2 and suspended at  $2 \times 10^6$  cells/mL buffer. At time zero, 1 nM FLPEP was added (upper trace in each panel). In addition, the receptor blocker tBOC was added ( $3 \times 10^{-6}\text{M}$ ) after 30 s to stop further binding of the stimulus (lower trace in each panel). The excitation wavelength was 340 nm. Top panel: Quin-2 fluorescence determined on channel B (of Figure 1) using a Corion 490-nm interference filter. The crossover from the superoxide assay has been subtracted. Middle panel: Oxidant production (superoxide equivalents) determined by the *para*-hydroxyphenylacetate assay. Fluorescence was observed at 400 nm (on channel A of Figure 1). Bottom panel: The rate of oxidant production was calculated as the first derivative of the data in the middle panel. Reproduced with permission from Ref. 33. Copyright 1985 Eaton Publishing Company.



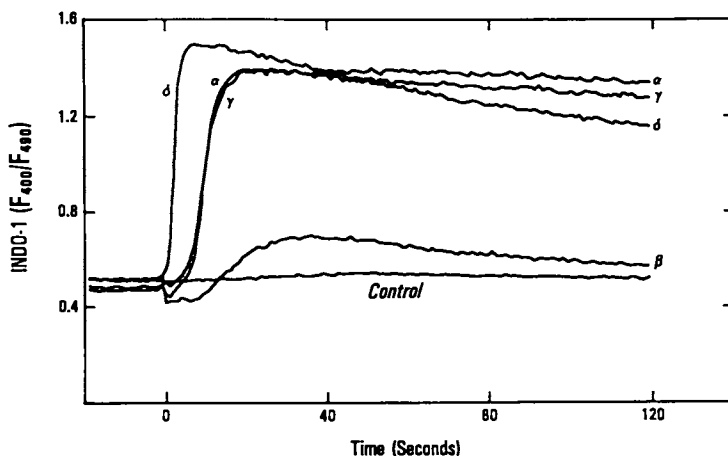


Figure 9. Increase of intracellular  $\text{Ca}^{2+}$  stimulated by various HCH isomers. Cells were labeled with Indo-1 and suspended at  $2 \times 10^6$  cells/mL buffer at  $37^\circ\text{C}$ . The HCH isomers were dissolved in DMSO and added to the cell suspensions such that the final HCH concentration was  $260 \mu\text{M}$  and the final DMSO concentration was 0.25% (v/v). The various isomers are indicated in the plot. The control is DMSO alone. The data are plotted as the ratio of fluorescence at 400 nm (measured on channel A) to that at 490 nm (measured through a Corion 490-nm interference filter on channel B).

The increase in  $\text{Ca}^{2+}$  is initiated rapidly and begins to recover after 1 min. The order of potency correlates fairly well with the solubilities of these compounds in organic solvents (37) and their abilities to accumulate in phospholipid vesicles (38), i.e.,  $\delta > \gamma > \alpha > \beta$ , but not with their insecticidal activity ( $\gamma \gg \delta > \alpha \gg \beta$ ; 39). At these concentrations, crystals of  $\beta$ -,  $\alpha$ -, and  $\gamma$ -HCH were evident in the cell suspensions when we made simultaneous measurements of the right-angle light scatter, indicating that the order of aqueous solubilities is  $\delta > \gamma > \alpha > \beta$ . However, stimulation by  $\delta$ -HCH at concentrations below its aqueous solubility limit shows a typical dose dependency of the response (Figure 10).

Figure 11 depicts two characteristics of the Indo-1-detected calcium response. The intracellular  $\text{Ca}^{2+}$  rise is primarily from intracellular stores because adding EGTA to chelate extracellular  $\text{Ca}^{2+}$  does not inhibit the response (Figure 11, upper panel). Secondly, treatment of neutrophils with pertussis toxin, which ADP-ribosylates a neutrophil G protein and causes a loss of cell responsiveness via receptor-mediated pathways (40,41), has minimal effect on the response to HCH (Figure 11, lower panel). Thus it can be concluded that HCH activation of neutrophils is independent of receptor-mediated activation of G proteins.

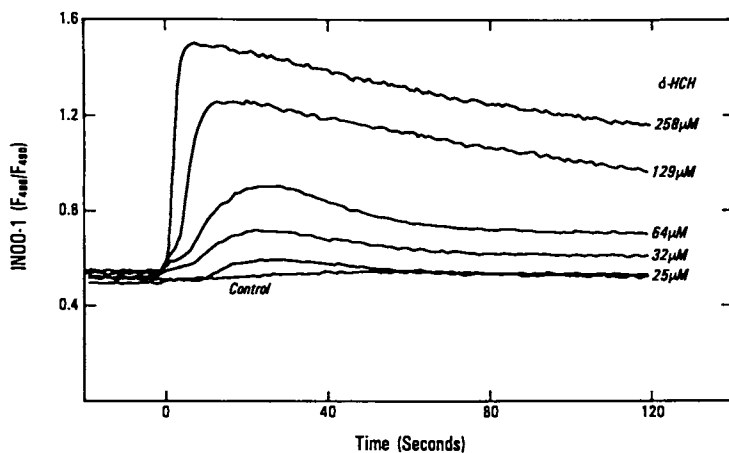


Figure 10. Dose-response curves for  $\delta$ -HCH stimulation of cytosolic  $\text{Ca}^{2+}$  increases measured in Indo-1-labeled cells. Experimental conditions are as in Figure 9.

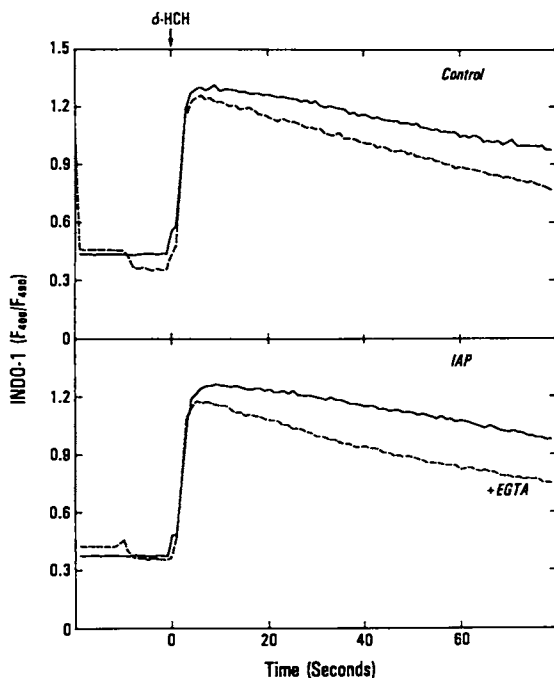


Figure 11. Effects of EGTA or treatment with islet activating protein (IAP or pertussis toxin) on the  $\delta$ -HCH-induced  $\text{Ca}^{2+}$  response detected in Indo-1-labeled cells. Cells were treated for 2 hours at  $37^\circ\text{C}$  with (IAP) or without (Control)  $10\ \mu\text{g}/\text{mL}$  IAP, then labeled with Indo-1. Cells were washed and resuspended at  $2 \times 10^6$  cells/mL buffer and stimulated with  $\delta$ -HCH (solid trace). In some cases (dashed traces), stimulation was preceded by the addition of  $5\text{-mM}$  EGTA 10 s before stimulation. Other experimental conditions are as in Figure 9.

**Summary**

We have described several fluorescence and spectroscopic assays for studying neutrophil activation. These types of assays can be used for a variety of cell types. These methods have the advantages of sensitivity, good time resolution, and the ability to measure responses simultaneously. We have used these methods to show (1) the relationship of  $\text{Ca}^{2+}$  to oxidant production and degranulation, (2) the relationships among aggregation and actin polymerization, and (3) the differential regulation of responses such as actin polymerization and oxidant production in terms of the number of receptors required to stimulate the response. These latter results may indicate that there is a unique pathway for regulation of actin polymerization. HCH activation of neutrophils is shown to be independent of receptor-G-protein coupling. Hence, HCH may be directly affecting G proteins or enzymes involved in phosphoinositide metabolism. This latter hypothesis is consistent with recent studies which show that HCHs inhibit several enzymes involved in phosphoinositide catabolism (42).

**Acknowledgments**

We thank Zenaida Oades and William Swann for excellent technical assistance. This work was supported by NIH grants AI17354, AI19032, AI22690, and RR00833. L.A.S is an Established Investigator of the American Heart Association. This is publication # 4944IMM from the Research Institute of Scripps Clinic.

**APPENDIX--Abbreviations used in this report**

C5a--Activated fifth component of complement.	IAP--Islet-activating protein or pertussis toxin.
DAG--Diacylglycerol.	IP <sub>3</sub> --Inositol trisphosphate.
DMSO--Dimethylsulfoxide.	NADPH-- $\beta$ -Nicotinamide adenine-dinucleotide phosphate, reduced form.
EGTA--Ethylene glycol bis(2-aminoethyl ether)- <i>N,N,N',N'</i> -tetraacetic acid.	PEP-- <i>N</i> -Formylhexapeptide or <i>N</i> -formyl-norleucyl-leucyl-phenylalanyl-norleucyl-tyrosyl-lysine.
F-actin--Filamentous actin.	PHPA-- <i>para</i> -Hydroxyphenylacetic acid.
FLPEP--Fluoresceinated <i>N</i> -formyl-norleucyl-leucyl-phenylalanyl-norleucyl-tyrosyl-lysine.	PMT--Photomultiplier tube.
FSC--Forward scatter.	SSC--Side scatter.
G protein--Guanine-nucleotide-binding protein.	tBOC--Tert-butoxy-carbonyl-phenylalanyl-leucyl-phenylalanyl-leucyl-phenylalanine.
HCH--1,2,3,4,5,6-hexachlorocyclohexane.	

**ADDENDUM**

The calcium indicator Fura2, which has not been discussed in detail in this manuscript, has been widely used as an intracellular calcium indicator (see Ref. 15 and also Cobbold, P.H.; Rink, T.J. *Biochem. J.* 1987, **248**, 313-328.

This probe utilizes dual excitation wavelengths and is observed at a single emission wavelength. The intracellular calcium probes Fluo3 and Rhod2, which have recently been introduced, have fluorescein-like and rhodamine-like spectral properties, respectively (Minta, A.; Harootunian, A.T.; Kao, J.P.Y.; Tsien, R.J. *J. Cell Biol* 1987, 105, 89a). These probes may be preferable for studies where long-wavelength excitation is desirable.

#### Literature Cited

1. Berkow, R. L.; Tzeng, D. Y.; Williams, L. V.; Baehner, R. L. *J. Lab. Clin. Med.* 1983, 102, 732-742.
2. Tolley, J. O.; Omann, G. M.; Jesaitis, A. J. *J. Leukocyte Biol.* 1987, 42, 43-50.
3. Omann, G. M.; Allen, R. A.; Bokoch, G. M.; Painter, R. G.; Traynor, A. E.; Sklar, L. A. *Physiol. Rev.* 1987, 67, 285-322.
4. Sklar, L. A. *Adv. Immunol.* 1986, 39, 95-143.
5. Olsson, I.; Venge, P. *Allergy* 1980, 35, 1-13.
6. Rossi, F. *Biochim. Biophys. Acta* 1986, 853, 65-89.
7. Sklar, L. A.; Finney, D. A.; Oades, Z. G.; Jesaitis, A. J.; Painter, R. G.; Cochrane, C. G. *J. Biol. Chem.* 1984, 259, 5661-5669.
8. Sklar, L. A. *Annu. Rev. Biophys. Biophys. Chem.* 1987, 16, 479-506.
9. Hyslop, P. A.; Sklar, L. A. *Anal. Biochem.* 1984, 141, 280-286.
10. Sklar, L. A.; Jesaitis, A. J.; Painter, R. G.; Cochrane, C. G. *J. Biol. Chem.* 1981, 256, 9909.
11. Whitin, J. C.; Chapman, C. E.; Simons, E. R.; Chovaniec, M. E.; Cohen, H. J. *J. Biol. Chem.* 1980, 255, 1874-1878.
12. Sklar, L. A.; McNeil, V. M.; Jesaitis, A. J.; Painter, R. G.; Cochrane, C. G. *J. Biol. Chem.* 1982, 257, 5471-5475.
13. Rink, T. J.; Tsien, R. Y.; Pozzan, T. *J. Cell Biol.* 1982, 95, 189-196.
14. Tsien, R. Y.; Pozzan, T.; Rink, T. J. *J. Cell Biol.* 1982, 94, 325-334.
15. Grynkiewicz, G.; Poenie, M.; Tsien, R. Y. *J. Biol. Chem.* 1985, 260, 3440-3450.
16. Roos, D.; Voetman, A. A.; Meerhof, L. J. *J. Cell Biol.* 1983, 97, 368-377.
17. Root, R. K.; Metcalf, J.; Oshino, N.; Chance, B. *J. Clin. Invest.* 1975, 55, 945-955.
18. Waggoner, A. *J. Membr. Biol.* 1976, 27, 317-334.
19. Seligmann, B. E.; Gallin, E. K.; Martin, D. L.; Shain, W.; Gallin, J. I. *J. Membr. Biol.* 1980, 52, 257-272.
20. Seligmann, B. E.; Gallin, J. I. *J. Clin. Invest.* 1980, 66, 493-503.
21. Thomas, J. A.; Buchsbaum, R. N.; Zimniak, A.; Racker, E. *Biochemistry* 1979, 18, 2210-2218.
22. Simchowit, L.; Roos, A. *J. Gen. Physiol.* 1985, 85, 443-470.
23. Simchowit, L. *J. Biol. Chem.* 1985, 260, 13248-13255.
24. Grinstein, S.; Elder, B.; Furuya, W. *Am. J. Physiol.* 1985, 248, C379-C385.

25. Grinstein, S.; Furuya, W. *Biochem. Biophys. Res. Commun.* 1984, 122, 755-762.
26. Yuli, I.; Snyderman, R. *J. Clin. Invest.* 1984, 73, 1408-1417.
27. Sklar, L. A.; Omann, G. M.; Painter, R. G. *J. Cell Biol.* 1985, 101, 1161-1166.
28. Sklar, L. A.; Oades, Z. G.; Finney, D. A. *J. Immunol.* 1984, 133, 1483-1487.
29. Sklar, L. A.; Hyslop, P. A.; Oades, Z. G.; Omann, G. M.; Jesaitis, A. J.; Painter, R. G.; Cochrane, C. G. *J. Biol. Chem.* 1985, 260, 11461-11467.
30. Lazzari, K. G.; Proto, P. J.; Simons, E. R. *J. Biol. Chem.* 1986, 261, 9710-9713.
31. Bass, D. A.; Parce, J. W.; DeChatelet, L. R.; Szejda, P.; Seeds, M. C.; Thomas, M. J. *Immunol.* 1983, 130, 1910-1917.
32. Howard, T. H.; Meyer, W. H. *J. Cell Biol.* 1984, 98, 1265-1271.
33. Omann, G. M.; Oades, Z. G.; Sklar, L. A. *BioTechniques* 1985, 3, 508-512.
34. Sklar, L. A.; Muller, H.; Swann, W. N.; Comstock, C.; Omann, G. M.; Bokoch, G. M. This volume.
35. Kuhns, D. B.; Kaplan, S. S.; Basford, R. E. *Blood* 1986, 68, 535-540.
36. English, D.; Schell, M.; Siakotos, A.; Gabig, T. G. *J. Immunol.* 1986, 137, 283-290.
37. Slade, R. E. *Chem. Ind. (London)* 1945, 64, 314-319.
38. Omann, G. M.; Lakowicz, J. R. *Biochim. Biophys. Acta* 1982, 684, 83-95.
39. Brooks, G. T. *Chlorinated Insecticides, Vol. 2, Biological and Environmental Aspects*; CRC: Cleveland, OH, 1974.
40. Bokoch, G. M.; Gilman, A. G. *Cell* 1984, 39, 301-308.
41. Okajima, F.; Ui, M. *J. Biol. Chem.* 1984, 259, 13863-13871.
42. Parries, G. S.; Hokin-Neaverson, M. J. *Biol. Chem.* 1985, 260, 2687-2693.

RECEIVED August 30, 1988

## Chapter 3

# Fluorescence Methods for the Analysis of Nucleic Acids in Recombinant Biological Products

Walter W. Holl and R. Lee Webb

Analytical, Physical, and Structural Chemistry Department, L-950, Smith  
Kline Beckman Corporation, 1500 Spring Garden Street,  
Philadelphia, PA 19101

Regulatory agencies currently set stringent standards on the quantities of nucleic acids allowed in recombinant biological products. In the pharmaceutical industry these requirements necessitate the quantification of trace amounts of nucleic acids in the presence of large quantities of protein and other excipients. Fluorescence methods offer advantages for such analyses, but also have limitations. The use of a variety of fluorescent dyes and techniques is described here, and practical examples of such use are presented.

There is currently an explosion in the application of recombinant DNA methods to a host of important problems ranging from medicine to agriculture. (See for example the entire issue of *Science* June 1987, 236, devoted to recombinant nucleic acid techniques.) The pharmaceutical industry as an example is pressing to provide biopharmaceuticals derived from these applications. Regulatory authorities and the general public have expressed concerns over the levels of nucleic acids to which individuals might be exposed. They have set stringent levels on the amounts of nucleic acids which may be contained in pharmaceutical preparations (often at the picogram level). In addition, most of the first wave of biopharmaceuticals are proteins, which require extensive separation and purification after production by genetically engineered organisms. During these purification/separation steps the levels of nucleic acids need to be monitored.

Current analytical methods have difficulty detecting picogram levels of nucleic acids, particularly when high levels of other biopolymers (e.g., proteins) are present. The most widely used assay method employed by the pharmaceutical industry involves a nick translation DNA hybridization method (1). This assay offers high sensitivity and selectivity but has a number of drawbacks.

0097-6156/89/0383-0045\$06.00/0  
• 1989 American Chemical Society

Limitations encountered in routine use include (a) the use of radioactive materials, (b) limited sensitivity in the presence of high protein concentrations, (c) long assay time of up to 5 days, (d) semiquantitative detection methods, and (e) the inability to automate the current procedure. In practice the assay often fails to achieve the desired sensitivity level set by the FDA of 10 picograms per dose, particularly when the dosage form contains high concentrations of proteins or excipients, which can interfere with the assay.

Fluorescence methods for the detection of nucleic acids have been known for twenty years or so since the pioneering work of LePecq and others (2-4). Strongly fluorescent dyes whose fluorescence is enhanced upon binding to nucleic acids (such as ethidium bromide) have been used to quantitatively estimate nucleic acids. These fluorescence methods offer the potential for high sensitivity using nonradioactive reactants, and they are quick, quantitative, relatively simple, inexpensive, and amenable to automation. For these reasons we have begun a preliminary investigation of a variety of commercially available dyes using current instrumentation, to determine their relative merits in detecting trace levels of nucleic acids in recombinant products.

Figure 1 shows the dyes studied. All these dyes are readily available, except for the bisacridine derivative (obtained from Dr. D. P. Kelly, University of Melbourne) and the bis-(methidium)-spermine. Several of these have been used for the quantification of nucleic acids in solution (4-7).

The most commonly used dye in fluorescence studies on nucleic acids is ethidium bromide. The dye has broad excitation bands centered around 280 and 460 nm and a strong emission around 600 nm. When the dye binds to DNA by an intercalative mechanism, its emission is greatly enhanced and slightly shifted in wavelength. In the simplest case with ethidium bromide saturating intercalating sites,

$$I_1 - I_0 = Kc$$

where  $I_1$  is the fluorescence of ethidium bound to nucleic acid,

$I_0$  is the fluorescence of free ethidium,

$K$  is a constant, and

$c$  is the concentration of nucleic acid.

The theory and application of this fluorescence method have been discussed in detail by LePecq and others (3,8). The assay requires that there is sufficient ionic strength to minimize ionic binding (e.g., 0.1M sodium chloride), that the pH is 4-10, that no heavy metals are present, that the fluorescence is not enhanced on binding to other excipients (e.g., proteins) and that at least portions of the nucleic acids are not complexed. These requirements can usually be met when dealing with recombinant products; in some cases the samples must be manipulated to create the appropriate conditions. In the intercalative method of dye binding, proteins rarely interfere with the assay, and procedures have been developed to remove the few interferences they may cause (e.g., the use of heparin or enzymatic digestion of the protein; 9).



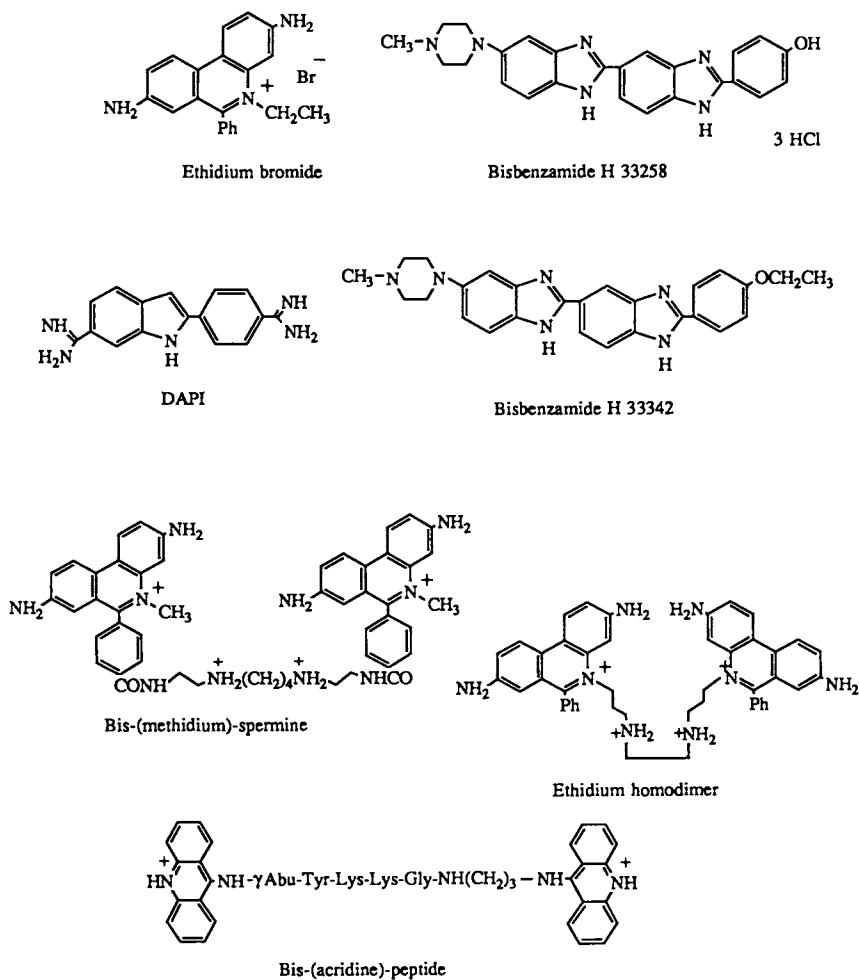


Figure 1. Dyes used for detection of nucleic acids by fluorescence.

**American Chemical Society  
Library**

1155 16th St., N.W.

In Connection with the American Chemical Society, Washington, D.C. 20036

ACS Symposium Series; American Chemical Society: Washington, DC, 1989.

The sensitivity of the fluorescence methods varies considerably with the instrument used. Advances in modern instrumentation and the power of today's computers allow for a much improved sensitivity. Using commercially available instruments and modern computers equipped with appropriate software, detection limits down to 10 pg of calf thymus DNA can be achieved using ethidium bromide. (We have achieved such levels using several Perkin-Elmer MPF66 instruments at various locations.)

It should be pointed out that when using ethidium bromide the sensitivity of the assays varies depending on the physical state of the nucleic acids (see Table I). Ethidium does not discriminate between RNA and DNA, although dyes are available which bind DNA exclusively, so the relative amounts of each may be determined by taking two sets of measurements. Alternatively, nucleases (DNA-ase or RNA-ase) can be used to exclusively remove one or the other in a mixture. Nucleic acids from different sources (see Table II) also show a variation in sensitivity, and the fluorescence assay lacks the selectivity of the hybridization technique. Nevertheless, for rapid screening or quality-control applications the fluorescence assay is still the method of choice.

Table I. Relative Fluorescence Intensities Obtained from Various Types of Nucleic Acids

Double-stranded DNA (calf thymus)	100
Single-stranded DNA	42
Heat-denatured DNA	55
Closed circular DNA	63
Ribosomal RNA (rat liver)	46

Table II. Relative Fluorescence Intensities Obtained Using DNA's from Various Sources

Calf thymus	100
Salmon testes	98
<i>Escherichia coli</i>	80
Human placenta	71

In current practice the fluorescence assay is often followed by the use of hybridization techniques when more selectivity is required. We have for instance used the fluorescence techniques to obtain data on the nucleic acid content of malaria vaccine proteins produced in *Escherichia coli*. The rapid turnaround time of the fluorescence assay is particularly useful during the early stages of purification to determine the optimal process conditions. After the final process has been arrived at and a variety of methods used to assess the nucleic acid content (including the hybridization techniques), the fluorescence method can be developed for routine quality-control purposes. In certain cases, particularly at high protein concentrations, the dye may bind to the protein with

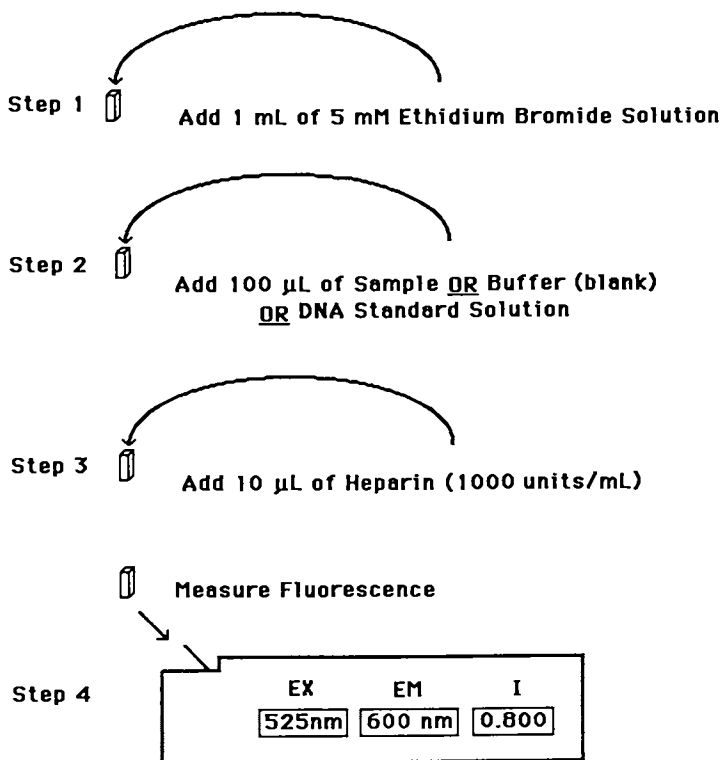
concomitant fluorescence changes. In these circumstances the binding can be overcome by the use of heparin or by digestion of the protein using proteolytic enzymes. Another source of interference experienced with the malaria sporozoite coat protein is strong binding of the protein to the DNA, preventing the dye from intercalating. Once again this is overcome by digestion of the protein, in this case with proteinase K.

A typical procedure is shown in Figure 2. Other dyes besides ethidium can be used, although ethidium has an advantage in that its excitation emission bands are well removed from any protein absorbances. A standard curve can be constructed for the nucleic acid of concern and the limits of detection established. In Step 3, proteolytic enzymes may be substituted for heparin, or the step may be bypassed in the case of proteins which do not interfere. After measurement of the unknown sample the nucleic acid concentration may be simply calculated or read from the standard curve.

The other dyes besides ethidium shown in Figure 1 have also been studied. The bisbenzamide (Hoechst) dyes (6) offer no improvement in detection limit over ethidium bromide, particularly when protein is present, because their excitation wavelength is close to the wavelengths of protein absorbances. The Hoechst dye 33258 has been used to determine adenine-thymine-rich regions in bacterial DNA (6), and its selectivity makes it useful for this purpose. DAPI suffers from the same drawbacks as ethidium in the presence of protein and gives no improvement in sensitivity, but it does show selectivity for DNA over RNA (5). Bis-(methidium)-spermine is not commercially available and was synthesized as outlined in reference 10 (with help from Professor P. B. Dervan and R. Hertzberg, which is gratefully acknowledged). This tightly binding dye gives enhanced sensitivity if the dye-to-DNA base pair ratio is adjusted appropriately (10). If the ratios are not correctly adjusted fluorescence quenching occurs. Since the DNA levels are usually unknown, complicated and time-consuming experimental procedures are required for a relatively small enhancement in sensitivity. Ethidium homodimer is commercially available (U.S. distributor, Molecular Probes, Inc., Eugene, Oregon), but it is relatively expensive. Under the correct conditions, detection limits slightly lower than those of ethidium can be obtained using this dye. The bisacridine peptide did not appear to offer an enhanced sensitivity over ethidium bromide, although dyes of this type may show selectivity for certain DNA sequences (11).

Care must be taken to ensure dyes are pure. The solid dyes are generally stable for prolonged periods (a year or more) when stored in the absence of light, heat, and moisture. Dilute solutions have much shorter lifetimes, particularly when exposed to heat and light, and stock solutions should be prepared frequently.

In order to further extend the utility of fluorescence methods the use of time-resolution methods, fluorescence polarization, and laser techniques should be explored. The addition of other dyes with enhanced fluorescence properties on binding and increased selectivity to various types of nucleic acids will be necessary to further develop more useful analytical methods.



step 5  $\text{Conc.} = \frac{(I_{\text{sample}} - I_{\text{blank}}) \times \text{Std conc.}}{(I_{\text{std}} - I_{\text{blank}})}$

Figure 2. Analytical procedure used for determining concentration of nucleic acids from fluorescence.

*Literature Cited*

1. Maniatis, T. *Molecular Cloning--A Laboratory Manual*; Cold Springs Harbor Laboratory: Cold Springs Harbor, NY; 1982, p. 324-325.
2. LePecq, J. B.; Paoletti, C. *Anal. Biochem.* 1966, *17*, 100.
3. LePecq, J. B. *Methods Biochem. Anal.* 1971, *20*, 57.
4. Karsten, U.; Wollenberger, A. *Anal. Biochem.* 1972, *46*, 135.
5. Kapuscinski, J.; Skoczylas, B. *Anal. Biochem.* 1977, *83*, 252.
6. Lutz, L. H.; Yayanos, A. A. *Anal. Biochem.* 1985, *144*, 1.
7. Markovits, J.; Roques, B. P.; LePecq, J. B. *Anal. Biochem.* 1979, *94*, 259.
8. Wehry, E. L., Ed. *Modern Fluorescence Spectroscopy*; Plenum Press: New York, 1981.
9. Karsten, U.; Wollenberger, A. *Anal. Biochem.* 1977, *77*, 464.
10. Dervan, P. B.; Becker, M. M. *J. Am. Chem. Soc.* 1978, *100*, 1968.
11. Kelly, D. P.; Mack, P. O.; Martin, R. F.; Wakelin, L. P. *Int. J. Peptide Protein Res.* 1985, *26*, 400.

RECEIVED August 23, 1988

## Chapter 4

# Dynamics of Interaction Among Ligand, Receptor, and G Protein

Larry A. Sklar, Heinz Mueller, William N. Swann, Christopher Comstock,  
Geneva M. Omann, and Gary M. Bokoch

Department of Immunology, Scripps Clinic and Research Foundation,  
10666 North Torrey Pines Road, La Jolla, CA 92037

A large number of cell-surface receptors (R) for hormones and other stimulatory ligands (L) are coupled to cell activation by guanine-nucleotide-binding proteins (G proteins). The dynamics of these fundamental, cell-triggering, LRG interactions have recently become accessible to real-time, spectroscopic analysis through (a) the development of fluorescent ligands for cell-surface receptors, (b) the application and refinement of real-time fluorescence (quantum yield and polarization) and flow cytometric methods, and (c) the introduction of convenient computer methods (i.e., the Simplex Algorithm) for multiparameter optimization on data sets of moderate size. We have examined the interactions of a fluorescent *N*-formylated peptide ligand--a synthetic analog of peptides released by bacteria during infection and inflammation--with its receptors on human polymorphonuclear leukocytes. By combining measurements in intact and permeabilized cells in which the LRG interactions are sensitive to the addition of guanine nucleotides, we have been able to analyze complex LRG dynamics. Models for the various receptor states, their rates of interconversion, and their apparent position in the cell activation pathway are evaluated. The merits and limitations of the various fluorescence methods are compared.

*Cellular Communication Mediated by Ligand-Receptor Interaction.* Communication between cells and the environment generally depends on the stereospecific association between ligands (L) and cell-surface, or in some cases intracellular, receptors (R). Ligands include chemo-attractants, neurotransmitters, hormones, and growth factors, and they either occur in the environment or arise as products of one cell or tissue type and elicit responses in specific target cells. Depending on the cell type and the ligand-receptor (LR) interaction, cellular responses to the association of ligands and receptors can range from milliseconds (ion fluxes responding to channel activation)

0097-6156/89/0383-0052\$06.00/0

© 1989 American Chemical Society

to hours (nuclear signals for cell differentiation). The responses often involve second, intracellular messengers generated through transmembrane coupling, particularly via a family of guanine-nucleotide-binding proteins (G proteins) (1,2).

An appreciation that cell responses to LR binding could be initiated prior to equilibrium occupancy and largely completed as equilibrium was approached motivated us to explore binding methodology with high temporal resolution. Generally speaking, radioligand methods are limited by (a) the time resolution intrinsic to any assay system which requires the separation of free and bound ligand and (b) analytical uncertainties arising from the perturbation of the distribution of free and bound ligand which occurs when the separation step requires a period comparable to the time constants in the system. In contrast, fluorescence methods raise the possibility of homogeneous, continuous, real-time analysis with millisecond resolution. This report focuses on real-time fluorescence approaches to study LR and LRG dynamics in cell preparations at receptor concentrations (approximately nanomolar) that approximate the natural abundance for many cell types. We will describe studies on a human white blood cell--the neutrophil or polymorphonuclear leukocyte, which is central in host defense and acute inflammation. As a model ligand, we have used a synthetic hexapeptide, *N*-formyl-Nle-Leu-Phe-Nle-Tyr-Lys-fluorescein (FLPEP), a stable synthetic analogue of formylated peptides derived from bacteria and similar to those ligands which the neutrophil encounters during host defense. Binding of this peptide to cell-surface receptors elicits a battery of neutrophil responses including chemotaxis, bactericidal free radical production, and degranulation.

*Fluorescence Methodology for Studying LR Systems.* Several distinct fluorescence methods have been successfully applied to this LR system (3,4). In the appendix we describe the basis of each technique, and its advantages and limitations. Of the available techniques, fluorescence polarization measurements can differentiate the free (rotationally mobile) and receptor-bound (immobilized) ligands at subnanomolar FLPEP concentrations, even in the presence of turbid, highly scattering cell suspensions ( $10^7$ /mL). Fluorescence flow cytometry is proving to be an extremely powerful and versatile tool which under optimal conditions can detect <1,000 fluoresceinated FLPEP molecules per cell and can discriminate cell-bound ligand in principal even when the free ligand in the surrounding volume exceeds  $1 \mu\text{M}$ . A third technique involves the use of a high-affinity antibody to fluorescein, which binds the free ligand in solution and specifically quenches the fluorescence of the fluorescein moiety, thereby discriminating free from bound ligand. Since fluorescein fluorescence is quenched at low pH (<5.5), it is possible to analyze the extent of ligand internalization by cells (i.e., its removal from the cell surface) by rapidly lowering the pH in the external cell medium. Extracellular ligand is rapidly quenched while intracellular ligand is protected from the pH change.

#### *Intracellular Signaling Pathways*

*G Protein Families.* Cell responses to the binding of stimulatory ligands (L) to cell-surface receptors (R) proceed through a multistep

pathway which involves R, guanine-nucleotide-binding proteins (G), and catalytic effector enzymes (E). Homologies among pathways are already evident (1,2,5). The signaling for many receptors involves a family of heterotrimeric G proteins. The alpha subunit of the proteins in this family contains the nucleotide binding site as well as the sites of interaction for both R and E. Amino acid sequence data indicate a relationship among the G proteins (6-8). The cysteine residue, which is four amino acids from the carboxy terminus, is the site of ribosylation by pertussis toxin. Ribosylation of this site is known to uncouple the communication between many receptors and G proteins (2,9-11). Ribosylation of the G protein causes a lowering of the affinity of the receptors. Reconstitution of G proteins into ribosylated membranes restores receptor-mediated signaling and high-affinity ligand binding (10,12). One receptor, rhodopsin, is also phosphorylated near its carboxy terminus by a receptor kinase (13). The protein arrestin preferentially binds phosphorylated rhodopsin, inhibiting the rhodopsin-transducin (the photoreceptor-G protein) interaction (14). Arrestin has no guanine nucleotide binding site and therefore terminates the rhodopsin activation pathway.

**LRG Interaction.** The mechanisms of the coupling among L, R, and G have begun to be investigated in several systems. From these studies a number of general principles have emerged (2):

1. The binding of an agonist to a receptor promotes the formation of a ternary LRG complex and an exchange of guanosine-5'-triphosphate (GTP) for guanosine-5'-diphosphate (GDP) on the G protein. The ternary complex is thus activated, promoting dissociation of LR from G and G into its subunits  $G_{\alpha}$  and  $G_{\beta\gamma}$ .

2. The ternary LRG complex, in the absence of guanine nucleotide, is stable, and the agonist is bound with high affinity to the receptor.

3. Free R has a low affinity. Processes which uncouple R from G, either guanine nucleotide binding to G or ribosylation of R, also give R a low affinity.

The physiologic LRG interaction actually involves at least five types of components: ligand, receptor, intact G or G protein subunits ( $\alpha$  and  $\beta\gamma$ ), GTP (which promotes LRG dissociation and activation), and GDP (which promotes LR dissociation from G but not G dissociation into its subunits). Little about the dynamics of these processes is known. The LRG states may be visualized, in shorthand, as a 3-dimensional array (Figure 1). A large number of questions concerning LRG states remain to be addressed:

1. Which of the LRG states exist physiologically?
2. What is the pathway of interaction during activation?
  - a. When do R and G couple? Is coupling dependent upon the presence of L? Can R and G be precoupled in a resting cell in the absence of L? If not, how rapid is the coupling of R and G once L binds to R?
  - b. How rapidly does guanine nucleotide bind, dissociate and exchange? What are the steps in the exchange? What is the rate-limiting step (the formation of LRG, the release of GDP, the binding of GTP)?



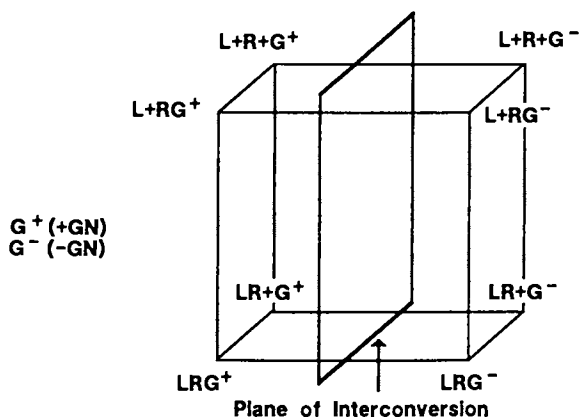


Figure 1. LRG States. One dimension represents LR coupling (top, L+R uncoupled; bottom, LR coupled); another represents RG coupling (front, RG coupled; back, R+G uncoupled); the third ("plane of interconversion") represents G interaction with nucleotide (bound, "G<sup>+</sup>", on left; G vacant, G<sup>-</sup>, on right). The available evidence suggests that activation proceeds through LRG<sup>+</sup> (first bound to GDP, lower front left), LRG<sup>-</sup> (vacant G in a ternary complex, lower front right), LRG<sup>+</sup> (adding GTP, lower front left), then LR+G<sup>+</sup> (now activated, lower rear left).

c. Does LR activate another G after the activation and dissolution of the first ternary complex LRG? What factors govern turnover or amplification (the lifetime of LR, the stoichiometry of R and G, the activity of receptor kinases, or internalization or sequestration of the receptor)?

d. What happens when R and G are uncoupled? Is R "vulnerable" to kinases, to G protein analogues like arrestin, or to internalization?

The answers to these questions and others depend upon a dynamic analysis of LRG interactions. The cell we study, the neutrophil, offers a number of exceptional advantages for the analysis of LRG dynamics.

**Neutrophils as a Model System for Studying LR Interactions.** Neutrophils are the most numerous of the white blood cells in man. They participate in host defense (bactericidal activity) and in the acute phase of inflammation. They contribute--through the release of granule proteases and the production of toxic oxygen species--to tissue injury resulting from inflammatory reactions. Resting neutrophils need to be activated to leave the circulation. When activated by chemoattractants, the cells change shape and adhere to the microvascular endothelium, penetrate the vascular basement membrane and chemotax to the site of developing inflammation. At the site the cells are stimulated, potentially by the same chemoattractants, to release inflammatory mediators.

Neutrophil function is regulated through surface receptors for a number of physiologic ligands. Stimulatory molecules include formyl peptides (synthetic analogues of peptides derived from bacterial membrane proteins), the activated fifth component of complement (C5a), the receptor-binding region of immune complexes, leukotriene B<sub>4</sub>, and platelet activating factor. The abundance of the receptor for each type of stimulatory ligand is typically 10<sup>4</sup>-10<sup>5</sup> receptors per cell with probably no more than a total of 10<sup>6</sup> stimulatory receptors per cell (11). Bokoch et al. (15) estimate that there are ~10<sup>6</sup> G in a neutrophil.

Studies on the neutrophil also benefit from the fact that considerable work has already gone into defining fluorescent ligands (formyl peptide agonists and antagonists and C5a) and real-time methodology for analyzing the dynamics of LRG interactions (3). While none of these neutrophil receptors has yet been sequenced, partial purification of the formyl peptide receptors has been reported (16). The formyl peptide receptor is particularly attractive because of the extensive structure-activity studies on peptide ligands by Freer and coworkers (17,18). The receptor is a trans-membrane glycoprotein with apparent molecular weight of 60,000 based on proteolysis (19) and photoaffinity (20) labeling studies.

#### **Definition of Receptor States in Neutrophils**

**Complexity of LR Dynamics in Intact Neutrophils at 37°.** At present, our most versatile assay to analyze receptor binding uses fluorescent ligand and a high-affinity antibody to fluorescein which discriminates free from receptor-bound hexapeptide ligand (FLPEP, *N*-formyl-Nle-Leu-Phe-Nle-Tyr-Lys-Fl). The assay has a time resolution of 1

second. In Figure 2, the specific binding and dissociation of FLPEP on intact neutrophils is displayed on a semilog plot. The experiment examines ligand dissociability as a function of time under conditions in which ligand binding was allowed to proceed for 15, 30, 60, or 120 s. Ligand dissociability following 2 min of binding is roughly linear on a log scale and is characterized by a dissociation half-time ( $t_{1/2}$ ) of approximately 2-3 min. At shorter periods of binding the dissociability is distinctly heterogeneous with a fast component ( $t_{1/2} \approx 10$  s) followed by a slow component similar to that observed at longer times. The magnitude of the fast component diminishes with the length of the binding period, and this component is largely absent 1 min after binding. Ligand internalization over short periods is measured in the same assay system by changing the extracellular pH and thereby quenching the fluorescence of extracellular ligand but not intracellular ligand. It was found that internalization at 37° has a half-time of  $\sim 3$  min (3).

An understanding of these LR dynamics requires both biological and mathematical insight. In this chapter we define these biological processes in terms of RG mechanisms and consider whether these processes reflect receptor in different states of activity. Next we develop a mathematical description to account for at least six separate processes: (1) ligand association, (2) rapid ligand dissociation, (3) slower dissociation, (4) internalization, and (5 and 6) two different interconversions among receptor forms.

*The slowly dissociating state appears to reflect receptor in an inactive form.* Cells can be stimulated in a pulse protocol in which the stimulus (FLPEP) is added, then at some later time, its binding to the receptor is interrupted by the addition of an antibody to fluorescein or of a receptor antagonist (tBoc-phe-leu-phe-leu-phe). A few seconds after the addition of the inhibitor, cell responses begin to decay (see Figure 8, Omann and Sklar, this volume). Six cell responses have been characterized in this manner (21). *Because the slowly dissociating receptor state (Figure 2) is found on cells at a time when cell responses have ceased, we suggested that this state was inactive; the rapidly dissociating state could be associated with cell activation.*

*Identity of the Rapidly Dissociating Receptor and its Relationship to LRG Interaction.* Permeabilized neutrophils as well as neutrophil membranes (not shown) provide systems for the analysis of LRG interactions because the G proteins are exposed to the extracellular medium. A binding experiment analogous to that performed on intact cells, but using permeabilized cells, is illustrated in Figure 3. After 15 s, 2 min, or 5 min (not shown) of ligand binding, dissociation in the absence of guanine nucleotide is essentially homogeneous (linear on a semilog plot) and characterized by a half-time of  $\sim 2$  min. When guanine nucleotide ( $10^{-5}$  M GTP $\gamma$ S) is added, the rate of dissociation increases markedly ( $t_{1/2} \approx 10$  s). Virtually all of the receptors (consistently  $\geq 90\%$ ) are sensitive to guanine nucleotide. An identical rapidly dissociating form is also produced if the permeabilized cells are exposed to pertussis toxin and their G proteins are exhaustively ribosylated (22). Okajima et al. (12) have reported that the low-affinity formyl peptide receptors

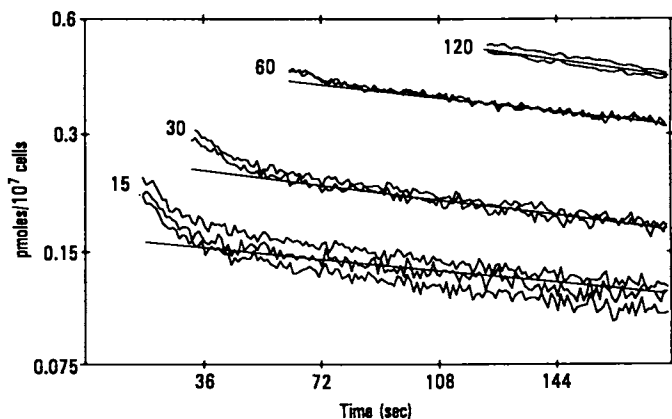


Figure 2. The binding and dissociation of FLPEP and receptor on intact neutrophils at 37°C. The data are plotted as the specific binding of FLPEP (pmoles/ $10^7$  cells) on a log plot versus time. Experimental details:  $10^7$  cells/mL were exposed at time 0 to 1 nM FLPEP. At 15, 30, 60, or 120 s, antibody to fluorescein is added to each sample. Fluorescence is monitored continuously during the additions. The data are derived from a point-by-point comparison of the fluorescence measured under conditions of receptor binding and receptor blockade. Data are representative of observations in more than 10 separate experiments. (Reproduced with permission from reference 22. Copyright 1987 Journal of Biological Chemistry.)

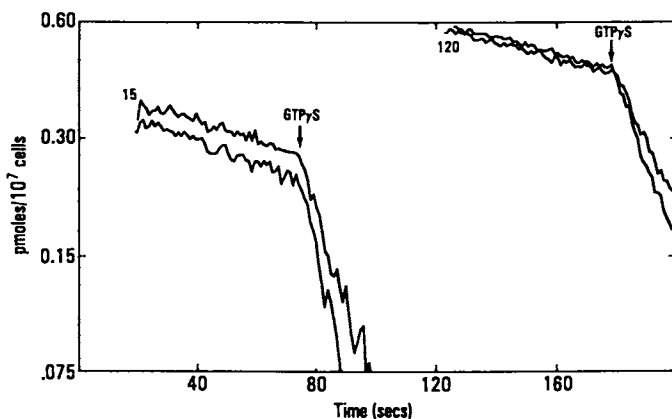


Figure 3. The binding and dissociation of FLPEP and receptor on permeabilized neutrophils at 37°C. The data are plotted as the specific binding (pmoles FLPEP bound/ $10^7$  cells) on a log plot versus time.  $10^7$  permeabilized cells/mL were exposed to 1 nM FLPEP at time 0. After 15 or 120 s, antibody to fluorescein was added to each sample. 60 seconds later,  $10^{-5}$  M GTP $\gamma$ S was added. (Reproduced with permission from reference 22. Copyright 1987 Journal of Biological Chemistry.)

formed after ribosylation of neutrophil membranes are restored to high affinity if G proteins are reconstituted into the membranes.

Thus three lines of evidence define the rapidly dissociating receptor as the LR complex. Conditions known to uncouple R from G--first, guanine nucleotide and second, pertussis toxin--produce LR; third, reconstitution of G protein restores receptor affinity, sensitivity to guanine nucleotide, and effector activation. In this sense, the ligand and binding behavior of this system is analogous to that of the beta-adrenergic receptor, where the LR and LRG complexes have already been studied with purified proteins and reconstituted membrane preparations (2,10).

*Assignments of the Fast and Slowly Dissociating Receptor Forms.* In the permeabilized cell or membrane, the rapidly dissociating form is apparently LR, whereas the slowly dissociating form (in the absence of guanine nucleotide), conversely, must be the ternary complex  $LRG^-$  (no nucleotide bound). While the rapidly dissociating form in the intact cell may also reflect LR, it is not reasonable to suggest that the slowly dissociating form in the intact cell is simply  $LRG^-$ , for several reasons. First,  $LRG^-$  should be an activatable form, but the slowly dissociating form in the cell appears to persist even after cell function has decayed. Second, guanine nucleotide, which is present in the cell, would be expected to bind to  $LRG^-$ , converting it into  $LR + G \cdot GTP$ , a rapidly dissociating state. Third, if slowly dissociating receptors are formed on intact cells at 4°C (under conditions where these receptors are trapped on the cell surface; 3) and cell membranes are prepared, these receptors are insensitive to guanine nucleotide (data not shown). For the present time we will tentatively describe this slowly dissociating form as LRX, a putatively inactive, GTP-insensitive state. In principle, this "LRX" state could form by modification of R (e.g., receptor kinase), modification of G, or by substitution of a protein like arrestin "masquerading" as a G protein. Having no guanine nucleotide binding site, such a protein might lock a receptor into a guanine-nucleotide-insensitive form which binds ligand with high affinity.

*Association Rate Constants for the Fast and Slowly Dissociating Receptor Forms.* Having assigned a tentative identity to these receptor forms, we may proceed to characterize them on the basis of their ligand binding characteristics. In order to examine association rate constants, we applied fluorescence polarization methods to the binding of FLPEP at nanomolar concentrations in turbid solutions (4). This is possible because FLPEP in solution is freely rotating (depolarized), while FLPEP on the receptor has restricted rotation (highly polarized). Using a T-format spectrofluorometer, simultaneous observation of the parallel and perpendicular components of the emission permits continuous observation of binding and dissociation.

Figure 4 shows an analysis of binding and dissociation of FLPEP in permeabilized cells in the absence (top panel) and the presence of GTPyS (lower panel). Dissociation is initiated, as indicated, by the addition of a receptor antagonist, tBoc-phe-leu-phe-leu-phe. The solid line is a fit to the data. The data from this experiment have

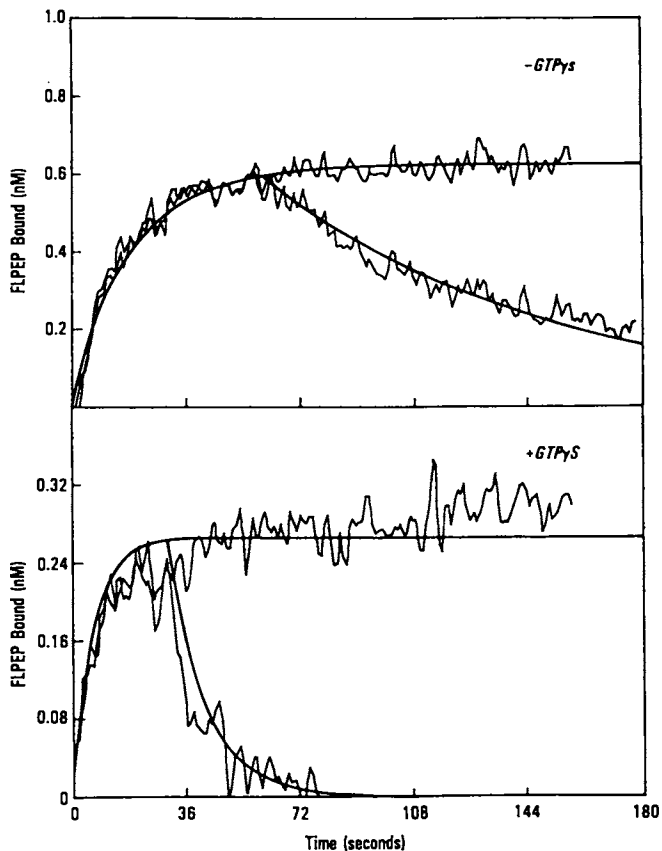
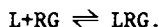


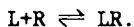
Figure 4. Continuous analysis by fluorescence polarization of FLPEP binding and dissociation to permeabilized neutrophils. Each curve represents the average of two determinations. The descending curves represent the effect of the addition of receptor antagonist after FLPEP had bound to the receptors. *Upper panel*, in the absence of GTPyS, receptor antagonist added at  $t = 60$  s; *lower panel*, in the presence of GTPyS, antagonist added at  $t = 30$  s. Solid lines are a fit to the data (see text).

In this experiment, the receptor concentration was determined to be  $1.2 \text{ nM}$ . At equilibrium, in the presence of  $1 \text{ nM}$  FLPEP,  $0.62 \pm 0.01 \text{ nM}$  ligand is bound in the upper panel;  $0.27 \pm 0.02 \text{ nM}$  is bound in the lower panel. The values of the dissociation constant ( $K_d$ ) in the equilibrium measurements are  $0.36 \times 10^{-9} \text{ M}$  and  $2.7 \times 10^{-9} \text{ M}$ , respectively. From the kinetic analysis, the values are  $0.33 \times 10^{-9} \text{ M}$  and  $2.6 \times 10^{-9} \text{ M}$ , respectively.

been taken to indicate reversible binding. In the upper panel, the interaction is putatively



In the lower panel, the interaction is putatively



The data in the upper and lower panels were fit simultaneously with a single association rate constant ( $k_a = 3.23 \times 10^7 \text{ M}^{-1} \text{ s}^{-1}$ ) and separate dissociation rate constants ( $k_d = 0.0108/\text{s}$ , upper panel;  $0.083/\text{s}$ , lower panel). The kinetic aspects of the fit were verified by the agreement with the equilibrium binding (see Figure 4 caption).

The fact that the binding is accommodated by a single-step reversible interaction does not prove that the interaction in the upper panel is between L and a preassociated  $RG^-$ . However, it implies that if there is an additional step, i.e.,



it is fast compared to binding or dissociation. In order to assess the possibility of additional steps, the experiment was carried out at  $15^\circ\text{C}$  with the idea that such a step might be slower and thus detectable. Preliminary measurements (data not shown) have been unable yet to resolve such a step. For analytical purposes we can regard ligand association or dissociation at  $37^\circ\text{C}$  in the presence or absence of guanine nucleotide as reflecting "pure" receptor states  $LR$  and  $LRG^-$ .

*A Glimpse of Transduction Mechanisms Using the Permeabilized Cell.* Transduction requires the formation of the ternary complex  $LRG \cdot \text{GDP}$ , the exchange of GTP for GDP ( $LRG \cdot \text{GDP} \rightarrow LRG^- \rightarrow LRG \cdot \text{GTP}$ ) and the dissolution of the active ternary complex. An analysis of the latter half of transduction, the interconversion of  $LRG^-$  to  $LR + G \cdot \text{GTP}$  is shown in Figure 5. When receptors are occupied in the absence of guanine nucleotide ( $LRG^-$ ), slow dissociation in the presence of antibody to fluorescein is observed. Adding guanine nucleotide at different concentrations promotes the formation of the rapidly dissociating receptor  $LR$  at different rates. The data are fit (solid lines) to a single-step conversion. Three rate constants are required: dissociation rates for  $LRG^-$  and  $LR$  (measured directly,  $\pm$  saturating guanine nucleotide) and a rate of conversion ( $k_{\text{conv}}$ ) from  $LRG^-$  to  $LR$ .

At the lower end of each solid line is the  $k_{\text{conv}}$  for that fit. Note that  $k_{\text{conv}}$  is proportional to the guanine nucleotide concentration. (At saturating guanine nucleotide ( $>10^{-5}$  GTPyS) conversion becomes nearly instantaneous.) The proportionality between  $k_{\text{conv}}$  (the overall event) and the concentration of guanine nucleotide (the first step, which requires the binding of guanine nucleotide) implies that the first step in the conversion is the rate-limiting event and that the second step (the dissolution of the ternary complex) is fast. Assuming the rate of interconversion ( $k_{\text{conv}} \times [LRG^-]$ )

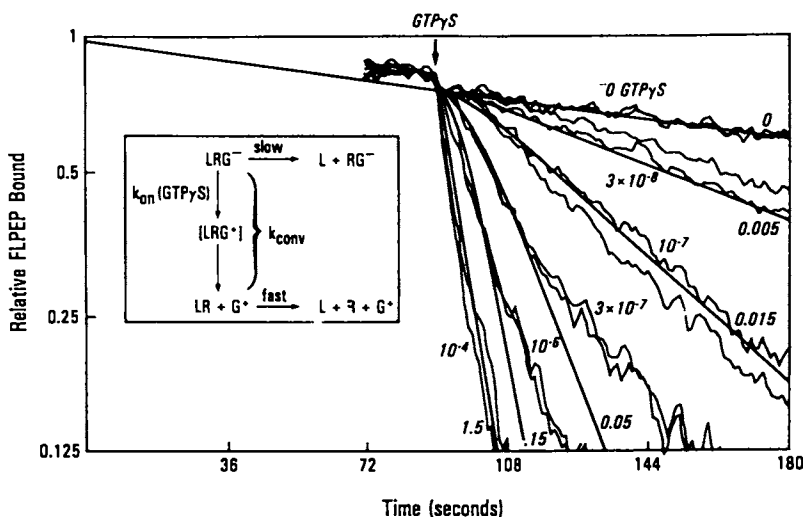
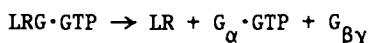


Figure 5. Guanine-nucleotide-dependent receptor interconversion from  $LRG^-$  to  $LR$ . Permeabilized cells ( $10^7/\text{mL}$ ) (no  $GTP\gamma S$ ;  $1 \text{ mM Mg}^{++}$ ) were allowed to bind FLPEP for 1 min. Data analysis begins with the addition of antibody to fluorescein (after 60 s, but not indicated). At 90 s (indicated),  $GTP\gamma S$  is added to induce interconversion to the rapidly dissociating state. The guanine nucleotide concentrations are shown (saturated at  $10^{-5} \text{ M}$ ). The solid lines are the fit to the onestep model shown in the inset, and the  $k_{\text{conv}}$  for the fit is shown at the end of each solid line. Data are plotted as the log of bound ligand (on a relative scale versus time).

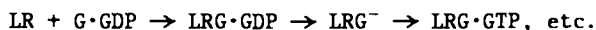


to be equal to the initial rate of binding of GTPyS ( $k_{on} \times [GTPyS] [LRG^-]$ ) provides a preliminary estimate for the bimolecular rate constant of GTPyS binding ( $\sim 2 \times 10^5/M^{-1}s^{-1}$ ). This estimate is within an order of magnitude of the rates of GTP binding to another G protein (23).

*Which Receptor States Contribute to Cell Activation?* Of the three states, LRG appears and breaks up during transduction and LRX forms after cell activation. The role of LR is less clear. Conceptually, an LR state in cells can be viewed either as a remnant of the ternary complex which dissociates during transduction



or as a precursor in a cycle of amplification



In an effort to begin to understand the role of the receptor states in the intact cell we compared the behavior of two different ligands at the formyl peptide receptor: the hexapeptide FLPEP and a tetrapeptide FMet-Leu-Phe-Lys-FL. These have been compared in binding and response assays. In binding measurements (not shown), the tetrapeptide (FMet-Leu-Phe-Lys-FL) dissociates more slowly from intact cells and from LRG but not from LR. Cell responses to these two peptides were assayed in pulse stimulation. After a saturating concentration of receptor antagonist is added, a few seconds elapse before oxidant production begins to decay for FLPEP, but more than 20 seconds elapse for FMet-Leu-Phe-Lys-FL. Since these ligands use the same receptor and the same biochemical pathway to elicit cell responses the differences could reflect the activity of LR and LRG. Two factors might contribute to activity: (1) the duration of ligand occupancy and (2) the rate of interconversion among the states. An increased lifetime of an active state could permit more G proteins to be sequentially activated.

### *Model Building*

*Analysis of Ligand Binding in the Intact Cell.* A model of LR dynamics in the intact cell consistent with the results of these studies is presented in Figure 6, and a fit to the data of a polarization binding experiment is shown. The model has these characteristics:

1. Two receptor states (LRG, LR) each can bind ligand at the same rate (rate 1,  $\sim 3 \times 10^7 M/s$ ).
2. LR and LRX dissociate with half-times comparable to those seen in the absence of interconversion (rate 3,  $t_{1/2} \approx 10$  s; rate 5,  $t_{1/2} \approx 100$  s).
3. The slowly dissociating state (LRX) is internalized (rate 6,  $t_{1/2} \approx 3$  min).
4. There is an interconversion between LR and LRX (rate 4,  $t_{1/2} \approx 10$  s).
5. The ternary complex LRG exists transiently (rate 2,  $t_{1/2} < 1$  s) consistent with the results of Figures 4 and 5 which suggest that

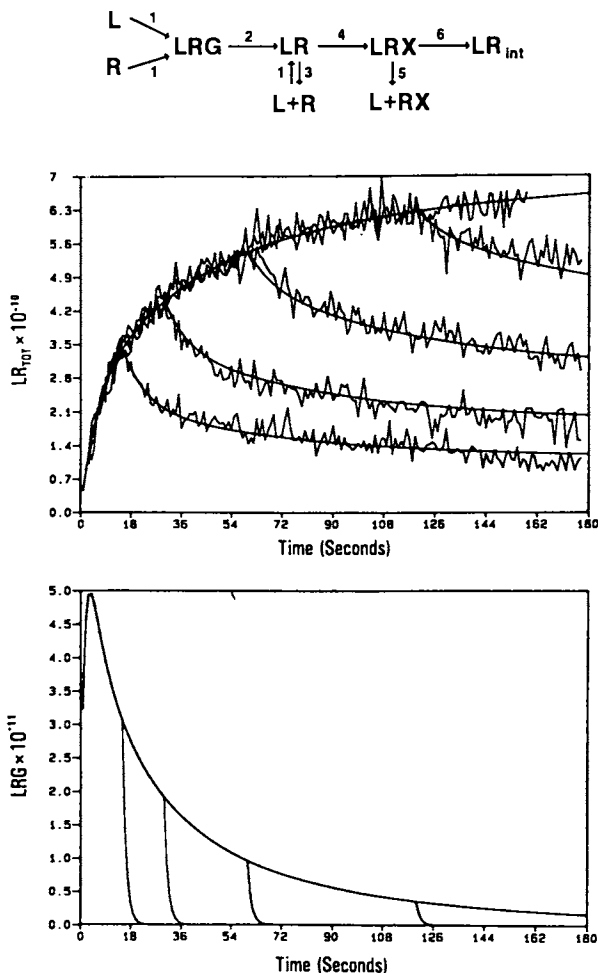


Figure 6. Interconverting receptor model. In the presence of L, membrane R and G become associated to form the ternary complex LRG, which is sequentially interconverted into LR and LRX prior to internalization.

**Middle panel:** The data are a continuous polarization analysis of ligand binding (1 nM FLPEP) to  $10^7$  cells/mL at  $37^\circ\text{C}$ , which represents  $\text{LR}_{\text{Tot}}$ , the sum of occupied receptors in all states. Dissociation is monitored following the addition of receptor antagonist to the different samples at 15, 30, 60, and 120 s. The smooth curves are a fit to the data using the model.

**Lower panel:** Calculated behavior of LRG in the model during binding and dissociation.

this state is formed rapidly and that it falls apart rapidly during activation.

We observe that the model accounts for the experimental data. The model predicts the behavior of the active state LRG to be analogous to cell activation itself. LRG rises in seconds, disappears in minutes as binding equilibrates, and, when binding is interrupted, disappears in a few seconds; as this state disappears, transduction also "collapses" and cell responses decay. The model should not be viewed as complete, however. For example, amplification steps, which permit the activation of multiple G proteins by a single receptor, would be built into the model by adding a reverse rate from LR to LRG. Such amplification would have to be verified experimentally.

### Prospects

Real-time spectroscopic methods can be used to measure the binding, dissociation, and internalization of fluorescent ligands with cell-surface receptors on cells and membranes. The time resolution available in these methods is sufficient to permit a detailed analysis of complex processes involved in cell activation, particularly receptor-G protein dynamics. A description of the kinetics and thermodynamics of these processes will contribute to our understanding of the basis of stimulus potency and efficacy.

These methods, when combined with real-time analysis of cell response (Omann and Sklar, this volume), also permit a quantitative analysis of the relationship between receptor occupancy and cell response.

### Acknowledgments

We thank Zenaida Oades for excellent technical assistance. This work was supported by NIH grants AI-17354, AI-19032, AI-22690, and RR00833. L.A.S. is an Established Investigator of the American Heart Association. This is publication #5080-IMM from the Research Institute of Scripps Clinic.

## APPENDIX: REAL-TIME METHODS FOR ANALYSIS OF LIGAND BINDING

### Method 1. Spectrofluorometric Method Using Antibody to Fluorescein

**Basis.** When the fluorescent ligand FLPEP is added to a cuvette containing neutrophils in the appropriate buffer the total fluorescence intensity is constant during the binding measurement whether or not the ligand binds to cell receptors; the ligand does not change its quantum yield when it binds to the receptor. (Over longer time periods, internalized ligand is acidified and begins to be quenched. The presence of  $\text{NH}_4^+$  inhibits such quenching.)

Antibody to fluorescein used at 25 nM ( $K_a > 10^{10} \text{ M}^{-1}$ ) rapidly binds and effectively quenches (>90%) FLPEP that is not yet bound to a receptor. When antibody to fluorescein is added to a cell suspension containing FLPEP, the antibody binds and quenches free FLPEP (discriminating between free and bound) but quenches the receptor-bound ligand only after it dissociates from the receptor. Dissociation of the ligand from the receptor thus is measured continuously.

**Calibration.** Quantitative binding analysis requires knowing the concentration of FLPEP, which can be determined for a stock solution of FLPEP by absorption spectroscopy. The quenching by the antibody is essentially quantitative, and the relative amounts of free and bound ligand are calculated from the relative fluorescence intensity.

There is a single assumption in these measurements--namely that the antibody only quenches free ligand. This has been demonstrated specifically by flow cytometry in experiments which show that there is no quenching of ligand on the cell (3). The kinetic analysis depends on rapid interaction of ligand and antibody, which in these experiments is essentially within the mixing time.

**Advantages.** The antibody technology is remarkably convenient. It requires only that a significant fraction of FLPEP be receptor bound ( $\geq 10\%$ ). The assay can be set up in a few minutes and is applicable to membranes, permeabilized cells, cells, or any other preparation in which the receptor concentration is in the range of 1 nM or greater. We use this assay routinely to analyze ligand dissociation kinetics.

**Limitations.** The assay is troublesome to use for:

- a. Very low receptor concentrations, in which background fluorescence becomes a consideration.
- b. High ligand concentrations (10 nM) where ligand is in great excess over receptor (1 nM), because the fraction of bound ligand is relatively small.
- c. Association-rate measurements in which continuous association analysis is preferable.

## Method 2. Fluorescence Polarization Analysis

**Basis.** The rotational mobility of a small ligand is relatively unrestricted in solution (anisotropy approaches 0). The mobility is restricted when the ligand binds to a large immobilized molecule such as the receptor. In a T-format fluorometer, the parallel and perpendicular components of the emission can be examined simultaneously. While precautions must be exercised in working with turbid suspensions, it is nonetheless practical to make continuous measurements of binding and dissociation.

**Calibration.** The quantitative transformation of polarization measurements into binding takes advantage of unique features of the FLPEP system. Weber's Law of the additivity of anisotropy is given by

$$\bar{r}\bar{Q} = \sum_i r_i Q_i X_i$$

where the anisotropy of the mixture is  $r = (I_{||} - I_{\perp}) / (I_{||} + 2I_{\perp})$ ,  $Q$  is the quantum yield of the mixture,  $r_i$  is the anisotropy of the  $i$ th component,  $Q_i$  is the quantum yield of the  $i$ th component, and  $X_i$  the mole fraction of the  $i$ th component.

Since the quantum yield is the same for free (*f*) and bound (*b*) ligand, we can write the observed anisotropy of the mixture *r* as

$$\bar{r} = r_f X_f + r_b X_b.$$

This states that for FLPEP the observed anisotropy is proportional to ratio of free to bound FLPEP. One measures  $r_f$  for the free ligand in the presence of cells and excess nonfluorescent peptide (or without cells at all). One measures  $r_b$  by obliterating (quenching) the fluorescence contribution of the free ligand component with antibody following the association of ligand with cell receptors. (Note: There is a small correction factor which takes into account the quenching efficiency of the antibody and the *r* value for FLPEP on the antibody.)

**Advantages.** Polarization measurements permit continuous binding analysis with subsecond resolution if required. When applied in stop-flow mixing conditions the technique has the best time resolution of the methods presently available.

**Limitations.** Of the three methods, polarization has the lowest signal-to-noise ratio, and is most limited in its ligand concentration range. It works best when a significant fraction of the ligand is bound to the receptor. For FLPEP and cells the practical range is 0.5 to 3 nM ( $K_d \leq L \leq R$ ). This method works best when free L is substantially depleted by the binding process.

### Method 3. Flow Cytometry

**Basis.** Ligand accumulates on single cells and is concentrated on cells compared to the concentration in the surrounding volume. In flow cytometry, in contrast to a cuvette system, only the individual cells and a small surrounding volume are illuminated. In short, the technology is biased against the detection of free ligand in the total volume. The bias can be adjusted by changing the illuminated volume (depending upon flow rate, beam size, beam shape). *At the present time, discrimination of free and bound ligand is possible at concentrations of free ligand approaching 1 μM.*

**Calibration.** Many approaches have been used to calibrate flow cytometric measurements, including the comparison of flow and nonflow techniques (radiolabels, spectrofluorometry). In recent years, commercial standards have been introduced which are calibrated in fluorescein equivalents/particle (e.g., 3,000 or 500,000). With labeled ligands, calibration requires determining the relative quantum yield of the ligand compared to pure fluorescein and using the standards to analyze the amount bound on cells. Our ligands (fluorescein isothiocyanate derivatives) are typically 50% as fluorescent as fluorescein.

**Advantages.** The advantages of flow cytometry are numerous. It is the most sensitive of the techniques, able to detect  $\leq 1,000$  fluorophores per cell (0.01 nM FLPEP). There is in addition no required total receptor concentration. It is effective for small numbers of

cells whether they are in a large or small volume. The concentration of ligand can be varied widely in both steady state and kinetic applications. It is effective for high- or low- $K_d$  ligands and does not require that a large fraction of the ligands be bound.

Techniques have already been developed which, in summary, permit analysis at equilibrium of receptor number,  $K_d$ , and by competition, the  $K_d$  of unlabeled ligands. In kinetic measurements, methods to measure association and dissociation of labeled (and by competition, unlabeled) ligands and internalization have been described (4,21, 24).

**Limitations.** Most commercial cytometers require 5-60 s to pressurize the cell sample and deliver it to the point of analysis. We developed a special sample chamber which delivers sample in three seconds in some machines (25). The fact that commercially available software has only recently been written and the reluctance of instrument manufacturers to make available source code has probably delayed by a few years the widespread application of this technology.

#### Literature Cited

1. Stryer, L.; Bourne, H. *Annu. Rev. Cell Biol.* 1986, 2, 391.
2. Gilman, A. G. *Annu. Rev. Biochem.* 1987, 56, 615.
3. Sklar, L. A.; Finney, D. A.; Oades, Z. G.; Jesaitis, A. J.; Painter, R. G.; Cochrane, C. G. *J. Biol. Chem.* 1984, 259, 5661.
4. Sklar, L. A. *Annu. Rev. Biophys. Biophys. Chem.* 1987, 16, 479.
5. Dixon, R. A. F.; Kobilka, B. K.; Strader, D. J.; Benovic, J. L.; Dohlman, H. G.; Frielle, T.; Bolanowski, M. A.; Bennett, C. D.; Rands, E.; Diehl, R. E.; Mumford, R. A.; Slater, E. E.; Sigal, I. S.; Caron, M. G.; Lefkowitz, R. J.; Strader, C. D. *Nature* 1986, 321, 75.
6. Itoh, H.; Kozasa, T.; Nagata, S.; Nakamura, S.; Katado, T.; Ui, M.; Iwai, S.; Ohtsuka, E.; Kawasaki, H.; Suzuki, K.; Kaziro, Y. *Proc. Natl. Acad. Sci. USA* 1986, 83, 3776.
7. Nukuda, T.; Tanabe, T.; Takahashi, H.; Noda, M.; Haga, K.; Haga, T.; Ichiyama, A.; Kangawa, K.; Hiranaga, M.; Matsuo, H.; Numa, S. *FEBS Lett.* 1986, 197, 305.
8. Didsbury, J. R.; Snyderman, R. *FEBS Lett.* 1987, 219, 259.
9. Stryer, L. *Annu. Rev. Neurosci.* 1986, 9, 87.
10. Smigel, M. D.; Ross, E. M.; Gilman, A. C. *Cell Membr. (N.Y.)* 1984, 2, 247.
11. Sklar, L. A. *Adv. Immunol.* 1986, 39, 95.
12. Okajima, F.; Katada, T.; Ui, M. *J. Biol. Chem.* 1985, 260, 6761.
13. Wilden, U.; Kuhn, H. *Biochemistry* 1982, 21, 3014.
14. Kuhn, H.; Hall, S. W.; Wilden, U. *FEBS Lett.* 1985, 176, 473.
15. Bokoch, G. M.; Bickford, K.; Bohl, B. J. *Cell Biol.* 1988, 106, in press.
16. Huang, C-K. *J. Leukocyte Biol.* 1987, 41, 63.
17. Freer, R. J.; Day, A. R.; Radding, J. A.; Schiffmann, E.; Aswanikumar, S.; Showell, H. J.; Becker, E. L. *Biochemistry* 1980, 19, 2404.

18. Freer, R. J.; Day, A. R.; Muthukumaraswamy, N.; Pinon, D.; Wu, A.; Showell, H. J.; Becker, E. L. *Biochemistry* 1982, *21*, 257.
19. Dolmatch, B.; Niedel, J. J. *Biol. Chem.* 1983, *12*, 7570.
20. Allen, R. A.; Jesaitis, A. J.; Sklar, L. A.; Cochrane, C. G.; Painter, R. G. *J. Biol. Chem.* 1986, *261*, 1854.
21. Sklar, L. A.; Hyslop, P. A.; Oades, Z. G.; Omann, G. M.; Jesaitis, A. J.; Painter, R. G.; Cochrane, C. G. *J. Biol. Chem.* 1985, *260*, 11461.
22. Sklar, L. A.; Bokoch, G. M.; Button, D.; Smolen, J. E. *J. Biol. Chem.* 1987, *262*, 135.
23. Ferguson, K. M.; Higashijima, T.; Smigel, M. D.; Gilman, A. G. *J. Biol. Chem.* 1986, *261*, 7393.
24. Sklar, L. A.; Sayre, J.; McNeil, V. M.; Finney, D. A. *Mol. Pharmacol.* 1985, *28*, 323.
25. Omann, G. M.; Coppersmith, W.; Finney, D. A.; Sklar, L. A. *Cytometry* 1985, *6*, 69.

RECEIVED August 23, 1988

## Chapter 5

# Detection of Calcium Signals in Neutrophils Using Fluorescent Dyes

### Effect of Hyperosmolality

Douglas E. Chandler, Carrie J. Merkle, and Charles J. Kazilek

Department of Zoology, Arizona State University, Tempe, AZ 85287

Previous studies indicate that osmotic gradients promote membrane fusion, while hyperosmotic conditions inhibit membrane fusion during exocytosis. Consistent with this idea is the observation that the release of lysosomal enzymes from rabbit neutrophils, induced by the chemotactic peptide *N*-formylmethionyl-leucyl-phenylalanine (FMLP), is inhibited almost 80% in a 700-mosmol/kg medium. Inhibition is immediate (within 10 s), increases with osmolality, and is independent of the osmoticant. Neutrophils loaded with the calcium indicator indo-1 exhibit an FMLP-induced calcium signal that is inhibited by hyperosmolality. Hyperosmolality (700 mosmol/kg) increases basal calcium levels and reduces the peak of the calcium signal elicited by FMLP at concentrations ranging from  $10^{-10}$  to  $10^{-7}$  M. Studies using chlorotetracycline, a dye that detects membrane-bound calcium within cells, show that part of the signal results from release of intracellularly sequestered calcium. Thus, in neutrophils, hyperosmolality inhibits not only exocytosis but also the calcium signal that initiates exocytosis.

Secretory cells synthesize, store, and, upon demand, release their products into the extracellular space by a process called exocytosis. Secretory materials are stored in membrane-bound granules and, during exocytosis, the plasma membrane of the cell and that of the secretory granule fuse, forming an aqueous pore through which the secretions escape. Several lines of evidence indicate that membrane fusion is promoted by formation of an osmotic gradient between the interior of the granule and the extracellular space. First, fusion of unilamellar phospholipid vesicles with a planar bilayer is promoted if the vesicles have a high inside osmotic strength. Cohen et al. (1,2) have shown that in such a system, calcium induces a prefusion adherence between the vesicular and planar membranes, which is followed by membrane fusion, providing that an osmotic gradient exists between the inside of the vesicle and the opposite side of the planar membrane. Second, hyperosmotic media inhibit exocytosis in a number of

0097-6156/89/0383-0070\$06.00/0

© 1989 American Chemical Society



cells, including the parathyroid gland, adrenal chromaffin cells, sea urchin eggs, and platelets (3-8). This has been interpreted as meaning that during exocytosis the material stored within the secretory granule becomes osmotically active, water moves in, the granule swells, and the osmotic gradient and/or granule swelling provides a driving force for membrane fusion. Indeed, calcium-induced granule swelling has been observed in an *in vitro* system, the isolated egg cortex (6,7). An alternative hypothesis is that expansion of the exocytic pocket is driven by hydration of the granule matrix after fusion.

Neutrophils represent an ideal system for studying osmotic effects on exocytosis. Stimulation of cytochalasin-B-treated neutrophils with the chemotactic peptide *N*-formylmethionyl-leucyl-phenylalanine (FMLP) results in a rapid compound exocytosis: up to 80% of lysosomal enzymes are released within 30 s (9-14). Secretion appears to be triggered by a rise in the level of cytosolic free calcium (15-18) promoted in part by entry of extracellular calcium through receptor-gated channels and in part by release of calcium that is sequestered or bound at some intracellular site (19-21). In this presentation, we augment our previously published data (22,23), which demonstrates that lysosomal enzyme release from neutrophils is inhibited under hyperosmotic conditions and that the rise in cytosolic calcium preceding secretion is inhibited as well.

Two fluorescent probes, indo-1 and chlorotetracycline, have been used for detecting calcium redistribution in neutrophils in response to chemotactic peptides. Indo-1, first described by Gryniewicz et al. (24), is a calcium chelator whose emission spectrum at 400 nm is very sensitive to calcium. It is a highly charged compound (see Figure 1) that is usually introduced in the form of an acetoxymethyl ester. The ester easily diffuses through cell membranes and is de-esterified by intracellular hydrolases, thereby producing the free acid, which is trapped in the cytoplasm. This probe is capable of monitoring cytosolic free calcium levels in the micromolar range (see Figure 2); indo-1 is highly specific for calcium and monitors only free calcium, not calcium bound to proteins or sequestered in organelles. Use of indo-1 and similar calcium probes, such as quin-2 and fura-2, is detailed in several recent publications (25-27).

CTC, used extensively to monitor calcium release in both whole cells and isolated organelles (28-33), is an amphipathic molecule that easily passes through cell membranes (see Figure 1). The fluorescence of this probe is enhanced more than fiftyfold by binding of calcium when the dye is intercalated into biological membranes. Thus, the strongest signal comes from dye molecules inserted into organelles that sequester calcium, such as mitochondria and smooth endoplasmic reticulum (see Figure 3). Release of organellar calcium is accompanied by dissociation of the dye-calcium complex and probable release of free probe into the cytoplasm and ultimately into the extracellular medium (Figure 3). Unlike dyes such as indo-1, CTC is not specific for calcium (magnesium and other divalent cations interfere) and at high concentrations can inhibit calcium-dependent cell responses (34-36). CTC, however, is a useful adjunct to indo-1 because it monitors release of calcium by organelles, while indo-1 monitors appearance of calcium in the cytoplasm.

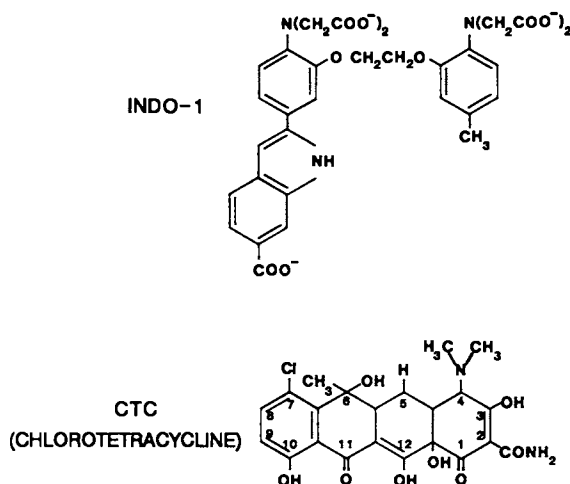


Figure 1. Structures of the fluorescent calcium probes indo-1 and chlorotetracycline.

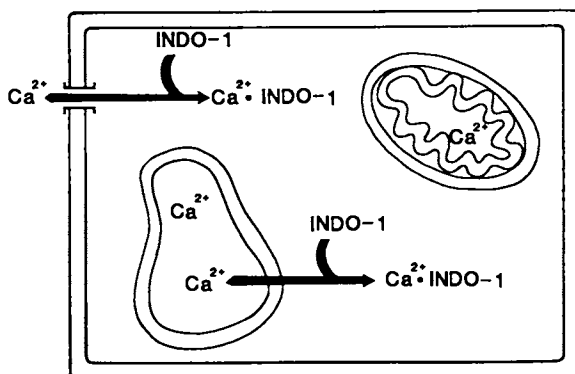


Figure 2. Reporting of cytosolic free calcium levels by indo-1. Increases in cytosolic calcium, due either to entry of extracellular calcium via calcium channels or to release of intracellular calcium sequestered in organelles such as smooth endoplasmic reticulum, results in formation of the indo-1-calcium complex. Fluorescence intensity at 400 nm (excitation at 340 nm) is proportional to the concentration of this complex; the dissociation constant for this complex is about 250 nM (24), making this probe useful for detecting calcium activities in the range of 25 to 2500 nM.

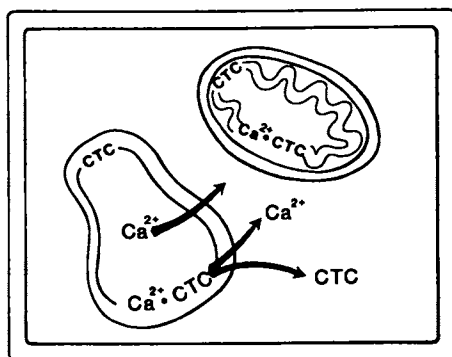


Figure 3. Reporting of intracellular calcium sequestration by chlorotetracycline (CTC). CTC preferentially partitions into cell membranes and its fluorescence in this environment is sensitive to calcium bound to the membrane; therefore its signal (excitation 400 nm, emission 530 nm) will come largely from organelles that bind or sequester calcium, such as smooth endoplasmic reticulum or mitochondria. Release of calcium from such organelles is accompanied by dissociation of the calcium-CTC complex, a decrease in CTC fluorescence and efflux of unbound probe from the organelle and from the cell.

### Methods

Rabbit peritoneal neutrophils were harvested and their release of  $\beta$ -glucuronidase was measured at 37°C, as described previously (13). For indo-1, neutrophils were washed twice in a calcium-free buffer, then loaded with 15  $\mu$ M indo-1 acetoxymethyl ester (24) for 40 min at 37°C at a density of  $5 \times 10^7$  cells/mL. The cells were then washed twice more in calcium-free buffer, resuspended to a density of  $1 \times 10^7$  cells/mL, and kept on ice. Prior to fluorometry, cells were diluted 4 $\times$  with the appropriate buffer at 37°C. For CTC, neutrophils were incubated with 20  $\mu$ M CTC at 37°C in the spectrofluorometer cuvette. All measurements were carried out using an SLM-Aminco SPF 500C fluorospectrometer interfaced with an IBM PC microcomputer.

### Results

Neutrophils, pretreated with cytochalasin B (5  $\mu$ g/mL), responded to FMLP with a rapid (<30 s) release of  $\beta$ -glucuronidase. Figure 4 shows that enzyme release is dose dependent in the range of FMLP concentrations from  $10^{-11}$  M to  $10^{-7}$  M (circles). If the osmolality is increased by the addition of 0.3-M sucrose to the buffer, enzyme release is inhibited (squares). The inhibition is as high as 80% at an FMLP concentration of  $3 \times 10^{-10}$  M, and can be overcome only partially by increasing the agonist concentration. The inhibition of enzyme release appears to depend on increased osmolality. Figure 5 shows that enzyme release decreases progressively as the osmolality of the medium is increased by addition of sodium HEPES (*N*-2-hydroxyethylpiperazine-*N'*-2-ethanesulfonic acid, sodium salt, pH 7.4) (triangles), sodium sulfate (squares), or sucrose (circles). The inhibition of enzyme release was accompanied by a reduction of the cytosolic calcium signal. Figure 6A shows that the emission of indo-1-loaded neutrophils at 400 nm undergoes a characteristic increase upon the addition of FMLP to a medium of normal osmolality (320 mosmol/kg). The increase is expressed as an abrupt peak followed by a slower decline to a plateau level. The indo-1 emission signal is extremely dependent on calcium levels in the submicromolar range; cytosolic calcium levels are estimated to be about 100-200 nM before stimulation and about 3  $\mu$ M at the peak of the FMLP-induced calcium transient. Cells placed in hyperosmotic media 2 min prior to FMLP addition exhibit indo-1 signals that are limited to a smaller initial peak with little or no plateau (Figure 6B-D). Modification of the calcium signal is similar regardless of the chemical nature of the osmoticant; increasing osmolality with sodium HEPES (trace A), sodium sulfate (trace B), or sucrose (trace C) produces the same result.

The calcium signal elicited by FMLP was further analyzed for dependence on extracellular calcium. In a calcium-containing medium of normal osmolality (Figure 7, trace 1), the signal consists of an abrupt peak at about 10 s after stimulation, a broad shoulder of elevated calcium lasting about 90 s, and a plateau of lower but still elevated calcium levels from 2 to 5 min after stimulation. Removal of extracellular calcium just before FMLP addition results in a markedly attenuated signal consisting of a single initial peak and a return to basal calcium levels within 60 s after stimulation (Figure 7, trace 2). This suggests that the initial peak results

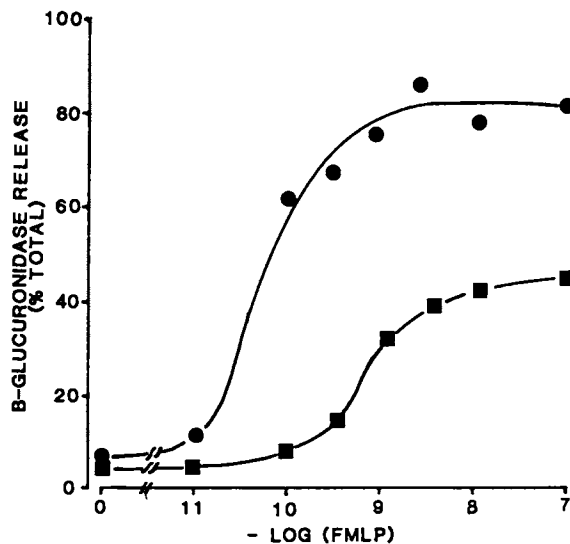


Figure 4. Effect of hyperosmolality on lysosomal enzyme release from rabbit neutrophils. Cells were preincubated 10 min at 37°C in either regular HEPES buffer at 320 mosmol/kg (●) or in HEPES buffer with 0.3-M sucrose at 680 mosmol/kg (■), 5 µg/mL cytochalasin B was added, cells were stimulated with FMLP, and β-glucuronidase was released into the medium during a 6-min period measured.

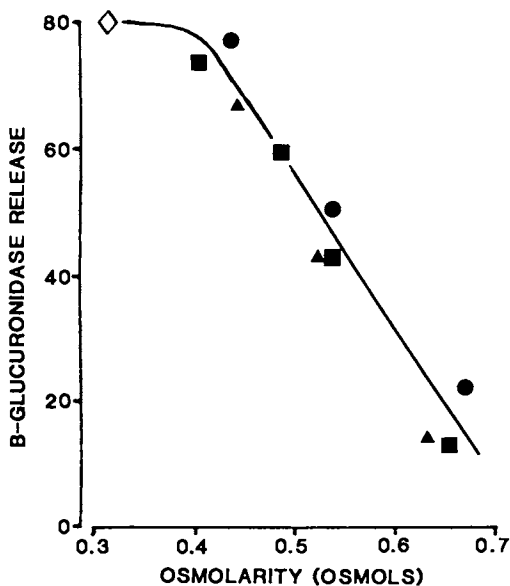


Figure 5. Inhibition of lysosomal enzyme release from neutrophils by increased osmotic strength. Cells were preincubated for 10 min at 37°C in regular buffer containing no additions ( $\diamond$ ), or containing sodium sulfate ( $\blacksquare$ ), sodium HEPES ( $\blacktriangle$ ), or sucrose ( $\bullet$ ) to increase the osmotic strength. Cells were treated with cytochalasin B (5  $\mu\text{g}/\text{mL}$ ) and FMLP ( $10^{-9}$  M) and  $\beta$ -glucuronidase was released into the medium measured.

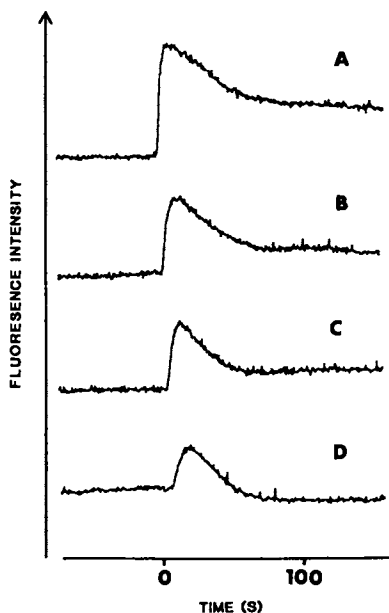


Figure 6. Effect of hyperosmolality on FMLP-induced calcium transients in indo-1-loaded neutrophils. Cells were incubated at 37°C in either regular buffer (A); regular buffer plus 0.15-*M* sodium sulfate, 662 mosmol/kg (B); 0.3-*M* sodium HEPES, 645 mosmol/kg (C); or 0.45-*M* sucrose, 870 mosmol/kg (D). All were treated with 5  $\mu\text{g}/\text{mL}$  cytochalasin B and stimulated with  $10^{-9}$  *M* FMLP. Excitation at 340 nm and emission at 400 nm.

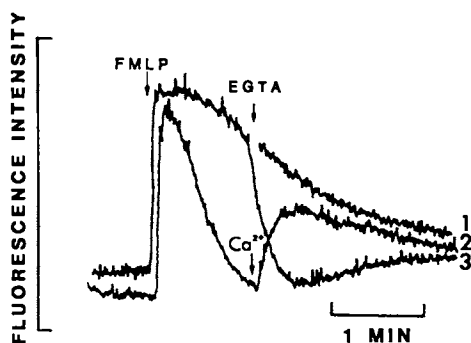


Figure 7. Sensitivity of the FMLP-induced calcium signal to removal of extracellular calcium. Indo-1-loaded neutrophils were stimulated with  $10^{-8}$  *M* FMLP in a medium of normal osmolality (320 mosmol/kg) and indo-1 fluorescence was recorded as described in Figure 6. Trace 1: Cells in a medium with normal calcium (1.5 *mM*). Trace 2: EGTA added to chelate extracellular calcium before stimulation; extracellular calcium (1.5 *mM*) readded 70 s after stimulation. Trace 3: Cells in a medium with normal calcium; EGTA added 70 s after stimulation to chelate extracellular calcium.

from release of intracellular calcium that is either bound or sequestered within an organelle. In contrast, the broad shoulder and lower plateau are completely eliminated, indicating that these later phases are generated by influx of extracellular calcium. This conclusion can be verified by showing that the addition of EGTA (ethyleneglycol-bis( $\beta$ -aminoethyl ether)-*N,N,N',N'*-tetraacetic acid) to chelate extracellular calcium at 70 s after stimulation results in an immediate decrease in the calcium signal to basal levels (Figure 7, trace 3); likewise, readdition of extracellular calcium to cells stimulated in the absence of calcium allows regeneration of the last phase in the calcium signal (Figure 7, trace 2).

In hyperosmotic media, the calcium signal is also attenuated, and again limited to a single immediate peak (Figure 8, trace 3). In this case, removal of extracellular calcium has little further effect on this initial peak (Figure 8, trace 2); evidently, the immediate release of intracellular calcium is reduced but not eliminated by increased osmolality. In contrast, the broad shoulder is completely missing; this second phase of the calcium signal appears to be sensitive to both extracellular calcium removal and to increased medium osmolality. The final phase of the signal between 2 and 5 min, although dependent on extracellular calcium, does not seem to be blocked by increased osmolality; readdition of calcium to a hyperosmotic medium 70 s after stimulation produces a normal final phase (Figure 8, trace 2) equal in magnitude to the final phase of the calcium signal seen in a control medium (trace 1).

Confirmation that FMLP-induced activation involves release of intracellular calcium was obtained by loading neutrophils with CTC. Addition of 20  $\mu$ M CTC to a neutrophil suspension resulted in a gradual increase in CTC fluorescence as the probe entered the cells and partitioned into intracellular membranes (Figure 9, upper panel). Addition of FMLP resulted in an abrupt decrease in fluorescence, suggesting release of calcium from intracellular membranes probed by CTC. The FMLP-induced release of calcium monitored by CTC was little affected by increased medium osmolality; a similar fluorescence decrease was seen in the presence of sodium HEPES (645 mosmol/kg) or sodium sulfate (662 mosmol/kg) (Figure 9, lower panel).

### Discussion

We have shown that lysosomal enzyme release from neutrophils is inhibited by hyperosmotic conditions, a finding that parallels observations in other cells and that could be interpreted as supporting the hypothesis that an osmotic gradient promotes membrane fusion during exocytosis. However, we also show that hyperosmolality reduces the FMLP-generated rise in cytosolic free calcium levels, the signal that initiates exocytosis. Thus, in neutrophils, the hyperosmotic inhibition of enzyme release may be due to the diminished calcium signal. The effect of osmolality on the calcium signal in other cells has not been studied and, until it is, a direct effect of osmolality on exocytosis cannot be assumed. Our observations, however, do not obviate the fact that hyperosmolality slows or inhibits membrane fusion both in *in vitro* systems where calcium is added exogenously (7) and in *in vivo* systems where the calcium signal is provided by ionophores rather than by calcium influx or by release of intracellular calcium (6).



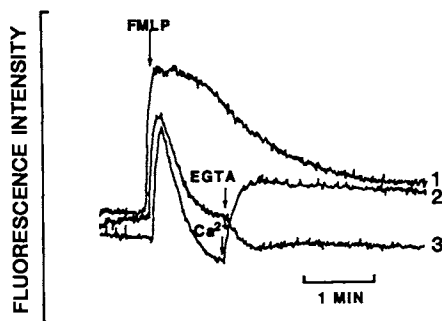


Figure 8. Sensitivity of the FMLP-induced calcium signal to hyperosmolality. Indo-1-loaded neutrophils were stimulated with  $10^{-8}$  M FMLP in a medium of high osmolality (645 mosmol/kg by addition of sodium HEPES), and indo-1 fluorescence was recorded as described in Figure 6. Trace 1: Cells in a medium with normal calcium and osmolality (reproduced from Figure 7). Trace 2: EGTA added to chelate extracellular calcium before stimulation; extracellular calcium (1.5 mM) readded 70 s after stimulation. Trace 3: Cells in a medium with normal calcium (1.5 mM); EGTA added 70 s after stimulation to chelate extracellular calcium.

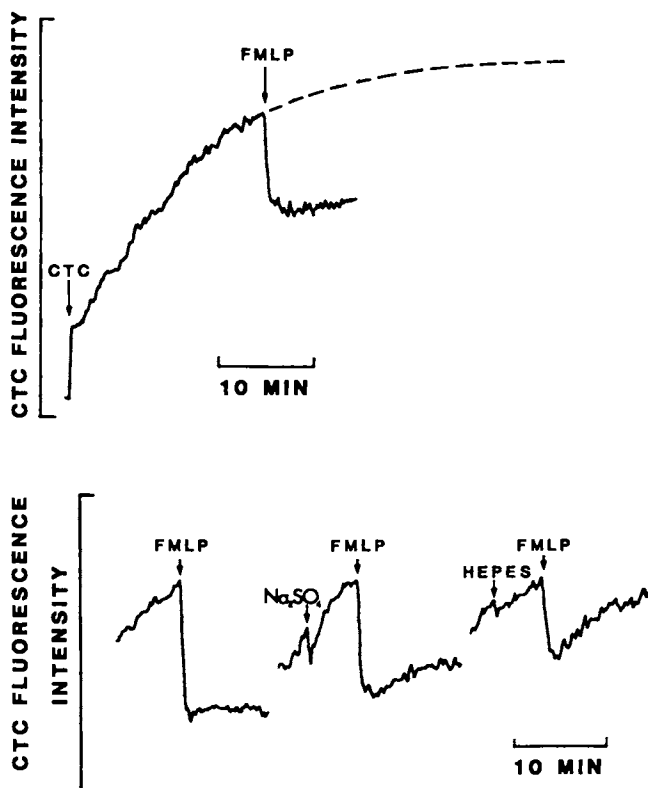


Figure 9. FMLP-induced release of intracellular calcium as monitored by CTC is not affected by hyperosmolality. Upper panel: Neutrophils were suspended in control medium containing  $20 \mu\text{M}$  CTC, and CTC fluorescence (excitation 400 nm, emission 430 nm) was monitored versus time at  $37^\circ\text{C}$ . Addition of  $10^{-8} \text{ M}$  FMLP at the arrow resulted in an abrupt decrease in CTC fluorescence. Lower panel: Increasing medium osmolality by addition of either sodium sulfate (middle trace) or sodium HEPES (right trace) had little effect on the FMLP-induced decrease in CTC fluorescence when compared to that seen in medium of normal osmolality (left trace).

Our results, here and in previous publications (22,23), show that the FMLP-induced calcium signal in neutrophils can be divided into three phases, as summarized in Figure 10. The first phase is an abrupt peak lasting up to 30 s after FMLP addition. It results from intracellular calcium release and leads to a peak cytosolic calcium signal of  $3.25 \mu\text{M}$ . The magnitude of this peak is reduced 70% in hyperosmotic media (23). The second phase consists of a broad shoulder 30 s to 90 s after stimulation. It depends on influx of extracellular calcium, presumably through receptor-gated channels, and is completely blocked at high osmolalities. The third phase, a plateau of lower but still elevated calcium levels (about  $0.4 \mu\text{M}$ ), is also dependent on extracellular calcium but is relatively unaffected by a high-osmolality medium.

The differing characteristics of these three phases suggest that FMLP initiates multiple intracellular signals, each of which controls a process that affects cytosolic calcium levels. These signals may be inositol phosphates formed during hydrolysis of phosphatidylinositol-4,5-bisphosphate, a crucial step in intracellular signaling in many cells, including neutrophils (37-39). For example, inositol-1,4,5-trisphosphate (IP3) initiates release of calcium from intracellular stores in many cells (40-42) and is probably responsible for producing the first phase of the FMLP signal. Inositol-1,3,4,5-tetrakisphosphate, a metabolite of IP3 that has been implicated in control of calcium channels in other cells (43), might initiate the second or third phase. These and other possibilities for multiple FMLP-generated signals in neutrophils will be subject to further study.

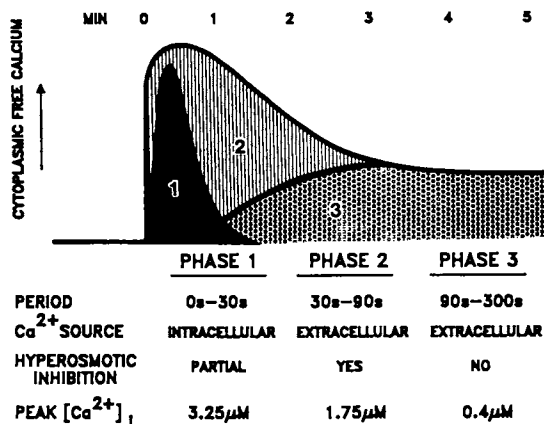


Figure 10. Three phases of the FMLP-induced calcium signal in rabbit neutrophils. (Reproduced from ref. 22. Copyright 1987 Elsevier Science Publishers, BV.)

Acknowledgment

This study was supported by NSF grant DCB-8407152 and NIH grant 1-K04-HD00619.

Literature Cited

1. Cohen, F. S.; Zimmerberg, J.; Finkelstein, A. J. *Gen. Physiol.* 1980, 75, 251-270.
2. Cohen, F. S.; Akabas, M. H.; Zimmerberg, J.; Finkelstein, A. J. *Cell Biol.* 1980, 98, 1054-1062.
3. Brown, W. M.; Pazoles, C. J.; Creutz, C. E.; Aurbach, G. D.; Pollard, H. D. *Proc. Natl. Acad. Sci. U.S.A.* 1978, 75, 876-880.
4. Hampton, R. Y.; Holz, R. W. *J. Cell Biol.* 1983, 96, 1082-1088.
5. Pollard, H. B.; Pazoles, C. J.; Creutz, C. E.; Scott, J. H.; Zinder, O.; Hotchkiss, A. J. *Biol. Chem.* 1984, 259, 1114-1121.
6. Zimmerberg, J.; Whitaker, M. *Nature (London)* 1985, 315, 581-584.
7. Zimmerberg, J.; Sardet, C.; Epel, D. *J. Cell Biol.* 1985, 101, 2398-2410.
8. Pollard, H. B.; Tack-Goldman, K.; Pazoles, C. J.; Creutz, C. E.; Shulman, N. R. *Proc. Natl. Acad. Sci. U.S.A.* 1977, 74, 5295-5299.
9. Goldstein, I.; Hoffstein, S.; Gallin, J.; Weissmann, G. *Proc. Natl. Acad. Sci. U.S.A.* 1973, 70, 2916-2920.
10. Goldstein, I. M.; Hoffstein, S. T.; Weissmann, G. *J. Immunol.* 1975, 115, 665-670.
11. Zurier, R. B.; Hoffstein, S.; Weissmann, G. *Proc. Natl. Acad. Sci. U.S.A.* 1973, 70, 844-848.
12. Hoffstein, S. T.; Goldstein, I. M.; Weissmann, G. *J. Cell Biol.* 1977, 73, 242-256.
13. Chandler, D. E.; Bennett, J. P.; Gomperts, B. D. *J. Ultrastruct. Res.* 1983, 82, 221-232.
14. Chandler, D. E.; Kazilek, C. J. *J. Cell Sci.* 1986, 83, 293-311.
15. Lew, P. D.; Wollheim, C. D.; Waldvogel, F. A.; Pozzan, T. *J. Cell Biol.* 1984, 99, 1212-1220.
16. Lew, P. D.; Monod, A.; Waldvogel, F. A.; Dewald, B.; Baggiolini, M.; Pozzan, T. *J. Cell Biol.* 1986, 102, 2197-2204.
17. Sklar, L. A.; Hyslop, P. A.; Oades, Z. G.; Omann, G. M.; Jesaitis, A. J.; Painter, R. G.; Cochrane, C. G. *J. Biol. Chem.* 1985, 260, 11461-11467.
18. White, J. R.; Naccache, P. H.; Molski, T. F. P.; Borgeat, P.; Sha'afi, R. I. *Biochim. Biophys. Res. Commun.* 1983, 113, 44-50.
19. Chandler, D. E.; Meusel, G.; Schumaker, E.; Stapleton, C. *Am. J. Physiol.* 1983, 245, C196-C202.
20. Smolen, J. E.; Korchak, H. M.; Weissmann, G. *Biochim. Biophys. Acta* 1981, 677, 512-520.
21. Stapleton, C. L.; Barnard, R. M.; Chandler, D. E. *Biochim. Biophys. Acta* 1983, 763, 225-230.
22. Chandler, D. E.; Kazilek, C. J. *Biochim. Biophys. Acta* 1987, 931, 175-179.
23. Kazilek, C. J.; Merkle, C. J.; Chandler, D. E. *Am. J. Physiol.* 1988, 254, C709-C718.
24. Gryniewicz, G.; Poenie, M.; Tsien, R. Y. *J. Biol. Chem.* 1985, 260, 3440-3450.

25. Tsien, R. Y.; Pozzan, T.; Rink, T. J. *J. Cell Biol.* 1982, **94**, 325-334.
26. Schackmann, R. W.; Chock, P. B. *J. Biol. Chem.* 1986, **261**, 8719-8728.
27. Tsien, R. Y.; Poenie, M. *Trends Biochem. Sci.* 1986, **11**, 450-455.
28. Caswell, A. H. *J. Membr. Biol.* 1972, **7**, 345-364.
29. Millman, M. S.; Caswell, A. H.; Hayes, D. H. *Membr. Biochem.* 1980, **3**, 291-315.
30. Chandler, D. E.; Williams, J. A. *J. Cell Biol.* 1978, **76**, 371-385.
31. Fabiato, A.; Fabiato, F. *Nature (London)* 1979, **281**, 146-148.
32. Gagerman, E.; Sehlin, J.; Taljedal, I.-B. *J. Physiol. (London)* 1980, **300**, 505-513.
33. Moran, D. J. *Exp. Zool.* 1984, **229**, 81-89.
34. LeBreton, G. C.; Sandler, W. C.; Feinberg, H. *Thromb. Res.* 1976, **8**, 477-485.
35. Gains, N. *Eur. J. Biochem.* 1980, **111**, 199-202.
36. Stapleton, C. L.; Mills, L. L.; Chandler, D. E. *J. Exp. Zool.* 1985, **234**, 289-299.
37. Naccache, P. H.; Sha'afi, R. I. In *New Insights Into Cell and Membrane Transport Processes*; Poste, G.; Crooke, S. T., Eds.; Plenum Press: New York, 1986; p 175-198.
38. Omann, G. M.; Allen, R. A.; Bokoch, G. M.; Painter, R. G.; Traynor, A. E.; Sklar, L. A. *Physiol. Rev.* 1987, **67**, 285-322.
39. Snyderman, R.; Smith, C. D.; Verghese, M. W. *J. Leukocyte Biol.* 1986, **40**, 785-800.
40. Berridge, M. J. *Biochem. J.* 1984, **220**, 345-360.
41. Krause, K.-H.; Schegel, W.; Wollheim, C. B.; Andersson, T.; Waldvogel, F. A.; Lew, P. D. *J. Clin. Invest.* 1985, **76**, 1348-1354.
42. Prentki, M.; Wollheim, C. B.; Lew, P. D. *J. Biol. Chem.* 1984, **259**, 13777-13782.
43. Irvine, R. F.; Moor, R. M. *Biochem. J.* 1986, **240**, 917-920.

RECEIVED August 30, 1988

## Chapter 6

# Element-Specific Epifluorescence Microscopy

### In Vivo Monitoring of Metal Biotransformations in Environmental Matrices

Todd K. Trout<sup>1,2</sup>, Gregory J. Olson<sup>1</sup>, Frederick E. Brinckman<sup>1</sup>,  
Jon M. Bellama<sup>2</sup>, and Robert A. Faltynek<sup>1</sup>

<sup>1</sup>Ceramics Division, National Bureau of Standards,  
Gaithersburg, MD 20899

<sup>2</sup>Department of Chemistry and Biochemistry, University of Maryland,  
College Park, MD 20899

Quantitative measurement of metal ion uptake in living cells is accomplished via staining the biota with an appropriate fluorogenic ligand, determining the emission photon flux by epifluorescence microscopy imaging (EMI), and relating the latter quantity to absolute metal ion concentration by atomic absorption analysis. By thus combining the techniques of element-specific fluorimetry and EMI, it is possible to observe the chemistry occurring during redox transformations of elements by colonies of living cells in reactions that have significant economic potential. The strengths, weaknesses, and future directions to be taken in improving this analytical method are discussed.

Life processes ultimately depend on the transport and reactivity of chemical elements and compounds. Modern biological studies have elegantly unraveled the complicated carbon-based metabolic cycles that are essential to the maintenance of many living things. Certain life forms, however, are energized by reduction-oxidation chemistry based upon elements other than carbon. For example, Sulfolobus and Thiobacillus bacteria utilize the oxidation of sulfide to sulfate to drive their metabolism (1,2). An important concomitant reaction during energy extraction from sulfide oxidation involves the disposition of the counter ion. Sulfide sources other than H<sub>2</sub>S contain metallic cations that are released into solution during the energy deriving process (3). Thus, the by-products from these natural transformations are an attractive source of rare or difficultly separated metals. For example, copper and uranium mine tailings containing low levels of the desired elements in pyritic matrices can be bioprocessed continuously by thiobacilli and other bacteria that turn insoluble sulfides into water soluble sulfates (4,5). Collection and concentration of aqueous runoff from mine tailings can therefore result in economic acquisition of strategic elements.

We bring up the above example of natural bioprocessing as a background to an important scientific question: how does one study

0097-6156/89/0383-0084\$06.00/0

© 1989 American Chemical Society

the detailed chemistry occurring around a specific element as it transforms *in vivo*? In the case of ore leaching bacteria, it would be of great interest to follow changes in coordination number, ligand type, and oxidation state that the natural process of sulfide oxidation imposes on a metal center. In a broader sense, there are many intriguing processes whereby ligand exchange and redox chemistry are apparently catalyzed by the workings of living organisms, but little indication of their mechanistic details have appeared due to a lack of methodology for *in vivo* study. Destructive techniques have been widely applied to determine the concentration of key elements in cells and other biota, but beside being incapable of use *in vivo*, they offer no information on the chemical nature of the element in question. For example, acid digestion of cells which have accumulated various organotin species, and subsequent traditional analysis by atomic absorption (AA) spectroscopy or element-specific spectrofluorimetry, will produce quantitative data on the amount of tin present, but will reveal nothing about the coordination environment of the metal on the cell surface prior to destruction.

With clear recognition that *in vivo* monitoring of chemical processes in biota must be as non-invasive and non-perturbing as possible, and that information should be obtained on specific chemical species rather than general chemical content, our group has begun development of techniques directed towards these ends. The method involves epifluorescence microscopy imaging (6) (EMI) of ions, employing ligands that are fluorogenic for the elements under consideration. Our approach is first to demonstrate that elements on cell surfaces can be qualitatively and quantitatively measured by EMI without destruction of the organism. As described below, the next step is to attain selective measurement of specific bond types and geometries via fluorogenic ligand design and proper choices of excitation or emission wavelength. Finally, we anticipate obtaining more detailed information on the environmental changes promoted on cell surfaces and substrates during processing by coupling EMI to microscopic Fourier transform infrared (FT-IR) analysis. We have previously shown that EMI employing fluorogenic ligands can be used as an on-line detector for HPLC (7). Our plan is, accordingly, to provide a bridge between element specific fluorometric analysis and quantitative, non-destructive determination of element uptake and distribution in living cells involved in bioprocessing.

#### Experimental (8)

##### Description of the Epifluorescence Microscopy Imaging (EMI) System.

A schematic diagram of the EMI system is given in Figure 1. Excitation and emission monochromators, microscope optics, and photomultiplier assemblies are products of Carl Zeiss GMBH, German Federal Republic. Computer control is via an IBM PC-XT microcomputer employing proprietary Zeiss software packages  $\lambda$ -Scan and MPP. All relative emission intensity values represent the average of at least 10 readings, with each reading being the average of 40 photomultiplier tube (PMT) measurements. All spectra are obtained with 1 nm resolution, with at least 20 PMT measurements averaged at each nm. Excitation radiation is provided by an Osram HBO 100 Super Pressure mercury lamp. Stepping motors are part of a

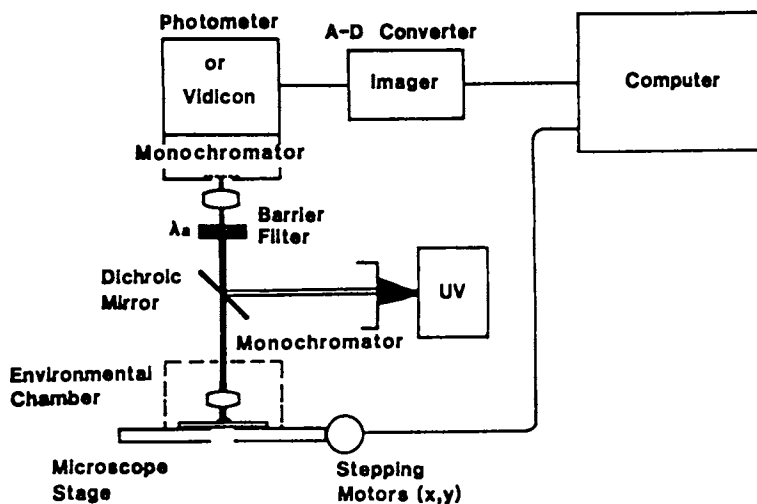


Figure 1. Schematic diagram for the Zeiss epifluorescence microscopy imaging system.



moveable stage designed in collaboration with Ealing Optical for precise translation of samples from the EMI apparatus to an adjacent FT-IR microscopy bench (vide infra).

The key features of the EMI system are the monochromators and PMT assembly, since the former allow for minor variations in excitation or emission wavelength that may be necessary to differentiate lumophores of closely related structure, and the latter provides a means of quantitating luminescent species under study. Each monochromator has a resolution capability of 1 nm, and we anticipate that by careful selection of excitation ( $\lambda_{ex}$ ) and emission ( $\lambda_{em}$ ) wavelengths, it will be possible to distinguish chemical centers that vary only by oxidation state or ligand type, rather than by elemental composition.

**Cultural Conditions.** *Pseudomonas fluorescens* strain 244 (Ps. 244) was obtained from Professor R.R. Colwell of the University of Maryland, College Park. The organism was cultured in Nelson nutrient broth (9) in Erlenmeyer flasks on a rotary shaker operated at 200 rpm and held at 29°C. Cells were harvested during the exponential growth phase and were washed twice with 10.0 mM piperazine N,N'-bis(2-ethanesulfonic acid) buffer (10) (PIPES), pH = 7.6. Cell density was controlled by first photometrically measuring the optical densities of the harvested cell suspensions employing a Klett-Summerson photometer (blue #42 filter), then diluting the cells with PIPES to a constant concentration of 4-6 mg cell dry weight/ml. cell suspension.

**Tin Analysis.** Measured quantities of Ps. 244 cells (4.0-6.0 mg dry weight) were exposed to 10.0 ppm tin solutions of the  $Bu_xSn^{(4-x)+}$  series (Bu = n-butyl group, x = 0,1,2,3) for at least 60 minutes, with the exception of experiments measuring the kinetics of tin uptake (vide infra). The cells were collected by centrifugation, and washed twice with 2.0 mL aliquots of PIPES. The cells were suspended in 1.0 mL of PIPES and were combined with 0.50 mL of  $5.0 \times 10^{-3}$  M flavonol (Aldrich) in EtOH, unless the concentration of flavonol was being systematically varied (see Results, Table I). Flavonol has been used widely as a fluorogen for tetravalent tin (11-13). The cells were collected by centrifugation, rewashed, and then suspended in 0.30 mL PIPES for EMI analysis in an optical quartz cell of approximately 0.5 mm pathlength. Luminescence data were collected through either a 63x oil immersion objective or a 40x hi-dry objective, employing the 366 nm mercury emission as  $\lambda_{ex}$ . Relative emission intensity measurements were made at 475 nm for tin analysis, the emission maximum for the tin-flavonol complexes examined in this work. Emission spectra are uncorrected.

In order to derive a quantitative relation between emission intensity as measured by EMI and actual metal content, cell samples were subjected to graphite furnace atomic absorption (GFAA) analysis (14). Atomic absorption experiments were performed both on cells which had been stained with a fluorescent reagent and on cells not exposed to a luminophore. After EMI analysis, 50  $\mu$ L of cell suspension were withdrawn from the 0.30 mL of sample used for EMI and were digested in 150  $\mu$ L of concentrated  $HNO_3$  for 90 minutes at 85°C. These solutions were then diluted to 1/10 of their concentration with deionized water, and the 150  $\mu$ L of these diluted

samples were combined with 50  $\mu\text{L}$  of 0.20M  $\text{K}_2\text{Cr}_2\text{O}_7$  prior to GFAA analysis. The purpose of the dichromate was to serve as a matrix modifier which enhances the sensitivity of GFAA towards the detection of tin (15). All GFAA measurements were acquired using a Perkin Elmer 460 Graphite Furnace Atomic Absorption Spectrometer. Protocol for tin GFAA analysis of the stained biota included drying at 85°C for 50s, ashing at 500°C for 10s, and atomizing at 2700°C for 6s. Absorption was measured at 225.7 nm. Similar methodology was employed for GFAA analysis of tin treated cell samples which were not exposed to flavonol, however it was seen that in these cases the dichromate matrix modification was not necessary.

Known concentrations of  $\text{Sn}^{4+}$  solutions were spiked into acid digested samples of *Ps. 244* which had been exposed to 10 ppm solutions of  $\text{Bu}_x\text{Sn}^{(4-x)+}$  ( $x = 0,1,2,3$ ). Atomic absorption analysis of these samples allowed for the calculation of the amount of tin accumulated on the cell by the method of multiple additions (16).

Substrates other than free cells were also examined for luminescence activity in the presence of tin and flavonol. For example, glass slides covered with a well-developed but uncharacterized biofilm growth were exposed to  $4.5 \times 10^{-4}$  M n-butyltin trichloride in ethanol for 60 min. The slides were subsequently rinsed with ethanol and exposed to  $1.4 \times 10^{-4}$  M flavonol for 15 min prior to EMI analysis. Controls containing either flavonol or organotin alone were prepared and analyzed for luminescence activity to complete the study. In a purely inorganic experiment, glass particles of 10-100  $\mu\text{m}$  diameter surface treated with sulfhydryl groups by Dr. W. Haller of the National Bureau of Standards were exposed first to aqueous  $\text{SnCl}_4$  solution, and then to flavonol in ethanol. Emission spectra of the surface-bound tin-flavonol complex were obtained by EMI.

**Zinc Analysis.** For EMI of zinc accumulation of *Ps. 244*, the ligand salicylaldehyde-2-quinolyldihydrazone (SAQH) was used. The SAQH was prepared by refluxing salicylaldehyde (Aldrich) with 2-hydrazinoquinoline (Kodak) as described by Sommer *et al.* (17). In methodology analogous to the tin work described above, known quantities of biomass were exposed to 1.0-30.0 ppm aqueous solutions of  $\text{ZnBr}_2$ . Cell samples were periodically withdrawn from the zinc solution in attempts to measure the kinetics of accumulation of the metal. For EMI analysis cells were suspended in 0.20 mL PIPES and were then treated with 0.10 mL of  $3.0 \times 10^{-3}$  M SAQH in EtOH. The cell samples were then rewashed and resuspended in 0.30 mL PIPES for EMI analysis ( $\lambda_{ex}=366$  nm,  $\lambda_{em}=498$  nm).

After EMI analysis, 50  $\mu\text{L}$  aliquots of cell suspensions were removed from the 0.30 mL samples and were digested as described in the above section of this report. A much higher sensitivity was observed for GFAA analysis of zinc solutions than was seen for solutions containing tin. Solutions of digested cell samples exposed to zinc had to be diluted by more than an order of magnitude more than solutions of cells which accumulated tin. Protocol for zinc GFAA analysis included drying at 85°C for 25s, ashing at 450°C for 25s, and atomizing at 2500°C for 6.5s. Absorption was measured at 212.9 nm.

Cell suspensions which were exposed to 1.0 ppm zinc were combined, and to this matrix known amounts of  $Zn^{2+}$  were added, to allow measurement of the amount of zinc accumulated by the cells via GFAA. In related work, cells treated with known concentrations of zinc solutions were systematically combined and thereby "diluted" with cells not exposed to zinc, to determine if GFAA and EMI analyses yield confirmatory results.

### Results and Discussion

Tin Analysis. Figures 2, 3 and 4 illustrate typical emission spectra obtained in the characterization of  $Sn^{4+}$ /flavonol interactions. As seen in Figure 2, the free ligand ( $5.0 \times 10^{-3}$  M) in ethanol in the absence of tin exhibits an emission maximum at 555 nm upon 366 nm excitation. Figures 3 and 4 show emission spectra of the  $Sn^{4+}$ /flavonol complex on irregularly shaped glass beads of 10-100  $\mu m$  diameter, and of  $BuSn^{3+}$ /flavonol accumulated by Pseudomonas 244 cells respectively. The glass bead study serves as a model of tin adhesion to a small heterogeneous surface from which spectra can be directly obtained only by microspectrofluorometric techniques. In vivo spectra of complexed tin on Pseudomonas 244 are essentially identical to those of the glass bead model system, exhibiting an emission maximum at 475 nm. A lower intensity residual peak at 550 nm in Figure 4 is due to uncomplexed flavonol, which was not completely removed from the cell membrane despite multiple washings.

The effect of variation of the molar ratio of ligand to metal ( $[L]:[M]$ ) present in a homogeneous solution on the emission intensity of the  $Sn^{4+}$ /flavonol complex is large (11). In order to measure the magnitude of this effect on the surface of a cell, relative emission intensity measurements at 457 nm were made on a series of Ps. 244 subsamples after primary treatment with equimolar concentrations of  $Sn^{4+}$  (10 ppm) followed by systematic variation of the concentration of flavonol to which they were exposed. Data are presented in Table I. It has been shown that a 1:1 complex is formed in solution between  $Sn^{4+}$  and flavonol (10). Those results are substantiated here, since at ligand:metal molar ratios ( $[L]:[M]$ ) much lower than 1:1 (samples 6-10) the luminescence intensity of the sample is diminished. Sample 1 indicates that flavonol which is not bound to accumulated tin does not give a significant emission at 457 nm, and sample 2 shows that excess flavonol either masks excitation or emitted radiation, or it may competitively bind and remove a fraction of the tin from the cell. Table I indicates that most of the tin in solution is accumulated by the cells and that the tin in solution is available for complexing, given that the maximum emissions are the samples which have nearly 1:1  $[L]:[M]$  ratios calculated by the concentrations of tin and flavonol to which the cell was exposed. Later work described in this report verifies that the capability of Ps. 244 to accumulate  $Sn^{4+}$  is sufficient to have removed essentially all of the tin from this solution. Sample 10 shows that the cells themselves, even upon treatment with tin, have little luminescence as compared to flavonol treated cells.

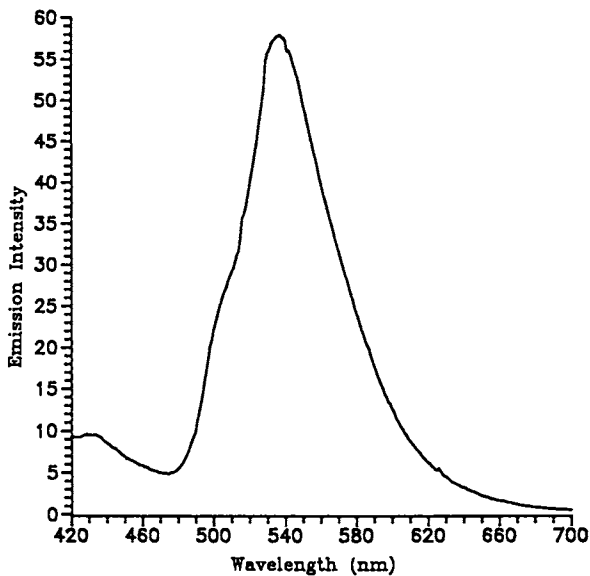


Figure 2. Emission spectrum of  $5.0 \times 10^{-3}$  M flavonol in ethanol.  
 $\lambda_{ex} = 366$  nm.

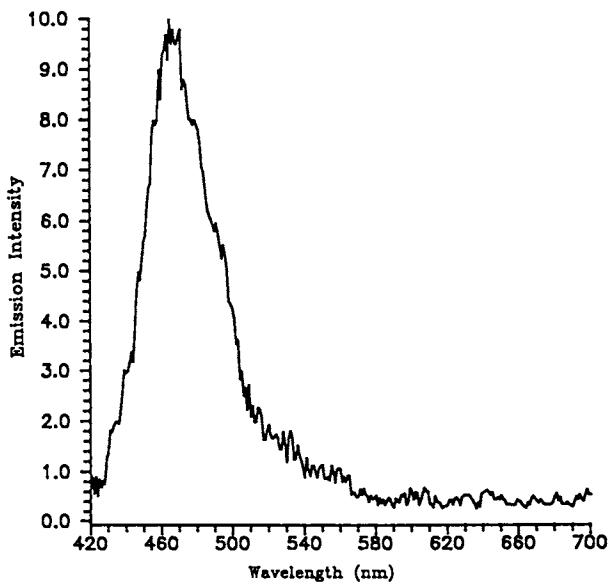


Figure 3. Emission spectrum of 10-100  $\mu$ m surface sulfhydryl derivatized glass beads following treatment with aqueous  $1.0 \times 10^{-3}$  M  $\text{SnCl}_4$  and ethanolic  $5.0 \times 10^{-3}$  M flavonol.  $\lambda_{ex} = 366$  nm.

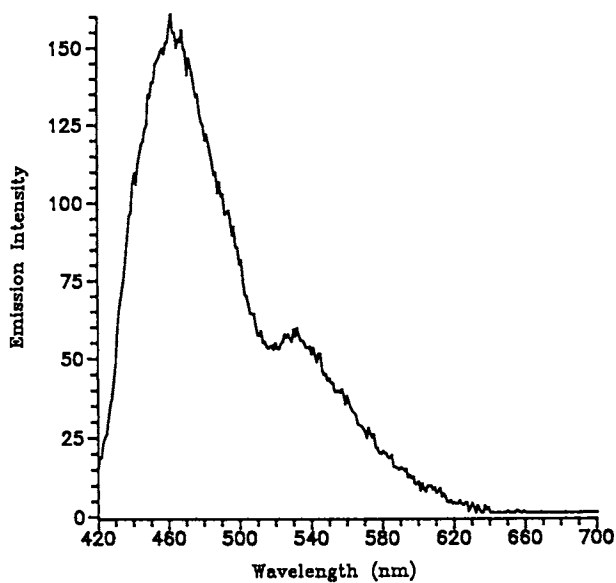


Figure 4. Emission spectrum of *Pseudomonas* 244 following treatment with aqueous  $2.0 \times 10^{-5}$  M n-butyltrichlorotin and 50% ethanolic  $1.0 \times 10^{-3}$  M flavonol.  
 $\lambda_{\text{ex}} = 366$  nm.

Table I. Variation of the Molar Ratio of [Flavonol]/[Sn<sup>4+</sup>] Applied to the Cells

Sample	mmoles Sn(IV)	mmoles Flavonol	Rel. Intensity at $\lambda(\text{em}) = 457$
1	0	$1.0 \times 10^{-4}$	10.58
2	$8.0 \times 10^{-5}$	$5.0 \times 10^{-4}$	53.23
3	$8.0 \times 10^{-5}$	$2.5 \times 10^{-4}$	87.61
4	$8.0 \times 10^{-5}$	$1.3 \times 10^{-4}$	75.93
5	$8.0 \times 10^{-5}$	$1.0 \times 10^{-4}$	83.35
6	$8.0 \times 10^{-5}$	$5.0 \times 10^{-5}$	54.65
7	$8.0 \times 10^{-5}$	$3.0 \times 10^{-5}$	36.22
8	$8.0 \times 10^{-5}$	$2.0 \times 10^{-5}$	23.92
9	$8.0 \times 10^{-5}$	$5.0 \times 10^{-6}$	12.19
10	$8.0 \times 10^{-5}$	0 . 0	0.33

The rate of Sn<sup>4+</sup> accumulation was monitored by treating cells with 10 ppm Sn<sup>4+</sup> at a time  $t = 0$  s, and periodically withdrawing uniform volumes of cell suspensions from the reaction container by micropipet, centrifuging the cells, washing the cells and staining the cells as described above then resuspending the cells in PIPES for EMI analysis. Figure 5 displays these data. Most of the Sn<sup>4+</sup> is accumulated in the first 4 minutes of exposure to Sn<sup>4+</sup>, in agreement with our earlier GFAA work (18). The EMI results are corroborated by GFAA results, obtained on the same samples after acid digestion. The similarity between these two curves suggests that our EMI methodology is a valid quantitative technique; the largest source of error appears to be in the pipetting of the cell suspensions, given the congruency of the minor fluctuations of the two curves.

Pseudomonas 244 cells were exposed to Bu<sub>x</sub>Sn<sup>(4-x)+</sup> ( $x = 0,1,2,3$ ) to compare the relative affinities the cells had for the differing species. The cells were exposed to 10 ppm solutions of the various tin species for over 2½ hours. After treating the cells with Sn<sup>4+</sup>, one half of the cells were analyzed by GFAA, the other half by EMI. GFAA results are contrasted to EMI results in Table II.

Table II. Relative Atomic Absorbance and Luminescence Intensities (at 457 nm) of Various Butyltin Moieties Accumulated on Cells

Sample	Relative GFAA	Relative EMI
Sn <sup>4+</sup> /flavonol	842	40.29
BuSn <sup>3+</sup> /flavonol	258	7.69
Bu <sub>2</sub> Sn <sup>2+</sup> /flavonol	100	6.23
Bu <sub>3</sub> Sn <sup>+</sup> /flavonol	155	-0.95
no tin added/flavonol	0	0.00

In general, adding organic groups to the tin appears to lessen the affinity of Pseudomonas 244 for the metal. This may be related to the relative toxicity of the organotin derivatives, as Bu<sub>3</sub>Sn<sup>+</sup> is the

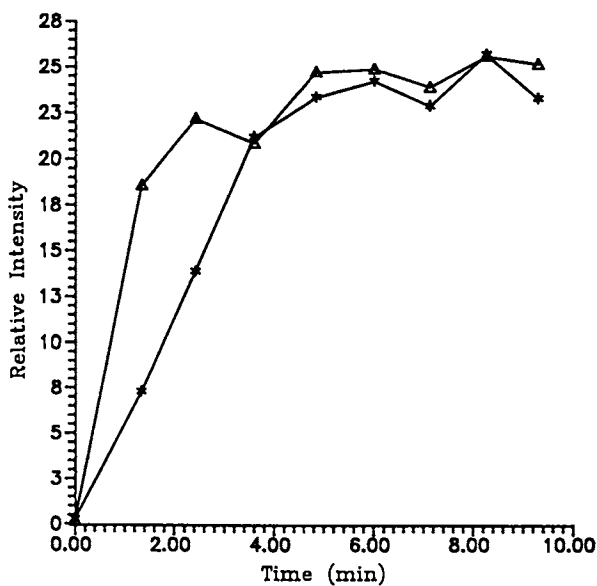


Figure 5. Kinetics of  $\text{Sn}^{4+}$  uptake by *Pseudomonas* 244 measured by EMI ( $\Delta$ ) and GFAA (\*) [ $\text{Sn}^{4+}$ ]<sub>0</sub> = 10 ppm in water.

most toxic species in this series of compounds (19). Tributyltin does not exhibit fluorescent properties with flavonol (20). The acid digested cell samples were combined, and by spiking known concentrations of  $\text{Sn}^{4+}$  solution into the digested cell matrix, GFAA analysis showed that the cells had accumulated about 1.6 mg of tin species/g cell dry weight.

Graphite furnace atomic absorption analysis of acid digested Ps. 244 cells exposed to the  $\text{Bu}_x\text{Sn}^{(4-x)+}$  ( $x=0,1,2,3$ ) series gave somewhat different results of relative accumulation and absolute metal content if the GFAA examination was preceded by EMI analysis. It was shown by GFAA that nearly a five-fold reduction in tin content was found in the cells which were treated with flavonol and subsequently rewashed several times as opposed to cells washed without prior treatment with flavonol. This corroborates data in Table I which suggest that flavonol can compete with coordination sites on the cell membrane for the tin. The flavonol ligand may preferentially chelate and thereby remove certain  $\text{Bu}_x\text{Sn}^{(4-x)+}$  species over others, thereby changing the apparent relative affinities for uptake between Ps. 244 and each species.

As a further example of the usefulness of EMI, we demonstrated the ability to image accumulation of  $\text{BuSn}^{3+}$  by a biofilm consisting of a mixed population of estuarine bacteria. The biofilms were grown on the surfaces of glass slides for two weeks. One of the slides was exposed to flavonol, but no tin. The emission spectrum resulting from the material on the slide, Fig. 6, indicates a relatively minor emission at 457 nm, the emission maximum for tin/flavonol complexes. A similar biofilm imaged after primary treatment with  $\text{BuSnCl}_3$  prior to staining with flavonol clearly displayed a more intense blue emission, Fig. 6, showing that the extant organisms adsorbed  $\text{BuSn}^{3+}$  from solution.

**Zinc Analysis.** *Pseudomonas* 244 was exposed to 27 ppm  $\text{Zn}^{2+}$  by combining 3.0 mL of cell suspension with 0.30 mL of 300 ppm aqueous  $\text{ZnBr}_2$ . The cells were allowed to accumulate  $\text{Zn}^{2+}$  for 5 hours. The  $\text{Zn}^{2+}$  treated cells were then combined with cells that were not exposed to zinc in systematically varied proportions by micropipet. These sample were centrifuged, and to each sample 0.20 mL of PIPES and 0.10 mL of  $3.0 \times 10^{-3}$  M SAQH were added, representing approximately a 3:1 [L]:[M] ratio in the sample containing only zinc treated cells. The cells were washed and analyzed by EMI, then digested and analyzed by GFAA as described earlier in this paper. Results are displayed in Figure 7. Again, a strong correlation is noted between results obtained by GFAA and EMI.

Several attempts were made to monitor the uptake of  $\text{Zn}^{2+}$  as a function of time. As a first attempt, the cells were exposed to 30 ppm  $\text{Zn}^{2+}$  at room temperature. The rate of uptake of the  $\text{Zn}^{2+}$  by the cells was much faster than was the case with  $\text{Sn}^{4+}$ ; it was impossible to measure an increase in zinc content of the cells above that of the initial  $\text{Zn}^{2+}$ -exposed sample either in fluorescence signal or GFAA signal by the methods described in this work. Reducing both the concentration of  $\text{Zn}^{2+}$  in solution (10 ppm and 1 ppm) and the temperature ( $0^\circ$ ) did not slow down the uptake process enough to monitor an increase in accumulated  $\text{Zn}^{2+}$ . By addition of known concentrations of  $\text{Zn}^{2+}$  to the cells exposed to a 1.0 ppm  $\text{Zn}^{2+}$  solution, it was found by GFAA that the amount of zinc accumulated



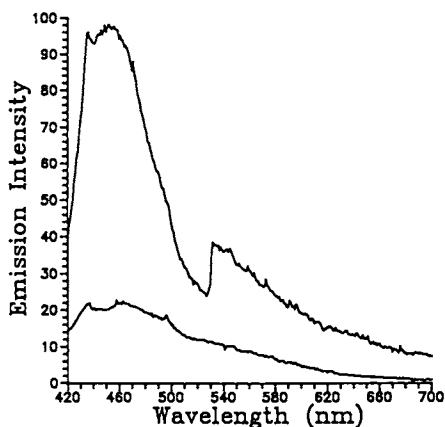


Figure 6. Emission spectra from biofilms of estuarine bacteria exposed to ethanolic  $4.5 \times 10^{-4}$  M n-butyltrichlorotin and ethanolic  $1.4 \times 10^{-4}$  M flavonol (upper trace) and to flavonol only (lower trace).

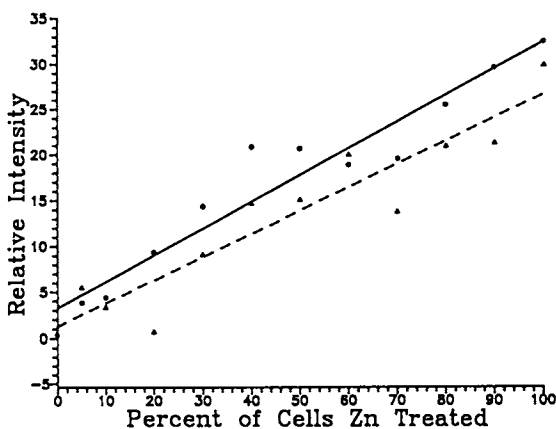


Figure 7. Correlation of EMI (▲) and GFAA (●) analysis for  $Zn^{2+}$  uptake by *Pseudomonas* 244.

by the Ps. 244 represented 0.36% of the dry mass of the organism. This analysis was performed after staining the biota with SAQH for EMI analysis. We have not evaluated whether SAQH reacts with  $Zn^{2+}$  intracellularly or only on the cell surface. Prior work has shown that tributyl- (17) and tripropyl- (21) tin binding is a chemical adsorption process rather than active transport.

### Conclusions and Future Directions

We have shown that the EMI technique is applicable to identification of cations in living cells and on other heterogeneous matrices. Strong correlations between emission intensity and compositional data from AA indicate that working curves can be generated for direct quantitative elemental analysis in living organisms in an essentially nondestructive fashion. The coupling of microscopy and traditional spectrofluorometric analysis represents a technique for following elemental uptake and disposition during bioprocessing.

Significant challenges remain in fine tuning the EMI technique to the point of obtaining chemical species selectivity. An obvious approach to the problem is to design new fluorogenic ligands that selectively complex to metal centers having differing chemical characteristics. For example, more highly substituted flavones may complex selectively with inorganic tin rather than with bulky organotins due to steric restrictions. The same argument can be used to potentially differentiate oxidation states: larger ligands may have more affinity toward lower oxidation state, larger ionic radius cations. Further need for novel ligand design is illustrated by the shortcomings of 3-hydroxyflavone itself. Although the ligand forms strongly emitting complexes with tin, it also forms luminescent compounds with many other elements, such as Zr(IV), Hf(III), Th(IV), Al(III) (22), Y(III) and In(III) (23). The fluorogenic ligand is not soluble in water alone, and it is arguable that the introduction of ethanol as a solvent makes the technique less than nondestructive. These points of concern apply as well to other fluorogenic ligands routinely used in spectrofluorimetric analysis, making ligand design a crucial factor in developing a more selective, less invasive EMI technique.

Another aspect of ligand design relates to efficient use of the precision emission and excitation monochromators in the EMI system. It would be of value to have a family of ligands exhibiting varying emission or excitation wavelengths, while all being selective for a single metal. In this manner, it might be possible to observe the imaging of different coordinate forms of the metal in question by choosing the proper  $\lambda_{ex}$  or  $\lambda_{em}$ .

In order to assess bond specific chemical changes occurring in matrices containing living cells, we are in the process of linking the EMI system to an Analect AQS-20 FT-IR spectrometer via a precision positioning stage. The strategy is to examine a substrate site by FT-IR microscopy and EMI prior to biota inoculation, and then reexamine the same location after bioleaching or bio-induced chemistry takes place. In this fashion, information on by products or chemical uptake from substrate can be obtained. We note that the wavelength limitation of infrared radiation makes it impossible to probe sub-cellular sites for specific vibrational frequencies.

Literature Cited

1. Brock, T.D. Thermophilic Microorganisms and Life at High Temperatures; Springer-Verlag: New York, 1978; pp 149-152.
2. Roy, A.B.; Trudinger, P.A. The Biochemistry of Inorganic Compounds of Sulfur; Cambridge University Press: Cambridge, 1970; pp 326-327.
3. Kelly, D.P.; Norris, P.R.; Brierley, C.L. In Microbial Technology: Current State and Future Prospects; (Bull, A.T.; Ellwood, D.C.; Ratledge, C., Ed.; Cambridge University Press: Cambridge, 1979; pp 263-308.
4. Olson, G.J.; Kelly, R.M. Biotechnol. Prog. 1986, **2**, 1.
5. Primrose, S.B. Modern Biotechnology; Blackwell Scientific Publications: Oxford, 1987; pp 83-84.
6. Siegel, J.I. Am. Lab. 1982, **14**(4), 65.
7. Blair, W.R.; Parks, E.J.; Olson, G.J.; Brinckman, F.E.; Valeiras-Price, M.C.; Bellama, J.M. J. Chromatogr. 1987, **410**, 383.
8. Certain commercial materials and equipment are identified in this report in order to adequately specify the experimental procedures. In no case does such identification imply recommendation or endorsement by the National Bureau of Standards, nor does it imply that the material or equipment identified is necessarily the best available for the purpose.
9. Nelson, J.D.; Blair, W.; Brinckman, F.E.; Colwell, R.R.; Iverson, W.P. Appl. Microbiol. 1973, **26**, 321.
10. Good, N.E.; Winget, D.; Winter, W.; Connoly, T.N.; Izawa, S.; Singh, R.M.M. Biochemistry 1966, **5**, 467.
11. Coyle, C.F.; White, C.E. Anal. Chem. 1957, **29**, 1486.
12. Blunden, S.J.; Chapman, A.H. Analyst 1978, **103**, 1266.
13. Vernon, F. Analytica Chim. Acta. 1974, **71**, 192.
14. Koirtzohann, S.R.; Kaiser, M.L. Anal. Chem. 1982, **54**, 1515A.
15. Parks, E.J.; Blair, W.R.; Brinckman, F.E. Talanta 1985, **32**, 633.
16. O'Haver, T.C. In Trace Analysis: Spectroscopic Methods for Elements; Winefordner, J.D., Ed.; Wiley-Interscience: New York, 1976; pp 41-42.
17. Sommer, L.; Maung-Gyee, W.P.; Ryan, D.E. Scripta Fac. Sci. Nat. Ujep Brunensis, Chemia 2 1972, **2**, 115.
18. Blair, W.R.; Olson, G.J.; Brinckman, F.E.; Iverson, W.P. Microb. Ecol. 1982, **8**, 241.
19. Evans, C.J.; Smith, P.J. J. Oil Col. Chem. Assoc. 1975, **58**, 160.
20. Blunden, S.J.; Smith, P.J. J. Organomet. Chem. 1982, **226**, 157.
21. Yamada, J.; Tatsuguchi, K.; Wantanabe, T. Agric. Biol. Chem. 1987, **42**, 1867.
22. Alford, W.C.; Shapiro, L.; White, C.E. Anal. Chem. 1951, **23**, 1149.
23. Results of this group, to be published.

RECEIVED September 22, 1988

## Chapter 7

# Luminescence Standards for Macro- and Microspectrofluorometry

Rance A. Velapoldi and Michael S. Epstein

Center for Analytical Chemistry, National Bureau of Standards,  
Gaithersburg, MD 20899

Requirements for standards used in macro- and micro-spectrofluorometry differ, depending on whether they are used for instrument calibration, standardization, or assessment of method accuracy. Specific examples are given of standards for quantum yield, number of quanta, and decay time, and for calibration of instrument parameters, including wavelength, spectral responsivity (determining correction factors for luminescence spectra), stability, and linearity. Differences in requirements for macro- and micro-standards are considered, and specific materials used for each are compared. Pure compounds and matrix-matched standards are listed for standardization and assessment of method accuracy, and existing Standard Reference Materials are discussed.

The inherent sensitivity and selectivity of spectrofluorometry, coupled with the advances in electro-optical components and computers, has led to the wide use of spectrofluorometry during the last three decades in diverse areas of analysis, including analytical chemistry, cellular biology, geochemistry, and mail sorting systems. The information obtained from these measurements has had a profound impact on all of these areas, for example, in assessing molecular interactions used for qualitative and quantitative analyses, chromatographic separations, cellular make-up and interactions, molecular volume, rotation and diffusion coefficients for large molecules, determination of porosities of geologic samples on a micro- and macro-scale, photochemical and kinetic processes, and energy transformation/conversion.

In general, luminescence measurements are relative rather than absolute, since the instrument characteristics and sample properties that determine the fluorescence intensities are often not well defined. Absolute luminescence measurements are difficult to perform and require time and instrumentation not available in most laboratories. Thus, luminescence measurements rely heavily on standards to determine instrument responses and parameters, the chemical composition of samples, and the characteristics of chemical systems. To

This chapter not subject to U.S. copyright  
Published 1989 American Chemical Society

avoid inaccuracy and confusion in luminescence measurements and data interpretation, reliable standards are needed.

*Definition and Uses of Standards.* In the context of this paper, the term "standard" denotes a well-characterized material for which a physical parameter or concentration of chemical constituent has been determined with a known precision and accuracy. These standards can be used to check or determine (a) instrumental parameters such as wavelength accuracy, detection-system spectral responsivity, and stability; (b) the instrument response to specific fluorescent species; and (c) the accuracy of measurements made by specific instruments or measurement procedures (assess whether the analytical measurement process is in statistical control and whether it exhibits bias). Once the luminescence instrumentation has been calibrated, it can be used to measure the luminescence characteristics of chemical systems, including corrected excitation and emission spectra, quantum yields, decay times, emission anisotropies, energy transfer, and, with appropriate standards, the concentrations of chemical constituents in complex samples.

Several books and symposium proceedings on luminescence standards and measurements have been published in the last several years, including: "Advances in Standards and Methodology in Spectrophotometry" (1), "Measurement of Photoluminescence" (2), "Standards in Fluorescence Spectrometry" (3), and "Modern Fluorescence Spectroscopy" (Volumes 1-4) (4). These books, the references within them, and the classic in the field, "Photoluminescence of Solutions" by C.A. Parker (5), provide the researcher with extensive information about luminescence standards and measurements.

In this chapter, we will review luminescence standards for macrospectrofluorometry and extend the discussion to standards for microspectrofluorometry. The term "luminescence" includes both fluorescence and phosphorescence; however, we will continue to use generally accepted terminology such as "spectrofluorometry" or "microspectrofluorometer," even though "spectroluminimetry" might be more representative or "luminescence spectrometer for measurements on a microscale" might be more correct (6). Although macrospectrofluorometric standards are discussed first, the comments basically hold for microspectrofluorometric standards, except in the special areas of stability and size and shape, which will be discussed later.

#### *Macrospectrofluorometric Standards*

*Requirements of Standards.* The general requirements for luminescence standards have been discussed extensively (3,7-9) and include stability, purity, no overlap between excitation and emission spectra, no oxygen quenching, and a high, constant quantum yield independent of excitation wavelength. Specific system parameters--such as the broad or narrow excitation and emission spectra, isotropic or anisotropic emission, solubility in a specific solvent, stability (standard relative to sample), and concentration--almost require the standard to be in the same chemical and physical environment as the sample. In the ideal case, the standard and the sample should be the same chemical in the same matrix. The best we can hope for is a judicious choice of well-characterized standards to cover most measurement situations. At the same time, the researcher and user must be aware

of the correct application of the standards and the limitations inherent in luminescence spectrometers and standards.

*Functions of Standards.* Fluorescent standards can be used for three basic functions: calibration, standardization, and measurement method assessment. In calibration, the standard is used to check or calibrate instrument characteristics and perturbations on true spectra. For standardization, standards are used to determine the function that relates chemical concentration to instrument response. This latter use has been expanded from pure materials to quite complex standards that are carried through the total chemical measurement process (10). These more complex standards are now used to assess the precision and accuracy of measurement procedures.

*Calibration.* In general, standards used for instrument calibration are physical devices (standard lamps, flow meters, etc.) or pure chemical compounds in solution (solid or liquid), although some combined forms could be used (e.g.,  $Tb^{3+} + Eu^{3+}$  in glass for wavelength calibration). Calibrated instrument parameters include wavelength accuracy, detection-system spectral responsivity (to determine corrected excitation and emission spectra), and stability, among others. Fluorescence data such as corrected excitation and emission spectra, quantum yields, decay times, and polarization that are to be compared among laboratories are dependent on these calibrations. The instrument and fluorescence parameters and various standards, reviewed recently (1,2,11), are discussed briefly below.

*Wavelength.* Three types of standards used for wavelength calibration are narrow-spectral-line low-pressure discharge sources and lasers; organic and inorganic species in solution; and narrow bands from the excitation sources (Xe, Hg) (e.g., see Refs. 11-16). For wavelength accuracies approaching 0.1 nm, narrow-line sources are recommended; several are listed in Table I. A few lines or many lines covering the wavelength region of interest can be used (17).

Procedures for calibrating both monochromators in a fluorescence spectrometer using narrow line sources have been discussed (15,18); care must be taken with placement of the calibration source.

For ease of use and wavelength accuracies of 1-2 nm, organic materials or inorganic ions in solution have been recommended as standards (Table II). However, these must be used carefully because (a) the peak maxima are matrix dependent, (b) narrow instrumental bandpasses are necessary, (c) impurities may affect peak location, and (d) the peak wavelength values have generally not been certified (11).

As mentioned previously (11), the wavelength position and stability of spectral lines from xenon or mercury excitation sources of spectrofluorometers may be variable with time, and such sources are difficult to use with certainty for the calibration of monochromators.

*Spectral Responsivity Standards (for Corrected Spectra).* Depending on the conditions, many different organic and inorganic compounds in various solvents have been used as standards for determining the spectral responsivity of instruments. Several measurement proce-

Table I. Spectral Lines from External Sources Used for Monochromator Wavelength Calibration

Wave-length <sup>a</sup> (nm)	Source		
	Line	Laser	Reference
202.55	Zn	-	17
253.65	Hg	-	15
296.73	Hg	-	15
325.03	-	He-Cd	14
365.01	Hg	-	15
404.66	Hg	-	15
435.84	Hg	-	15
514.54	-	Ar	14
546.07	Hg	-	15
576.96	Hg	-	15
579.07	Hg	-	15
632.82	-	He-Ne	14
692.95	Ne	-	17
724.52	Ne	-	17
752.55	-	Kr	14
799.30	-	Kr	14
852.11	Cs	-	17
894.35	Cs	-	17

<sup>a</sup>Wavelengths in air.

Table II. Luminescence Wavelength Standards--Organics in Solution and Inorganic Ions in Glass Matrices

Material	Matrix	Wavelength (nm) <sup>a</sup>		Reference
		$\lambda_{ax}$	$\lambda_{em}$	
Phenanthrene	n-C <sub>6</sub> H <sub>12</sub>	211-346	-	19
Gd <sup>3+</sup>	Borate Glass	248-274	312	20
Tb <sup>3+</sup>	Borate Glass	220-379	486	20
Sm <sup>3+</sup>	Phosphate Glass	-	562-707	20
Eu <sup>3+</sup>	Phosphate Glass	318-526	578-612	21
Anthracene, Naphthalene, Ovalene	Polymer Blocks	-	300-550	22

<sup>a</sup>Wavelengths rounded to nearest nanometer.

dures, including absolute measurements, can be used to determine the various correction factors given in equations 1 and 2.

*Excitation Spectra* (11,19):

$$X(\lambda_x) = X_m(\lambda_x)k[\rho(\lambda_x)/\tau(\lambda_x)]N(\lambda_x)[\tau'(\lambda_x)]^{-1} \quad (1)$$

where  $X(\lambda_x)$  is the corrected spectrum,  $X_m$  is the measured excitation spectrum including corrections for stray radiation;  $k$  is a constant;  $\rho(\lambda_x)/\tau(\lambda_x)$  is the beam-splitter correction factor;  $N(\lambda_x)$  is the reference detector wavelength response including the transmittance of the detector window; and  $\tau'(\lambda_x)$  is the transmittance of the sample cell window.

For excitation spectra, the accuracy of the correction procedure can be checked by comparing the corrected, normalized values with the absorbance spectrum (19) or determining if any peaks from the source are observed in the corrected excitation spectrum (23).

*Emission Spectra* (11,24):

$$E(\lambda_x, \lambda_m) = E_{\lambda_x} \alpha(\lambda_x) R(\lambda_m) C(\lambda_x, \lambda_m) y_{p, \lambda_m}(\lambda_x) \quad (2)$$

where  $E(\lambda_x, \lambda_m)$  is the measured spectrum [called  $J(\lambda_x, \lambda_m)$  in Ref. 23],  $\lambda_x$  and  $\lambda_m$  indicate wavelength ranges of excitation and emission optical properties, respectively,  $E_{\lambda_x}$  is the spectral irradiance of the sample at  $\lambda_x$ ,  $\alpha(\lambda_x)$  is the absorbance of the sample at  $\lambda_x$ ;  $R(\lambda_m)$  is the spectral responsivity of the detection system;  $C(\lambda_x, \lambda_m)$  is the correction due to sample effects (refractive index, reabsorption, emission anisotropy); and  $y_{p, \lambda_m}(\lambda_x)$  is the spectral photon yield of luminescence.

Procedures for determining the spectral responsivity or correction factors in equation 2 are based on radiance or irradiance standards, calibrated source-monochromator combinations, and an accepted standard. The easiest measurement procedure for determining corrected emission spectra is to use a well-characterized standard and obtain an instrumental response function, as described by equation 3 (17). In this case, quinine sulfate dihydrate has been extensively studied and issued as a National Bureau of Standards (NBS) Standard Reference Material (SRM).

$$E(\lambda_x, \lambda_m) = E_s [R'(\lambda_m)] \quad (3)$$

where  $E_s$  is the corrected emission spectrum of the standard in appropriate units and  $R'(\lambda_m)$  is the detection system responsivity including various correction factors.

The instrument response function can then be used to correct emission spectra obtained from molecules over the same wavelength range. Corrections for differences in index of refraction must be made if other solvents are used. Of the many standards often recommended and used for determining spectral responsivity, a few for which digital data exist are listed in Table III. Although literally hundreds of publications recommend various materials as standards, few provide digital data for corrected excitation and emission spectra. Thus, in addition to the documentation on standards recommended by Chapman et al (29) and expanded by others (7,9,11,26), we recommend reporting digital data at appropriate wavelength intervals for corrected luminescence spectra.



Table III. Standards for Corrected Excitation and Emission Spectra

Material <sup>a</sup>	Wavelength range (nm)	Solvent	Reference
<i>Excitation Spectra<sup>b</sup></i>			
2-Aminopyridine	220-325	1.0N H <sub>2</sub> SO <sub>4</sub>	19
Quinine Sulfate	280-380	1.0N H <sub>2</sub> SO <sub>4</sub>	19
Quinine Sulfate	270-400	0.1N HClO <sub>4</sub>	11
3-Aminophthalimide	340-425	99% EtOH	19
Proflavine	390-470	0.05M Acetate	19
Fluorescein	450-510	0.1N NaOH	19
Rhodamine B	490-570	99% EtOH	19
Methylene Blue	570-680	99% EtOH	19
<i>Emission Spectra</i>			
2-Aminopyridine	320-455	1.0N H <sub>2</sub> SO <sub>4</sub>	25,26
2-Naphthol	333-500	0.02N Acetate	25,26
Quinine Sulfate	400-590	1.0N H <sub>2</sub> SO <sub>4</sub>	26
Quinine Sulfate	375-675	0.1N HClO <sub>4</sub>	17
$\beta$ -Carboline	380-630	1.0N H <sub>2</sub> SO <sub>4</sub>	27
3-Aminophthalimide	435-645	1.0N H <sub>2</sub> SO <sub>4</sub>	26
Cresyl Violet	570-815	MeOH	28

<sup>a</sup>Use laser grade or appropriately purified materials.

<sup>b</sup>Absorption maxima  $\leq 0.02$ .

The corrected excitation and emission spectra for quinine sulfate from previous work (17) and from a round-robin exercise (11) are given in Figure 1. The coefficients of variation are also given at each point to indicate the amount of agreement in measured values from the ten laboratories participating in the round-robin exercise.

Several solid materials, such as organics dissolved in plastics (22,23), phosphors sintered with polytetrafluoroethylene (30), phosphors (31), and lumogen-T (23), have been suggested as calibration standards. But most of the publications suggesting these materials (except Ref. 31) have not included digital data for the corrected spectra. Additional information, precautions, and pitfalls to be aware of in the use of various standards have been summarized in Reference 11 and the references cited therein.

*Quantum-Yield and Quantum-Counter Standards.* The materials recommended as quantum-yield and quantum-counter standards are summarized in Table IV. As can be seen, several of the materials suggested as spectral responsivity standards have also been suggested as quantum-yield and quantum-counter standards. The materials listed in Table IV cover the wavelength range from 200 to almost 800 nm, giving an excellent choice for the researcher. Quantum counters that operate further into the red are still needed, especially for the area of

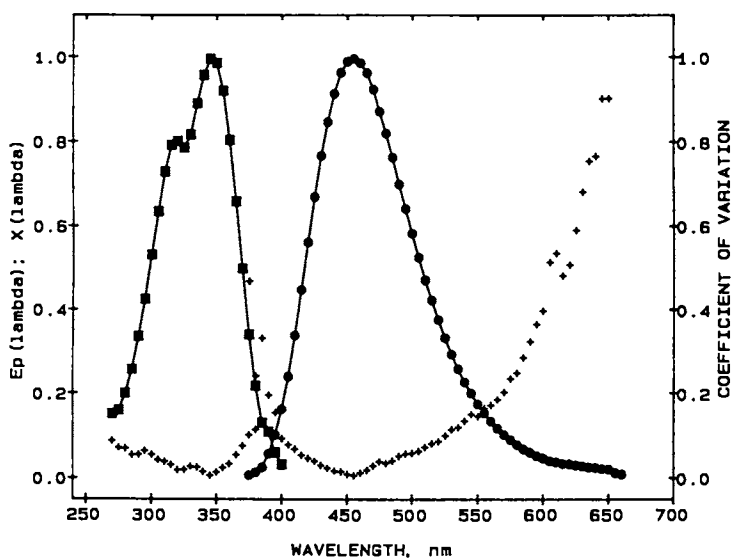


Figure 1. Average corrected emission spectrum (-●-) and excitation spectrum (-■-) for quinine sulfate in 0.1 mol/L  $\text{HClO}_4$  obtained during round-robin test with ten laboratories; coefficient of variation at each wavelength (+).

Table IV. Quantum Yield and Quantum Counter Standards

Material <sup>a</sup>	$\lambda$ Range (nm)	Solvent (Conc. in mol/L)	Quantum Yield <sup>b</sup>	% Flatness <sup>c</sup>	Ref.
Quinine Sulfate	200-400 <sup>d</sup>	H <sub>2</sub> SO <sub>4</sub> (0.1) <sup>e</sup>	0.51±0.03	5	32-34
Quinine Sulfate	"	H <sub>2</sub> SO <sub>4</sub> (1.0)	0.55±0.03	-	34
Quinine Sulfate	"	HClO <sub>4</sub> (0.1,1.0)	0.60±0.04	-	17
2-Aminopyridine	280-315	H <sub>2</sub> SO <sub>4</sub> (0.1,1.0)	0.66±0.05	-	35
$\beta$ -Carboline	330-370	H <sub>2</sub> SO <sub>4</sub> (1.0)	0.60±0.02	-	27
DPH <sup>f</sup>	290-390	PFN <sup>g</sup>	0.52±0.02 <sup>i</sup>	-	38
DPA <sup>h</sup>	330-405	Hexane	0.95-1.00	-	9
Fluorescein	400-520	NaOH (0.1) <sup>j</sup>	0.92±0.03	-	9
Cresyl Violet	510-635	MeOH	0.54±0.03	-	28
Rhodamine B	360-590	MeOH <sup>k</sup>	0.68±0.04	2	26, 34, 39, 40
Rhodamine 590(6G)	360-590	EtOH	0.95±0.03	5	41
CZ144 <sup>l</sup>	220-700	CH <sub>2</sub> Cl <sub>2</sub>	0.75±0.15	4	24
CZ682	485-780 <sup>m</sup>	CH <sub>2</sub> Cl <sub>2</sub>	0.59±0.23	4	24

Material <sup>a</sup>	$\lambda$ Range (nm)	Solvent (Conc. in mol/L)	Quantum Counter Conc. (g/L)	% Flatness <sup>c</sup>	Ref.
DANS <sup>n</sup>	210-400	NaOH (0.1)	2.5	3	36, 37
Coumarin 440	360-400	MeOH	1.44	2	39
Coumarin 535	360-490	MeOH	0.58	2	39
[Ru(bipy) <sub>3</sub> ] <sup>2+</sup>	280-560	MeOH	10.0	2	9
Rhodamine B	360-590	MeOH <sup>k</sup>	5.0	2	26, 34, 39, 40
Rhodamine 575	360-590	MeOH <sup>k</sup>	1.32	8	39
Rhodamine 590(6G)	360-590	MeOH	2.83	5	39
HITC <sup>o</sup>	350-700	MeOH	2.8	-	42
Nile Blue A <sup>p</sup>	360-590 <sup>q</sup>	MeOH	1.30	2	39
Nile Blue A	280-700	Ethylene Glycol	2.2	-	42
Oxazine 725	360-590 <sup>q</sup>	MeOH	1.75	2	39
Oxazine 170 <sup>r</sup>	255-700	Ethylene Glycol	1.50	-	42
Basic Blue 3 <sup>s</sup>	240-700	Ethylene Glycol	4.1	-	42
CZ144 <sup>l</sup>	220-700	CH <sub>2</sub> Cl <sub>2</sub>	6.0	4	24
CZ682	485-780 <sup>m</sup>	CH <sub>2</sub> Cl <sub>2</sub>	8.0	4	24

<sup>a</sup>Use laser grade materials. <sup>b</sup>Use dilute solutions ( $A < 0.01$ ); uncertainties based on literature or recommendations (9). <sup>c</sup>Over wavelength range. <sup>d</sup>Note red edge shift. <sup>e</sup> $[H^+]$  concentration. <sup>f</sup>1,6-diphenyl-1,3,5-hexatriene. <sup>g</sup>Perfluoro-*n*-hexane. <sup>h</sup>9,10-diphenylanthracene; quantum yield uncertain, needs more work if warranted due to narrow bands. <sup>i</sup>Based on quantum yield of 0.83 for 9,10-DPA in cyclohexane; corrected value should be 0.60, using 0.95 for 9,10-DPA (9). <sup>j</sup>Fluorescein is relatively unstable in NaOH; more stable in NaHCO<sub>3</sub>. <sup>k</sup>MeOH recommended to avoid polarization problems in viscous solvents (43). <sup>l</sup>Benzopyryllium salts. <sup>m</sup>Used with Rhodamine B, gave 200-780 nm range. <sup>n</sup>Sodium 1-dimethylaminonaphthalene-5-sulfonate. <sup>o</sup>1,1',3,3',3',3'-hexamethylindotricarbocyanine. <sup>p</sup>2-amino-7-(dimethylamino)-3,4-benzophenazonium perchlorate. <sup>q</sup>QC's can be used at longer wavelengths, comparator used Rhodamine B as reference standard (39). <sup>r</sup>2,7-bis(ethylamino)-6-methyl-3,4-benzophenazonium perchlorate. <sup>s</sup>2,7-bis(diethylamino)phenazonium chloride.

energy conversion. Quantum-yield measurements are difficult to make, and quantum counters are relatively easy to use; however, both are subject to several sources of error that have been discussed extensively (1-3,9) and summarized recently (11).

**Decay Time.** Many organic and inorganic materials in various solvents have been suggested as decay-time standards. Selected standards listed in Table V cover the decay-time range from nanoseconds to

Table V. Materials Used as Standards for Fluorescence Decay Time,  $\tau$

Substance	Solvent	$\tau$ (ns)	Reference
2-Aminopyridine	0.1, 1.0N H <sub>2</sub> SO <sub>4</sub>	9.6	35
Anthracene	c-C <sub>6</sub> H <sub>12</sub>	5.23±0.05 <sup>a</sup>	45
$\beta$ -Carboline	1.0N H <sub>2</sub> SO <sub>4</sub>	22.03±0.12	27
1-Cyanonaphthalene	c-C <sub>6</sub> H <sub>12</sub>	18.23 <sup>a</sup>	45
1-Cyanonaphthalene	Gas phase <sup>b</sup>	24.1 <sup>a</sup>	45
DNMA <sup>c</sup>	CH <sub>2</sub> Cl <sub>2</sub>	2.40 <sup>a</sup>	45
DPH <sup>d</sup>	c-C <sub>6</sub> H <sub>12</sub>	32.5±0.05 <sup>a</sup>	38
DPH	c-C <sub>6</sub> H <sub>12</sub>	15.7±0.02	38
DPH	C <sub>6</sub> H <sub>6</sub>	6.1±0.01	38
Fluorescein	0.1N NaOH	4.5±0.03 <sup>e</sup>	46
3-Methylindole	c-C <sub>6</sub> H <sub>12</sub>	4.36 <sup>a</sup>	45
3-Methylindole	C <sub>2</sub> H <sub>5</sub> OH	8.17 <sup>a</sup>	45
1-Methylindole	c-C <sub>6</sub> H <sub>12</sub>	6.24 <sup>a</sup>	45
1,2-Methylindole	C <sub>2</sub> H <sub>5</sub> OH	5.71 <sup>a</sup>	45
POPOP	C <sub>2</sub> H <sub>5</sub> OH	1.35±0.2	47
PPO <sup>g</sup>	c-C <sub>6</sub> H <sub>12</sub>	1.42 <sup>a</sup>	45
PPOP <sup>h</sup>	c-C <sub>6</sub> H <sub>12</sub>	1.10±0.02 <sup>a</sup>	48
$\gamma$ -Pyrenebutyrate	H <sub>2</sub> O+KI	18.0-115 <sup>i</sup>	49
Quinine sulfate	0.1N H <sub>2</sub> SO <sub>4</sub> +KCl	0.2-19.2 <sup>f, i</sup>	49
Quinine sulfate	1.0N H <sub>2</sub> SO <sub>4</sub>	20.4 <sup>f</sup>	50
Quinine sulfate	10.0N H <sub>2</sub> SO <sub>4</sub>	21.8 <sup>f</sup>	50
Quinine sulfate	0.1N H <sub>2</sub> SO <sub>4</sub>	19.1, 3.63 <sup>f</sup>	45
Quinine sulfate	0.1N H <sub>2</sub> SO <sub>4</sub>	19.3 <sup>f</sup>	46
Rhodamine B	C <sub>2</sub> H <sub>5</sub> OH	2.88±0.06	51
Eu <sup>3+</sup>	Silicate glass	2.68±0.03 ms	21
Gd <sup>3+</sup>	Borate glass	4.10±0.01 ms	20
[Ru(bipy) <sub>3</sub> ] <sup>2+</sup>	H <sub>2</sub> O	0.64±0.02 $\mu$ s	52
Sm <sup>3+</sup>	Phosphate glass	1.91±0.03 ms	20

<sup>a</sup>Values for degassed solutions. <sup>b</sup>With one atmosphere cyclohexane. <sup>c</sup>N,N-dimethyl-1-naphthylamine. <sup>d</sup>Trans-1,6-diphenyl-1,3,5-hexatriene. <sup>e</sup>Average of 13 literature values (see Ref. 50). <sup>f</sup>Values from many authors agree for a single exponential, but there appear to be two exponentials that show wavelength dependence. <sup>g</sup>2,5-Diphenyloxazole. <sup>h</sup>p-Bis(2-phenyloxazolyl)benzene. <sup>i</sup>Decay time dependent on Cl<sup>-</sup> or I<sup>-</sup> concentration.

milliseconds. Caveats apply to the use of these materials as standards and to the experimental setup (summary in ref. 11): e.g., some researchers suggest that quinine sulfate should not be used as a decay-time standard because its decay cannot be described with a single exponential (45); care must be exercised in the type of scatterer used and the placement of the pulsed source (47).

*Sensitivity, Linearity, and Stability of Instruments.* Quinine sulfate has been suggested as a standard for determining the limit of detection and linearity of instruments (44). Some organic materials dissolved in plastics have been suggested as standards because of their stability (22), and many inorganic ions dissolved in glasses are quite stable.

The same requirements for material stability do not necessarily hold in the macro- and micro-environments. For example, organic species generally photobleach when irradiated. In macromolecules, this degradation is usually quite slow and measurements can be made with little or no noticeable change in fluorescence intensity. Most laboratories periodically make a new working standard at low concentrations from a solid or stock solution that has been stored in the dark. For critical measurements, however, it is recommended that new standard stock and working solutions be prepared just before use. In the microenvironment, photobleaching is a more significant problem, as will be discussed shortly.

#### *Microspectrofluorometric Standards*

The discussion of microspectrofluorometric standards will parallel the previous discussion of macrostandards and will delineate the additional requirements for standards that are used in the microscopic environment. Haaijman (53) has reviewed the various materials and procedures used for making measurements on a microscopic scale.

*Requirements of Standards.* Standards used in the calibration of microspectrofluorometric instrumentation must meet more stringent requirements than those used in macromolecules. The effect of increased excitation flux as well as spatial effects under magnification make many macromolecule standards unsatisfactory for micromeasurements. Following are some of the requirements for fluorescence standards that are strongly influenced by a change from the macro- to the micro-environment.

*Stability.* The stability of the luminescence signal can be degraded by the increased power of the excitation radiation under microscopic illumination, particularly when the fluorophor is an organic molecule. The radiation flux density impinging on the sample using incident (epi-) illumination can be 4 or more orders of magnitude higher than in a macrospectrofluorometer. This increase in excitation radiation power can lead to rapid photobleaching of organic compounds in solution which show no appreciable degradation during irradiation in the macroenvironment. As shown in Figure 2, for example, the fluorescence intensity of fluorescein isothiocyanate (FITC), commonly used as a tagging reagent in fluorescence immunoassay, decays rapidly when exposed in the microscope, decreasing as much as 50% in less than 30 s. For comparison, the stability of a

uranium-doped microsphere under the same conditions is also shown. Though techniques are available to reduce photobleaching, such as protecting agents (54), sample deoxygenation (55), pulsed laser excitation (56), rapid excitation shutters (57), and specimen fixation (58), none is universally applicable to all instrument and analysis conditions. Furthermore, if photobleaching cannot be totally eliminated, then a standard which is used to relate an instrument signal to analyte concentration must photobleach at an identical (or at least similar) rate under the same experimental conditions as the sample.

Thus, in the microenvironment, calibration standards have different requirements than standards that are used to relate the instrument signal to compound concentration. Standards used to calibrate the response of a microspectrofluorometer for day-to-day or instrument-to-instrument comparisons must not photobleach. Conversely, a standard used to quantify the concentration of an analyte in a sample must photobleach in a manner identical to that of the sample.

Ideally, techniques to reduce photobleaching, such as the addition of UV absorbers, solution deoxygenation, and the use of nanosecond-pulsed lasers or fast shuttering to decrease sample exposure (54-58), can be applied successfully to both standards and samples. For example, Velapoldi and Gjelsvik (57) used an automated microspectrofluorometer, which included fast shutters and computer-controlled scanning and data accumulation, to make reproducible measurements within milliseconds (or at most a second). The short illumination time reduced the photooxidation of the organic standard and the analyte, making organic standards viable alternatives to inorganic ion-doped glasses and allowing fluorescence measurements of organics without photodegradation. In this case, porosities of both macroscopic and microscopic geologic samples were determined. The standard was cast and ground as part of the 30- $\mu\text{m}$ -thick geologic thin section. Repetitive measurements (3-5, total irradiation time less than 1 s) at the same position on both the cast standard and the thin section showed no photobleaching and yielded coefficients of variation of approximately 2%. However, prolonged irradiation (>10 s) resulted in photobleaching of the organic fluorophor. Figure 3 shows the porosity on a microscale for a geologic thin section from a drilling core.

Haaijman (53) took a different approach for the standardization of microscopic immunofluorescence measurements using FITC. Rather than using special instrumentation or procedures to reduce photobleaching, he designed a standard using FITC bound to aminoethyl-Sephadex beads, in which the amount of bound fluorophor was quantified using absorbance measurements. Though the response of the FITC-labeled beads to changes in physicochemical variables (i.e., pH and duration of excitation) was not identical to that of FITC-labeled cells, the discrepancies were not considered major and the beads were deemed to be adequate for immunofluorescence microscopy and superior to other available standards.

These problems are not as significant in the macroenvironment, where many standards can be used for both calibration and standardization, since photodegradation of the sample is usually not significant, running around 5-10%. However, if measurements of the highest accuracy or of small differences are required, these uncertainties

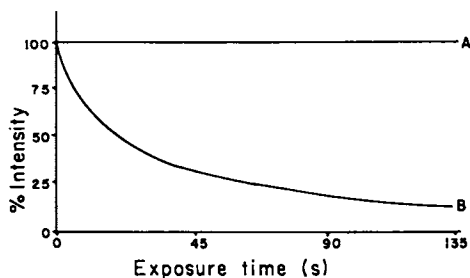


Figure 2. Irradiation of uranyl glass microspheres (A) and FITC-labeled microbeads (B) demonstrate photobleaching and stability of both materials.

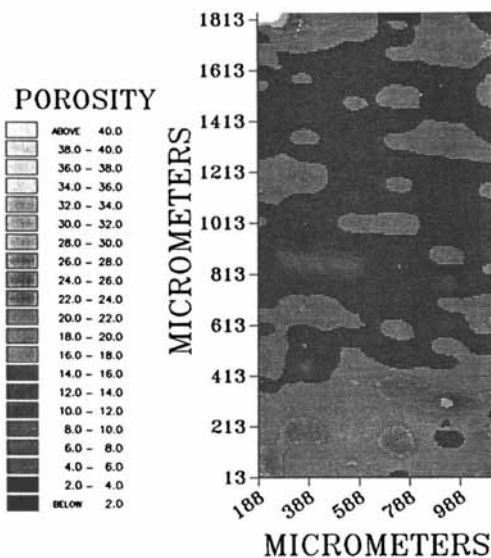


Figure 3. Porosity measurements on a microscopic scale for a small ( $2\text{ cm} \times 2\text{ cm} \times 30\text{ }\mu\text{m}$ ) thin section of sandstone impregnated with fluorophor-doped polymer. Average porosity = 16.3%; range of porosities = 1.8-42%.

may be too large, and as discussed previously, new working standards should be prepared.

*Size and Shape.* The dimensions of the standard are more critical in the microenvironment than in the macroenvironment, since microscopic measurements commonly require changes in field apertures and magnification. If a microscopic standard has a small ( $\mu\text{m}$ -sized), well-defined shape, such as a sphere or cylinder, an accurate intensity/volume relationship can be established, which should be independent of the microscope optics. Standardization is thus valid no matter what microscope parameters are employed, as long as the spectral characteristics of the standard and the sample are quite similar or identical.

*Use of Macrostandards in the Microenvironment.* Macrostandards, such as uranyl ion-doped glass microscope slides, have been used as standards for microspectrofluorometric measurements by several authors (59,60). The appeal of such an approach is obvious, because well-characterized and stable standards are readily available and easy to use. However, as discussed by Sernetz and Thær (61), the diameter or thickness of a macrostandard will be greater than the excitation and emission field diameters of the microspectrofluorometer, and thus the fluorescence emission will be a function of microscope parameters that define the volumes illuminated and observed, such as objective magnification and numerical aperture, emission and excitation aperture size, and focal point. These parameters will be difficult to reproduce on two or more different microscopes and will be subject to focusing errors when using the same microscope. Use of a macrostandard will be further complicated by errors due to prefilter and postfilter effects and would be impossible for nonphotometric (i.e., visual) detection schemes.

*Use of Microstandards in the Microenvironment.* The most common approach to preparing microstandards is to place a fluorophor in or to bind it to a stable, nonfluorescing host of well-defined shape. Ploem (62) used microdroplets of FITC solution in micro-wells in a perspex slide, but found significant photobleaching under illumination. More successful were microcapillaries (61-63) of about 6  $\mu\text{m}$  inside diameter and 50 mm length filled with fluorophor solution. These standards did not photobleach as much as the microdroplets, since the excited portion of the fluorophor solution, which was less than 40  $\mu\text{m}$  in length, was continuously renewed by convectional flow and diffusion. However, a specific length of capillary had to be isolated using the microscope measuring aperture.

Velapoldi et al. (64) used a similar approach but prepared fibers of uniform diameter (5-45  $\mu\text{m}$ ) from inorganic ion-doped glasses. The fluorescence parameters of these materials can be changed by substituting various ions, such as  $\text{Tb}^{3+}$ ,  $\text{Sm}^{3+}$ ,  $\text{Eu}^{3+}$ ,  $\text{Mn}^{2+}$ ,  $\text{UO}_2^{2+}$ ,  $\text{Cu}^+$ , and  $\text{Sn}^{2+}$ . They show excellent stability under irradiation using incident excitation (measurement imprecision of 1% under continuous irradiation in the microscope for 24 h) and have a fluorescence flux density proportional to the fiber length. Recently, microspheres (5-40  $\mu\text{m}$  diameter) of these ion-doped glasses have been prepared and evaluated (65). Ions can be selected to produce either sharp ( $\text{Tb}^{3+}$ ,  $\text{Sm}^{3+}$ ,  $\text{Eu}^{3+}$ ) or broad ( $\text{Mn}^{2+}$ ,  $\text{UO}_2^{2+}$ ,  $\text{Cu}^+$ ,



Sn<sup>2+</sup>) spectral distributions. The spheres exhibit a fluorescence flux density proportional to the radius cubed (Figure 4). They are similar in size and shape to cells and have a distinct advantage over fibers or capillaries in that no physical parameters (i.e., capillary length) need to be defined by the microscope optics. Figures 5a and b illustrate homogeneously and nonhomogeneously uranium-doped glass microspheres. The luminescence intensity distribution was obtained using an automated microspectrofluorometer system with a scanning mirror or stage (0.1 to 2.5  $\mu\text{m}$  step resolution), which was scanned in a raster mode (100x100), yielding 10,000 data points of fluorescence flux density as a function of x,y position.

Many inorganic ion-doped glasses luminesce, giving coverage from the ultraviolet to the red (Table VI). In addition, ions that undergo interconfigurational electronic transitions upon absorption and emission of radiation, such as Pb<sup>2+</sup>, show emission maximum shifts as large as 150 nm upon changing matrices (Figure 6), whereas ions

Table VI. Characteristics of Luminescence from Inorganic Ion-Doped Glasses

Element	Spectra Type <sup>a</sup>	Luminescing Species	Excitation Range (nm) <sup>b</sup>	Useful Emission Range (nm) <sup>c</sup>
Tl	Broadband	Tl <sup>+</sup>	215-260	250-370
Pb	Broadband	Pb <sup>2+</sup>	241-295	270-480
Ag	Broadband	Ag, Ag <sup>+</sup>	250-320	290-430
Ce	Broadband	Ce <sup>3+</sup>	215-317	310-420
Eu	Broadband	Eu <sup>2+</sup>	230-400	325-650
Sn	Broadband	Sn <sup>+</sup>	265	370-450
Cu	Broadband	Cu <sup>+</sup>	254-445	385-600
Bi	Broadband	Bi <sup>3+</sup>	319	390-525
U	Broadband	(UO <sub>2</sub> ) <sup>2+</sup>	340-480	490-620
Mn	Broadband	Mn <sup>2+</sup>	356-422	500-680
Cd	Broadband	CdS	350-470	560-790
Fe	Broadband	Fe <sup>3+</sup>	458	570-650, 800-880
Cr	Broadband	Cr <sup>3+</sup>	585	710-1000
Mo	Broadband	Mo <sup>3+</sup>	980	990-1030
Gd	Narrowband	Gd <sup>3+</sup>	220-280	311
Tm	Narrowband	Tm <sup>3+</sup>	265-350	350, 383, 455
Dy	Narrowband	Dy <sup>3+</sup>	340-380	475, 576
Tb	Narrowband	Tb <sup>3+</sup>	250-378	495, 544, 580, 620
Sm	Narrowband	Sm <sup>3+</sup>	403-469	563, 572, 599, 647, 705
Eu	Narrowband	Eu <sup>3+</sup>	340-395	578, 591, 611, 653, 700
Pr	Narrowband	Pr <sup>3+</sup>	440-475	610, 710, 890
Nd	Narrowband	Nd <sup>3+</sup>	530-585	890, 1060

<sup>a</sup>Shape of the spectral distribution; broadband spectra have a bandwidth at half height of greater than 5 nm. <sup>b</sup>The wavelength range observed to excite luminescence in the ion-doped glass. <sup>c</sup>The approximate wavelength range over which luminescence has been observed (broadband) or the approximate wavelengths at which luminescence maxima occur (narrowband). All wavelengths are approximate since they represent an average value taken from different references using various excitation sources and base glass compositions (65).

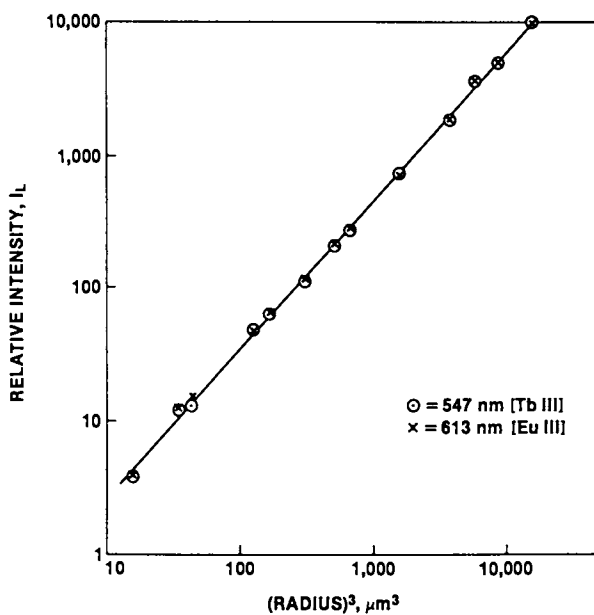


Figure 4. Relative luminescence flux versus the cube of the radius for  $\text{Tb}^{3+}$ - and  $\text{Eu}^{3+}$ -doped microspheres. Similar plots are obtained for  $(\text{UO}_2)^{2+}$ - and  $\text{Mn}^{2+}$ -doped microspheres.

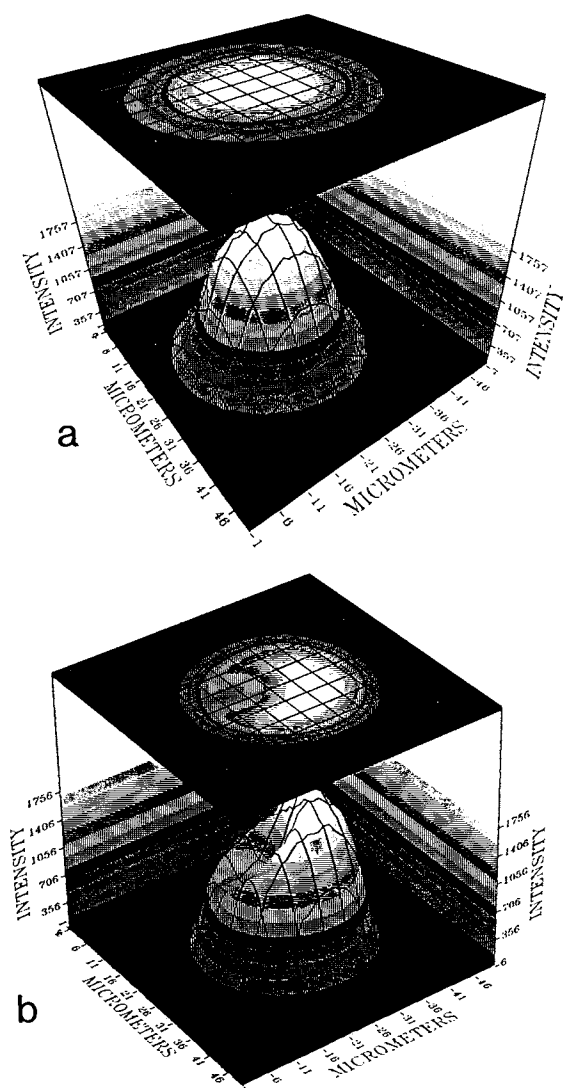


Figure 5. Two- and three-dimensional representations of relative luminescence flux of uranyl ion-doped glass beads, measured in a  $100 \times 100$  raster with 10,000 data points. Depicted are a homogeneously doped bead (a) and a nonhomogeneously doped bead (b).

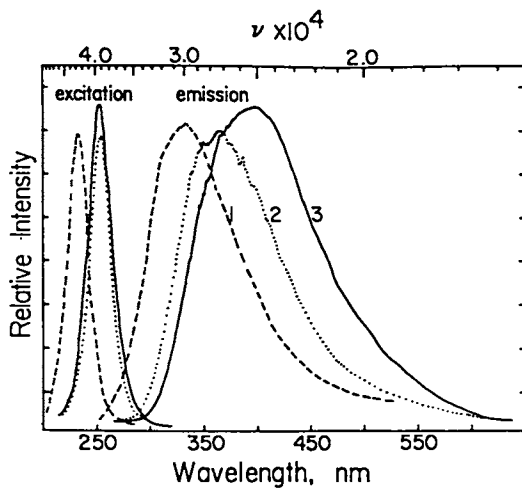


Figure 6. Corrected spectra for  $\text{Pb}^{2+}$ -doped phosphate (1), borate (2), and silicate (3) glasses. Excitation shown as relative intensity; emission shown as relative quanta/unit bandwidth.

that undergo intraconfigurational electronic transitions, such as  $\text{Eu}^{3+}$ , show emission maximum shifts of only a few nanometers (8). Thus the choice of the right ion and matrix gives some variety of luminescence characteristics.

Although inorganic ion-doped glasses are ideal as standards for calibration, they have limited application for relating instrument signal to analyte concentration because only a small number of different spectral distributions are available (relative to the myriad of organic species). There are likely to be only a few cases in which the spectral distribution of a specific class is similar enough to the analyte spectrum to be useful. The use of uranium-doped glasses for the quantification of FITC-labeled species (65) is one such case. The fact remains, though that a standard of the same material as the sample is preferred for standardization.

The approach to standardization used by Haaijman (53) and others (66,67), in which the fluorophor is incorporated within or bound to the surface of a plastic sphere, is more versatile than the use of inorganic ion-doped spheres, since the standard can be tailored exactly to the specifications required by the analyte species. However, this approach increases the uncertainty of the measurement because the photobleaching characteristics of both the standard and the sample must be considered. The ideal approach is to employ both types of standards. The glass microspheres can be used to calibrate instruments and set instrument operating parameters on a day-to-day basis, and the fluorophor-doped polymer materials can be used to determine the concentration-instrument response function.

#### *Applications of Macro Spectrofluorometric Standards*

**Standardization.** Standardization in analytical chemistry, in which standards are used to relate the instrument signal to compound concentration, is the critical function for determining the relative concentrations of species in a wide variety of matrices. Environmental Standard Reference Materials (SRM's) have been developed for various polynuclear aromatic hydrocarbons (PAH's). Information on SRM's can be obtained from the Office of Standard Reference Materials, National Bureau of Standards, Gaithersburg, MD 20899. Summarized in Table VII, these SRM's range from "pure compounds" in aqueous and organic solvents to "natural" matrices such as shale oil and urban and diesel particulate materials.

**Pure Compound SRM's.** Pure compound SRM's (or standards) are convenient to use for environmental samples such as water, where little sample extraction is necessary. Generator columns (SRM 1644) were developed to provide differing concentrations of pure PAH's by varying the temperature of the bath in which the generator column is placed (68). Figure 7a illustrates the raw fluorescence signal obtained during the SRM certification process using the standard addition method for determining benzo [a] pyrene concentrations by an "on stream" fluorescence technique. Figure 7b is a plot of the intensities, showing the best least-squares fits to data collected at four different temperatures. In this case, the instrument response as a function of concentration can be determined for a specific PAH while the unknown sample is measured by the same process (assuming

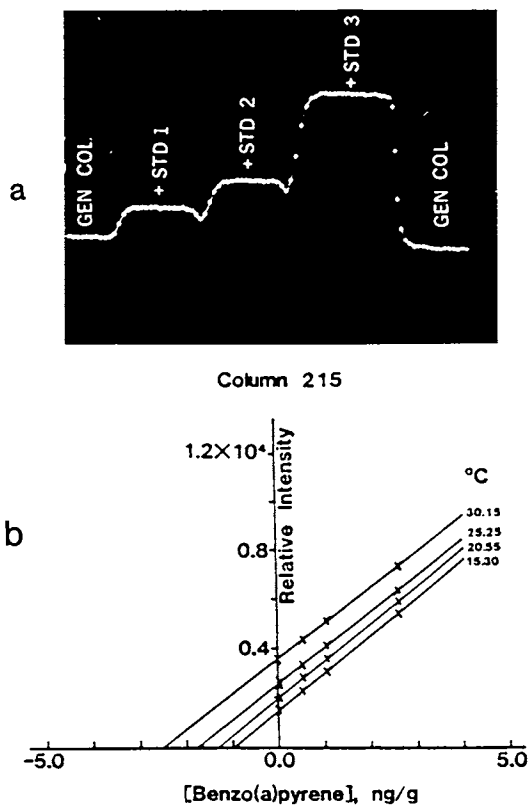


Figure 7. (a) Multichannel analyzer CRT display of raw data using standards-addition technique and (b) raw data (x) and fitted least-squares line (—) for the calculation of the benzo[a]pyrene concentration in the generator column effluent at four temperatures.

Table VII. Standard Reference Materials (SRM's) for the Determination of Polycyclic Aromatic Hydrocarbons (PAH's)<sup>a</sup>

SRM #	SRM Name	Certified Compounds
Pure Solutions:		
1644	Generator columns for PAH	Anthracene, benzo[a]-anthracene, benzo[a]pyrene
1647	Priority pollutant PAH in acetonitrile	16 PAH's
1587	Nitrated PAH in methanol <sup>b</sup>	6 nitrated PAH's
1596	Dinitropyrenes in solvent	4 nitrated pyrenes (3 dinitro and 1 nitro)
Natural Matrix Materials:		
1580	Organics in shale oil <sup>c</sup>	5 PAH's + 4 oxygen-nitrogen-containing compounds
1582	Petroleum crude oil <sup>c</sup>	5 PAH's + dibenzothiophene
1588	Cod liver oil <sup>c,d</sup>	- - -
1597	Complex PAH mixture from coal tar <sup>c</sup>	9 PAH's
1648	Urban particulate matter <sup>c,e</sup>	- - -
1649	Urban dust/organics <sup>c</sup>	5 PAH's
1650	Diesel particulate material <sup>c</sup>	6 PAH's

<sup>a</sup>Office of Standard Reference Materials, National Bureau of Standards, Gaithersburg, MD 20899. <sup>b</sup>Nitrated PAH's do not fluoresce but can be made to fluoresce by passing through a Zn or Pt column to reduce nitro groups to amino groups. <sup>c</sup>Information values for other organics in certificate. <sup>d</sup>Certified values for pesticides and PCB's. <sup>e</sup>Certified values for inorganic constituents.

only that the same specific PAH is present in the unknown sample). Liquid chromatographic techniques can be used to separate complex mixtures of PAH's (See, for example, Refs. 69,70), and the PAH of interest determined by that mode.

Another useful standard is SRM 1647, priority pollutant polynuclear aromatic hydrocarbons (in acetonitrile). It can be used to calibrate liquid chromatographic instruments (retention times, instrument response), to determine percent recoveries, and to fortify aqueous samples with known PAH concentrations. Figure 8 illustrates the HPLC separation and UV detection (fluorescence is also used extensively) for the 16 priority pollutants.

*Matrix SRM's.* Matrix SRM's can be used for a variety of functions. Taylor (71) reviewed the uses of matrix standards, which include: (a) method development and evaluation, (b) establishment of measurement traceability, and (c) assurance of measurement compatibility. During certification of these matrix SRM's, the selectivity of fluorescence

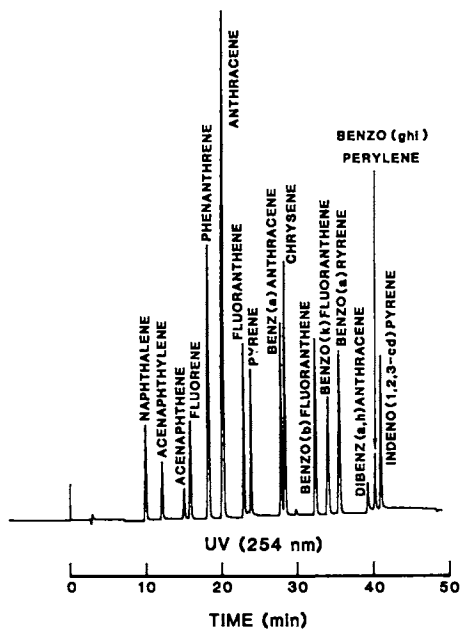


Figure 8. Reversed-phase HPLC separation of SRM 1647, priority pollutant polynuclear aromatic hydrocarbons (in acetonitrile), using UV detection.



detection was used to simplify analytical procedures. For example, in the certification processes of SRM's 1648 (urban particulate matter) and 1649 (urban dust/organics), UV detection and quantification of selected PAH's gave quite uninterpretable reversed-phase HPLC chromatograms (Figure 9) unless normal-phase fraction separations were done before the reversed-phase determinations (Figure 10) (72,73). Reversed-phase HPLC separations using fluorescence detection with wavelength programming provided "single step" quantification (Figure 11). These do not truly relate concentration to instrument response but instead relate concentration to the total chemical measurement process, including extraction, separation, and instrument response. This response function may be biased compared to the one obtained for the pure compound solutions, simply because the chemical measurement process response is included.

If the sample and standard have essentially the same matrices (e.g., air particulates or river sediments), one can go through the total measurement process with both the sample and the standard in order to (a) check the accuracy of the measurement process used (compare the concentration values obtained for the standard with the certified values) and (b) obtain some confidence about the accuracy of the concentration measurements on the unknown sample since *both* have gone through the same chemical measurement process (except sample collection). It is not recommended, however, that pure standards be used to standardize the total chemical measurement process for natural matrix type samples: chemical concentrations in the natural matrices could be seriously misread, especially since the pure PAH probably would be totally extracted in a given solvent, whereas the PAH in the matrix material probably would not be. All the parameters and matrix effects, including extraction efficiencies, are carefully checked in the certification process leading to SRM's.

Direct Reversed-Phase LC Analysis  
of Air Particulate Extract

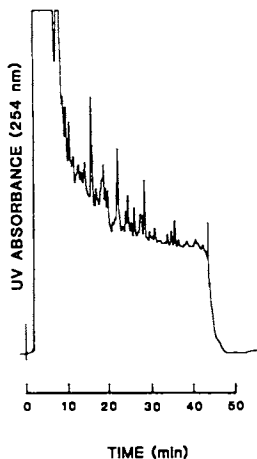


Figure 9. Reversed-phase HPLC analysis of PAH's extracted from SRM 1649, urban dust/organics, with UV detection, not preceded by normal-phase HPLC clean-up (Reprinted from reference 72. Copyright 1984 American Chemical Society.)

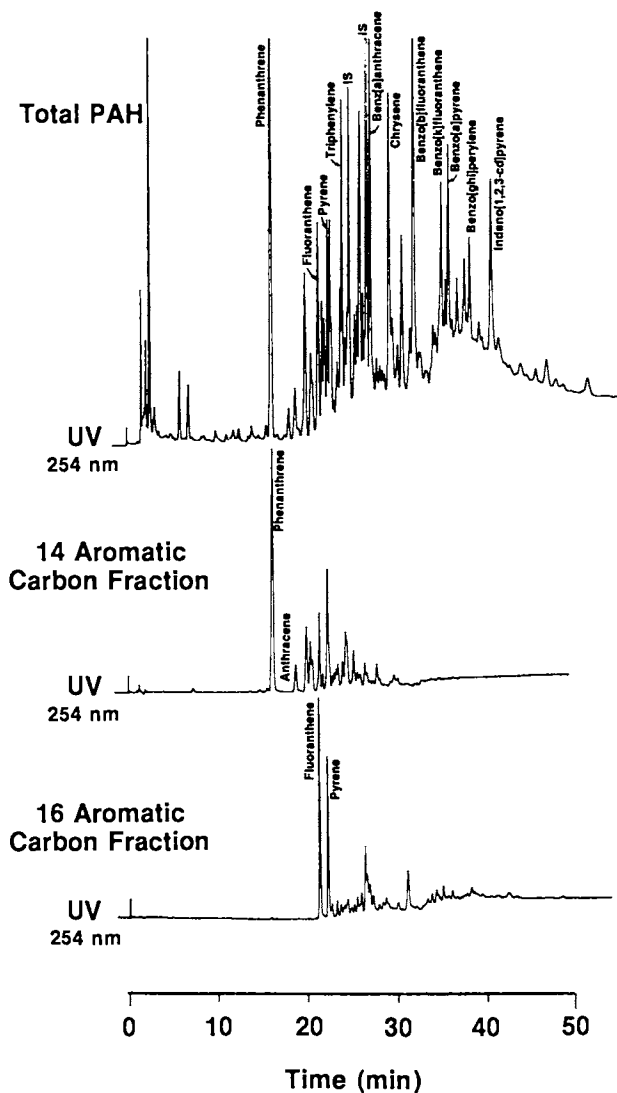


Figure 10. Reversed-phase HPLC analysis of PAHs extracted from SRM 1649, urban dust/organics, with UV detection, preceded by normal-phase HPLC fractionation based on ring carbon number. (Reprinted from reference 72. Copyright 1984 American Chemical Society.) *Continued on next page.*

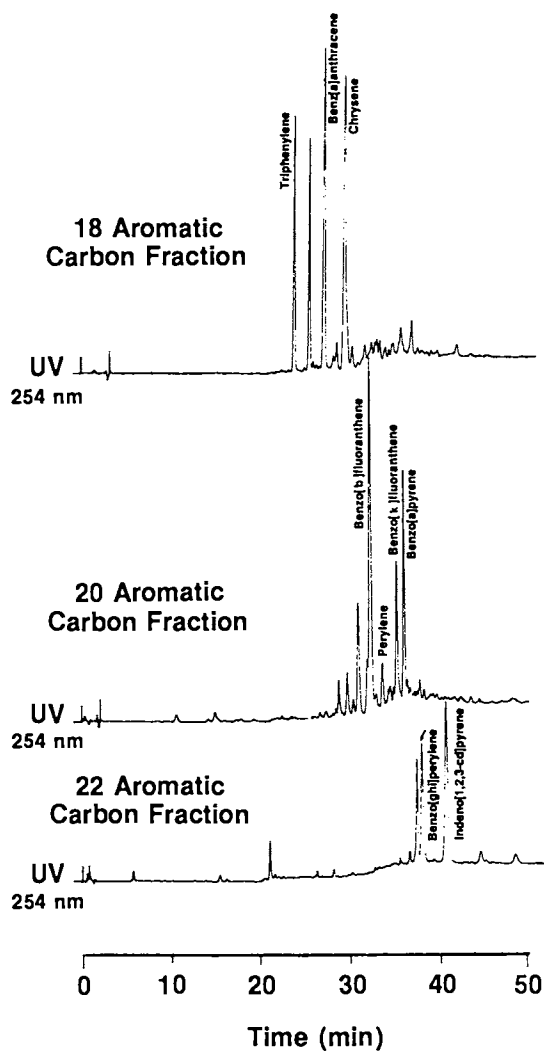


Figure 10. Continued.

**Bidimensional Fluorescence Wavelength Programming  
LC Analysis of Air Particulate Extract**

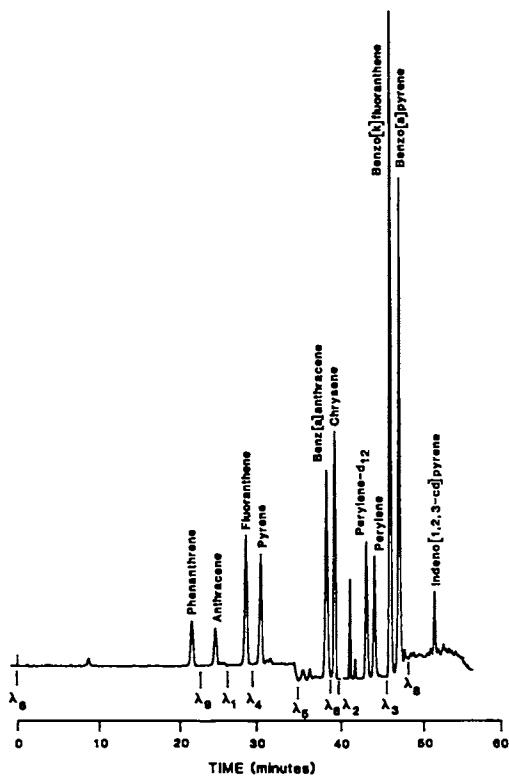


Figure 11. Reversed-phase HPLC analysis of total PAH's extracted from SRM 1648, urban particulate matter, with programmed fluorescence detection. (Reprinted from reference 72. Copyright 1984 American Chemical Society.)

*Standards for the Future.* In general, more standards that cover a wider wavelength range are needed for calibration, and natural matrix standards are needed for standardization and measurement assessment. Analysts should advise suppliers of standards (e.g., national laboratories) about which matrices are being commonly collected and which compounds need to be certified. In microspectrofluorometry, more fluorophor-tagged materials are needed, as well as increased stability of the organic-tagged species. Until we have stable organic species that will not photobleach under incident irradiation, we will need better correlation of the fluorescence flux of the stable, inorganic ion-doped spheres to the concentration of the organic species. This requirement may not hold for some new types of automated instrumentation (especially microspectrofluorometers) or for flow systems, since the residence times of any individual fluorophor under the microscope objective should be short enough to preclude photobleaching. Nevertheless, static investigations of samples such as cells to give locational information certainly will continue to be of interest, and the stable standards will continue to serve a useful calibration function in the future.

#### *Literature Cited*

1. Burgess, C.; Mielenz, K. D., Eds. *Advances in Standards and Methodology in Spectrophotometry*; Analytical Spectroscopy Library; Elsevier Science: Amsterdam, 1987; Vol. 2.
2. Mielenz, K. D., Ed. *Optical Radiation Measurements; Measurement of Photoluminescence*; Academic: New York, 1982; Vol. 3.
3. Miller, J. D., Ed. *Techniques in Visible and Ultraviolet Spectrometry, Standards in Fluorescence Spectrometry*; UV Spectrometry Group, Chapman and Hall: London, 1981; Vol. 2.
4. Wehry, E. L., Ed. *Modern Fluorescence Spectroscopy*; Plenum: New York, Vol. 1, 1976; Vol. 2, 1976; Vol. 3, 1981; Vol. 4, 1981.
5. Parker, C. A. *Photoluminescence of Solutions*; Elsevier: Amsterdam, 1968.
6. Mielenz, K. D. *Anal. Chem.* 1976, 48, 1093-4.
7. Demas, J. N.; Crosby, G. A. *J. Phys. Chem.* 1971, 75, 991.
8. Velapoldi, R. A. *J. Res. Nat. Bur. Stand., Sect. A* 1972, 76, 641.
9. Demas, J. N. In *Optical Radiation Measurements; Measurement of Photoluminescence*; Mielenz, K. D., Ed.; Academic: New York, 1982; Vol. 3, pp 195-248.
10. Velapoldi, R. A.; Hertz, H. S. In *The Importance of Chemical Speciation in Environmental Processes*; Bernhard, M.; Brinckman, F. E.; Sadler, P. J., Eds.; Springer-Verlag: Berlin, 1986; pp 685-710.
11. Velapoldi, R. A. In *Advances in Standards and Methodology in Spectrophotometry*; Burgess, C.; Mielenz, K. D., Eds.; Elsevier Science: Amsterdam, 1987; Vol. 2, pp 175-193.
12. Miller, J. N. In *Techniques in Visible and Ultraviolet Spectrometry*; Miller, J. D., Ed.; Chapman and Hall: London, 1981; Vol. 2, pp 8-14.
13. Mielenz, K. D. In *Optical Radiation Measurements; Measurement of Photoluminescence*; Mielenz, K. D., Ed.; Academic: New York, 1982; Vol. 3, pp 1-87.

14. Burke, R. W.; Velapoldi, R. A. In *Recommended Reference Materials for the Realization of Physicochemical Properties*; Marsh, K. N., Ed.; Blackwell Scientific: Oxford, England, 1987; pp 465-489.
15. *Annual Book of ASTM Standards*; American Society for Testing and Materials: Philadelphia, PA, 1987; Sec. 14, pp 479-481.
16. Harrison, G. R. *M.I.T. Wavelength Tables*; M.I.T. Press: Cambridge, MA, 1983; Vol. 2.
17. Velapoldi, R. A.; Mielenz, K. D. *NBS Spec. Publ. 260-64* 1980.
18. Guilbault, G. G. *Practical Fluorescence; Theory, Methods, and Techniques*; Marcel Dekker: New York, 1973, p. 150.
19. Melhuish, W. H. In *Optical Radiation Measurements; Measurement of Photoluminescence*; Mielenz, K. D., Ed.; Academic: New York, 1982; Vol. 3, pp 115-138.
20. Reisfeld, R. *J. Res. Nat. Bur. Stand., Sect. A* 1972, 76, 613.
21. Velapoldi, R. A.; Reisfeld, R.; Boehm, L.; *Phys. Chem. Glasses* 1973, 14, 101.
22. West, M. A.; Kemp, D. R. *Am. Lab.* 1977, 9 (3), 37.
23. Brecht, E. *Anal. Chem.* 1983, 58, 384.
24. Costa, L. F.; Mielenz, K. D.; Grum, F. In *Optical Radiation Measurements; Measurement of Photoluminescence*; Mielenz, K. D., Ed.; Academic: New York, 1982; Vol. 3, pp 139-174.
25. Melhuish, W. H. *Appl. Opt.* 1975, 14, 26.
26. Melhuish, W. H. *J. Res. Nat. Bur. Stand., Sect. A* 1972, 76, 547.
27. Ghiggino, K. P.; Skilton, P. F.; Thistlethwaite, P. J. *J. Photochem.* 1985, 31, 113.
28. Magde, D.; Brannon, J. H.; Cremers, T. L.; Olmstead, J., III *J. Phys. Chem.* 1979, 83, 696.
29. Chapman, J. H.; Förster, Th.; Kortüm, G.; Parker, C. A.; Lippert, E.; Melhuish, W. H.; Nebbia, G. *Appl. Spectrosc.* 1963, 17, 171.
30. Weidner, V. R.; Mavrodineanu, R.; Eckerle, K. L. *Appl. Opt.* 1986, 25, 832.
31. Shelton, C. F. *NBS Tech. Note 417* 1968.
32. Fletcher, A. N. *Photochem. Photobiol.* 1969, 9, 439.
33. Gill, J. E. *Photochem. Photobiol.* 1969, 9, 313.
34. Melhuish, W. H. *J. Phys. Chem.* 1961, 72, 793.
35. Meech, S. R.; Phillips, D. *J. Photochem.* 1983, 23, 193.
36. Weber, G.; Teale, F. W. J. *Trans. Faraday Soc.* 1957, 53, 646.
37. Himel, C. M.; Mayer, R. T. *Anal. Chem.* 1970, 42, 130.
38. Cehelnik, E. D.; Cundall, R. B.; Palmer, T. F. *Chem. Phys. Lett.* 1976, 27, 586.
39. Demas, J. N.; Pearson, T. D. L.; Cetron, E. J. *Anal. Chem.* 1985, 57, 51.
40. Melhuish, W. H. *N.Z. J. Sci. Technol, Sect. B* 1955, 37, 142.
41. Drexhage, K. H. *J. Res. Nat. Bur. Stand., Sect. A*, 1976, 80, 421.
42. Kopf, U.; Heinz, J. *Anal. Chem.* 1984, 56, 1931.
43. Taylor, D. G.; Demas, J. N. *Anal. Chem.* 1979, 51, 717.
44. *Annual Book of ASTM Standards*; American Society for Testing and Materials: Philadelphia, Pa., 1987; Sec. 14, pp 545-550.
45. Lampert, R. A.; Chewter, L.A.; Phillips, D.; O'Connor, D. V.; Roberts, A.J.; Meech, S. R. *Anal. Chem.* 1983, 55, 68.

46. Barrow, D. A.; Lentz, B. R. *Chem. Phys. Lett.* 1984, 104, 163.
47. Lakawicz, J. R.; Cherek, H.; Baltur, A. *J. Biochem. Biophys. Methods* 1981, 5, 131.
48. Raynor, D. M.; McKinnon, A. E.; Szabo, A. G.; Hackett, P. A. *Can. J. Chem.* 1976, 54, 3246.
49. Chen, R. F. *Anal. Biochem.* 1974, 58, 593.
50. Chen, R. F. *J. Res. Nat. Bur. Stand., Sect. A* 1972, 76, 593.
51. Harris, J. M.; Lytle, F. E. *Rev. Sci. Instrum.* 1979, 48, 1469.
52. Van Houten, J. *J. Am. Chem. Soc.* 1976, 98, 4853.
53. Haaijman, J. J. Ph.D. Thesis, Organization for Health Research, Institute for Experimental Gerontology, Rijswijk, Netherlands, 1977.
54. Picciolo, G. L.; Kaplan, D. S. *Adv. Appl. Microbiol.* 1984, 30, 197.
55. Rollie, M. E.; Patonay, G.; Warner, I. M. *Anal. Chem.* 1987, 59, 180.
56. Bergquist, N. R.; Nilsson, P. *Ann. N.Y. Acad. Sci.* 1975, 254, 157.
57. Velapoldi, R. A.; Gjelsvik, N. A. In *Microbeam Analysis, 1987*; Geiss, R. H., Ed.; San Francisco Press: San Francisco, 1987, pp 202-204.
58. Fukuda, M.; Tsuchihashi, Y.; Takamatsu, T.; Nakanishi, K.; Fujita, S. *Histochemistry* 1980, 65, 269.
59. Jongsma, A. P. M.; Hijmans, W.; Ploem, J. S. *Histochemie*, 1971, 25, 329.
60. Kaplan, D. S. Ph.D. Dissertation, George Washington University, Washington, DC, 1985.
61. Sernetz, M.; Thær, A. *J. Microsc. (Oxford)* 1970, 91, 43.
62. Ploem, J. S. In *Standardization in Immunofluorescence*; Holborow, E. J., Ed.; Blackwell Scientific: Oxford and Edinburgh, 1970; pp 137-153.
63. van der Ploeg, M.; Ploem, J. S. *Histochemie* 1973, 33, 61.
64. Velapoldi, R. A.; Travis, J. C.; Cassatt, W. A.; and Yap, W. T. *J. Microsc. (Oxford)* 1976, 103, 293-303.
65. Epstein, M. S.; Velapoldi, R. A.; Blackburn, D. *Evaluation of Luminescent Glass Spheres as Calibration Standards for Microspectrofluorimetry*; National Bureau of Standards: Gaithersburg, MD; Annual Task Report to Food and Drug Administration, 1984, 1985, 1986; also, paper to be submitted.
66. Schwartz, A. *Quantitative Fluorescein Microbead Standards*; Flow Cytometry Standards Corporation: Research Triangle Park, NC 27709, [1985] technical brochure.
67. Bangs, L. B. *Am. Biotechnol. Lab.* May/June 1987, 10.
68. Velapoldi, R. A.; White, P. A.; May, W. E.; Eberhardt, K. R. *Anal. Chem.* 1983, 55, 1896.
69. Wise, S. A. In *Handbook of Polycyclic Aromatic Hydrocarbons*; Björseth, A., Ed.; Marcel Dekker: New York, 1983; Vol. 1, pp 183-256.
70. Wise, S. A. In *Handbook of Polycyclic Aromatic Hydrocarbons*; Björseth, A., Ed.; Marcel Dekker: New York, 1985; Vol. 2, pp 113-197.

71. Taylor, J. K. *Handbook for SRM Users*; NBS Spec. Publ. 260-100, 1985; For Sale By: Superintendent of Documents, U.S. Government Printing Office, Washington, DC 20402.
72. May, W. E.; Wise, S. A. *Anal. Chem.* 1984, *56*, 225.
73. Wise, S. A.; Benner, B. A.; Chesler, S. N.; Hilpert, L. R.; Vogt, C.R.; May, W. E. *Anal. Chem.* 1968, *58*, 3067

RECEIVED August 22, 1988



## Chapter 8

# Peroxyoxalate Chemiluminescence Reaction

### A Versatile Method for Activation of Fluorophore Luminescence

Richard S. Givens, Richard L. Schowen, John Stobaugh,  
Theodore Kuwana, Francisco Alvarez, Nikhil Parekh, Bogdan Matuszewski,  
Takao Kawasaki, Osborne Wong, Mirko Orlović, Hitesh Chokshi,  
and Kenichiro Nakashima

Center for Bioanalytical Research and Department of Chemistry,  
University of Kansas, Lawrence, KS 66045

Investigations have shown that the peroxyoxalate chemiluminescence reaction can be effectively used for a postcolumn detector in high-performance liquid chromatography (HPLC). The reaction generates the fluorescent state of certain suitable acceptors, such as 2-cyanobenz[*f*]isoindole (CBI) derivatives of amino acids, peptides, amines, and related primary amines. The derivatization method makes use of the reaction of 2,3-naphthalenedicarboxaldehyde and cyanide (NDA/CN) as a new fluorogenic and chemiluminescent reagent for analysis of primary amine functions. While the method has proven to be superior to standard fluorescence assays for low-level detection of amino acids and peptides, optimizing the method's sensitivity remains the current goal of this research. For this reason, the contributing parameters for efficient generation of chemiluminescence for the assay of CBI derivatives based on oxalate-hydrogen peroxide activation have been identified and investigated. Among the important factors are: (i) the nature of the leaving group on the oxalate ester, (ii) the fluorescence properties of the NDA/CN analyte, (iii) the fluorescence-quenching capabilities of the oxalate ester and its reaction products, (iv) solvent effects, and (v) the effects of added catalysts.

In order to optimize the chemiluminescence response, we have investigated the mechanism of the complex reactions leading to chemical generation of chemiluminescence. A new peroxyoxalate-hydrogen peroxide reaction mechanism has emerged from our preliminary studies on the five contributing factors listed above. Two kinetic models are discussed, one for the

NOTE: Dedicated to the Memory of Professor Takeru Higuchi (1916–1987)

0097-6156/89/0383-0127\$08.00/0

• 1989 American Chemical Society

mechanism of the reaction in organic solvents and the second for mixed aqueous-organic solvents. The latter model is particularly adaptable to quantitative rate studies and has become the focus of efforts to develop the peroxyoxalate chemiluminescence reaction as a postcolumn detector for HPLC.

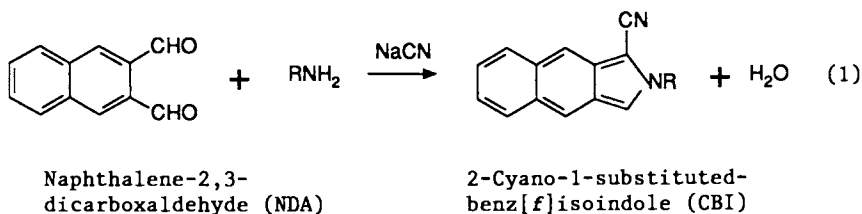
Applications of the oxalate-hydrogen peroxide chemiluminescence-based and fluorescence-based assays with NDA/CN derivatives to the analysis of amino acids and peptides are included. The sensitivity of the chemiluminescence and fluorescence methods is compared for several analytes. In general, peroxyoxalate chemiluminescence-based methods are 10 to 100 times more sensitive than their fluorescence-based counterparts. The chief limitation of chemiluminescence is that chemical excitation of the fluorophore apparently depends on its structure and oxidation potential.

The potential for improved chemiluminescent detection is large, since the efficiency for activation of the acceptor is less than 0.01%. A thousand-fold increase in signal could be anticipated from this reaction.

The Center for Bioanalytical Research was established in 1983 to further the already existing studies in the areas of bioanalytical and pharmaceutical chemistry at the University of Kansas, which were directed toward the discovery and development of exquisitely sensitive methods for bioanalysis. Among the areas of interest were fluorogenic methods for the assay of primary amines, amino acids, oligopeptides, and proteins. Methods for primary amines and amino acids have been extensively studied, for example, and a number of excellent sensitive fluorogenic reagents have emerged. One of the most popular is the combination of *ortho*-phthalaldehyde (OPA) and 2-mercaptoethanol (2-ME), discovered by Roth (1), examined by Simons and Johnson (2,3), and developed for precolumn or postcolumn derivatization of amino acids in high-performance liquid chromatography (HPLC) analyses by a number of workers, including Bensen and Hare (4).

A number of drawbacks in the application of the OPA/2-ME reagent system include the instability of the fluorescent isoindole derivative (5-7); the use of the noisome reagent 2-mercaptoethanol; the low and solvent-dependent fluorescence efficiencies (8,9) of the isoindole; and--perhaps the most limiting--the effective restriction of the OPA assay to primary aliphatic amines and to amino acids. Most oligopeptides and polypeptides do not give fluorescent adducts. (However, see Ref. 10.)

The initial discoveries of the extension of the aromatic ring of the *ortho*-phthalaldehyde (OPA) to a naphthalene-2,3-dicarboxaldehyde (NDA) and the substitution of cyanide (CN<sup>-</sup>) for 2-ME as the nucleophile have provided the Center with a much more versatile reagent system (5,11), which maintains the sensitivity for primary aliphatic amines and amino acids, and now is known to form fluorescent products with oligopeptides, proteins, and other related analytes that possess a primary amine function (Equation 1).



The derivatization process (5) is accomplished in aqueous media at basic pH (pH 7-10) in a matter of approximately 15 min to yield a 2-cyanobenz[f]isoindole (CBI), which is stable for 10 to 12 hr in solution. As shown in Figure 1, the absorption characteristics of the CBI adducts are also readily accessible for assay by standard fluorescence or ultraviolet detection. In addition to the absorption between 200 and 300 nm, there are two maxima in the visible spectrum at approximately 420 and 440 nm accessible for fluorescence or ultraviolet detection. A probable mechanism (5,11) for the CBI formation is illustrated in Scheme 1.

The stability of the CBI derivative is sufficient for its isolation and complete characterization (11), an accomplishment that is not realized with most OPA adducts. Thus, the CBI derivatives of a number of representative amino acids and amines have been isolated and their fluorescent properties determined as a function of the media and other relevant parameters encountered in reverse-phase HPLC (RP-HPLC).

Perhaps most encouraging in these discoveries was the observation that NDA/CN<sup>-</sup> worked equally well for derivatization of dipeptides and higher homologues of the primary amino acid series. Again, a stable, fluorescent, isolatable derivative was obtained. One of the most important initial findings was the high fluorescence efficiency of the CBI adduct (12). Tables 1 and 2 list the efficiencies for a representative group of mono-, di-, and tripeptides and a limited comparison of the CBI efficiencies with the more traditional OPA (8) and dansyl (9) derivatives, respectively.

As noted, the fluorescence efficiencies of the CBI adducts are invariably greater than those of OPA or dansyl analogs, generally ranging from 0.4 to 0.8, with the exception of the bis-CBI adduct of

Table I. Effects of Peptide Substituents on Fluorescence Quantum Efficiencies ( $\phi_F$ ) of 1-Cyano-N-substituted Benz[f]isoindoles (CBI) in Aqueous Acetonitrile

CBI derivative	R	$\phi_F$
	-Gly	0.73
	-Gly-Gly	0.48
	-Gly-Gly-Gly	0.59
	-Ala	0.75
	-Ala-Ala	0.54
	-Lys	0.55
	-Lys-CBI	0.03

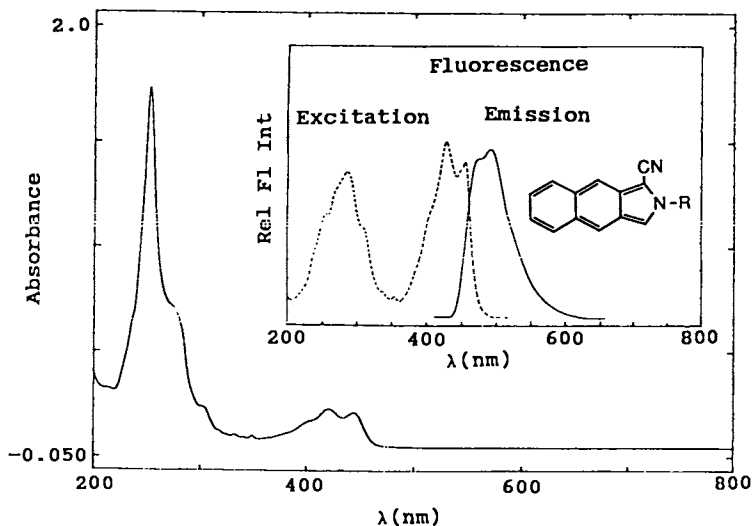
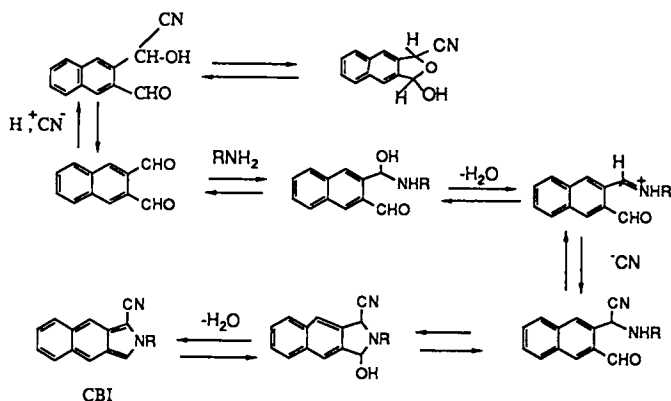


Figure 1. Absorption and fluorescence spectra of the cyanobenz-[f]isoindole chromophore: CBI-Ala.



Scheme 1. Probable mechanism for CBI formation.

Table II. A Comparison of Fluorescence Quantum Efficiencies ( $\Phi_F$ ) of OPA, Danysl, and CBI Derivatives in Aqueous-Organic Mixed Solvents

Labeled Amino Acid	OPA (8)	Danysl (9)	CBI (12)
Ala	0.40		0.75
Gly	0.39	0.065	0.73
Tyr	0.33	0.068	
Val	0.34	0.091	
Lys	0.34		0.55
Gly·Gly	0.14		0.48
Gly·Gly·Gly	0.081		0.59

lysine. This amino acid has two primary amine functions, both of which react with NDA/CN<sup>-</sup>. The weak fluorescence of the bis-CBI adduct suggests that an intramolecular complex of the two newly formed chromophores may result in a significant increase in the internal decay or quenching of the first excited singlet state (13). Efforts to circumvent the quenching effect or to improve on the emission efficiency of the lysine bis-adduct have largely been ineffective.

If reaction time is kept short, however, the derivatization process can be intercepted at the mono-adduct form, which is sufficiently fluorescent for assay purposes. It should be noted that the fluorescence efficiencies of the CBI adducts are relatively insensitive to the water content of the solvent mixture (11,12) in contrast with earlier reports on the dansyl derivatives, which lose an order of magnitude of efficiency in aqueous-based solvent systems (9).

Figure 2 is a chromatogram of 18 primary amino acids that were first converted to the CBI adducts with NDA/CN<sup>-</sup> in borate buffer (pH 9.5) and then separated by RP-HPLC (5,14). The trace represents 20 pmol of each amino acid injected followed by elution through an Ultrasphere ODS (4.6 × 250 mm) column with a gradient that consisted initially of 10% tetrahydrofuran/phosphate buffer (pH 6.8) (solvent A), to which was added a 55% acetonitrile/10% methanol/phosphate buffer (solvent B), producing a final mixture of 40% solvent A and 60% solvent B. The limits of detection and the relative sensitivity of the assay are considerably enhanced with laser-induced fluorescence (LIF) detection, as reported earlier by Roach and Harmony (15). At a signal-to-noise ratio of 2, a conventional fluorescence detector (Kratos FS-980) is sensitive to levels as low as 10 to 30 fmol for the amino acids listed in Table III. However, with LIF, the improvement in detection limits is approximately two orders of magnitude, i.e., 0.1 to 0.4 fmol. A further comparison of the limits for NDA/CN<sup>-</sup> and those for OPA/2-ME using LIF is given in Table III. In this direct comparison of the two tagging reagents, the NDA/CN<sup>-</sup> method is approximately thirtyfold better.

The versatility of the reagent system in the assay of small peptides is nicely illustrated in Figures 3 through 5. Neurotensin, a polypeptide composed of 13 amino acids, and three fragments from partial hydrolysis were derivatized with NDA/CN<sup>-</sup> and separated by

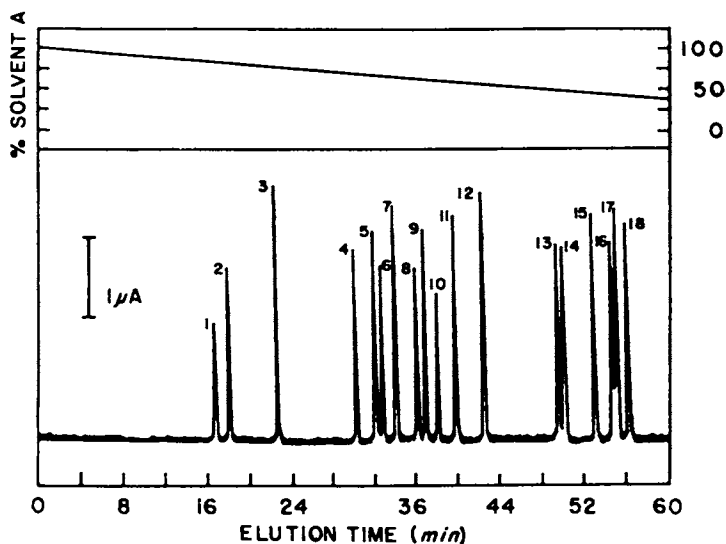


Figure 2. Gradient-elution profile (5) of 18 amino acids derivatized with NDA/CN<sup>-</sup>. The peak numbers correspond to those listed in Table III. Each peak represents 20 pmol of the individual amino acids. The chromatographic conditions are described in the text. (Reprinted from reference 5. Copyright 1987 American Chemical Society.)

Table III. Detection Limits of OPA/2-ME and NDA/CN<sup>-</sup> Derivatized Amino Acids Using Conventional and Laser-Induced Fluorescence (LIF) Detection<sup>a</sup>

Amino Acid	Abbr	Detection limits <sup>b</sup> (fmol)			
		OPA		NDA	
		Conventional	LIF	Conventional	LIF
1. Cysteic acid	cya	N/A	N/A	33	N/A
2. Aspartic acid	asp	170	4.7	23	0.16
3. Glutamic acid	glu	200	4.4	20	0.16
4. Asparagine	asn	210	10.4	21	0.43
5. Histidine	his	510	7.0	22	0.36
6. Glutamine	gln	1070	7.8	18	0.33
7. Serine	ser	280	6.4	18	0.11
8. Arginine	arg	240	14.6	10	0.27
9. Glycine	gly	420	6.8	18	0.16
10. Threonine	thr	290	6.9	25	0.23
11. Alanine	ala	250	10.3	19	0.20
12. Tyrosine	tyr	250	8.5	15	0.24
13. Valine	val	N/A	N/A	20	0.28
14. Methionine	met	280	10.5	17	0.28
15. Tryptophan	trp	460	12.3	15	0.36
16. Isoleucine	ile	180	14.2	19	0.32
17. Phenylalanine	phe	340	13.2	15	0.27
18. Leucine	leu	N/A	N/A	15	N/A

<sup>a</sup>Reported in Ref. 15.<sup>b</sup>Detection limits based on signal-to-noise ratio of 2.

RP-HPLC (Figure 3) (Wong, O. S., unpublished results). These oligopeptides were easily identified and monitored at the picomole level.

Figure 4 shows the time course of the enzymatic hydrolysis of a 2.5-nmol sample of *met*-enkephalin, a pentapeptide, which was monitored by the NDA/CN<sup>-</sup> methodology (5) by RP-HPLC with fluorescence detection. The sequential enzymatic hydrolysis of the N-terminal amino acids was followed as they were released. Figure 4A shows the initial release of tyrosine, the N-terminal amino acid, which is then followed by release of glycine (4B), the second amino acid in the sequence. The final hydrolyzate (4C) indicates that the peptide includes a second glycine, a phenylalanine, and a methionine, which constitute the remaining amino acids. The sequential arrangement was established with additional determinations at intermediate hydrolytic stages (not shown) to be Tyr·Gly·Gly·Phe·Met in accord with the known structure. Lastly, Figure 5 demonstrates that *leu*-enkephalin in plasma can be detected with NDA/CN<sup>-</sup> down to 0.32 nmol/mL using conventional fluorescence detection methods, still considerably above the normal endogenous levels of these opiate pentapeptides (de Montigny, Ref. 14 and unpublished results).

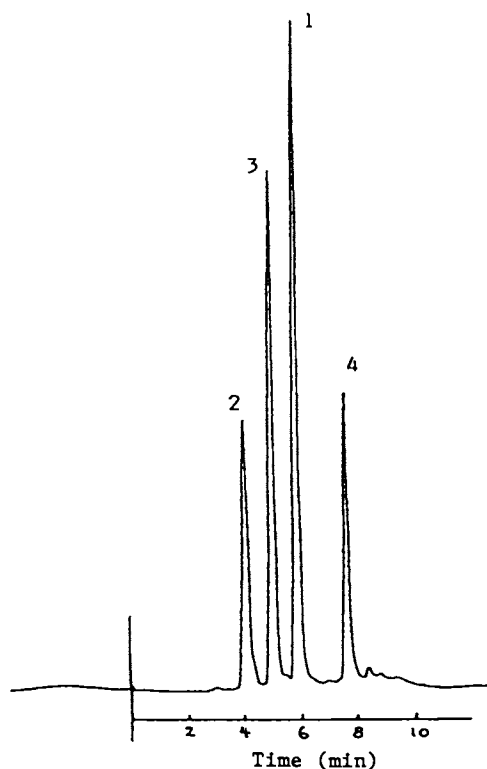


Figure 3. Chromatogram of neurotensin-CBI (NTS) and neurotensin-fragment-CBI products (Wong, O. S., unpublished results).

Peptides derivatized with NDA/CN. HPLC conditions: 4.6 × 150 mm TSK-gel ODS-120T column, 5 μm; mobile phase: (A) 10% MeCN, 50 mM phosphate buffer, pH 3; (B) 73% MeCN, 50 mM phosphate buffer, pH 3; 1.0 mL/min; 10 μL injection; Shimadzu R-530 fluorescence detector, 420 nm (ex)/490 nm (em), 12 μL flow cell; LKB dual pump gradient system.

- |    |  |          |
|----|--|----------|
| 1. | NTS (1-13) Glu-Leu-Tyr-Glu-Asn-Lys-Pro-Arg-Arg-Pro-Tyr-Ile-Leu | 5.5 pmol |
| 2. | NTS (1-11) Glu-Leu-Tyr-Glu-Asn-Lys-Pro-Arg-Arg-Pro-Tyr         | 5.0 pmol |
| 3. | NTS (1-8) Glu-Leu-Tyr-Glu-Asn-Lys-Pro-Arg                      | 5.0 pmol |
| 4. | NTS (1-6) Glu-Leu-Tyr-Glu-Asn-Lys                              | 5.0 pmol |



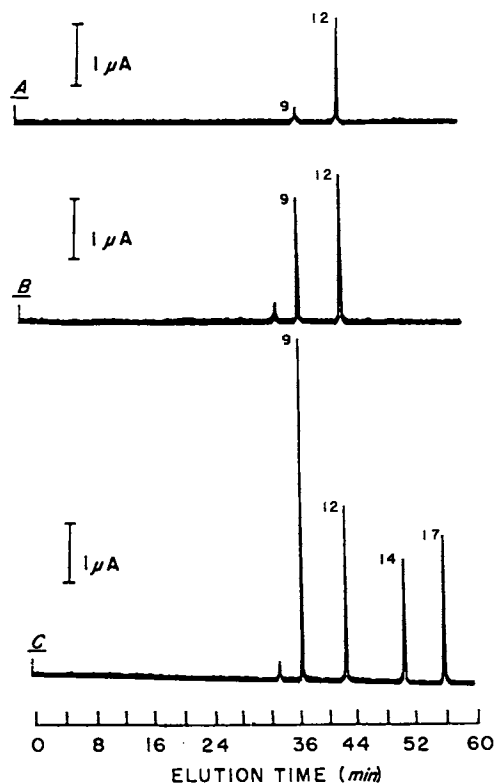


Figure 4. Enzymatic hydrolysis of met-enkephalin (2.5 nmol) showing the sequential release of amino acids and the final mixture. The amino acids were identified from the retention times of the standard amino acid mixture: 9, Gly; 12, Tyr; 14, Met; 17, Phe. (Reprinted from reference 5. Copyright 1987 American Chemical Society.)

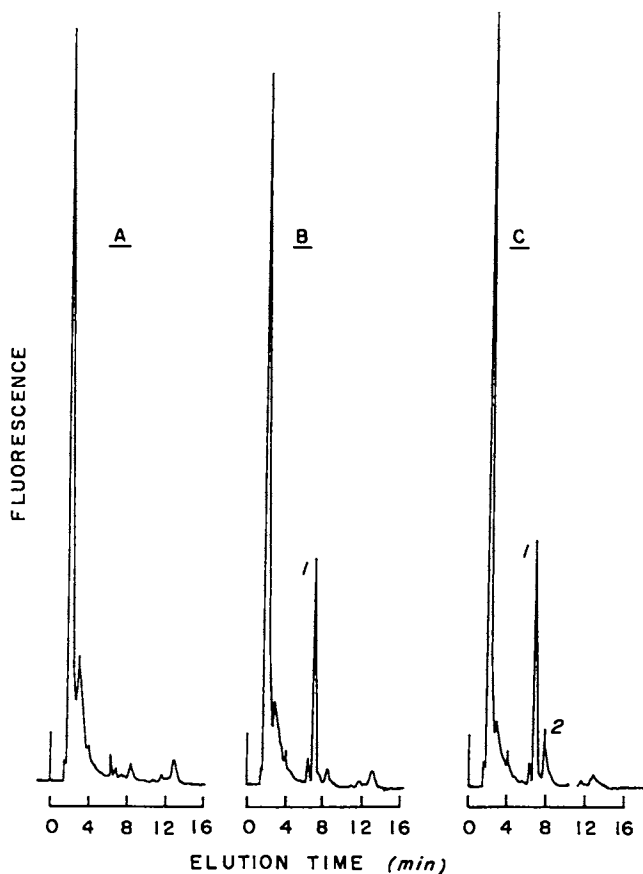


Figure 5. Chromatograms of a blank (A) and plasma samples spiked with *leu*-enkephalinamide (B, 1, 1.25 nmol/mL) and *leu*-enkephalin (C, 2, 0.32 nmol/mL) (de Montigny, Ref. 14 and unpublished results).

Though these examples may be impressive illustrations of the power of NDA/CN<sup>-</sup> as a fluorogenic reagent for oligopeptides, important applications require detection limits well below those we have attained above (e.g., leu-enkephalin). Some of the inherent limitations are the selectivity of the reagent for the analyte, the quantitative reaction with the substrate, and the stability of the reagent against unwanted, interfering side reactions. Other significant contributions to the limits of detection arise from the fluorescence method itself. Contributors to the noise and background signals include the stray light from the source, scattered light, emission from fluorescent impurities, excitation lamp instability, and Raman emission. These latter factors reduce the signal-to-noise ratio in fluorescence assays and thus keep the lower limits of detection relatively high.

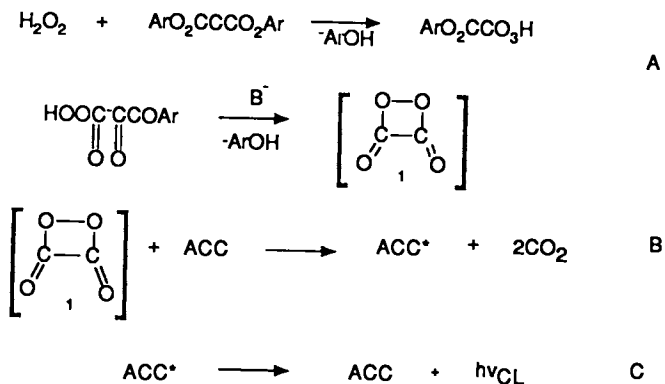
An alternative method, one which requires no light source, is the chemical generation of the fluorescent state, i.e., the chemiluminescent method. Though a variety of chemiluminescent reactions are available, the peroxyoxalate method presents enough versatility and sufficient flexibility in its application to warrant investigation in conjunction with our NDA/CN<sup>-</sup> methodology. Historically, the use of a reaction between an oxalate ester and hydrogen peroxide in the presence of certain fluorescent molecules has been known to produce the corresponding fluorescence emission with good efficiency (16). Rauhut's studies on the mechanism of the reaction reported 20 years ago (16) suggested the intermediacy of a 1,2-dioxetanedione (1, Scheme 2), an analog of other 1,2-dioxetane derivatives known to produce chemiluminescence. While the intermediacy or even the existence of compound 1 has never received experimental support, it remains the suggested chemical precursor to the chemiluminescent step.

In the chemiluminescence-based HPLC detection system, illustrated schematically in Figure 6, the oxalate ester and hydrogen peroxide are introduced to the eluent stream at postcolumn mixer M<sub>2</sub>, which then flows through a conventional fluorescence detector with the exciting lamp turned off or a specially built chemiluminescence detector. The two reagents are combined at mixer M<sub>1</sub>, rather than being premixed, to prevent the slow hydrolytic reactions of the oxalate ester.

Our initial attempts with this design using the NDA/CN<sup>-</sup> system were encouraging far beyond our expectations. Our enthusiasm was sustained when we found that dipeptide-CBI derivatives could be detected at the femtomole level (Tables IV and V) and that such limits of detection with our purified derivatives under less-than-

Table IV. Application of NDA/CN Labels for RP-HPLC with Chemiluminescence Detection

CBI Derivative	Amount Injected (pmol)	Peak Height (mm)	Peak Height (mm/pmol)
dI-Ala	3.6	695	199
d-Ala-d-Ala	2.5	540	216



Scheme 2. Mechanism for hydrogen peroxide-oxalate ester generation of chemiluminescence. Ar = aryl; B<sup>-</sup> = a base.

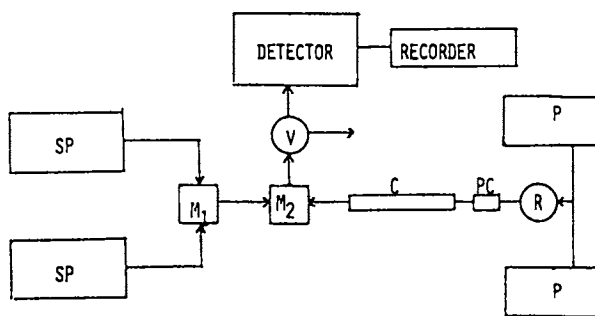


Figure 6. Chemiluminescent HPLC postcolumn reactor system.

Table V. Comparison of Limits of Detection (LOD) for Dansyl and NDA Derivatives Employing Fluorescence and Chemiluminescence Detection for RP-HPLC

Derivative	Chemiluminescence*		Fluorescence		Ratio CL/FL
	Peak Height (mm/pmol)	Relative Peak Height	LOD (fmol)	LOD (pmol)	
Dansyl-Gly	10	1.0	100-150	7	50-70
Dansyl-Asp	25	2.5	60	11	180
CBI-Ala	196	19.6	8	4	500

\*A conventional fluorescence detector with a 15- $\mu$ L sample cell was employed.

Table VI. RP-HPLC Chemiluminescence Sensitivity in Previous Studies with Oxalate Esters  
[All studies used 2,4,6-trichlorophenyl oxalate with H<sub>2</sub>O<sub>2</sub>]

Chemiluminescent Analyte	LOD (fmol)	Ref.
1. Dansyl-Amino Acids* -----	2 - 5	17
2. Fluorescamine-Catecholamines -----	10 - 20	a
3. Dansyl-Amines -----	0.8- 14	18,19
NBD (7-nitrobenzo-2-oxa-1,3-diazole)-		
Amines -----	19 - 270	18,19
OPA (o-phthalaldehyde)-Amines -----	94 - 580	18,19
4. PAH (polynuclear aromatic hydrocarbons) ---	100-125,000	b
5. Amino-PAH -----	0.1- 10	c

a. Imai, K., et al. *Anal. Biochem.* 1981, 112, 99-104.

b. Birks, J. W., et al. *Anal. Chem.* 1983, 55, 432.

c. Birks, J. W., et al. *Anal. Chem.* 1984, 56, 1096; Weinberger, R. *J. Chromatogr.* 1984, 288, 445.

\*Using a chemiluminescence detector with 60- $\mu$ L sample cell.

optimal conditions were essentially an order of magnitude better than those obtained with the dansyl-Gly and dansyl-Asp derivatives as reported by Imai (17) and Melbin (18,19) (see Table VI).

To our surprise and satisfaction, the general approach worked; the CBI derivatives did chemiluminescence, and the sensitivity enhancement was 30- to 50-fold over fluorescence! With this success, we embarked on a more thorough study of chemiluminescence with the goal of optimizing the method. Identifiable parameters that affected the efficiency of light emission from a chemically generated fluorescent molecule included:

- (1) the nature of the phenolic leaving group,
- (2) the fluorescence properties of the CBI derivatives (analytes),

- (3) the fluorescence quenching capabilities of the oxalate ester and its products (especially the phenol),
- (4) solvent effects on the fluorescence emission, and
- (5) the effects of additional reagents and catalysts normally encountered in HPLC assays.

To understand how these parameters affected the efficiency of the chemiluminescent reaction, we examined the mechanism originally proposed by Rauhut (16). As shown in Scheme 2, hydrogen peroxide reacts with an oxalate ester, such as 2,4,6-trichlorophenyl oxalate (TCPO), in a two-step process to form a reactive intermediate for which Rauhut suggested structure 1, the 1,2-dioxetanedione. The dioxetanedione then interacts with an acceptor (ACC) to produce two molecules of CO<sub>2</sub> and the excited state of the acceptor. The last stage of the sequence is fluorescence emission from the acceptor.

A useful division of the contributing mechanistic features of any chemiluminescence process involving excitation of a "spectator" fluorophore is given in Equation 2. To optimize the chemical efficiency ( $\phi_{CHEM}$ ), we have also undertaken a systematic investigation of the reaction condition variables that are encountered in typical HPLC assays.

$$\phi_{CL} = \phi_{CHEM} \cdot \phi_{EXCH} \cdot \phi_{FL} \quad (2)$$

where  $\phi_{CL}$  is the total chemiluminescence quantum efficiency,  
 $\phi_{CHEM}$  is the efficiency of the chemical reaction,  
 $\phi_{EXCH}$  is the efficiency of the energy exchange from chemical potential to electronic excitation energy, and  
 $\phi_{FL}$  is the fluorescence efficiency.

More recent work on the analogous dioxetanes (2 in Figure 7) and dioxetanones (3 in Figure 7) by Turro (20), Schuster (21,22), and Adam (23) has shown that excitation of the acceptor can occur by two different processes: direct energy transfer to the acceptor from dioxetane, or oxidation of the acceptor by dioxetanone, followed by chemical decomposition of the dioxetanone and electron transfer back to the radical cation of the acceptor, yielding its singlet excited state. That neither of these two mechanisms alone accounts for the peroxyoxalate system was clearly indicated by the earlier work of Turro (20), who found no correlation of chemiluminescence intensity to either the excitation energy or the oxidation potential of the acceptor (Figure 7).

Indeed, our own examination (24) of the time course of the TCPO-H<sub>2</sub>O<sub>2</sub>-induced chemiluminescence of diphenylanthracene (DPA) in ethyl acetate with varying concentrations of triethylamine revealed a biphasic emission profile, a result that is inconsistent with a single reactive (light-producing) intermediate in this reaction (Figure 8). With increasing amine concentration (from curve a to b to c), the biphasic profile is shifted toward a single maximum, but the analytical form of the light intensity decay is biexponential, indicating that more than one active intermediate remains. In fact,

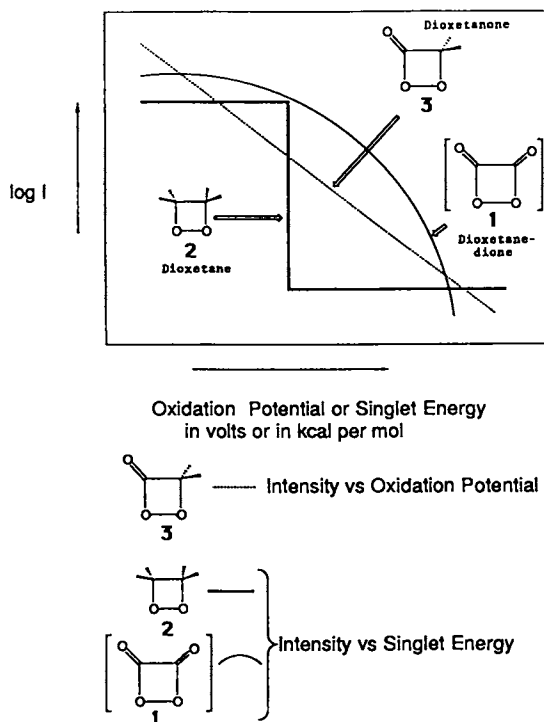


Figure 7. Absence of a linear correlation of either oxidation potential or singlet energy to chemiluminescence efficiency for the peroxyoxalate reaction.

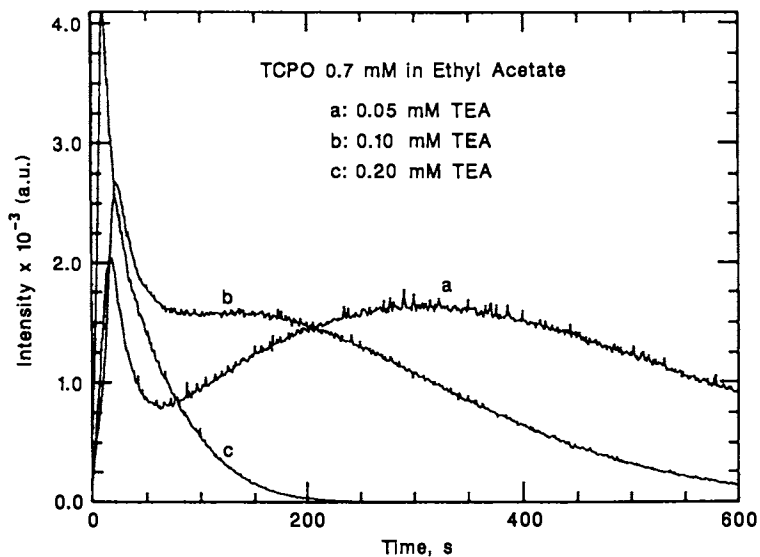


Figure 8. Observed decay curves for TCPO-H<sub>2</sub>O<sub>2</sub>-DPA chemiluminescence. TEA, triethylamine; a.u., arbitrary units. (Reproduced from Ref. 24. Copyright 1986 American Chemical Society.)



careful scrutiny of the published time-curves in the seminal report of Rauhut et al. (16) reveals parallel behavior for similar chemiluminescent reactions that they examined.

To confirm that the emission under each of the two maxima detected in our study was in fact that of DPA, the wavelength dependence was monitored as a function of the intensity with each one. As shown in Figure 9, the emission spectra are those of the DPA fluorescent excited state.

From these results, we have constructed a mathematical model (24) for the time-dependent emission which incorporates three reactive intermediates:

$$I = \frac{dh\nu}{dt} = fk_a[X] + gk_b[Y]$$

$$I = [OX]_0 \left\{ \frac{fk_a}{(k_T - k_x)} (e^{-k_x t} - e^{-k_T t}) + \frac{gk_b k_x k_y k_z}{(k_T - k_x)} \left[ \frac{(e^{-k_x t} - e^{-k_b t})}{(k_y - k_x)(k_b - k_x)} + \frac{(e^{-k_T t} - e^{-k_b t})}{(k_y - k_T)(k_b - k_x)} \right] + \frac{gk_b k_x k_y k_z}{(k_T - k_y)} \left[ \frac{(e^{-k_y t} - e^{-k_b t})}{(k_y - k_x)(k_b - k_y)} \right] \right\} \quad (3)$$

where  $[OX]_0$  is the initial oxalate concentration,  $h\nu$  is the photon count,  $f$  is the fraction of X that goes to  $X'$ ,  $g$  is the fraction of Y that goes to  $Y'$ ,  $k_x$ ,  $k_y$ ,  $k_z$ ,  $k_a$ , and  $k_b$  are the rate constants for the reactions shown in Scheme 3, and  $k_T$  is the sum of  $k_a$  and  $k_b$ . X,  $X'$ , Y,  $Y'$ , and Z represent the necessary putative chemical intermediates shown in the reactions scheme.

Two of these intermediates (X and Y) lead to the chemiluminescent process, and a third (Z) serves as a bridge or "way station" between the two light-inducing species. A schematic representation based on this kinetic model is shown in Scheme 3. This model correctly simulates the series of time-dependent intensity curves, as is seen by comparing Figure 10 to Figure 8. Thus, the chemical generation of the "reactive intermediate(s)" is a much more complex process than originally envisioned by Rauhut (16). This finding is in agreement with recent work by Cundall (25), but contrasts with earlier reports, which repeatedly proposed a single intermediate, i.e., the dioxetanedione mechanism (26-29).

Fortunately, as the reaction is transferred from a purely organic solvent system to mixed organic-aqueous media, which are employed in most RP-HPLC separations, the apparent multiplicity of maxima in the time profile of the intensity dependence seems to be suppressed or to collapse to a reasonably simple biexponential-like dependence. As shown in Figure 11, simply changing the solvent from ethyl acetate to 95% aqueous acetonitrile and the catalyst from triethylamine to imidazole produces a single maximum profile, one that is more easily modeled mathematically, as defined in Equation 4:

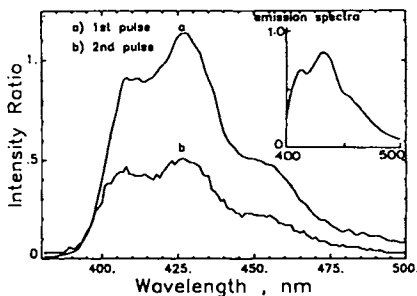
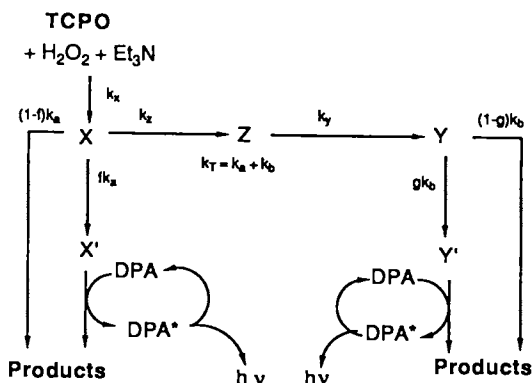


Figure 9. Chemiluminescence emission spectra from the two pulses with DPA as the acceptor; inset is DPA fluorescence spectrum. (Reproduced from Ref. 24. Copyright 1986 American Chemical Society.)



Scheme 3. General mechanism for the TCPO-H<sub>2</sub>O<sub>2</sub>-DPA chemiluminescence. (Reproduced from Ref. 24. Copyright 1986 American Chemical Society.)

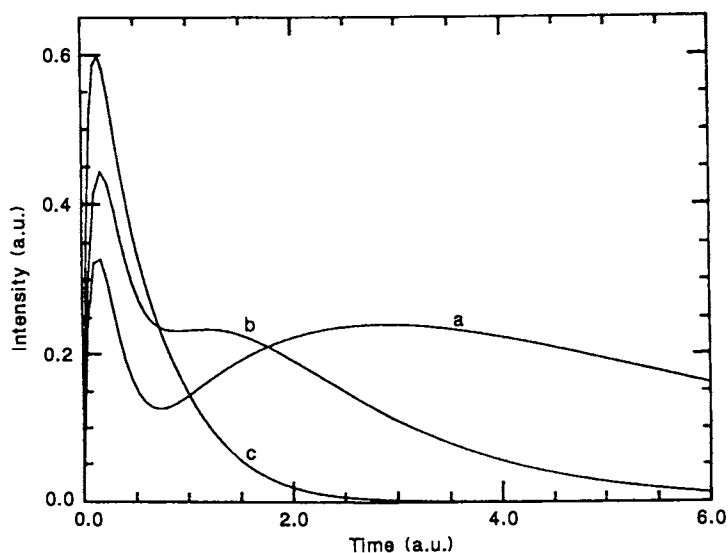


Figure 10. Simulated decay curves from the kinetic analysis of the TCPO- $\text{H}_2\text{O}_2$ -DPA chemiluminescence. Arbitrary units (a.u.) used on both axes. (Reproduced from Ref. 24. Copyright 1986 American Chemical Society.)

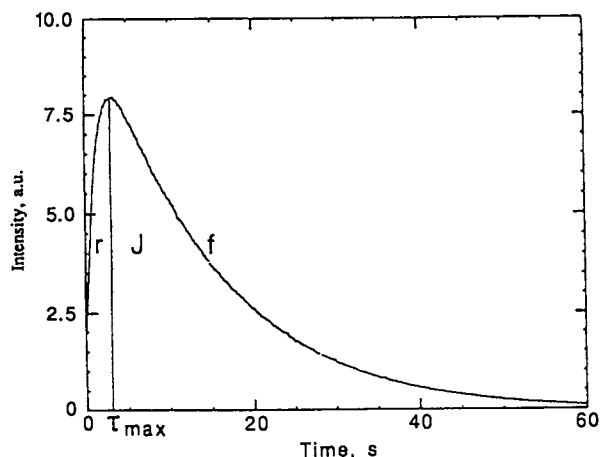


Figure 11. Time-dependent emission for aqueous acetonitrile chemiluminescence of TCPO- $\text{H}_2\text{O}_2$ -imidazole system measured at 430 nm.

$$I(t) = \frac{Mr}{f-r} (e^{-rt} - e^{-ft}) \quad (4)$$

where  $I(t)$  is the emission intensity,  
 $M$  is the (theoretical) initial maximum intensity,  
 $r$  is the rise rate constant,  
and  $f$  is the fall rate constant.

This model permits a determination of the rate constants for the rise of the chemiluminescence intensity and its subsequent decay and, more importantly, allows a quantitative assessment of the effects of reaction conditions, such as solvent variation, temperature, or additives, on the rates ( $r$  and  $f$ ), the time required ( $\tau_{max}$ , Equation 5), the intensity ( $J$ , Equation 6), and the efficiency ( $Y$ , Equation 7) of a particular chemiluminescent reaction (see also Figure 12).

$$\tau_{max} = [\ln(f/r)]/(f-r) \quad (\text{Time required for the emission to reach maximum}) \quad (5)$$

$$J = M(r/f) \quad (\text{Maximum intensity}) \quad (6)$$

$$Y = \int_0^{\infty} I(t) dt = M/f \quad (\text{Quantum efficiency}) \quad (7)$$

Such an analysis has been conducted for the TCPO-H<sub>2</sub>O<sub>2</sub>-DPA reaction by varying the solvent, the temperature, and the concentrations of the reactants. Some of the results from this study are presented in Table VII.

The rate constants for phenol release (2,4,6-trichlorophenol; TCP) were determined spectrophotometrically at 298 nm in both the presence and the absence of the fluorophore (DPA) and were shown to be independent of DPA at the concentrations employed. The time-dependent release of TCP monitored at 298 nm, which is shown in

Table VII. Effect of H<sub>2</sub>O<sub>2</sub> Concentration on the TCPO-H<sub>2</sub>O<sub>2</sub>-DPA Reaction

[H <sub>2</sub> O <sub>2</sub> ] (mM)	Rise Rate Constant, $r$ ( $\times 10^3 \cdot s^{-1}$ )	Fall Rate Constant, $f$ ( $\times 10^2 s^{-1}$ )	Maximum Intensity, $J$ (au)	Quantum Efficiency, $Y$ ( $\phi \times 10^4$ )
1.25	3.0	3.6	1.7	2.9
2.50	3.2	3.5	1.8	3.2
5.0	3.4	3.2	2.5	4.5
10.0	3.7	2.6	3.5	6.7
30.0	11.0	2.2	4.9	10.0
120.0	22.5	3.0	5.9	8.4

[TCPO] = 0.75 mM  
[DPA] = 0.075 mM  
[Imidazole] = 2.5 mM  
25°C  
pH 7.0

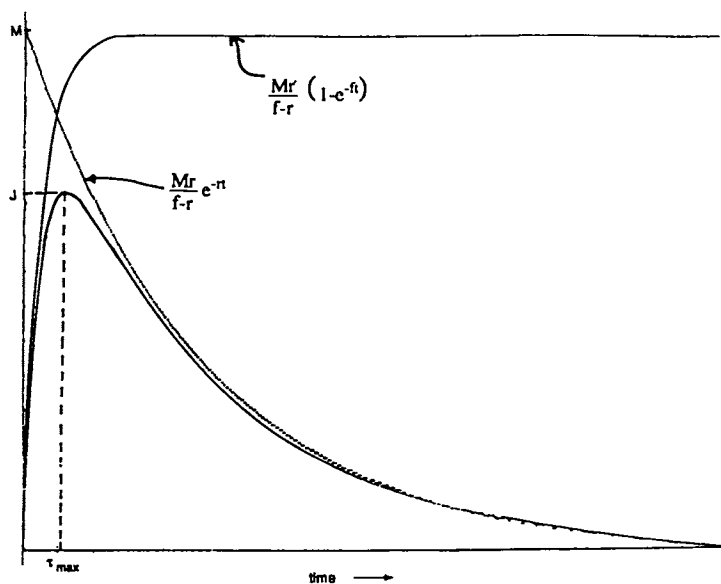


Figure 12. Efficiency, lifetime, and intensity of single-maximum model.

American Chemical Society  
Library

1155 16th St. NW

In Luminescence Applications, C. D. Givens, M.; ACS Symposium Series, American Chemical Society, Washington, DC, 1989.

Washington, D.C. 20036

Figure 13, indicates that the first mole of phenol is released in <30 s, the same elapsed time for the chemiluminescence to reach a maximum intensity. In fact, the measured rate constant  $r$ , for the rise in the chemiluminescence emission, is identical to the rate of the first phenol's release from the oxalate ester. Furthermore, the slower rate of release of the second phenol ligand has a rate constant that is identical to the chemiluminescence decay rate  $f$ . Thus, the model allows a quantitative analysis of the reaction mechanism, heretofore not available to us. We intend to continue this avenue of investigation in order to optimize the chemiluminescence efficiencies under HPLC conditions and to delineate further the mechanism for peroxy-oxalate chemiluminescence.

We have also investigated other oxalate esters as a potential means to improve the efficiency. The most commonly used oxalates are the 2,4,6-trichlorophenyl (TCPO) and 2,4-dinitrophenyl (DNPO) oxalates. Both have severe drawbacks: namely, their low solubility in aqueous and mixed aqueous solvents and quenching of the acceptor fluorescence. To achieve better solubility and avoid the quenching features of the esters and their phenolic products, we turned to difluorophenyl oxalate (DFPO) derivatives 5 and 6 (Figure 14). Both the 2,4- and the 2,6-difluoro esters were readily synthesized and were shown to be active precursors to DPA chemiluminescence. In fact, the overall efficiency of the 2,6-difluorophenyl oxalate 5 is higher than for TCPO in the chemical excitation of DPA under the conditions outlined earlier. Several other symmetrical and unsymmetrical esters were also synthesized, but all were less efficient than either TCPO or 2,6-DFPO (Figure 14).

The quenching effects of these esters and the phenolic products were also measured using standard Stern-Volmer quenching procedures, and the quenching constants ( $K_q$ ) were recorded (Table VIII). Neither the difluoro derivatives nor their phenols posed a serious problem to the chemiluminescence of either the CBI- or dansyl-labeled amino acids.

Table VIII. Quenching Effects by Oxalates and Product Phenols on CBI- and Dansyl-Labeled Amino Acids

Quencher	CBI-Ala ( $K_q$ in $M^{-1}$ )	Dansyl-Asp ( $K_q$ in $M^{-1}$ )
Phenyl Oxalate		
2,4-difluoro	40	30
2,6-difluoro	43	50
2,4,6-trichloro	120	54
2,4-dinitro	580	900
Phenols		
2,4-difluoro	14	0.4
2,6-difluoro	11	0.7
2,4,6-trichloro	11	0.9
2,4-dinitro	290	600

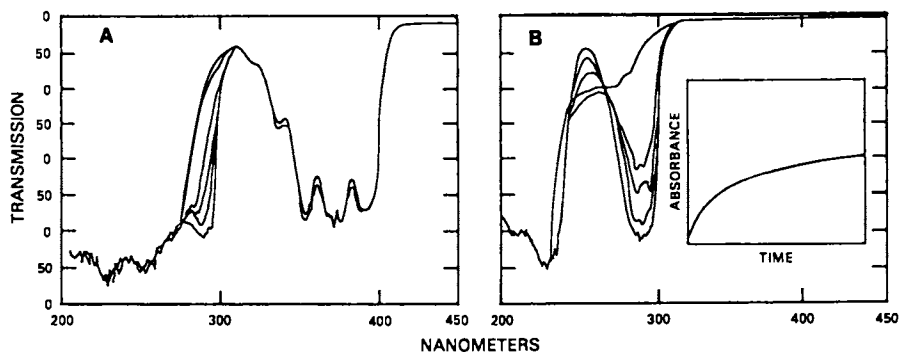
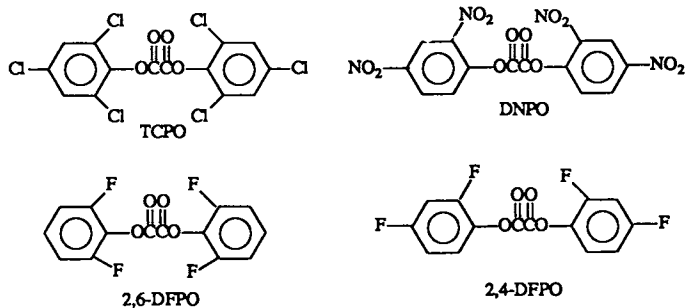


Figure 13. Release of TCP ( $\lambda_{max} = 298 \text{ nm}$ ) from the TCPO- $\text{H}_2\text{O}_2$  reaction, with and without DPA, in acetonitrile-imidazole buffer (75% aq. acetonitrile) monitored by absorbance change. A, In the presence of DPA. B, Without DPA present.

A



B

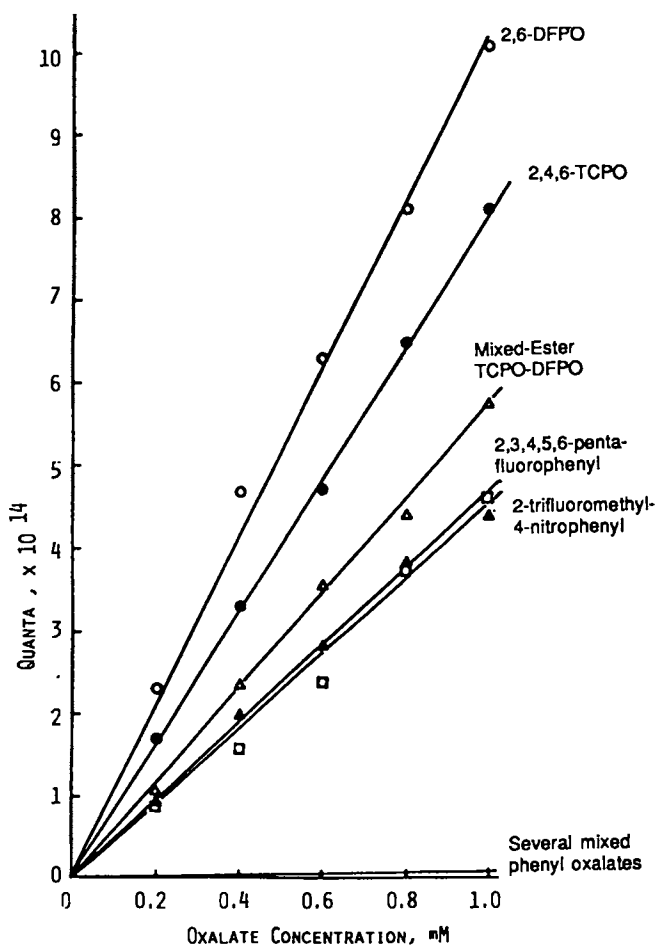


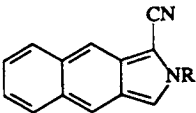
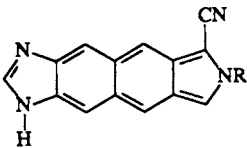
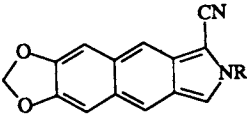
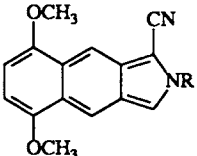
Figure 14. Oxalate esters synthesized (A) and oxalate dependence on the chemiluminescence quantum efficiency (B).

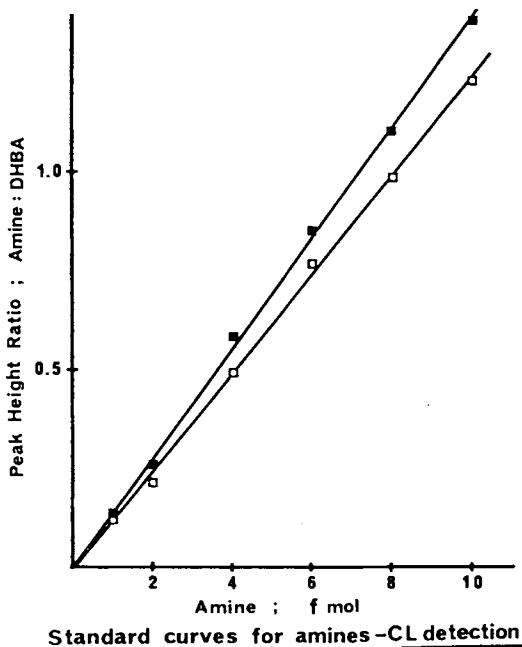


Finally, we have also attempted to improve on the fluorescence and chemiluminescence efficiencies of the labeling reagent, the naphthalene dialdehyde. Derivatives 7, 8, and 9 (Table IX) have been synthesized and studied. As shown in Table IX, none of these new derivatives presents an advantage over the parent unsubstituted CBI-Ala.

It is appropriate at this juncture to illustrate the power of chemiluminescence in an analytical assay by comparing the limits of sensitivity of the fluorescence-based and the chemiluminescence-based detection for analytes in a biological matrix. The quantitation of norepinephrine and dopamine in urine samples will serve as an illustrative example. Dopamine, norepinephrine, and 3,4-dihydroxybenzylamine (an internal standard) were derivatized with NDA/CN<sup>-</sup>, and chemiluminescence was used to monitor the chromatography and determine a calibration curve (Figure 15). The limits of detection were determined to be less than 1 fmol injected. A typical chromatogram is shown in Figure 16.

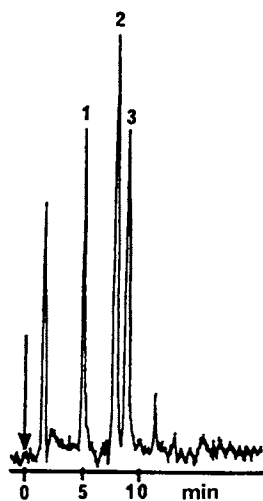
Table IX. Fluorescence Efficiencies ( $\Phi_F$ ), Chemiluminescence Efficiencies ( $\Phi_{CL}$ ), and Emission Maxima ( $\lambda_{max}$ ) for Substituted Benz[*f*]isoindoles of Simple Amino Acids

Reagent	Structure	$\Phi_F$	$\Phi_{CL}$	$\lambda_{max}$
CBI-Ala		0.75	0.014	480
IMCBI-Gly 7		0.61	0.028	510
MDCBI-Gly 8		0.62	0.014	475
DMCBI-Ala 9		0.62	0.0093	500



■ ; Norepinephrine :  $r = 0.999$   
 □ ; Dopamine :  $r = 0.999$

Figure 15. Standard curves for norepinephrine and dopamine vs. dihydroxybenzylamine as an internal standard (Kawasaki, T.; Wong, O.; Imai, K.; Higuchi, T., in preparation).



#### HPLC Conditions

Pump; LKB 2150 HPLC Pump, ISCO 314  
 Detector; ATTO AC-2220 (Luminomonitor I)  
 60  $\mu$ L flow cell  
 Column; TSK gel ODS-120T; 150 x 4.6 mm, 5  $\mu$ m  
 Eluent; 10mM potassium hydrogen phthalate,  
 pH 2.5/MeCN = 50:50, v/v  
 Flow rate; 1 ml/min  
 Reagent; 0.5 mM DNPO/MeCN, 1 ml/min  
 12.5 mM H<sub>2</sub>O<sub>2</sub>/MeCN, 2 ml/min

#### Peaks

1 = norepinephrine  
 2 = 3,4-dihydroxybenzylamine (I.S.)  
 3 = dopamine

\* each peak: 1 fmole

Figure 16. Chromatogram of cyanobenz[f]isoindole derivatives of catecholamines.

A similar analysis using a Farrand fluorometer fitted with a 10- $\mu$ L flow cell gave limits of fluorescence detection of 1 pmol; i.e., it was  $10^3$  less sensitive than the chemiluminescence analyses. This increased level of sensitivity has been realized for several other systems that are amenable to the NDA/CN<sup>-</sup> derivatization method (Kawasaki, T.; Wong, O.; Imai, K.; Higuchi, T., in preparation). These results encouraged further efforts in the development of the peroxyoxalate chemiluminescent method for HPLC-detectors.

Though we and others (17-19) have demonstrated the utility and the improved sensitivity of the peroxyoxalate chemiluminescence method for analyte detection in RP-HPLC separations for appropriate substrates, a substantial area for improvement and refinement of the technique remains. We have shown that the reactions of hydrogen peroxide and oxalate esters yield a very complex array of reactive intermediates, some of which activate the fluorophor to its fluorescent state. The mechanism for the ester reaction as well as the process for conversion of the chemical potential energy into electronic (excited state) energy remain to be detailed. Finally, the refinement of the technique for routine application of this sensitive method, including the optimization of the efficiencies for each of the contributing factors, is currently a major effort in the Center for Bioanalytical Research.

#### *Acknowledgments*

This research was supported by the Center for Bioanalytical Research, the Kansas Advanced Technology Commission, and Oread Laboratories, Inc.

#### *Literature Cited*

1. Roth, M. *Anal. Chem.* 1971, **43**, 880-882.
2. Simons, S. S., Jr.; Johnson, D. F. *J. Am. Chem. Soc.* 1976, **98**, 7098-7099.
3. Simons, S. S., Jr.; Johnson, D. F. *J. Chem. Soc., Chem. Commun.* 1977, (11), 374-375.
4. Bensen, J. R.; Hare, P. E. *Proc. Natl. Acad. Sci. U.S.A.* 1975, **72**, 619-622.
5. de Montigny, P.; Stobaugh, J. F.; Givens, R. S.; Carlson, R. G.; Srinivasachar, K.; Sternson, L. A.; Higuchi, T. *Anal. Chem.* 1987, **59**, 1096-1101.
6. Sternson, L. A.; Stobaugh, J. F.; Repta, A. J. *Anal. Biochem.* 1985, **144**, 233-246.
7. Wong, O. S.; Sternson, L. A.; Schowen, R. A. *J. Am. Chem. Soc.* 1985, **107**, 6421-6422.
8. Chen, R. F.; Smith, P. D.; Maly, M. *Arch. Biochem. Biophys.* 1978, **189**, 241-250.
9. Chen, R. F. *Arch. Biochem. Biophys.* 1967, **120**, 609.
10. Joys, T. M.; Kim, H. *Anal. Biochem.* 1979, **94**, 371-377.
11. Carlson, R. G.; Srinivasachar, K.; Givens, R. S.; Matuszewski, B. K. *J. Org. Chem.* 1986, **51**, 3978-3983.
12. Matuszewski, B. K.; Givens, R. S.; Srinivasachar, K.; Carlson, R. G.; Higuchi, T. *Anal. Chem.* 1987, **59**, 1102-1105.

13. De Schryuer, F. C.; Collart, P.; Vandendriessche, J.; Goedeweck, R.; Seinnen, A.; Van der Auweraer, M. *Acc. Chem. Res.* 1987, 20, 159-166.
14. de Montigny, P. PhD Thesis, The University of Kansas, Lawrence, KS, 1986.
15. Roach, M. C.; Harmony, M. D. *Anal. Chem.* 1987, 59, 411-415.
16. Rauhut, M. M.; Bollyky, L. J.; Roberts, B. G.; Loy, M.; Whitman, R. H.; Iannotta, A. V.; Semsel, A. M.; Clarke, R. A. *J. Am. Chem. Soc.* 1967, 89, 6515-6522.
17. Kobayashi, S.; Imai, K. *Anal. Chem.* 1980, 52, 424.
18. Melbin, G. J. *J. Liq. Chromatogr.* 1983, 6, 1603-1616.
19. Melbin, G.; Smith, B. E. *J. Chromatogr.* 1984, 312, 203-210.
20. Lechtken, P.; Turro, N. J. *Mol. Photochem.* 1974, 6, 95-99.
21. Schuster, G. B. *Acc. Chem. Res.* 1979, 12, 366-373.
22. Schmidt, S. P.; Schuster, G. B. *J. Am. Chem. Soc.* 1980, 102, 306-314.
23. Adam, W.; Cueto, O. *J. Am. Chem. Soc.* 1979, 101, 6511-6515.
24. Alvarez, F. J.; Parekh, N. J.; Matuszewski, B.; Givens, R. S.; Higuchi, T.; Schowen, R. L. *J. Am. Chem. Soc.* 1986, 108, 6435-6437.
25. Catherall, C. L. R.; Palmer, T. F.; Cundall, R. B. *J. Chem. Soc., Faraday Trans. 2* 1984, 80, 823-836; 837-849.
26. Imai, K.; Miyaguchi, K.; Honda, K. *Bioluminescence and Chemiluminescence: Instruments and Applications* Volume II; van Dyke, K., Ed., CRC Press: Boca Raton, FL, 1985, Chapter 5, p 65-76.
27. McCapra, F.; Perring, K.; Hard, R. J.; Hann, R. A. *Tetrahedron Lett.* 1981, 5087-5091.
28. Mohan, A. G.; Turro, N. J. *J. Chem. Educ.* 1974, 51, 528-529.
29. Sigvardson, K. W.; Birks, J. W. *Anal. Chem.* 1983, 55, 432-435.

RECEIVED September 6, 1988

## Chapter 9

# Applications and Interactions in Solid-Surface Luminescence Analysis

Robert J. Hurtubise, S. M. Ramasamy, Job M. Bello,  
Greg J. Burrell, and Linda A. Citta

Chemistry Department, University of Wyoming, Laramie, WY 82071

Solid-surface room-temperature phosphorescence (RTP) is a relatively new technique which has been used for organic trace analysis in several fields. However, the fundamental interactions needed for RTP are only partly understood. To clarify some of the interactions required for strong RTP, organic compounds adsorbed on several surfaces are being studied. Fluorescence quantum yield values, phosphorescence quantum yield values, and phosphorescence lifetime values were obtained for model compounds adsorbed on sodium acetate-sodium chloride mixtures and on  $\alpha$ -cyclodextrin-sodium chloride mixtures. With the data obtained, the triplet formation efficiency and some of the rate constants related to the luminescence processes were calculated. This information clarified several of the interactions responsible for RTP from organic compounds adsorbed on sodium acetate-sodium chloride and  $\alpha$ -cyclodextrin-sodium chloride mixtures. Work with silica gel chromatoplates has involved studying the effects of moisture, gases, and various solvents on the fluorescence and phosphorescence intensities. The net result of the study has been to improve the experimental conditions for enhanced sensitivity and selectivity in solid-surface luminescence analysis.

Solid-surface luminescence analysis involves the measurement of fluorescence and phosphorescence of organic compounds adsorbed on solid materials. Several solid matrices such as filter paper, silica with a polyacrylate binder, sodium acetate, and cyclodextrins have been used in trace organic analysis. Recent monographs have considered the details of solid-surface luminescence analysis (1,2). Solid-surface room-temperature fluorescence (RTF) has been used for several years in organic trace analysis. However, solid-surface room-temperature phosphorescence (RTP) is a relatively new technique, and the experimental conditions for RTP are more critical than for RTF. In addition, the fundamental interactions needed for RTP are only

0097-6156/89/0383-0155\$06.00/0

• 1989 American Chemical Society

partly understood. Von Wandruszka and Hurtubise (3) employed several spectral techniques to show that the anion of *p*-aminobenzoic acid was held by two sodium acetate molecules, which was one aspect that allowed RTP to be detected. The RTP lifetimes and the intensities of the anion of *p*-aminobenzoic acid adsorbed on sodium acetate-sodium chloride mixtures were also investigated (4). Short- and long-decaying phosphorescent components were observed from the anion adsorbed on sodium acetate and on sodium acetate-sodium chloride mixtures.

Filter paper has been used extensively as a matrix to obtain RTP from organic compounds. Nevertheless, little is known about the interactions that cause RTP from organic compounds adsorbed on filter paper. Schulman and Parker (5) postulated that hydrogen bonding of ionic organic molecules to hydroxyl groups of the filter paper was the main interaction which provided a rigid sample matrix for RTP. Lue-Yen Bower and Winefordner (6) reported that RTP by the heavy-atom effect for aromatic hydrocarbons adsorbed on filter paper was caused by silver ion forming a  $\pi$ -complex with the  $\pi$ -electron cloud of the aromatic hydrocarbons. Andino et al. (7) employed X-ray photoelectron spectroscopy to understand the surface processes in RTP where heavy-atom ions were used. They commented that the extent of penetration of the heavy atom or ions appeared to exceed that of the organic compound. If the filter paper is packed with salts or sugars, the matrix can hold the phosphor rigid, and relatively strong RTP signals can be obtained (8). McAleese and Dunlap (9) considered a matrix-isolation mechanism for RTP from cellulose paper samples which was based on the swelling property of cellulose in the presence of strongly polar solvents. For example, after the matrix was dried, the molecules became trapped between cellulose chains, and this permitted the necessary rigidity for the phosphor. In other work, Dalterio and Hurtubise (10) used several spectral techniques and showed that several hydrogen-bonding interactions could occur between phosphors and filter paper. Ramasamy and Hurtubise (11) investigated the effects of temperature on the RTP and RTP properties of the anion of *p*-aminobenzoic acid adsorbed on sodium acetate. Their results supported a rigidly held mechanism for the RTP of the anion of *p*-aminobenzoic acid adsorbed on sodium acetate. In later work, they studied the room-temperature luminescence properties of the anion of *p*-aminobenzoic acid adsorbed on sodium acetate-sodium chloride mixtures (12). The results revealed that several factors were important for maximum RTP from this anion.

### *Short Historical Survey*

Sawicki (13) used solid-surface fluorescence techniques extensively in the 1960's for air pollution research. In 1967, Roth (14) reported the RTP of several pharmaceuticals adsorbed on filter paper. Schulman and Walling (15) showed that several organic compounds gave RTP when adsorbed on filter paper. Paynter et al. (16) reported the first detailed analytical data for RTP and gave limits of detection, linear dynamic ranges, and reproducibilities for the compounds. Since publication of these two studies (15,16), several researchers have used solid-surface luminescence analysis in trace organic analysis (1,2).

**Recent Uses of Solid-Surface Luminescence Analysis in Environmental Analysis.** Vo-Dinh and coworkers have shown very effectively how solid-surface luminescence techniques can be used for environmentally important samples (17-22). RTP has been used for the screening of ambient air particulate samples (17,18). In addition, RTP has been employed in conjunction with a ranking index to characterize polynuclear aromatic pollutants in environmental samples (19). A unique application of RTP reported recently is a personal dosimeter badge based on molecular diffusion and direct detection by RTP of polynuclear aromatic pollutants (20). The dosimeter is a pen-size device that does not require sample extraction prior to analysis. The dosimeter can detect various polynuclear aromatics at the ppb level after 1 hour of exposure. It has been shown that the RTP of aza-arenes can be enhanced by using mercury(II) chloride as a heavy atom (21). Also, sensitized fluorescence spectrometry with a solid organic substrate can be used to detect trace amounts of polynuclear aromatic compounds (22).

#### **Experimental Considerations**

Several solid surfaces, such as filter paper, sodium acetate, and silica gel chromatoplates with a polyacrylate binder, have been used in solid-surface luminescence work (1,2). Experimentally it is relatively easy to prepare samples for analysis. With filter paper, for example, a small volume of sample solution is spotted onto the surface, the filter paper is dried, and then the measurement is made. In many cases, an inert gas is passed over the surface during the measurement step to enhance the RTP signal. For powdered samples, the sample preparation procedure is somewhat more involved. Commercial instruments can be readily used to measure the luminescence signals, and a variety of research instruments have been developed to obtain the solid-surface luminescence data (1,2).

**Solid-Surface Luminescence with  $\alpha$ -Cyclodextrin-NaCl Mixtures.** It was recently reported that an 80%  $\alpha$ -cyclodextrin-NaCl mixture could be employed as a matrix to obtain RTF and RTP analytical data (23,24). Cyclodextrins are cyclic oligosaccharides constructed from  $\alpha$ -(1,4)-linked glucose units arranged in a torus. Cyclodextrins have been shown to form inclusion compounds with molecules that fit into their hydrophobic cavity (25). They are commercially available as  $\alpha$ -,  $\beta$ -, and  $\gamma$ -cyclodextrins, and researchers have shown that they have many uses (25,26). In this work, we showed that it was relatively easy to detect nanogram amounts of mixtures of benzo(a)pyrene and benzo(e)pyrene using RTF and RTP. It was found that benzo(a)pyrene gave RTF on 80%  $\alpha$ -cyclodextrin-NaCl, whereas benzo(e)pyrene gave both RTF and RTP on the mixture. Also, the RTF intensity of benzo(e)pyrene was 16 times less than the RTF intensity of benzo(a)pyrene. Figure 1a shows the RTF emission spectra for several mixtures of benzo(a)pyrene and benzo(e)pyrene adsorbed on 80%  $\alpha$ -cyclodextrin-NaCl, and Figure 1b gives a standard RTF emission spectrum for benzo(a)pyrene adsorbed on the cyclodextrin matrix. As a comparison of the two figures shows, benzo(a)pyrene can be readily detected in the presence of different amounts of benzo(e)pyrene. Figure 2 gives the RTP spectra for benzo(e)pyrene in the presence of benzo(a)pyrene.

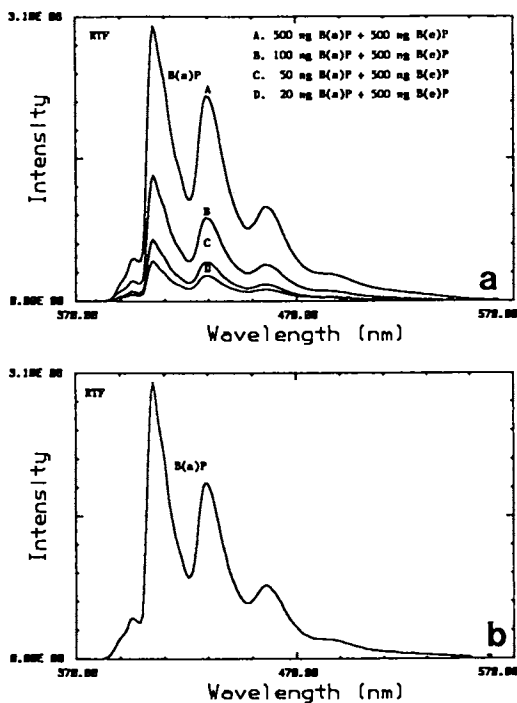


Figure 1. (a) Room-temperature fluorescence spectra of benzo(*a*)pyrene on 80%  $\alpha$ -cyclodextrin-NaCl in the presence of benzo(*e*)pyrene.  $\lambda_{\text{ex}} = 369$  nm. (b) Room-temperature fluorescence spectrum of 500 ng of benzo(*a*)pyrene on 80%  $\alpha$ -cyclodextrin-NaCl.  $\lambda_{\text{ex}} = 300$  nm.



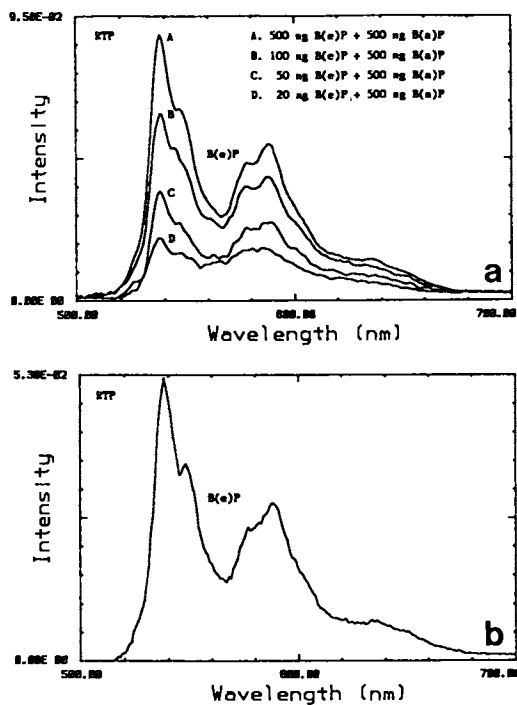


Figure 2. (a) Room-temperature phosphorescence spectrum of benzo(e)pyrene on 80%  $\alpha$ -cyclodextrin-NaCl in the presence of benzo(a)pyrene.  $\lambda_{ex} = 284$  nm. (b) Room-temperature phosphorescence spectrum of benzo(e)pyrene on 80%  $\alpha$ -cyclodextrin-NaCl.  $\lambda_{ex} = 284$  nm.

By comparing these spectra with the reference spectrum of benzo(e)pyrene in Figure 2b, it can be seen that benzo(e)pyrene can be identified at nanogram levels with a relatively large amount of benzo(a)pyrene present. In addition, by using selective excitation it was possible to detect both benzo(a)pyrene and benzo(e)pyrene at the nanogram levels in mixtures using one RTF scan. In other work, a 3-dimensional plot of RTF emission from a benzo(a)pyrene and benzo(e)pyrene mixture was obtained. As Figure 3 shows, the fluorescence bands for both compounds were easily observed. The 3-dimensional plot is advantageous because more comprehensive luminescence information is obtained than in 2-dimensional plots.

*Interactions in Solid-Surface Luminescence Temperature Variation.* Solid-surface luminescence analysis, especially solid-surface RTP, is being used more extensively in organic trace analysis than in the past because of its simplicity, selectivity, and sensitivity (1,2). However, the interactions needed for strong luminescence signals are not well understood. In order to understand some of the interactions in solid-surface luminescence we recently developed a method for the determination of room-temperature fluorescence and phosphorescence quantum yields for compounds adsorbed on solid surfaces (27). In addition, we have been investigating the RTF and RTP properties of the anion of *p*-aminobenzoic acid adsorbed on sodium acetate as a model system. Sodium acetate and the anion of *p*-aminobenzoic acid have essentially no luminescence impurities. Also, the overall system is somewhat easier to study than compounds adsorbed on other surfaces, such as filter paper, because sodium acetate is more simple chemically.

Solid-surface fluorescence and phosphorescence quantum yield values were obtained from +23° to -180°C for the anion of *p*-aminobenzoic acid adsorbed on sodium acetate (11). Phosphorescence lifetime values were also obtained for the adsorbed anion from +23° to -196°C. Table I gives the fluorescence and phosphorescence quantum yield values acquired. The fluorescence quantum yield values remained practically constant as a function of temperature. However, the phosphorescence quantum yield values changed substantially with temperature. The phosphorescence lifetime experiments indicated two decaying components. Each component showed a gradual increase in phosphorescence lifetime with cooler temperatures, but then the increase appeared to level off at the coldest temperatures.

Several fundamental luminescence parameters were calculated for the anion of *p*-aminobenzoic acid on sodium acetate (11). The triplet formation efficiency ( $\phi_t$ ), the rate constant for phosphorescence ( $k_p$ ), and the rate constant for the radiationless transition from the triplet state ( $k_m$ ) were calculated. The results showed that the  $k_p$  and  $\phi_t$  values were constant with temperature, but that  $k_m$  changed with temperature. At room temperature, 0.39 was the average  $k_m$  value for the short- and long-decaying components. At -180°C the average value of  $k_m$  was 0.080; thus the rate constant for  $k_m$  changed by a factor of 4.9 from room temperature to -180°C. Equation 1 can be used to comment on the mechanism of solid-surface phosphorescence.

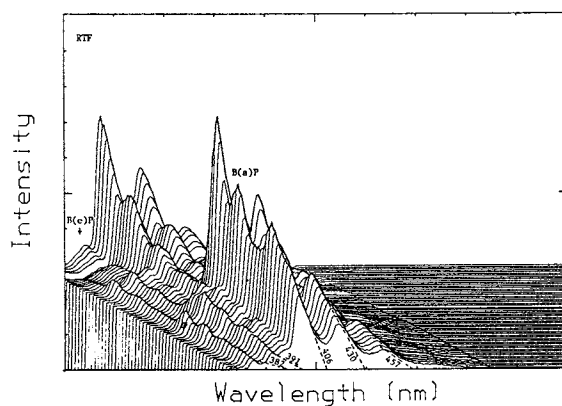


Figure 3. Three-dimensional plot of the room-temperature fluorescence of a mixture of 500 ng each of benzo(*a*)pyrene and benzo(*e*)pyrene on 80%  $\alpha$ -cyclodextrin-NaCl. Numbers along dashed lines show the approximate wavelengths (nm) represented by these lines. The excitation wavelength was varied from 250 nm (front spectrum) to 370 nm (back spectrum) at 2-nm increments. Benzo(*a*)pyrene emitted from approximately 380 nm to 540 nm, and benzo(*e*)pyrene emitted from 365 nm to 505 nm.

$$\phi_p = (\phi_t) \frac{k_p}{k_p + k_m} \quad (1)$$

where  $\phi_p$  is the phosphorescence quantum yield. Because  $k_m$  showed the greatest change with temperature, it would have the greatest effect on  $\phi_p$ . The results showed that  $k_m$  was a function of temperature, and the more rigid the matrix at lower temperature, the smaller the value of  $k_m$ . The variation of  $k_m$  with temperature showed that the RTP was a function of how rigidly the *p*-aminobenzoic anion was held. Oxygen and moisture were not major contributing factors to the decrease of  $\phi_p$  as temperature increased because of the experimental conditions used in the work.

The phosphorescence lifetimes for the *p*-aminobenzoic acid anion adsorbed on sodium acetate as a function of temperature were evaluated in a manner similar to the one discussed by Oelkrug and coworkers (28-30) for polycyclic aromatic hydrocarbons adsorbed on  $\gamma$ -alumina. In general, the solid-surface phosphorescence lifetime curves for the anion of *p*-aminobenzoic acid followed Equation 2.

Table I. Fluorescence and Phosphorescence Quantum Yield Values for the Anion of *p*-Aminobenzoic Acid Adsorbed on Sodium Acetate Over a Wide Temperature Range<sup>a</sup>

Temperature (°C)	Fluorescence quantum yield, $\phi_f$	Phosphorescence quantum yield, $\phi_p$
23	0.19±0.06 <sup>b</sup>	0.40±0.07
0	0.18±0.07	0.37±0.05
-40	0.20±0.10	0.43±0.18
-80	0.21±0.05	0.55±0.16
-120	0.20±0.05	0.63 <sup>c,d</sup> (0.05) <sup>e</sup>
-140	0.24±0.04	0.59 <sup>c,d</sup> (0.02) <sup>e</sup>
-160	0.22±0.04	0.48 <sup>d</sup> ±0.16 <sup>b</sup>
-180	0.22±0.06	0.61 <sup>c,d</sup> (0.05) <sup>e</sup>

<sup>a</sup>The results are the average of at least four determinations except for three of the samples. The  $\phi_p$  value at -160°C is the average of three determinations.

<sup>b</sup>95% confidence limits.

<sup>c</sup>Average of duplicate determinations.

<sup>d</sup>Temperature held for two hours prior to quantum yield measurements.

<sup>e</sup>Range. Data taken from Ref. 11.

$$1/\tau_p - 1/\tau_p^0 = k_1 \exp(-E_a/RT) \quad (2)$$

where  $\tau_p$  is the phosphorescence lifetime at a given temperature and  $\tau_p^0$  is the phosphorescence lifetime when the exponential term is zero or is very small. The exact meanings of the preexponential factor ( $k_1$ ) and the activation energy term ( $E_a$ ) are not fully developed (31). The  $k_1$  and  $E_a$  terms were evaluated from Equation 2 and found to be roughly comparable to the values for naphthalene adsorbed on highly activated alumina (11,30). Generally, the smaller the  $k_1$  and  $E_a$  values, the more strongly the compound interacts with the surface (29,30). In the future, Equation 2 should be a useful means of comparing various surfaces for RTP in solid-surface phosphorescence analytical work.

*Sodium Acetate-Sodium Chloride Mixtures.* Ramasamy and Hurtubise (12) obtained RTF and RTP quantum yields, triplet formation efficiency, and phosphorescence lifetime values for the anion of *p*-aminobenzoic acid adsorbed on sodium acetate and on several sodium acetate-sodium chloride mixtures. Rate constants were calculated for phosphorescence and for radiationless transition from the triplet state. The results showed that several factors were important for maximum RTP from the anion of *p*-aminobenzoic acid. One of the most important of these was how efficiently the matrix was packed with sodium acetate molecules. A similar conclusion was found for RTF; however, the RTP quantum yield increased more dramatically than the RTF quantum yield.

As discussed earlier by Senthilnathan and Hurtubise (4), before a saturated ethanol solution of sodium acetate is formed, the solid-surface RTP is less than the RTP from samples prepared with solutions that are saturated with sodium acetate. It was shown by Ramasamy and Hurtubise (12) that both the RTF and RTP quantum yields of the *p*-aminobenzoic acid anion increased as the amount of sodium acetate increased in the solid mixtures. Figure 4 shows the quantum yield of fluorescence ( $\phi_f$ ) and the quantum yield of phosphorescence ( $\phi_p$ ) versus the log of the ratio of millimoles of dissolved sodium acetate to the millimoles of dissolved *p*-aminobenzoic acid anion. There are two major portions to each graph--namely, the region before saturation of the ethanol with sodium acetate and the region beyond the saturated ethanol solution. The ethanol solution refers to the solution used to prepare the sample prior to solid-surface measurements in the dry state (12). The ethanol solution is saturated at a log value of 3.36 on the abscissa in Figure 4. As shown in Figure 4, in the region before saturation, there is an approximately linear increase in the  $\phi_f$  and  $\phi_p$  values as the sodium acetate concentration increases. A much more dramatic increase in  $\phi_f$  and  $\phi_p$  occurs beyond a saturated solution of sodium acetate in Figure 4, with the largest  $\phi_f$  and  $\phi_p$  values obtained for pure sodium acetate. The results in Figure 4 strongly indicated that how effectively the matrix was packed was a major factor in yielding high  $\phi_f$  and  $\phi_p$  values. Tighter

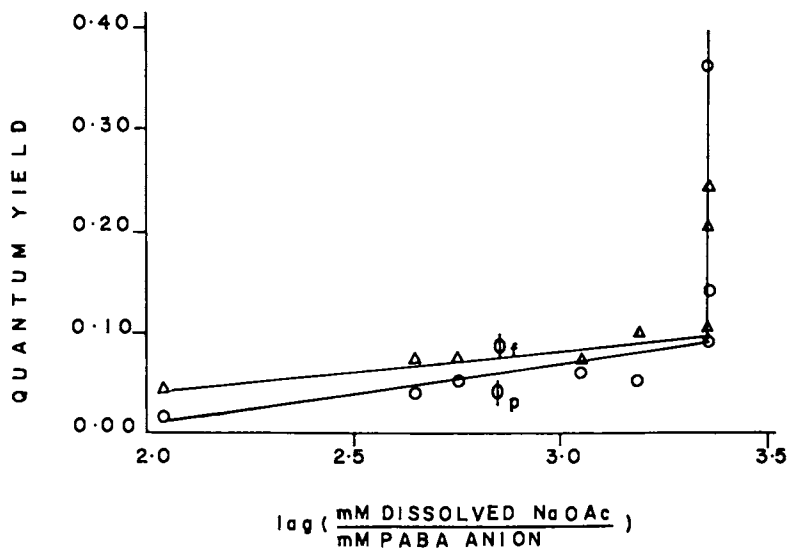


Figure 4. Graphs of fluorescence quantum yield ( $\phi_f$ ) and phosphorescence quantum yield ( $\phi_p$ ) versus log of the ratio of millimoles of dissolved sodium acetate to millimoles of *p*-aminobenzoic acid anion. (Reproduced from reference 12. Copyright 1988 American Chemical Society.)

packing would permit the matrix to hold the *p*-aminobenzoic acid anion rigidly. As indicated in Figure 4, the increase in  $\phi_p$  is greater than for  $\phi_f$ .

#### Other Studies

Burrell and Hurtubise (32) investigated calibration curves extended well beyond the normal linear range for RTF and RTP of benzo(f)quinoline adsorbed on a silica gel chromatoplate under neutral and acidic conditions. As the benzo(f)quinoline concentration increased, the RTF curves leveled off, whereas the RTP curves passed through a maximum and then decreased. The extended calibration curves along with fluorescence and phosphorescence spectra and phosphorescence lifetimes for benzo(f)quinoline revealed differences in the RTF and RTP phenomena. For example, it was determined that RTF could arise from molecules adsorbed on the surface and in multilayers of molecules, whereas phosphorescence was only generated from molecules adsorbed on the surface of the chromatoplate and not in the multilayers.

In other work, the effects of nitrogen, air, oxygen, and humidity on the RTF and RTP of benzo(f)quinoline adsorbed on silica gel chromatoplates are being investigated. The results indicate that the RTF is affected very differently than the RTP.

#### Conclusions

Solid-surface luminescence analysis is a useful approach for organic trace analysis because of its simplicity, sensitivity, and selectivity. It will continue to be used in environmental analysis and other areas not only for the reasons mentioned above but also because it is readily adaptable to field work. By developing a fundamental understanding of the interactions responsible for strong RTF and RTP signals, the advantages and disadvantages of the luminescence approach will be more specifically defined in the future.

#### Literature Cited

1. Hurtubise, R. J. *Solid Surface Luminescence Analysis*; Marcel Dekker: New York, 1981.
2. Vo-Dinh, T. *Room Temperature Phosphorimetry for Chemical Analysis*; Wiley: New York, 1984.
3. Von Wandruszka, R. M. A.; Hurtubise, R. J. *Anal. Chem.* 1977, **49**, 2164.
4. Senthilnathan, V. P.; Hurtubise, R. J. *Anal. Chem.* 1985, **57**, 1227.
5. Schulman, E. M.; Parker, R. T. *J. Phys. Chem.* 1977, **81**, 1932.
6. Lue-Yen Bower, E.; Winefordner, J. D. *Anal. Chim. Acta* 1978, **102**, 1.
7. Andino, M. M.; Kosinski, M. A.; Winefordner, J. D. *Anal. Chem.* 1986, **58**, 1730.
8. Niday, G. T.; Seybold, P. G. *Anal. Chem.* 1978, **50**, 1577.
9. McAleese, D. L.; Dunlap, R. B. *Anal. Chem.* 1984, **56**, 2244.
10. Dalterio, R. A.; Hurtubise, R. J. *Anal. Chem.* 1984, **56**, 336.
11. Ramasamy, S. M.; Hurtubise, R. J. *Anal. Chem.* 1987, **59**, 432.
12. Ramasamy, S. M.; Hurtubise, R. J. *Anal. Chem.*, in press.

13. Sawicki, E. *Talanta* 1969, 16, 1231.
14. Roth, M. J. *Chromatogr.* 1967, 30, 276.
15. Schulman, E. M.; Walling, C. J. *J. Phys. Chem.* 1973, 77, 902.
16. Paynter, R. A.; Wellons, S. L.; Winefordner, J. D. *Anal. Chem.* 1974, 46, 736.
17. Vo-Dinh, T. In *Identification and Analysis of Organic Pollutants in Air*; Keith, L. J., Ed.; Butterworth Publishers: Boston, 1984; Chap. 16.
18. Vo-Dinh, T.; Bruewer, T. J.; Colovos, G. C.; Wagner, T. J.; Jungers, R. J. *Environ. Sci. Technol.* 1984, 18, 477.
19. Vo-Dinh, T.; Abbott, D. W. *Environ. Int.* 1984, 10, 299.
20. Vo-Dinh, T. *Environ. Sci. Technol.* 1985, 19, 997.
21. Abbott, D. W.; Vo-Dinh, T. *Anal. Chem.* 1985, 57, 41.
22. Vo-Dinh, T.; White, D. A. *Anal. Chem.* 1986, 58, 1128.
23. Bello, J. M.; Hurtubise, R. J. *Anal. Lett.* 1986, 19, 775.
24. Bello, J. M.; Hurtubise, R. J. *Appl. Spectrosc.* 1986, 40, 790.
25. Szejtli, J. *Cyclodextrins and Their Inclusion Complexes*; Akademiai Kiado: Budapest, 1982.
26. Saenger, W. In *Inclusion Compounds*; Atwood, J. L.; Davies, J. E. D.; MacNicol, D. D., Eds.; Academic Press: New York, 1984, Vol. 2, Chap. 8.
27. Ramasamy, S. M.; Senthilnathan, V. P.; Hurtubise, R. J. *Anal. Chem.* 1986, 58, 612.
28. Kessler, R. W.; Uhl, S.; Honnen, W.; Oelkrug, D. *J. Lumin.* 1981, 24/25, 551.
29. Plauschinat, M.; Honnen, W.; Krablchier, G.; Uhl, S.; Oelkrug, D. *J. Mol. Struct.* 1984, 115, 351.
30. Oelkrug, D.; Plauschinat, M.; Kessler, R. W. *J. Lumin.* 1979, 18/19, 434.
31. Honnen, W.; Krablchier, G.; Uhl, S.; Oelkrug, D. *J. Phys. Chem.* 1983, 87, 4872.
32. Burrell, G. J.; Hurtubise, R. J. *Anal. Chem.* 1987, 59, 965.

RECEIVED August 22, 1988



## Chapter 10

# Multidimensional Fluorescence Analysis of Cyclodextrin Solvent-Extraction Systems

Lisa A. Blyshak, Gabor Patonay, and Isiah M. Warner

Department of Chemistry, Emory University, Atlanta, GA 30322

The theory and development of a solvent-extraction scheme for polynuclear aromatic hydrocarbons (PAHs) is described. The use of  $\gamma$ -cyclodextrin (CD $\gamma$ ) as an aqueous phase modifier makes this scheme unique since it allows for the extraction of PAHs from ether to the aqueous phase. Generally, the extraction of PAHs into water is not feasible due to the low solubility of these compounds in aqueous media. Water-soluble cyclodextrins, which act as hosts in the formation of inclusion complexes, promote this type of extraction by partitioning PAHs into the aqueous phase through the formation of complexes. The stereoselective nature of CD $\gamma$  inclusion-complex formation enhances the separation of different sized PAH molecules present in a mixture. For example, perylene is extracted into the aqueous phase from an organic phase anthracene-perylene mixture in the presence of CD $\gamma$  modifier. Extraction results for a variety of PAHs are presented, and the potential of this method for separation of more complex mixtures is discussed.

In recent years, the analytical utility of cyclodextrins has become increasingly evident. These compounds, which are cyclic oligosaccharides formed from the enzymatic degradation of starch by bacteria, have been used in a variety of analytical systems. The resulting compounds consist of 6, 7, or 8 glucopyranose units attached by  $\alpha$ -1,4 linkages, and they are referred to as  $\alpha$ -,  $\beta$ -, and  $\gamma$ -cyclodextrins respectively. These homologues are torus-shaped and have a relatively nonpolar internal cavity, which results from the C1 chair conformation of individual glucose residues and the specific manner in which the glucose units are linked (1). Primary and secondary hydroxyl groups are located at the cavity edges, and glycosidic oxygen bridges line the interior of the cavity as depicted in Figure 1. The positioning of the hydroxyl groups enhances cyclodextrin solubility in water. The glycosidic oxygen bridges give the cavity a polarity which is about the same as that

0097-6156/89/0383-0167\$06.00/0

© 1989 American Chemical Society

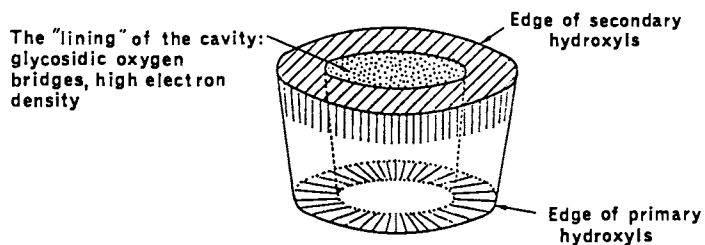


Figure 1. Functional structural scheme of cyclodextrins.  
(Reprinted with permission from Ref. 1. Copyright 1982  
Akademiai Kiado.)

of ethanol (2). This nearly nonpolar internal environment allows cyclodextrins to incorporate nonpolar species, provided the sizes of the guest and the host are compatible. Some pertinent physical data for the cyclodextrins are given in Table I.

Table I. Important Characteristics of Cyclodextrins<sup>a</sup>

Parameter	Type of Cyclodextrin		
	$\alpha$	$\beta$	$\gamma$
Molecular weight -----	972	1135	1297
Diameter of cavity (Å) -----	4.7-6	8	10
Volume of cavity (Å <sup>3</sup> ) -----	176	346	510
Number of water molecules --- taken up by cavity.	6	11	17
Diffusion constant at 40°C <sup>b</sup> -	3.443	3.224	3.000
Crystal form (from 60% aq. isopropanol).	Hexagonal plates or blade-shaped needles.	Monoclinic parallel- ograms.	Quadratic plates or prisms.
Solubility in water (g/100 mL at 25°C).	14.5	1.85	23.2
Molecules per unit cell -----	4	2	6
Water of crystallization (%)	10.2	13.2-14.5	8.13-17.7

<sup>a</sup>Reprinted with permission from Ref. 1.

<sup>b</sup>Craig, L. C.; Pulley, A. O. *Biochemistry* 1961, 1, 89.

Unlike other organized media such as micelles, cyclodextrins are rigid molecules. Formation of complexes with nonpolar molecules is based on a stereoselective interaction. Inclusion complexes form if the size of the guest molecule is compatible with the CDx cavity size (1,3). If the guest is too large to fit inside the cavity, no complex will form. In many cases an inclusion complex may form if some hydrophobic portion of the guest is compatible with the cavity size. Usually, the molecule orients itself in order to attain maximum contact between the apolar cavity and the hydrophobic portions of the included molecule (4). Side chains affect the degree of complexation based on their size and polarity. Each of the three common cyclodextrins has a characteristic cavity size due to the number of glucose residues in the compound, and as a result each one interacts to different degrees with molecules of varying dimensions.

Complexation occurs as a result of several weak interactions, including hydrogen bonding, van der Waals forces, and hydrophobic interactions; no covalent bonds are formed during the process (3). Another factor influencing complex formation is the decrease in ring strain afforded by formation of an inclusion complex with a nonpolar molecule (1). The inclusion process releases high-energy water from the CDx cavity.

Cyclodextrins can solubilize hydrophobic molecules in aqueous media through complex formation (5-8). A nonpolar species prefers the protective environment of the CDx cavity to the bulk aqueous solvent. In addition, cyclodextrins create a degree of structural rigidity and molecular organization for the included species. As a result of these characteristics, these macrocycles are used in studies of fluorescence and phosphorescence enhancement (9-11), stereoselective catalysis (12,13), and reverse-phase chromatographic separations of structurally similar molecules (14,15). These same complexing abilities make cyclodextrins useful in solvent extraction.

Although aqueous samples may be easily extracted with a variety of organic solvents (16), samples collected in organic matrices are more difficult to work with and often require lengthy sample preparation. One method for extracting organic samples is that of Rosen and Middletown (17). This method is limited because it is time consuming and requires large amounts of solvents. An alternative to this technique presented by Natusch and Tomkins uses the polar organic solvent dimethyl sulfoxide (DMSO) to extract PAHs from hydrocarbon solvent (18). Although DMSO is useful for separating PAHs from nonpolar organic solvents, selective interactions with specific compounds are limited. Our interest was to find a polar solvent which could be used to selectively extract PAHs from an organic-phase mixture based on a particular characteristic of the analyte molecules.

The method described here makes use of the ability of cyclodextrins to include molecules based on stereoselective interactions. In general, appreciable extraction of PAHs into the aqueous phase is not feasible because most PAHs have very low solubilities in water (19,20). The interesting feature of this method is that the use of an aqueous CDx modifier enhances the extraction of selected species into the aqueous layer while retaining other species in the bulk organic phase. The extraction efficiency is related to the degree of CDx complexation and thus to the size and hydrophobicity of the compounds to be extracted. This method may be particularly useful for simplifying complex mixtures of organic material such as oil samples or air sample adsorbates that are usually soluble in organic solvents. Such samples contain a variety of PAHs, which would make them amenable to separations by extraction into an aqueous phase. A few studies on the use of cyclodextrins for extraction have been described. Most such extractions use small solvent volumes and require precipitation of the complex from the aqueous solution (21); then the solid complex must be treated with an organic solvent to remove the guest from the solid matrix (22). Although the reagent volumes are small in these extractions, the separation procedure is tedious.

In conventional solvent extraction, a solute is partitioned between two immiscible solvents. Here,  $\gamma$ -CDx is used as an aqueous-phase modifier to increase the aqueous solubilities of several PAHs and thus to increase their aqueous-phase extraction efficiencies. In most cases, the degree of extraction depends on the fit of the potential guest into the CDx cavity. Thus, the stereoselective behavior of these macrocycles gives them the potential to discriminate between organic-phase solutes in an extraction. After extraction, analytes of interest that have been transferred to the aqueous phase may be identified without removal from the CDx complex or may be back-extracted into a suitable

solvent, such as cyclohexane. This technique is simpler than previous CDx extraction methods because the aqueous-phase complex is amenable to a variety of manipulations. The scheme described here may enhance existing knowledge of CDx behavior in two-phase systems and may also serve as a sample-preparation technique for reverse-phase chromatography.

In this study, a  $\gamma$ -CDx modifier was used to extract several PAHs as single components and to extract several binary mixtures. The data were collected using fluorescence measurements, which allow both identification and quantitation of the fluorophore in solvent extraction. Important experimental considerations such as solvent choice, temperature, and concentrations of the modifier and the analytes are discussed. The utility of this method as a means of simplifying complex PAH mixtures is also evaluated. In addition, the coupling of cyclodextrin-modified solvent extraction with luminescence measurements for qualitative evaluation of components in mixtures will be discussed briefly.

### *Experimental Section*

**Reagents.** Perylene was obtained from Sigma Chemical Company (St. Louis, Missouri). All other PAHs were supplied by Aldrich Chemical Company (Milwaukee, Wisconsin) and were reported to contain less than 3% impurities. All PAHs were used without further purification. Isopropyl ether (99%) for extraction work was also purchased from Aldrich. Hydroquinone, a fluorescent stabilizer present in the ether, was removed prior to solution preparation by rotary evaporation. Fluorometric-grade 1-butanol was supplied by Fisher Scientific Company (Fair Lawn, New Jersey). All solutions for extractions of PAHs were prepared by evaporating portions of a stock cyclohexane solution and diluting to the appropriate volume with isopropyl ether. Fluorescence measurements were performed on 1:10 dilutions of the stock and final organic phase solutions. The effect of dissolved CDx on the fluorescence intensity of the organic phase PAH was minimized by dilution with isopropyl ether.

Cyclodextrin solution for extraction studies was prepared at a concentration of  $1.00 \times 10^{-2}M$  by dissolving solid  $\gamma$ -CDx in deionized water (Continental Water Systems, Atlanta, Georgia). Fresh solution was prepared daily to prevent bacterial growth and CDx decomposition from interfering with complexation and extraction. Cyclodextrin was purchased from Advanced Separation Technologies, Inc. (Whippany, New Jersey) and was used as received. Solid CDx from one lot number was used for all extractions.

Samples for studies of CDx effects on fluorescence enhancement in organic solution were prepared using pyrene, because pyrene possesses a long lifetime and is very susceptible to quenching and enhancement in solution (23). An aliquot of pyrene stock solution in cyclohexane was placed under a nitrogen purge to evaporate the cyclohexane. Samples were redissolved in a 1:4 mixture of isopropyl ether and 1-butanol, which was saturated with aqueous CDx solution. Pyrene samples were also prepared in which the organic solvent was not saturated with CDx solution. The mixed solvent was used in order to minimize the effects of ether evaporation and thus allow more accurate quantitation. Fluorescence measurements were made on diluted samples of these solutions. The solvent used to make up the

final volume for the dilutions of both sample types was the mixed solvent. This procedure was followed in order to mimic the conditions used for the preparation of extraction samples for fluorescence analysis. Peak areas of the resulting fluorescence spectra from both saturated and unsaturated samples were compared to determine the effect of CDx on PAH fluorescence in the organic phase.

**Extraction Procedure and Apparatus.** Extractions were performed by vigorously shaking equal volumes of aqueous  $10^{-2}M$   $\gamma$ -CDx and  $10^{-5}M$  PAH solutions for 2 min at room temperature. The two layers were separated in a separatory funnel. Since fluorescence enhancement is often observed for luminophores in aqueous CDx media, fluorescence measurements were made on the organic phase. Fluorescence in organic media is not expected to be strongly affected by CDx because of the generally low solubility of the oligosaccharides in nonpolar media (1). Extractions were also performed without CDx to ensure that no appreciable extraction occurred in the absence of CDx. In addition, an organic-phase volume change was noted for some extractions. These changes are reflected in the data calculations. To ensure that total fluorescence was linearly related to PAH concentration, both the initial  $10^{-5}M$  organic phase solution and the organic phase after extraction were diluted with more of the initial organic solvent to a concentration to  $10^{-6}M$  before measurements were made. This dilution diminishes the effect of dissolved cyclodextrin on fluorescence intensities of PAHs. Extraction efficiencies were evaluated by monitoring the fluorescence of the diluted organic samples. Since the fluorescence peak area is proportional to concentration, peak-area values were substituted into the equation for the distribution ratio  $D$ :

$$D = \frac{[P]_a}{[P]_o} \quad (1)$$

where  $[P]_a$  is the final PAH concentration in the aqueous phase and  $[P]_o$  is the final PAH concentration in the organic phase. Extraction efficiencies reported here were determined according to the equation,

$$\%E = \frac{100D}{D + V_o/V_w} \quad (2)$$

where  $D$  is the distribution ratio,  $V_o/V_w$  is the volume ratio of the organic and aqueous phases, and  $\%E$  is the percent extracted into the aqueous phase.

All samples were monitored using a Perkin-Elmer 650-10S Fluorescence Spectrophotometer. Fluorescence excitation and emission wavelengths for the PAHs in this study were obtained from Berlman (24). The resulting spectra were analyzed using an Apple II+ computer by integrating peak areas to determine total changes in

fluorescence. Fluorescence peak areas were used because total fluorescence peak areas are insensitive to peak shifts and peak ratio changes and, thus, accurately reflect changes in analyte concentration. Binary mixtures of two PAH species were quantitated using fluorescence intensity measurements in regions of sole emission for each compound and comparing these data to calibration curves also based on fluorescence intensity at the wavelengths chosen for sole emission. The mixtures quantitatively studied were anthracene-perylene, pyrene-perylene and pyrene-coronene. The wavelengths chosen for sole emission for these studies were 385 nm for anthracene, 375 nm for pyrene, 475 nm for perylene, and 480 nm for coronene. Several two-dimensional spectra of PAH mixtures were obtained using a vidicon-based video fluorometer which provides multiple emission spectra as a function of multiple excitation wavelengths (25).

### Results and Discussion

The extraction efficiencies for the PAHs studied are given in Table II along with the dimensions of each PAH. As expected, the larger PAHs showed larger extraction efficiencies because they could more adequately fill the 9.5-Å cavity of  $\gamma$ -CDx. Comparative extractions using pure deionized water rather than CDx did not result in appreciable extraction efficiencies for any of the PAHs studied. In the CDx extractions, pyrene, perylene, and coronene were extracted from isopropyl ether with respective extraction efficiencies of 38.2%, 95.1%, and 93.7%. Relating this information to the relative dimensions of each compound indicates that the extraction procedure is related to the bulkiness of the PAH and the tightness of its fit in the CDx cavity. Large, bulky guest molecules such as perylene and coronene are capable of fitting tightly in  $\gamma$ -CDx because their molecular dimensions closely approximate the diameter of the cyclodextrin. Thus, these compounds give very large extraction efficiencies.

Table II. Extraction Efficiencies (%) for Several PAHs using Cyclodextrin-Modified Extraction

Compound	Molecular Dimensions <sup>a</sup> (angstroms)	%Extracted <sup>b</sup>
Anthracene	5.0 × 9.2	0.60 ± 2.0
Pyrene	7.1 × 8.9	38.2 ± 1.9
Perylene	9.1 × 9.2	95.1 ± 2.6
Coronene	9.2 × 9.2	93.7 ± 4.0

<sup>a</sup> Estimate based on bond lengths.

<sup>b</sup> Extracted from isopropyl ether into 10<sup>-2</sup>M  $\gamma$ -CDx.

The smaller molecules do not extract appreciably when the CDx modifier is used. Even though anthracene is reported to complex with  $\gamma$ -CDx, its formation constant may not be large enough to permit

extraction in this system. Roughly 100% of the anthracene remained in the organic layer. The data obtained thus far suggest that the PAH must not only fit inside the cavity, but must also form a strong complex in order to transfer satisfactorily to the aqueous phase. Thus, extraction efficiency is related to the compatibility of the CDx and PAH dimensions, as is seen by comparing %E to PAH dimensions. Extraction may also be inhibited by the formation of ternary complexes between small PAHs, organic solvent molecules, and CDx. The presence of organic solvent in the CDx cavity would change the polarity of the cavity, making the cavity environment similar to that of the bulk organic solvent. Should this occur, the drive for complexation would be lessened since complexation is promoted by the polarity change experienced by the guest molecule. The more tapered molecules, such as anthracene and pyrene, which cannot fill the cavity as well as larger species, would leave room in the cavity for solvent molecules to enter and, thus, would have smaller extraction efficiencies.

In addition to the size of the potential guest species, other factors may influence the degree of extraction possible for particular PAHs. For example, temperature is known to affect the formation constants for inclusion complexes (1). At lower temperatures, the stability of certain complexes is increased. Thus, lowering the temperature at which extractions are performed may increase extraction efficiencies. The solvent choice may also be useful in establishing the degree to which certain PAHs extract. If ternary complex formation is a problem during the solvent extraction process, the polarity of the organic solvent may also provide a means of altering extraction efficiencies. As the solvent polarity approaches the polarity of the cyclodextrin cavity, the extraction efficiencies for PAHs may decrease. The effects of solvent polarity are currently under study.

Since many of the organic solvents form insoluble complexes with cyclodextrin (1), solvent choice was crucial in designing the solvent-extraction scheme. Wishnia and Lappi reported the complexation of various organic solvents with the cyclodextrins (26). Thus, solvent choice must be based upon a knowledge of CDx complexation behavior. In preliminary extraction studies, solvents such as cyclohexane and chloroform formed such stable complexes with  $\gamma$ -CDx that, when shaken, a white precipitate formed in the aqueous phase, and the organic phase volume decreased appreciably. Any PAH present in these systems was completely extracted from the organic phase, possibly as a solid ternary complex. This method, however, is not true solvent extraction, since a solid species forms during the separation. To avoid this problem, we used a small solvent molecule which did not complex appreciably with  $\gamma$ -CDx. Isopropyl ether was chosen as the organic solvent because it did not precipitate when mixed with aqueous CDx. Various other organic solvents may also be used for this type of extraction, but most of these are volatile and, thus, not suitable for a quantitative study. Ethers appear to be especially amenable to use in cyclodextrin-modified extraction. It is important to remember, however, that the use of  $\alpha$ -CDx and  $\beta$ -CDx may require other solvent systems, since the CDx cavity size affects the formation of crystalline ternary complexes.



The utility of CDx solvent extraction for separating mixtures was evaluated by measuring the individual extraction efficiencies of the components in several binary PAH mixtures. The results of these mixture analyses are shown in Table III.

Table III. Extraction Efficiencies (%E) of Components in Binary PAH Mixtures

Components of Binary Mixture	%E for Component 1	%E for Component 2
Anthracene-perylene	0.0 ± 3.1	89.6 ± 5.4
Pyrene-perylene	40.9 ± 4.2	93.5 ± 3.1
Pyrene-coronene	42.3 ± 8.4	92.3 ± 0.9

The data indicate that the extracted percentages of components in these mixtures were independent of one another. Of the three mixtures extracted, separation of PAHs was relatively good for only one of them. This mixture of anthracene and perylene was easily separated because anthracene did not extract into aqueous  $\gamma$ -CDx solution but perylene extracted reasonably well. For those mixtures in which both species had a reasonable extraction into the modified aqueous phase, separation of the two compounds was not possible. Since excess CDx was available for complexation, the extraction of one component did not interfere with the extraction of the other. This problem might be resolved by decreasing the CDx concentration so that the PAHs would compete with one another in the complexation process. Figures 2 and 3 show the total-luminescence contour plots of two binary PAH mixtures before and after extraction with aqueous  $\gamma$ -CDx. The second of these mixtures, anthracene-coronene (Figure 3), again illustrates the potential for separating mixtures when one component has a low extraction efficiency.

The utility of extraction with aqueous CDx modifier appears to lie in the potential for simplifying complex mixtures of PAHs. Interpretation of the data suggests that extractions of this type are useful for separating large PAHs from small ones based on the strength of complex formation. Only those species that are of the right size to form strong complexes with cyclodextrin are capable of being extracted. This technique is useful for discriminating among analytes present in an organic matrix. Combining cyclodextrin-modified solvent extraction with available luminescence techniques may provide analysts with a useful technique for identification of components in complex mixtures.

After extraction, each phase may be studied independently in order to obtain a useful qualitative evaluation of the components in the original sample. The selectivity and specificity of fluorescence analysis can be especially beneficial in identification of PAHs. For example, some components could be identified by examining the fluorescence spectra of the organic and aqueous phases. Characteristic peak shapes may reveal identities of the components. For more complicated systems in which the spectra overlap, lifetime measurements may be used to identify components (27).

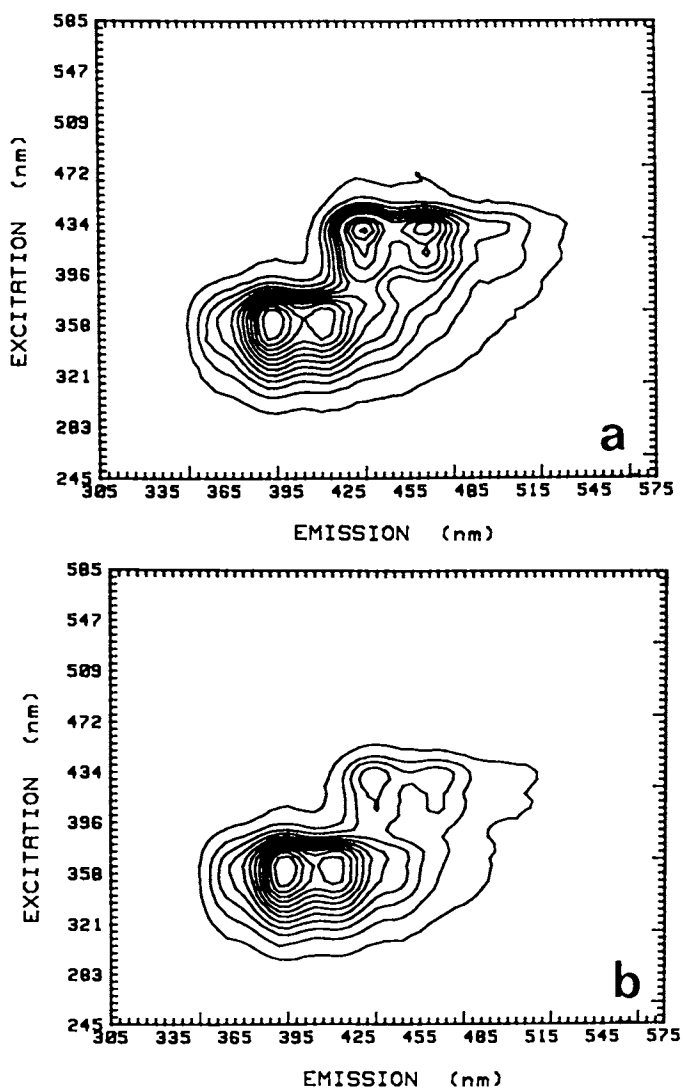


Figure 2. Total-luminescence contour plots of an anthracene-perylene mixture prior to extraction (a) and following extraction (b) with  $\gamma$ -cyclodextrin.

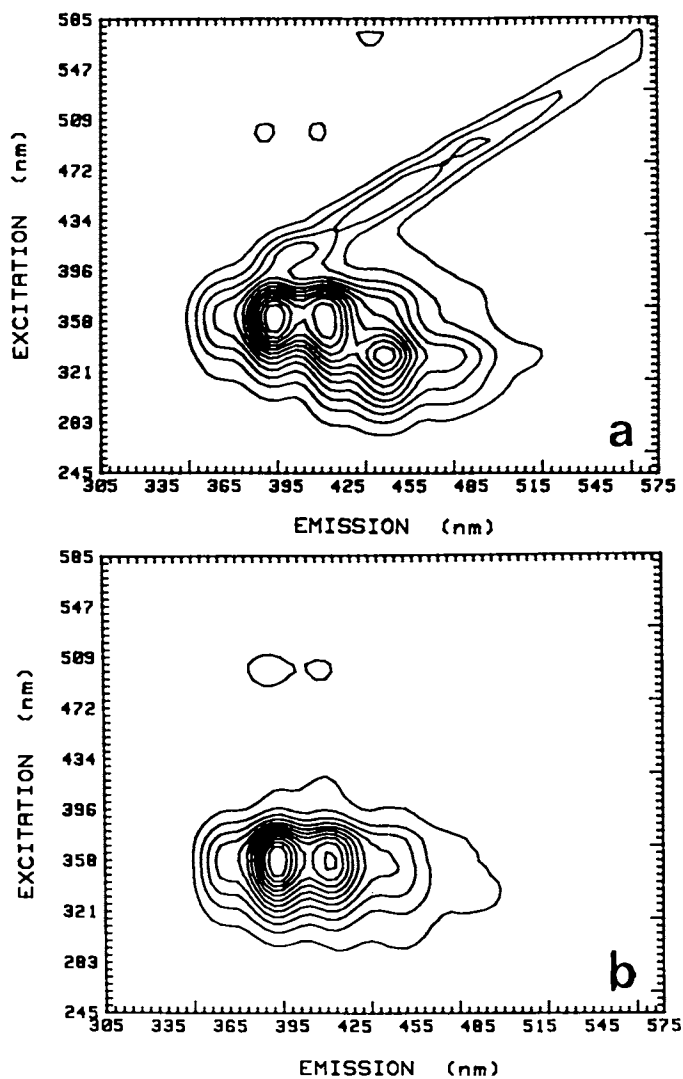


Figure 3. Total-luminescence contour plots of an anthracene-coronene mixture prior to extraction (a) and following extraction (b) with  $\gamma$ -cyclodextrrin.

Modern instruments capable of obtaining excitation-emission matrices (EEMs) allow use of new data-analysis techniques to resolve overlapped spectra. Resolution techniques such as the ratio method (28) and others (29,30) may provide further differentiation of the components present in the phases separated by solvent extraction.

### Conclusion

Cyclodextrin-modified solvent extraction has been used to extract several PAHs from ether to an aqueous phase. Data evaluation shows that the degree of extraction is related to the size of the potential guest molecule and that the method successfully separates simple binary mixtures in which one component does not complex strongly with CDx. The most useful application of cyclodextrin-modified solvent extraction is for the simplification of complex mixtures. The combined use of CDx modifier and data-analysis techniques may simplify the qualitative analysis of PAH mixtures.

### Literature Cited

1. Szejtli, J. *Cyclodextrins and Their Inclusion Complexes*; Akademiai Kiado: Budapest, Hungary, 1982.
2. Schlenck, W.; Sand, D. M. *J. Am. Chem. Soc.* 1961, **83**, 2312.
3. Saenger, W. *Angew. Chem. Int. Ed. Engl.* 1980, **19**, 344-362.
4. Bender, M. L.; Komiyama, M. *Cyclodextrin Chemistry*; Springer-Verlag: New York, 1978.
5. Cline Love, L. J.; Weinberger, R. *Spectrochim. Acta, Part B* 1983, **38**(11/12), 1421-1433.
6. Lach, J. L.; Chin, T. F. *J. Pharm. Sci.* 1964, **53**, 924.
7. Hamanda, Y.; Nambu, N.; Nagai, T. *Chem. Pharm. Bull.* 1975, **23**, 1205.
8. Cohen, J.; Lach, J. L. *J. Pharm. Sci.* 1963, **52**, 132.
9. Jules, O.; Scypinski, S.; Cline Love, L. J. *Anal. Chim. Acta* 1985, **169**, 355-360.
10. Scypinski, S.; Cline Love, L. J. *Anal. Chem.* 1984, **56**, 322-327.
11. Cline Love, L. J.; Grayeski, M. L.; Noroski, J.; Weinberger, R. *Anal. Chim. Acta* 1985, **170**, 3-12.
12. Breslow, R.; Kohn, U.; Siegel, B. *Tetrahedron Lett.* 1976, 1645-1646.
13. Kitaura, Y.; Bender, M. L. *Bioorg. Chem.* 1975, **4**, 237-249.
14. Armstrong, D. W.; DeMond, W.; Czech, B. D. *Anal. Chem.* 1985, **57**, 481-484.
15. Armstrong, D. W.; DeMond, W. *J. Chrom. Sci.* 1984, **22**, 411-415.
16. Caton, J. E.; Barnes, Z. K.; Kubota, H.; Griest, W. H.; Maskarinec, M. P. *Adv. Identif. Anal. Org. Pollut. Water* 1981, **1**, 329-344.
17. Rosen, A. A.; Middletown, F. M. *Anal. Chem.* 1955, **27**, 790.
18. Natusch, D. F. S.; Tomkins, B. A. *Anal. Chem.* 1978, **50**(11), 1429-1434.
19. Pearlman, P. S.; Yalkowsky, S. H.; Banerjee, S. J. *Phys. Chem. Ref. Data* 1984, **13**(2), 555-562.
20. Schwarz, F. P. *J. Chem. Eng. Data* 1977, **22**, 273-277.
21. Matsunaga, K.; Imanaka, M.; Ishida, T.; Oda, T. *Anal. Chem.* 1984, **56**, 1980-1982.
22. Harangi, J.; Nanasi, P. *Anal. Chim. Acta* 1984, **156**, 103-109.

23. Kalyanasundaram, K.; Thomas, J. K. *J. Am. Chem. Soc.* 1977, **99**, 2039-2044.
24. Berlman, I. B. *Handbook of Fluorescence Spectra of Aromatic Molecules*, 2nd ed.; Academic: New York, 1971.
25. Warner, I. M.; Fogarty, M. P.; Shelley, D. C. *Anal. Chim. Acta* 1979, **109**, 361-372.
26. Wishnia, A.; Lappi, S. J. *J. Mol. Biol.* 1974, **82**, 77.
27. Warner, I. M.; Patonay, G.; Thomas, M. P. *Anal. Chem.* 1985, **57**, 463A-483A.
28. Fogarty, M. P.; Warner, I. M. *Anal. Chem.* 1981, **53**, 259-265.
29. Moran, M. G.; Kowalski, B. R. *Anal. Chem.* 1979, **51**, 776A-789A.
30. Appellof, C. J.; Davidson, E. R. *Anal. Chem.* 1981, **53**, 2053-2056.

RECEIVED August 18, 1988

## Chapter 11

# Characterization of Aquatic Humic Acid Fractions by Fluorescence Depolarization Spectroscopy

Marvin C. Goldberg and Patricia M. Negomir

U.S. Geological Survey, Box 25046, MS 424, Lakewood, CO 80225

Humic materials collected from the Okefenokee swamp in Georgia had been fractionated on the basis of their hydrophobicity and proton affinity. Six fractions resulted from the separation process, and these fractions were studied by fluorescence spectroscopy to gain information about their internal structure, and behavior in water. The equivalent spherical molar volume of the humic fractions was determined by two methods. The range of molar volumes, including results from both methods, was from 738 to 4630 cubic centimeters per mole. It was established that each of the humic fractions had two fluorophores. The complete emission and excitation spectra are given for these fractions as well as the phase resolved emission spectra of both fluorophores for each fraction. Each fraction had two excitation maxima: A higher energy peak between 340 and 358 nanometers (nm) and a lower energy peak between 390 and 398 nm. The unresolved emission maxima for all six fractions ranged from 445 to 478 nanometers but the phase resolved emission maxima ranged from 405 to 410 nm for the high energy peak and 460 to 480 nm for the low energy peak. The shape of the fractions as rotors in water is aspherical; however, dynamic depolarization measurements indicate that as the size of the fractions decreases the asphericity of the molecule decreases.

In this chapter, we present the theory and results of measurements on humic acid fractions using fluorescence techniques. The fluorescence techniques are attractive for this application because of the natural fluorescence of humic materials, the high sensitivity of fluorescence detection, and the ability to directly observe the morphology of the molecule in aqueous solutions without the need for drying or applying harsh chemical conditions. Several interesting types of information are obtained from fluorescence measurements:

1. Fluorescence lifetime measurements can increase the analytical specificity when analyzing mixtures (1-4) and can indicate changes in chemical binding of the fluorophores under various environmental conditions (5).
2. Depolarization measurements, coupled with fluorescence lifetimes, are correlated with rates of molecular rotation to obtain estimates of molecular conformation, volume, and shape.

This chapter not subject to U.S. copyright  
Published 1989 American Chemical Society

Applications of fluorescence emission spectroscopy to detect chemical signatures from water are well documented. M.C. Goldberg discusses in Meyers and Welch (6) the application of fluorescence spectroscopy coupled with Raman spectroscopy to measure water characteristics using a remote sensor. In many of these applications the material producing the signature is aquatic humic acids. Goldberg and Devonald (7) developed a fluorescence technique for quantitatively determining the amount of organic material in surface water films. Specific applications were given for the Houston Ship Channel in Texas, where the fluorescence excitation spectrum was used to specify the types of materials present and the fluorescence emission spectrum was used for quantification. The treatment depended on adequate standards and some prior knowledge of the film composition. Goldberg and Wilson (8) describe the use of fluorescence spectroscopy as an analytical technique to determine thiamine and ferricyanide in water and wastewater.

This chapter presents new information about the physical properties of humic acid fractions from the Okefenokee Swamp, Georgia. Specialized techniques of fluorescence depolarization spectroscopy and phase-shift fluorometry allow the nondestructive determination of molar volume and shape in aqueous solutions. The techniques also provide sufficient data to make a reliable estimate of the number of different fluorophores in the molecule their respective excitation and emission spectra, and their phase-resolved emission spectra. These measurements are possible even in instances where two fluorophores have nearly identical emission spectra. The general theoretical background of each method is presented first, followed by the specific results of our measurements. Parts of the theoretical treatment of depolarization and phase-shift fluorometry given here are more fully expanded upon in (5,9-11). Recent work and reviews of these techniques are given by Warner and McGown (12).

### *Materials*

The humic material used in this study was collected at the Sill Dam on the Suwannee River outlet of the Okefenokee Swamp in Stephen Foster State Park near Fargo, Ga. Several schematics for fractionating humic materials into isolates have been advanced in the literature. For the work done in this paper we chose the method of Leenheer (13-14), which fractionates the humic materials based on their hydrophobicity and proton affinity. The humic fractions for this study were supplied by Leenheer. The original humic sample was collected by passing the Okefenokee swamp sample through three filter cartridges containing, in series, Amberlite XAD-8 resin, MSC-1 hydrogen saturated cation exchange resin and Duolite A-7 anion-exchange resin in free base form.<sup>1</sup> Leenheer (13) provides flow charts for the chemical isolation procedures. The hydrophobic acid, base and neutral isolates were obtained from the XAD-8 resin, the hydrophilic acids from the MSC-1 resin and the strong hydrophobic and strong hydrophilic acids from the Duolite A-7 resin.

### *Principles of Depolarization Measurements.*

Any factor that affects the size or shape of a molecule, the hindered movement of a fluorophore within a molecule, or the energy transfer within the molecule will affect the measured depolarization of its fluorescence emission. Therefore, the conformation of humic fractions in solution can be studied as a function of pH, ionic strength, temperature, and other factors by depolarization measurements. The principle of the method is that excitation of fluorescent samples with polarized light stimulates

emission that is also polarized. This occurs because molecules with absorption dipole moments closely parallel to the polarization plane of the exciting light are selectively excited. Also, molecules excited by polarized light have absorption dipole moments closely parallel to one another. Because the emission dipole moments of excited molecules have a fixed angular relation to their absorption moments, the emission moments will also tend to be parallel, resulting in polarized emission in the absence of processes such as rotation that scramble the fixed angular relationship between absorbing and emitting dipoles. Any rotation of a molecule that occurs after excitation by polarized light and before fluorescence emission takes place, contributes to the partial depolarization of the emitted light. This depolarization is easily measured. From these data and the fluorescence lifetimes, the rotational relaxation time can be calculated.

A depolarization measurement consists of exciting a fluorescent sample with linearly polarized light and measuring the polarization of emitted light at right angles to the plane of excitation. The polarization of the emitted light is defined as

$$P = (I_{\parallel} - I_{\perp}) / (I_{\parallel} + I_{\perp}) \quad (1)$$

Where  $I_{\parallel}$  and  $I_{\perp}$  are the measured intensities when the detector polarizer is respectively oriented parallel and perpendicular to the plane of the exciting light.

Several different factors contribute to the depolarization of emitted fluorescence relative to the polarization of the excitation light. Most of these can be controlled by experimental parameters, but two factors are intrinsic to the method and must be evaluated:

1. One intrinsic cause of depolarization in solution is the nature of the photoexcitation process. When a compound is excited with polarized light, the probability of excitation is greatest for those fluorophores with absorption dipole moments parallel to the excitation polarization plane. In a sample with a random distribution of absorption dipole moments, as in an isotropic solution, the probability of excitation by linearly polarized light is proportional to  $\cos^2\theta$  (where  $\theta$  is the angle between an absorption dipole moment and the plane of excitation polarization). This results in an angular distribution of absorption dipole moments in the excited molecules. The light emitted from excited fluorophores is polarized parallel to their emission dipole moment. If the absorption and emission dipoles are colinear and no other causes of depolarization exist, then the angular distribution of dipoles results in a maximum emission polarization of  $P = 0.5$  (5).

2. In general, the absorption and emission dipoles are not colinear but have an intrinsic angular difference within the fluorophore. This difference causes some amount of depolarization of the emitted light, relative to the exciting light. The angular displacement of the emission and absorption dipoles can be determined by measuring the depolarization in a dilute, vitrified solution, where rotation is not possible and radiationless energy transfer (see below) has only a small probability.

In addition to the intrinsic causes of depolarization, several experimentally controllable factors can contribute to a change in orientation of the emission dipole moment:

1. Radiationless transfer of energy among fluorophores results in depolarization because of a broadening in the distribution of emission dipole orientations. Because energy transfer is strongly dependent on the distance between emitter and absorber, depolarization can be used to measure the average distance between fluorophores when other contributions to the depolarizations are subdued. The method is most useful when the average separation of absorbing centers is about 5 nm, which corresponds to concentrations of approximately 0.013 M. Therefore, radiationless energy transfer is measured in viscous, moderately concentrated solutions (to minimize rotational diffusion).

2. Rotational diffusion during the lifetime of the excited state of the fluorophores



also contributes to a change in orientation of the emission dipole moment between the times of energy absorption and emission. The molecular rotation rate and, hence, the degree of depolarization from this cause are greatest in solutions of low viscosity. Rotational diffusion, therefore, is measured in solutions of low viscosity and low concentration (to minimize radiationless energy transfer).

Generally, it is easy to experimentally separate the depolarization effects of energy transfer and rotational diffusion of humic material. Viscosity can be controlled in aqueous solutions by adding glycerol or sucrose, and concentrations of humic material as small as 40 ppm provide conveniently strong fluorescence signals. By using dilute, low-viscosity solutions, the effects of intermolecular energy transfer are minimized, and the effects of rotationally caused depolarization are maximized. The resultant measured depolarization is determined by rotational motion of the fluorophore and the intrinsic offset of its absorption and emission dipoles. The following section describes how the contribution from the intrinsic dipole offset can be measured and the rate of molecular rotational diffusion determined by making measurements at a series of viscosities or a series of temperatures or both. The rate of rotational diffusion can be related to molar volume if the shape of the molecule and the microviscosity of its environment are known or assumed.

*Molecular Rotational Diffusion.* Rotational diffusion is the dominant intrinsic cause of depolarization under conditions of low solution viscosity and low fluorophore concentration. Polarization measurements are accurate indicators of molecular size. Two types of measurements are used: steady-state depolarization and time-dependent (dynamic) depolarization.

*Steady-State Fluorescence Depolarization Spectroscopy.* For steady state depolarization measurements, the sample is excited with linearly polarized light of constant intensity. Observed values of  $P$  depend on the angle between the absorption and emission dipole moment vectors. In equation 2 (9),  $P_0$  is the limiting value of polarization for a dilute solution of fluorophores randomly oriented in a rigid medium that permits no rotation and no energy transfer to other fluorophores:

$$P_0 = (3\cos^2\beta - 1) / (\cos^2\beta + 3), \quad (2)$$

where  $\beta$  is the angle between the absorption and emission dipole moment vectors.  $P_0$  can range from a maximum of  $1/2$  to a minimum of  $-1/3$ , as  $\beta$  varies from  $0$  to  $90^\circ$ . To a first approximation,  $P_0$  is a property of the fluorophore only, environmental effects being small enough to neglect. For the case of a fluorophore bound to a larger molecule,  $P_0$  depends on the intrinsic offset of the absorption and emission dipoles and on any restricted rotation of the fluorophore that is independent of the overall rotation of the larger molecule. Restricted rotation of the fluorophore will increase with temperature, decreasing the value of  $P_0$ . This effect is discussed by Lakowicz (5, chap. 5).

When rotational diffusion occurs, additional depolarization will result. Molecules that rotate rapidly, traversing a large angle during the emission lifetime, can effect complete randomization of polarization of the emitted light. More slowly rotating molecules, which have rotational periods of the same order of magnitude as the emission lifetime, will cause partial depolarization of the emitted light. Under conditions of partial depolarization, a molar volume can be calculated from Equation 3, which is one form of the Perrin equation (5).

$$(1/P - 1/3) = (1/P_0 - 1/3)[1 + (3\tau/p)] \quad (3)$$

where:  $P$  = observed depolarization of emission from all causes,  
 $P_0$  = depolarization of the emission due only to intrinsic causes, without any other depolarizing factors,

$\tau$  = the lifetime of the emitting fluorophore, and  
 $\rho$  = the rotational relaxation time of the molecule after excitation.

The rotational relaxation time,  $\rho$ , is related to the molecular volume by the equation:

$$\rho = 3\eta V / RT \quad (4)$$

where  $\eta$  = the solution viscosity,  
 $V$  = equivalent volume of a spherically rotating molecule,  
 $R$  = the gas constant, and  
 $T$  = temperature in Kelvins.

The quantity  $\eta V / RT$  is equal to six times the rotational period. The rotational relaxation time,  $\rho$ , should be shorter than the fluorescence lifetime,  $\tau$ , for these equations to apply. It is possible to perform calculations for nonspherical molecules such as prolate and oblate ellipsoids of revolution, but in such cases, there are different rotational rates about the different principal axes.

When equation 4 is substituted into 3, equation 5 is obtained:

$$(1/P - 1/3) = (1/P_0 - 1/3)(1 + \tau RT / \eta V) \quad (5)$$

Equation 5 has the form  $y = mx + b$ , the equation of a straight line, with  $y = (1/P - 1/3)$ ,  $x = T/\eta$ ,  $m = \text{slope } (1/P_0 - 1/3)(\tau R / V)$ , and  $b = \text{the intercept } (1/P_0 - 1/3)$ . Therefore a graph of  $1/P$  vs  $T/\eta$ , known as a Perrin plot, (see Figures 1a-f) should yield a straight line with a slope  $m$  and intercept  $1/P_0$ . The molecular equivalent-sphere volume can be determined from the slope by substituting  $P_0$ ,  $\tau$ ,  $R$  and  $m$  into equation 6:

$$V = (1/P_0 - 1/3)(\tau R / m). \quad (6)$$

The intercept,  $1/P_0$ , is called the anisotropy of the molecule and is an indication of the nonrotational depolarization of the molecule. This 'intrinsic' depolarization is due to the segmental motion of the fluorophores within the molecule; the depolarization due to energy transfer and the angular difference in transition dipole moments of the absorbing and emitting states.

Experimentally, the quantity  $T/\eta$  is varied for Perrin plots either by holding  $T$  constant and changing  $\eta$  or by holding  $\eta$  constant and changing  $T$ . Usually,  $\eta$  is varied in aqueous solutions by adding sucrose or glycerol. When  $T$  is constant, the viscosity of pure water and the viscosity of pure glycerol or saturated sucrose solution determine the upper and lower limiting values of  $T/\eta$ . If the molecule containing the fluorophore changes its conformation at some given temperature, as might occur with high temperature denaturation, a temperature-varying Perrin plot will have an abrupt change of slope at that temperature (15). It is possible to identify a conformation change dependent on a variable such as pH, by plotting  $1/P$  against pH (or other variable), at constant  $T/\eta$ . Because  $1/P$  is related to  $1/V$  through equation 5 or 9, its value will remain constant at constant  $T/\eta$ , as long as  $V$  and  $\tau$  do not change.

*Effect of Multicomponent Signals on Depolarization Measurements.* If two or more components contribute to the signal, as with the humic materials, the measured value of  $P$  will be a weighted average of the  $P$  values from each component. Therefore, weighted averages of  $\tau$  and  $P$  must be used in equation 5. This concern has not been discussed in the literature and Equations 7 and 8 offer a method for obtaining weighted values for  $\tau$  and  $P$  that require measuring the phase-resolved lifetimes of each fluorophore. Weighted values for  $\tau$  and  $P$  can be calculated as follows:

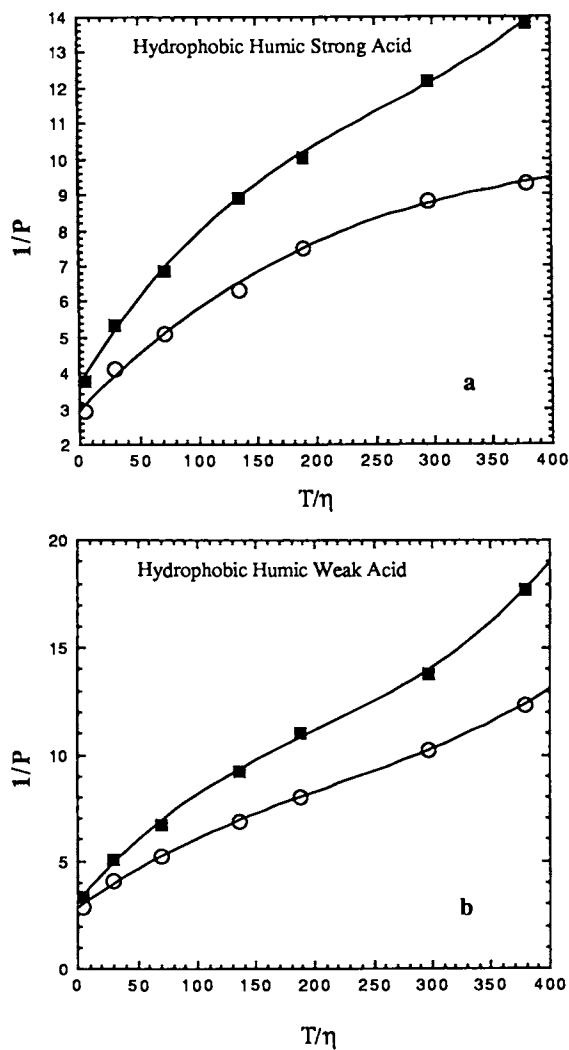


Figure 1. Perrin plots of the two fluorophores (open circles and solid squares) in hydrophobic humic strong (a) and weak (b) acids. (Continued on next page.)

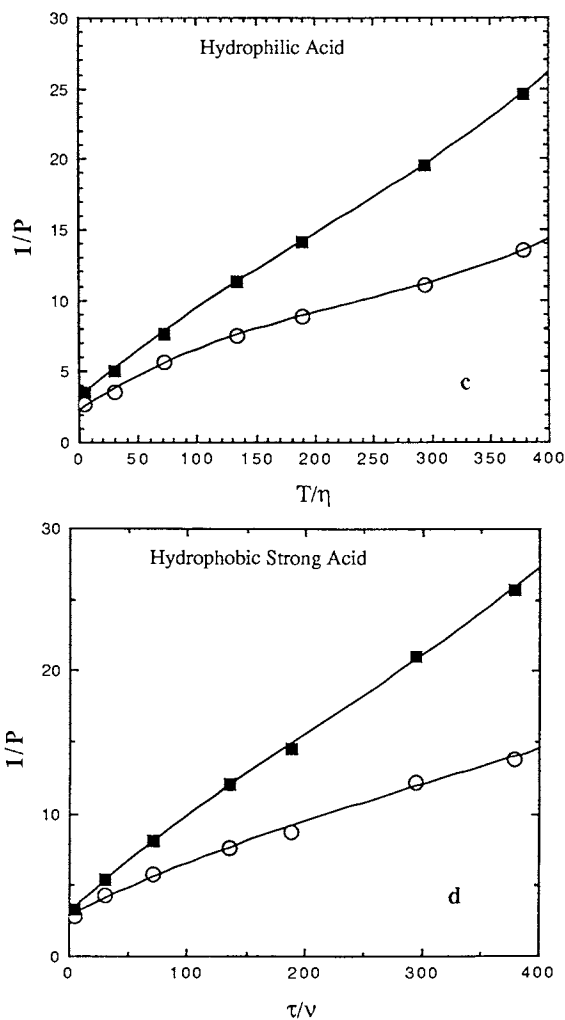


Figure 1. Continued. Perrin plots of the two fluorophores (open circles and solid squares) in hydrophilic (c) and hydrophobic strong (d) acids.

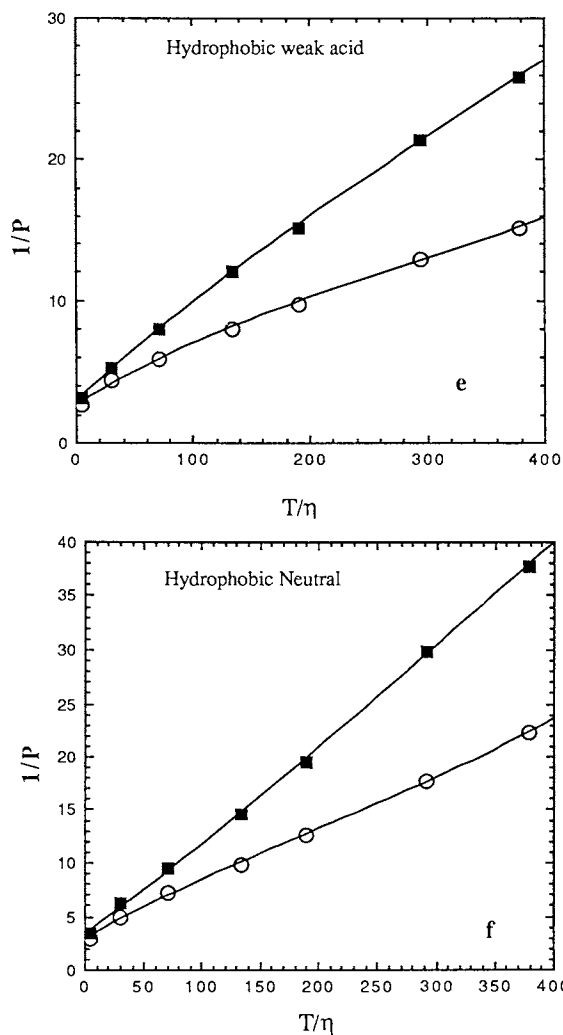


Figure 1. Continued. Perrin plots of the two fluorophores (open circles and solid squares) in hydrophobic weak acid (e) and neutral (f) fractions.

$$\tau' = \sum_i \tau_i f_i \quad (7)$$

$$P' = \sum_i P_i f_i \quad (8)$$

where the subscript  $i$  indicates measured values for the pure  $i$ th component,  $f_i$  is a weighting factor proportional to the phase-resolved signal intensity of the  $i$ th component, and  $\tau'$  and  $P'$  are the sample weighted average lifetime and limiting polarization, respectively. The weighting factors are determined from the phase-resolved lifetime measurements, which are discussed later under "Phase-Resolved Emission Spectra". For a sample with more than one fluorophore, Equations 5 and 6 become the equivalent Equations 9 and 10.

$$(1/P - 1/3) = (1/P_0 - 1/3) + (1/P_0 - 1/3)(\tau RT/\eta V) \quad (9)$$

$$V = (1/P_0 - 1/3)(\tau R/m) \quad (10)$$

Equations 9 and 10 were used to obtain the molar volumes of the humic fractions.

Fluorescence spectroscopy studies indicate that humic molecules, like proteins, are flexible and it is possible that the chromophores undergo segmental motion that is distinct from that of the overall molecule. That is, there may be "nonglobal rotation" as well as global rotation, as suggested by Chen and Scott (16). The Perrin plot is not linear in cases of multiple relaxation times and if the global relaxation is slow compared to the segmental rotation, the Perrin plot is concave towards the  $x$ -axis. At higher values of  $T/\eta$  essentially all the polarization will be lost even if the global relaxation is slow. Even though the rotation may be rapid, if it is hindered rotation the segmental rotation will result in partial depolarization of the light. This results in a lowering of  $P_0$  which is read in Figures 1a - f as the intercept of the extrapolated curved line with the  $y$ -axis. According to Chen and Scott (16), this apparent limiting polarization can be used to calculate the angle over which the flexible subunit can move. They introduce the equation

$$P'_0/P = (3 \cos^2\theta - 1)/2 \quad (11)$$

where  $\theta$  is the average angle of the cone describing the range of motion of the subunit,  $P'_0$  is the apparent limiting anisotropy and  $P$  is the anisotropy (17). The slope is read as the straight line portion of the curves in Figures 1a-f and applied in equation 10 to obtain the equivalent-sphere molar volume. The difference between the extrapolated intercept of the linear portion of the line on the  $y$  ordinate and the extrapolated intercept of the curved line is attributed to the internal rotation of the fluorophores in the molecule (5).

*Molar Volume and Shape of Humic Fractions.* Each of the six humic fractions was placed in aqueous solution at pH 6.5 and depolarization measurements made. Generally, concentrations between 40 and 60 ppm provided sufficient fluorescence signal intensity to make all the required measurements and maintain the solutions sufficiently dilute to avoid depolarization by energy transfer. Fluorophoric lifetimes were determined on the SLM 4800 phase spectrophotofluorometer as were the depolarization measurements. The  $T/\eta$  ratios were changed for each of the measurements plotted in Figures 1 a-f by changing the glycerol to water ratio in the

solutions containing the humic fractions. The molar volumes of the humic fractions are listed in Table I as calculated by Equation 10.

Table I. Volume of Humic Fractions

Humic Fraction	Volume in cm <sup>3</sup> /mole
Hydrophobic Humic Strong Acid	4630
Hydrophobic Humic Weak Acid	2280
Hydrophilic Acid	2190
Hydrophobic Strong Acid	1940
Hydrophobic Weak Acid	1530
Hydrophobic Neutral	1000

#### *Dynamic Depolarization Spectroscopy.*

*Pulsed method.* Using a pulsed or modulated excitation light source instead of constant illumination allows investigation of the time dependence of emission polarization. In the case of pulsed excitation, the measured quantity is the time decay of fluorescent emission polarized parallel and perpendicular to the excitation plane of polarization. Emitted light polarized parallel to the excitation plane decays faster than the excited state lifetime because the molecule is rotating its emission dipole away from the polarization plane of measurement. Emitted light polarized perpendicular to the excitation plane decays more slowly because the emission dipole moment is rotating towards the plane of measurement.

With a modulated light source, the phase difference between the perpendicular and parallel components of the emission is measured. The time delay of the perpendicular component of emission is longer than that of the parallel component because the molecule requires a certain period of time to rotate into the perpendicular orientation where it can be detected through the perpendicular polarizer.

Both pulse and modulation methods permit an estimate of a spherical volume for a macromolecule and are especially useful for determining deviations from molecular sphericity.

*Time Resolved Fluorescence Depolarization.* In Equation 3, it is assumed that the polarization decays to zero as a single exponential function, which is equivalent to assuming that the molecular shape is spherical with isotropic rotational motion. Multiexponential decays arise from anisotropic rotational motion, which might indicate a nonspherical molecule, a molecule rotating in a nonuniform environment, a fluorophore bound to the molecule in a manner that hinders its motion, or a mixture of fluorophores with different rotational rates.

In principle, pulsed excitation measurements can provide direct observation of time-resolved polarization decays and permit the single-exponential or multiexponential nature of the decay curves to be measured. In practice, however, accurate quantification of a multiexponential curve often requires that the emission decay be measured down to low intensity values, where obtaining a satisfactory signal-to-noise ratio can be a time-consuming process. In addition, the accuracy of rotational rate measurements close to a nanosecond or less are severely limited by the pulse width of the flash lamps. As a result, pulsed-excitation polarization measurements are not commonly used for short rotational periods or for careful measurements of rotational anisotropy.

*Modulation Method*

The interpretation of emission phase-angle shifts in the light modulation method is more complicated than the analysis of decay curves from pulsed excitation, but the modulation technique is more rapid and can determine rotational rates and degree of anisotropy on a subnanosecond scale. Experimentally, the sample is excited with polarized, sinusoidally modulated light. The phase-angle difference,  $\Delta$ , between the perpendicular and parallel polarized components of the emission is measured. The relationship between  $\tan \Delta$  and molecular rotations has been derived by Weber (10). The dependence of  $\tan \Delta$  on the limiting polarization, excited state lifetime, rotational diffusion rate, and the light modulation frequency is given in Equation 12.

$$\tan \Delta = \frac{2R\tau^2\omega r_o}{\frac{1}{9}m_o(1 + \omega^2\tau^2) + \left(\frac{2R\tau}{3}\right)(2+r_o) + (2R\tau)^2} \quad (12)$$

where  $R$  = rotational rate,  
 $\tau$  = fluorescence lifetime,  
 $\omega = 2\pi\nu$  excitation modulation frequency,  
 $\nu$  = modulation frequency of the oscillator,  
 $r_o$  = fluorescence anisotropy which would be observed in the absence of rotational diffusion, and  
 $m_o = (1 + 2r_o)/(1 - r_o)$ .

The maximum value of  $\tan \Delta$  is given by:

$$\tan \Delta_{max} = \frac{P_o \omega \tau}{\left\{ 1 + \left[ (1 - P_o^2) (1 + \omega^2 \tau^2) \right]^{1/2} \right\}} \quad (13)$$

The value of  $\tan \Delta$  depends upon the modulation frequency, the excited state lifetime, and the rate of rotation. The value decreases to zero when the rotation period is either longer or shorter than the excited state lifetime and is a maximum when the two times are comparable in magnitude.  $\tan \Delta$  also increases as the modulation frequency increases. For spherical rotators, the measured value of  $\tan \Delta$  for a given modulation frequency and excited state lifetime allows the rotational rate to be calculated from

$$2R\tau^2 + 2R\tau \left[ \frac{2+r_o}{3} - \left| \frac{r_o}{\tan \Delta} \right| (\omega\tau) \right] + \frac{1}{9} m_o (1 + \omega^2\tau^2) = 0 \quad (14)$$

Then the molecular volume may be determined as for steady state measurements using Equation 6.

For spherical rotators, the measured value of  $\tan \Delta_{max}$  is independent of the rate of rotation. However, for non spherical rotators, the measured value of  $\tan \Delta_{max}$  depends on the molecular shape and is always smaller than the measured value of  $\tan \Delta_{max}$  for spherical molecules. Nonsphericity can be detected by calculating the  $\tan$



$\Delta_{\max}$  for spherical molecules (using Equation 13) and then measuring the sample throughout a temperature range that causes the sample rotation rate to vary in the region of  $\tan \Delta_{\max}$ . If the measured  $\tan \Delta_{\max}$  is smaller than the calculated value, the molecule is nonspherical. One can distinguish between anisotropic rotation and the segmental motion of the fluorophores on the molecule, hindered rotation, both of which cause a tangent defect (the difference between the experimentally measured tangent maximum and the calculated tangent maximum). The decrease in value of  $\tan \Delta_{\max}$  (tangent defect) caused by hindered rotation (segmental motion of the fluorophores within the molecule) can be as large as 100 percent, much larger than for anisotropic rotations, which seldom exceed 25 percent. By noting the magnitude of the tangent defect, the cause can be assigned to either anisotropic rotation of the molecule or hindered rotation of the fluorophores.

### Measurements

Measurements of  $\tan \Delta$  as a function of temperature for the six humic fractions are plotted in Figures 2a-f. These measurements were made at pH 6.5. These plots show a maximum between 6 °C and 25 °C. Equation 15 offers another method for the calculation of the molar volume based on the anisotropy of the molecule and the temperature and viscosity at the experimental maximum of the  $\tan \Delta$  plots. The consequences of obtaining the volume in this manner are discussed by Mantulin and Weber (18).

$$V_{SE} = \frac{NkT_o}{6\eta_o R_o} \quad (15)$$

where  $V_{SE}$  = the Stokes-Einstein volume

$R_o$  = The rotational rate and at the maximum is  $1/2\rho_o$

$\eta_o$  = the viscosity of the solution at  $T_o$  and

$T_o$  = temperature of the solvent at which  $\tan \Delta$  goes through a maximum. These values are presented in Table II.  $V_{SE}$  (the Stokes-Einstein volume) is calculated for a spherical molecule; if the molecule is aspherical this calculation ( $V_{SE}$ ) is called  $V_{\text{apparent}}$ . The  $V_{\text{apparent}}$  can be smaller or larger than the Stokes-Einstein volume and varies from the equivalent sphere volume obtained by solution of equations 3,4 and 5.

The difference between  $V_{\text{apparent}}$ , the apparent Stokes-Einstein volume and  $V_{\text{Perrin}}$  (Equations 3,4 and 5) is attributed to deviation in shape of the rotating molecule, from a sphere. Weber, (10) and Mantulin and Weber(18), discuss the solution of equations leading to a shape assignment assuming the molecule is an ellipsoid. The ratios of  $V_{\text{Perrin}}/V_{\text{apparent}}$  presented in Table II. range from 4 to 1.4. If a molecule is a spherical rotor in water the value of  $V_{\text{apparent}}$  should be equal to the value of  $V_{\text{Perrin}}$ . The data in Table II lead to the conclusion that as the size of the humic fraction decreases, the asymmetry of the humic fraction, decreases; that is, its shape approaches sphericity. Based on this reasoning the hydrophobic neutral should be much closer to sphericity than the hydrophobic humic strong acid fraction. These data do not allow us to differentiate between ellipsoidal rotators and those that have other types of aspherical shapes.

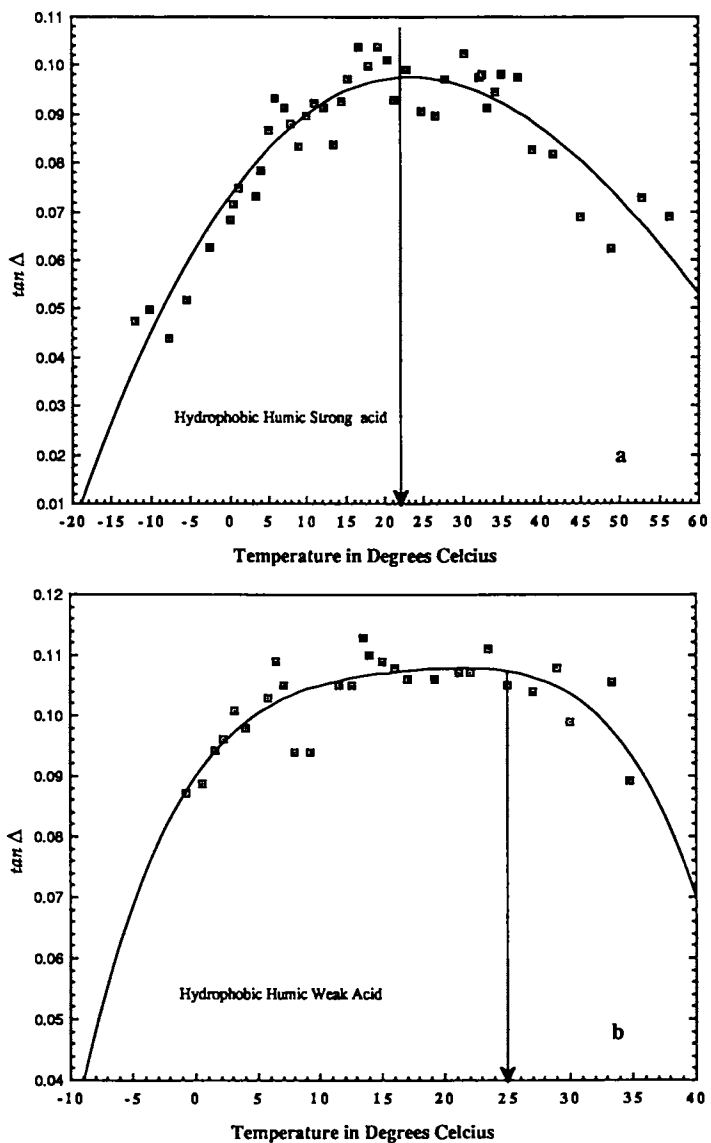


Figure 2. Tangent  $\Delta$  plotted against temperature for hydrophobic humic strong (a) and weak (b) acids. The arrow marks the curve maximum.

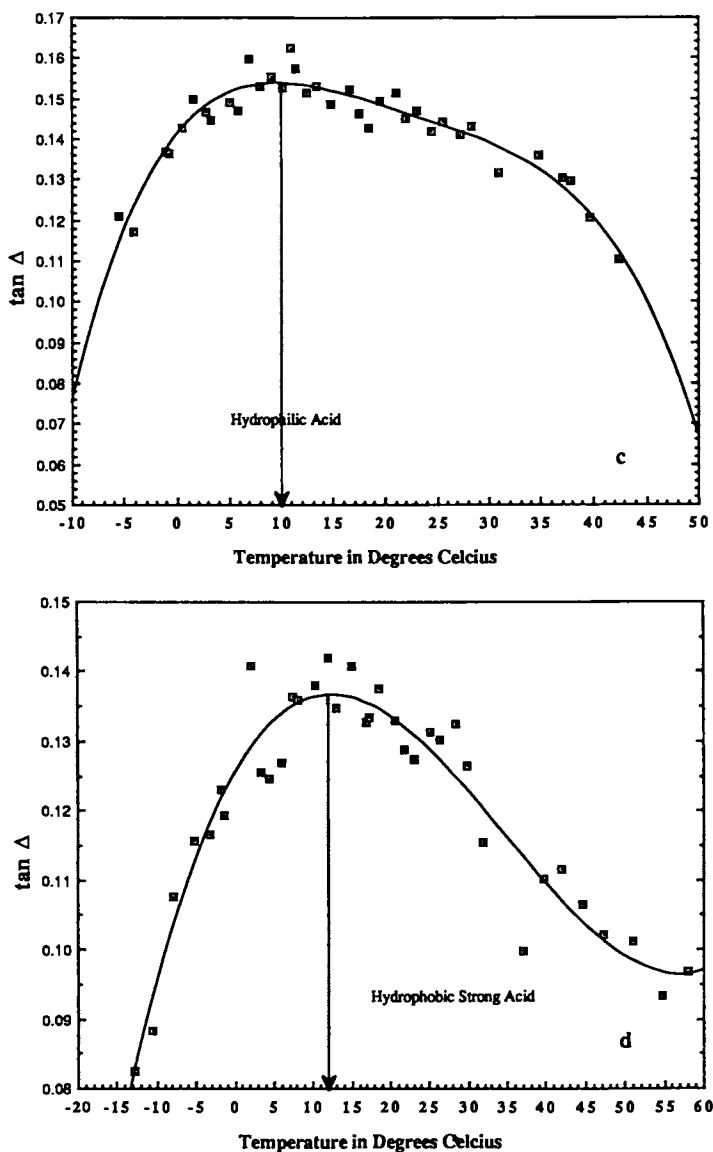


Figure 2. Continued. Tangent  $\Delta$  plotted against temperature for hydrophilic (c) and hydrophobic strong (d) acids. The arrow marks the curve maximum. (Continued on next page.)

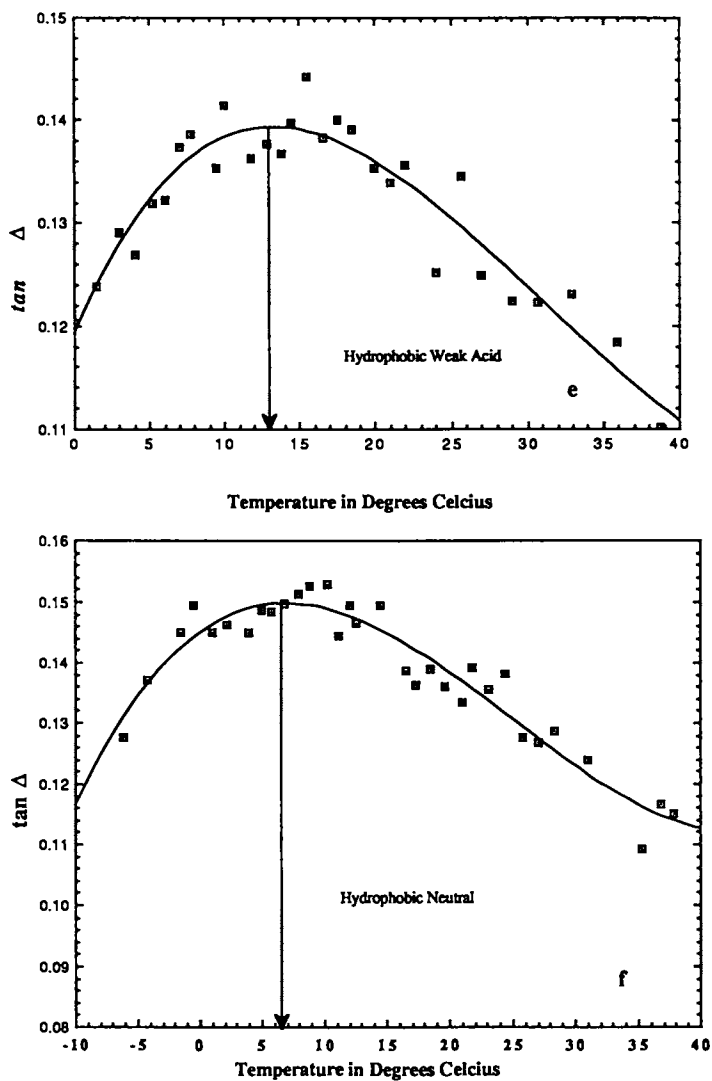


Figure 2. Continued. Tangent  $\Delta$  plotted against temperature for hydrophobic weak acid (e) and neutral (f) fractions. The arrow marks the curve maximum.

Table II. Comparison of Stokes-Einstein ( $V_{\text{apparent}}$ ) Volume to the Perrin Volume

Humic Fraction	$V_{\text{apparent}}$ ( $\text{cm}^3/\text{mole}$ )	$V_{\text{Perrin}}$ ( $\text{cm}^3$ ) ( $\text{cm}^3/\text{mole}$ )	$V_{\text{Perrin}}/V_{\text{apparent}}$
Hydrophobic Humic Strong Acid	1150	4630	4.0
Hydrophobic Humic Weak Acid	1190	2280	1.9
Hydrophilic Acid	865	2190	2.5
Hydrophobic Strong Acid	872	1940	2.2
Hydrophobic Weak Acid	926	1530	1.7
Hydrophobic Neutral	738	1000	1.4

#### *Excitation-Emission Spectra.*

Figures 3a-f show the emission and excitation spectra for all six humic fractions. The excitation and emission maxima are listed in Table III along with the maxima of the phase-resolved emission spectra. In each case the emission spectrum was scanned with the excitation maximum wavelength held constant, and the excitation spectrum was scanned with the emission maximum wavelength held constant. Several interesting features are noted. The two humic samples (Figures 3a,b) each have two excitation maxima and it appears that a double peak has been merged into the emission scan as evidenced by the shoulder on the high energy side of the emission peak. Similarly it seems evident that the exaggerated shoulders in the emission spectra of all the fractions point to the inclusion of two emission peaks in each spectrum. This evidence suggests the presence of two chromophores in each humic fraction.

The hydrophobic humic weak acid has a double peak in the excitation spectrum and its longer wavelength peak is of higher intensity than those in the spectra of the other fractions. This longer wavelength peak, which occurs in the spectra of all the humic fractions, progressively diminishes in the series; hydrophobic humic weak acid > hydrophobic humic strong acid > hydrophobic weak acid > hydrophobic strong acid > hydrophobic neutral > hydrophilic acid.

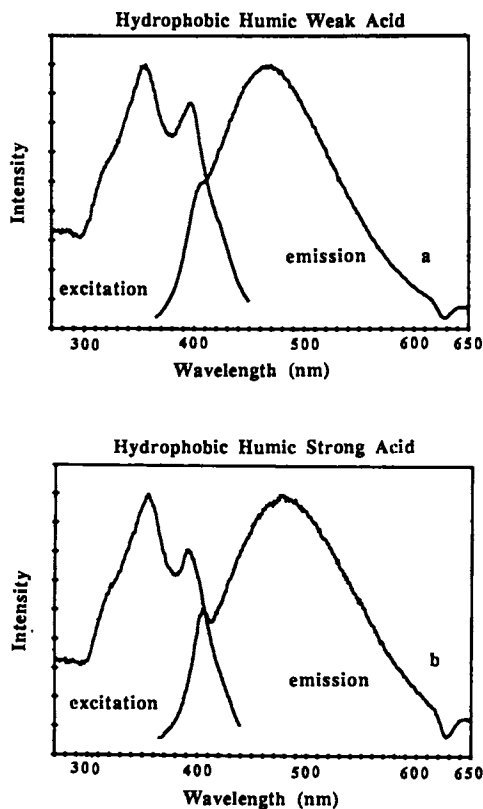


Figure 3. Excitation-emission spectra for hydrophobic humic weak (a) and strong (b) acids.

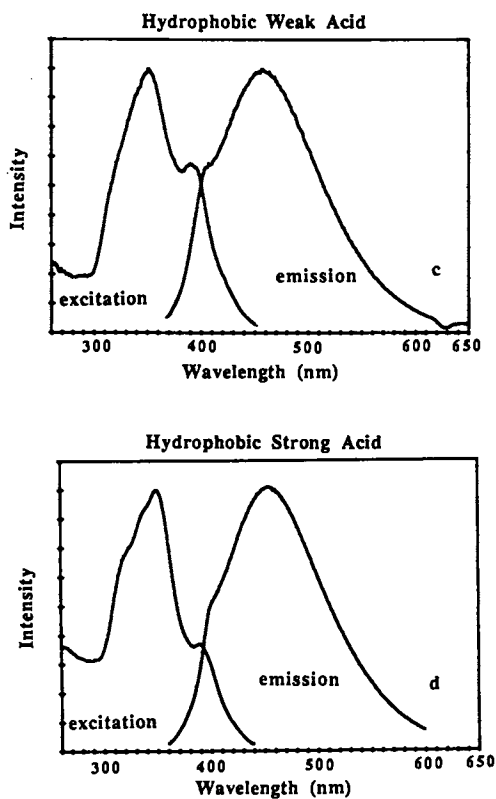


Figure 3. Continued. Excitation-emission spectra for hydrophobic weak (c) and strong (d) acids. (Continued on next page.)

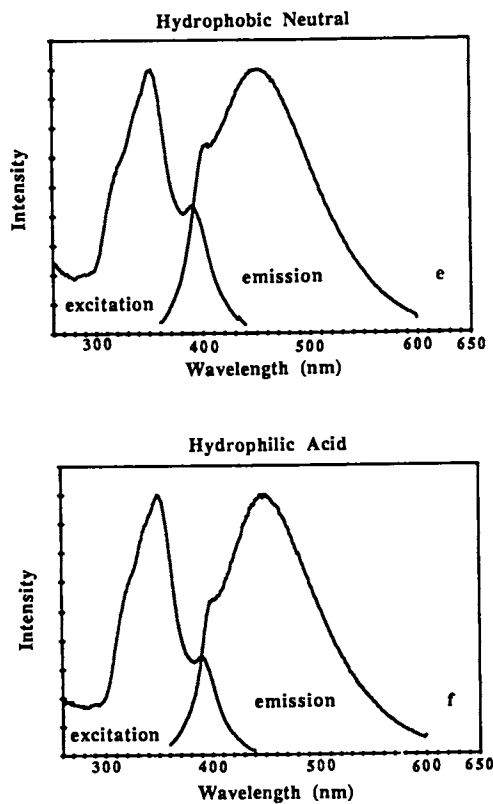


Figure 3. Continued. Excitation-emission spectra for hydrophobic neutral (e) and hydrophilic acid (f) fractions.



Table III. Humic Fractions Fluorescence Excitation and Emission Maxima and Phase-Resolved Emission Maxima

Humic Fraction	Excitation Maxima (in nm)	Emission Maxima (in nm)	Emission Maxima Phase Resolved (in nm)
Hydrophobic humic weak acid	358, 398	475	405, 480
Hydrophobic humic strong acid	358, 393	478	405, 480
Hydrophobic weak acid	350	450	410, 470
Hydrophilic acid	350	448	405, 460
Hydrophobic strong acid	340	445	410, 470
Hydrophobic neutral	353	455	405, 470

*Fluorophore Composition of Humic Acid Fractions.* If a single fluorophore is present in a molecule, (a) the short-wavelength limit of the emission spectrum should correspond to the 0-0 band emission from the first excited electronic state of the fluorophore, (b) the long-wavelength limit of the excitation spectrum should correspond to the 0-0 band excitation from the ground electronic state of the fluorophore and (c) the excitation band should end at the wavelength where the emission band begins. A small amount of band overlap can be explained by thermal vibrational excitation that occurs after electronic excitation but before fluorescent emission (9). However all the spectra shown in Figures 3 a-f have large band overlaps, of 80 nm or more. This overlap is strong evidence for the existence of more than one fluorophore. Additional evidence for this conclusion is seen in the phase-resolved spectra.

#### *Phase-Resolved Emission Spectra*

*Theory.* If two or more fluorophores with different emission lifetimes contribute to the same broad, unresolved emission spectrum, their separate emission spectra often can be resolved by the technique of phase-resolved fluorometry. In this method the excitation light is modulated sinusoidally, usually in the radio-frequency range, and the emission is analyzed with a phase sensitive detector. The emission appears as a sinusoidally modulated signal, shifted in phase from the excitation modulation and partially demodulated by an amount dependent on the lifetime of the fluorophore excited state (5, Chapter 4). The detector phase can be adjusted to be exactly out-of-phase with the emission from any one fluorophore, so that the contribution to the total spectrum from that fluorophore is suppressed. For a sample with two fluorophores, suppressing the emission from one fluorophore leaves a spectrum caused only by the other, which then can be directly recorded. With more than two fluorophores the problem is more complicated but a number of techniques for deconvoluting the complex emission curve have been developed making use of several modulation frequencies and measurement phase angles (19).

For single exponential fluorescence decay, as is expected for a sample containing just one fluorophore, either the phase shift or the demodulation can be used to calculate the fluorescence lifetime  $\tau$ . When the excitation light is modulated at an angular frequency  $\omega = 2\pi\nu$ , the phase angle  $\phi$ , by which the emission modulation is shifted from the excitation modulation, is related to the fluorescence lifetime by:

$$\tan \phi = \omega\tau \quad (16)$$

The demodulation  $m$  is related to the fluorescence lifetime by:

$$m = (1 + \omega^2 \tau^2)^{-1/2} \quad (17)$$

If the signal decay is a single-exponential curve, equations 16 and 17 result in values for  $\tau$  that are in agreement with each other. Dissimilar values indicate multiexponential decay, which usually means that the sample contains more than one fluorophore. Multiexponential decay can be resolved by using a phase fluorometer with phase sensitive detection. A time-independent, direct-current signal is produced that is proportional to the cosine of the difference between the phase angle of the detector ( $\phi_D$ ) and the phase angle of the fluorescence ( $\phi$ ):

$$F(\lambda, \phi_D) = k F(\lambda) \cos(\phi_D - \phi) \quad (18)$$

where

$F(\lambda, \phi_D)$  = the measured direct current signal,

$k$  = a proportionality constant that includes sample and instrumentation factors as well the modulation factor of the exciting light,

$F(\phi)$  = the direct current intensity component of the fluorescence emission,

$\phi_D$  = the detector phase angle, and

$\phi$  = the fluorescence phase angle.

For a given fluorophore at a given wavelength, the maximum phase-resolved signal intensity is obtained when  $\phi_D = \phi$ , and the minimum signal is obtained when the entire signal from the given component is cancelled out at  $\phi_D = \phi + 90^\circ$ .

Consider a sample with two fluorophores, A and B, whose lifetimes ( $\lambda_A$  and  $\lambda_B$ ) are each independent of emission wavelength and are different from one another. By setting  $\phi_D = \phi_A + 90^\circ$ , the contribution from A is nulled out and the scanned emission spectrum represents only the contribution from B. Similarly, the spectrum for A is obtained by setting  $\phi_D = \phi_B + 90^\circ$ . In practice, finding the correct value of  $\phi_D$  for this direct nulling approach can be tedious, so more indirect but faster methods are often used. If the spectrum is scanned with a series of different detector phase angles, spectra of the separate fluorophores can be generated by best fit routines, or a set of simultaneous equations can be generated allowing a matrix solution for the contributions of the fluorophores (19). For these techniques, equations 19 and 20 apply (11,20)

$$\tan \phi = \frac{\sum_i f_i \sin \phi_i \cos \phi_i}{\sum_i f_i \cos^2 \phi_i} \quad (19)$$

and

$$m^2 = \left( \sum_i f_i \cos^2 \phi_i \right)^2 + \left( \sum_i f_i \sin \phi_i \cos \phi_i \right)^2 \quad (20)$$

where:  $\phi$  = the experimentally measured phase-shift angle,

$m$  = the experimentally measured demodulation,

$\phi_i$  = the phase shift due to the  $i$ th component,

$f_i$  = the fractional contribution of the  $i$ th component to the measured quantities.

By measuring  $\phi$  and  $m$  at several modulation frequencies, a set of simultaneous equations can be generated that allow a determination of the best values for fluorophore lifetime and fractional contributions. The  $f_i$  values from these calculations are the quantities that are used in Equations 7 and 8 to obtain weighted values of  $\tau$  and  $P_0$ .

#### *Phase-Resolved Spectra.*

Humic materials fractionated on the basis of hydrophobicity and proton affinity continue to exhibit two fluorophores as discussed in the section "Excitation-Emission Spectra. Strong evidence to establish the existence of at least two chromophores is seen in the phase-resolved spectra. These spectra are shown in Figures 4 a-f. They consist of the phase-resolved emission spectrum of each of the two fluorophores plotted separately and the normal emission spectrum of the humic fraction. If the nulling out of one fluorophore is exact then the sum of the two separate phase resolved spectra should be additive to equal the normal spectrum. In these figures the normal emission spectrum was measured separately from the two phase resolved emission spectra. The phase resolved spectra were then superimposed onto the scan of the normal emission spectrum.

#### *Conclusions.*

Fluorescence polarization spectroscopy is a powerful tool that is useful in measuring the properties of humic fractions. It was found that six humic fractions, separated on the basis of their hydrophobicity and proton affinity were different in size, ranging from 1000 to 4630 cm<sup>3</sup>/mole when measured by the conventional Perrin plot. Using the method of dynamic depolarization and calculating the volume from the tangent delta plots yielded sizes ranging from 738 to 1190 cm<sup>3</sup>/mole. This difference in volume between the two methods of determination is due to the asphericity of the molecules as they rotate in water. The excitation-emission spectra of these humic fractions were very similar though the emission spectra of the larger molecules shifted slightly towards lower wavelengths as a function of molecular size. The excitation spectra exhibited two maxima. The lower energy maximum decreased in intensity also as a

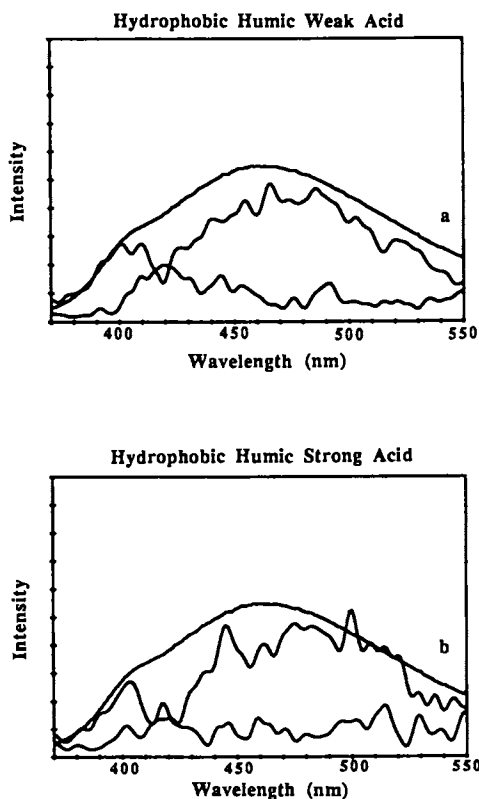


Figure 4. Phase-resolved plots of the six humic fractions superimposed on the normal emission scan for each fraction. The emission spectrum of the first fluorophore was suppressed and a scan was made of the second fluorophore; then the second fluorophore was suppressed and an emission scan was made of the first fluorophore. Fractions: hydrophobic humic weak (a) and strong (b) acids.

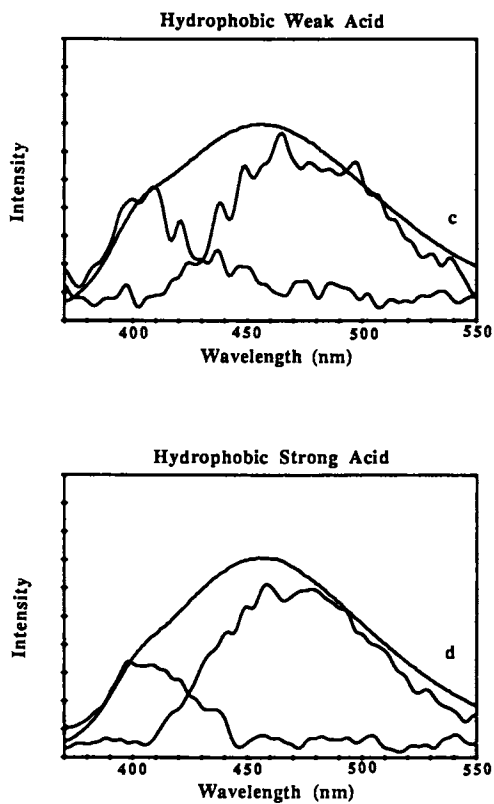


Figure 4. Phase-resolved plots, continued. Fractions: hydrophobic weak (c) and strong (d) acids. (Continued on next page.)

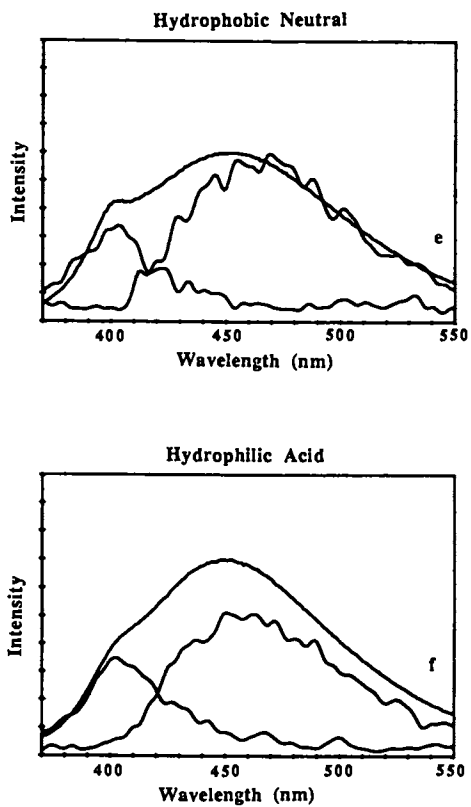


Figure 4. Phase-resolved plots, continued. Fractions: hydrophobic neutral (e) and hydrophilic acid (f).

function of the size of the humic fraction. The overlap of the 0-0 band of the excitation ground electronic state with the 0-0 band of the first excited electronic emission state is strong evidence for the existence of more than one fluorophore in each of the humic fractions. Additional evidence is supplied by the phase resolved emission spectra of all the fractions. It was possible to obtain two phase resolved emission spectra with different maxima for each fraction. This indicates that two fluorophores are present in each fraction. The phase-resolved spectra of all six fractions have one emission maximum between 470 and 580 nm and the second emission maximum between 405 and 410 nm. The unresolved emission spectra have maxima between 445 and 478 nm and two excitation maxima, one between 340 and 358 nm and the other between 390 and 398 nm.

All these data are adequate to characterize these fractions and to differentiate one from another.

#### *Literature Cited*

1. Love, L.B.C.; Upton, L.M. *Anal. Chem.* 1980, *52*, 496-499.
2. Weiner, E. R.; Goldberg, M.C. *Am. Lab.* 1982, *50*, 1583-1584.
3. Demas, J.N. *Excited State Lifetime Measurements*; Academic: New York, 1983; Chapter 1.
4. Goldberg, M.C. *Proc. 26th Rocky Mountain Conference*, 1984, p 110.
5. Lakowicz, J.R. *Principles of Fluorescence Spectroscopy*; Plenum: New York, 1983
6. Meyers, W.; Welch, R.I. In *Manual of Remote Sensing*; Bowden, L.W.; Pruitt, E.L., Eds.; American Society of Photogrammetry: Falls Church, VA, 1975; Vol. II, Chapter 19. pp 1497-1501.
7. Goldberg, M.C.; Devonald, D.H. *U. S. Geol.Surv., J. Res.* 1973, *1*, 709-717.
8. Goldberg, M.C.; Wilson, J.K. *Proc. Am.Chem.Soc.168th Natn Mtg., Atlantic City, NJ*, 1974.
9. Parker, C. A. *Photoluminescence of Solutions*; Elsevier: New York, 1968; p 57.
10. Weber, G. *J. Phys.Chem.* 1977, *66*, 4081-4091.
11. Weber, G. *J. Phys. Chem.* 1981, *85*, 949-953.
12. Warner, I. M.; McGown, L. B. *Anal. Chem.* 1988, *60*, 162R-174R.
13. Leenheer, J. A.; Noyes, T. I. *U. S. Geol.Surv.,Water Supply Pap.* 2230 1984, 16 p.
14. Leenheer J.A. *Environ. Sci.Technol.* 1984, *15*, 578-87.
15. Ellerton, R.N.; Isenberg, I. *Biopolymers* 1969, *8*, 767-786.
16. Chen, R.F.; Scott C.H. In *advances in Luminescence Spectroscopy*; Cline-Love, L. J.; Eastwood, D., Eds.; ASTM Spec. Tech. Publ. 863 1983 p 26-39
17. Gottlieb, Y.; Whal, P. *J. Phys. Chem.* 1963, *60*, 849-56.
18. Mantulin W. W.; Weber, G. *J. Chem. Phys.* 1977, *66*, 4092-99.
19. McGown, L. B.; Bright, F. V. *Anal. Chem.* 1984, *56*, 1400A-1415A.
20. Jameson, D. M.; Weber, G. *J. Phys. Chem.* 1981, *85*, 953-958.

RECEIVED September 12, 1988

## Chapter 12

# Use of Fluorescent 1,3-Disubstituted 2(1*H*)Pyridones for Environmental Analysis

David A. Nelson, James H. Bush, James R. Beckett,  
Douglas M. Lenz, and David W. Rowe

Department of Chemistry, University of Wyoming, Laramie, WY 82071

Fluorescent derivatives were prepared from a series of alkyl halides and alcohols using derivatizing reagents prepared from 3-carbamoyl-2(1*H*)pyridone and 3-phenyl-2(1*H*)pyridone. These derivatives were designed to be analyzed by high-performance liquid chromatography (HPLC) using fluorescence detection, and they could be measured at the picomole level. The derivatization chemistry is applicable to a wide variety of organic compounds. Derivatives were also prepared from amines, phenols, acrylonitrile, and heptachlor. A series of six pyridone sulfonates was synthesized for use as fluorescent, site-specific, water-tracing compounds.

The development of fluorescent derivatizing reagents for high-performance liquid chromatography (HPLC) is an area of considerable interest, mainly because of the inherent sensitivity gain of fluorescence detection over ultraviolet detection and because of the availability of reasonably priced, sensitive fluorescence detectors. The use of laser-induced fluorescence detectors for HPLC has already been reported by several research groups (1-3), and no doubt such detectors will soon be commercially available. When used with micro-bore HPLC technology, such detectors can achieve extremely sensitive levels of detection (4). New fluorescent reagents tailored for specific purposes are likely to become increasingly important for environmental analyses.

Reports on the use of fluorescent derivatives abound (5). Some reagents have become widely used. The dansyl group is probably the most thoroughly studied. Dansyl chloride has been widely used as a fluorescent derivatizing reagent for HPLC (6,7). It reacts readily with primary and secondary amino groups (7) and with phenols (8), but forms derivatives of alcohols very slowly (9). The lower detection limit for dansyl derivatives of aliphatic amines is in the range of 300 femtomoles per injection.

Dansyl chloride does have some drawbacks when used with reverse-phase HPLC. One of these is that the quantum yield of fluorescence varies greatly with the polarity of the solvent for dansyl derivatives (10,11). As the polarity of the solvent increases, the

0097-6156/89/0383-0206\$06.50/0

• 1989 American Chemical Society



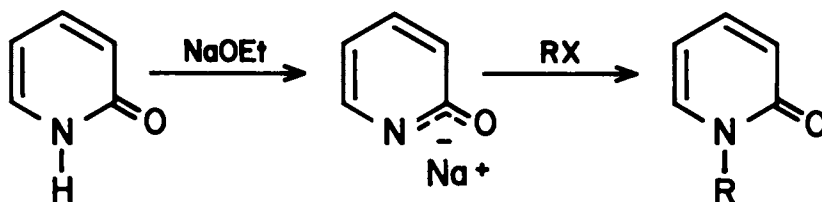
fluorescence quantum yield decreases, and it is smallest in water, a common solvent for reverse-phase liquid chromatography. For example, the value of the quantum yield of fluorescence for dansyl-*dl*-tryptophan in water is 0.068, compared to 0.70 in dioxane, and the wavelength of the emission maximum for the tryptophan derivative can vary as much as 78 nm with varying solvents (11). If solvent programming is being used to develop the HPLC chromatogram, this difference in emission maximum could result in a widely varying signal.

The fluorescent signal will change with variation in quantum yield of fluorescence and with molar absorptivity. Not only do fluorescence quantum yields vary with the different dansyl derivatives formed, but so do the molar absorptivities (12). Another problem is exemplified by the 30-nm difference in the emission maxima of the dansyl derivatives of phenol and 2,4,5-trichlorophenol (13). It would be convenient if the quantum yields and molar absorptivities were constant within a set of derivatives. Finally, the fluorescent signal from dansyl derivatives decreases in acidic solution (13) due to protonation of the dimethylamino group.

Other limitations found in fluorescent derivatives include quenching by oxygen, metals, or other species, chemical or photochemical instability, and biodegradability.

The fluorescence of certain 1,3-disubstituted 2(1H)pyridones has been noted in the literature (14-16), but little spectroscopic information has been reported. We have found that pyridone compounds having a 1-alkyl group and an electron-withdrawing 3-group, such as -CONH<sub>2</sub>, -COOR, -CN, or -C<sub>6</sub>H<sub>5</sub>, absorb at about 320 nm and emit at about 380 nm with a high quantum efficiency. Studies made with 1-methyl-3-carbamoyl-2(1H)pyridone show that its fluorescence efficiency is essentially constant over the range of pH 1-12, and constant in aqueous methanol or aqueous acetonitrile mixtures in which the percentage of organic solvent varies from 0 to 75% (Table I). The pyridone ring system is quite stable chemically.

We inferred that these properties might be exploited in a series of unique derivatizing reagents designed specifically for trace analysis of organic compounds using HPLC separation and fluorescence detection. The use of these pyridones for the analytical purposes reported here is based on their acidic properties. Treatment of a 1H-2-pyridone with a base converts the pyridone to its salt.



Scheme I

The salt is an ambient nucleophile and can undergo either N or O alkylation. Chung and Tieckelmann (17) have shown that unsubstituted pyridone sodium salts in acetonitrile or dimethylformamide solvent form primarily the *N*-alkylated product. Using 3-substituted

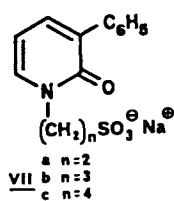
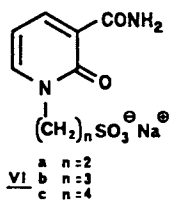
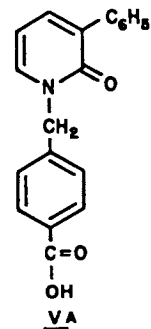
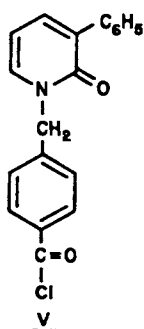
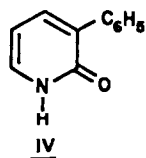
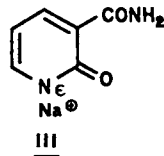
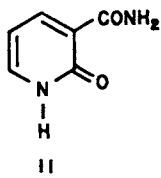
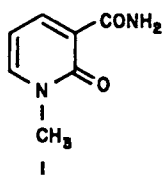
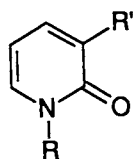


Table I Fluorescence as a Function of Solvent Composition for Two 3-Substituted 2(1H)-Pyridone Compounds

Compound I: R=CH<sub>3</sub>, R'=CONH<sub>2</sub>Compound Va: R=CH<sub>2</sub>C<sub>6</sub>H<sub>4</sub>COOH, R'=C<sub>6</sub>H<sub>5</sub>

Solvent	Relative Fluorescence	
	I	Va
100% water-----	1.00	0.40
Methanol:		
25%-----	0.82	0.42
50%-----	0.76	0.43
75%-----	0.72	0.46
100%-----	0.56	0.38
Acetonitrile:		
25%-----	0.81	0.43
50%-----	0.77	0.42
75%-----	0.68	0.40
100%-----	0.49	0.24

pyridones under the conditions reported in this study, *N*-alkylated products were formed exclusively.

The chemistry described above has been exploited in three ways:

1. Direct use of pyridone sodium salts as fluorescent derivatizing reagents.
2. Synthesis of a more specific fluorescent acid chloride derivatizing reagent.
3. Synthesis of pyridone sulfonates as water-tracing compounds.

### Results and Discussion

**1. Pyridone Sodium Salts as Nucleophilic Fluorescent Derivatizing Reagents.** A derivatizing reagent was prepared by converting 3-carbamoyl-2(1H)pyridone to its sodium salt (III) with sodium hydroxide. Reagent III is reasonably stable but must be used under anhydrous conditions. The reagent can be used to derivatize a wide variety of organic compounds, based on the general principles of nucleophilic substitution and addition reactions. Figure 1 shows the separation of a series of derivatives formed from alkyl bromides with Reagent III. The reaction given in Figure 2 shows the selective reaction of III with the insecticide heptachlor. Only one of the seven chlorine atoms is reactive.

Michael additions of III to reactive acceptors appear feasible. Derivatives were formed from acrylonitrile and ethyl acrylate. Although these were not fully characterized, they were observed by HPLC analysis.

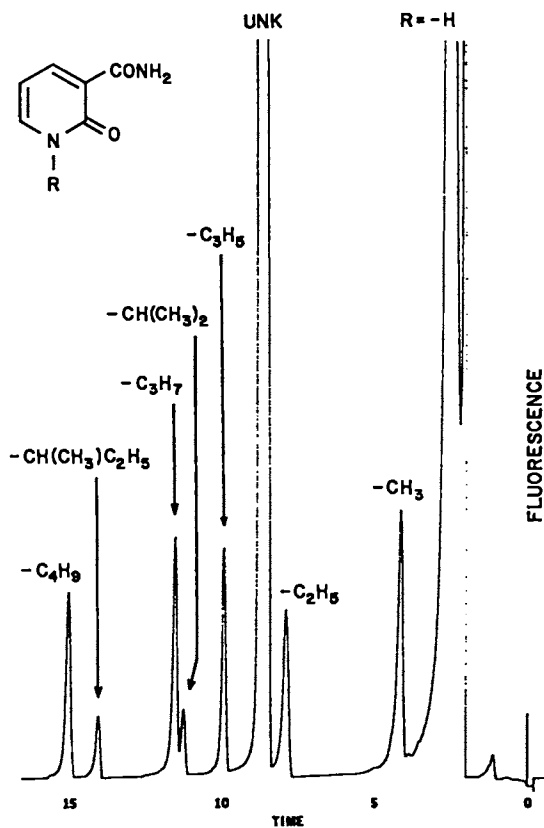


Figure 1. Chromatogram showing separation of alkyl bromide derivatives of Reagent III. Conditions as described in the text under "HPLC Separation Conditions."

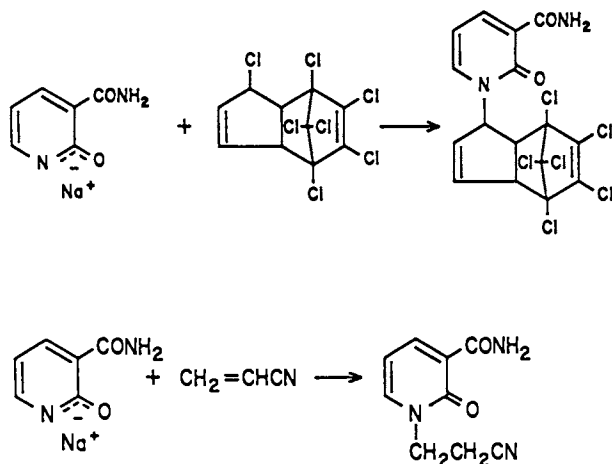
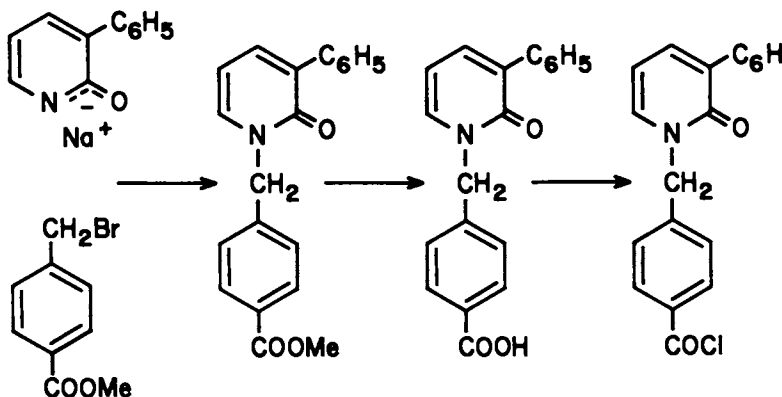


Figure 2. Formation of derivatives of heptachlor and acrylonitrile.

2. *Pyridone Acid Chlorides as Fluorescent Derivatizing Reagents.* A second derivatizing reagent, a fluorescent acid chloride, was synthesized from the sodium salt of 3-phenyl-2(1H)pyridone (IV). The salt of IV can be converted into Reagent V by the reaction shown in Scheme II.



Scheme II

This fluorescent acid chloride can be used to form derivatives of alcohols, amines, and phenols. Using these fluorescent derivatives, an analysis of a series of *n*-alcohols from  $\text{C}_1$  to  $\text{C}_4$  was developed. A chromatogram produced by this technique is shown in Figure 3. Derivatives were also formed from ammonia, dimethylamine, and phenol. A derivative was formed from pentachlorophenol but was not fully characterized. The quantum yields of fluorescence of the alcohol derivatives of V were lower than those of the alkyl halide derivatives of III.

3. *Water-Tracing Compounds.* Another application of these fluorescent pyridones has been the development of a series of compounds useful as ground-water tracers. Smart and Laidlaw have outlined several qualities desirable in fluorescent water-tracing compounds (18).

The properties of an organic tracing compound should minimize loss while in transit. There are two main sources of dye loss, non-adsorptive loss and adsorptive loss. Nonadsorptive losses can be due, among other reasons, to photochemical decomposition, chemical decay, pH effects, and biodegradation of the compound by microorganisms. Adsorption of the tracer onto both organic and inorganic substrates is often irreversible and can be a source of much loss. In tests conducted by Smart and Laidlaw, adsorption was the least prevalent in compounds containing sulfonic acid groups. This seemed to be due to their low  $\text{pK}_a$ , which gives an anionic group that repels the usual anionic charges<sup>a</sup> of the adsorbents.

Many of the properties of the 3-phenyl- and 3-carbamoyl-2(1H)-pyridones indicate that they may be useful as water tracers. As already shown these compounds are intensely fluorescent. They show

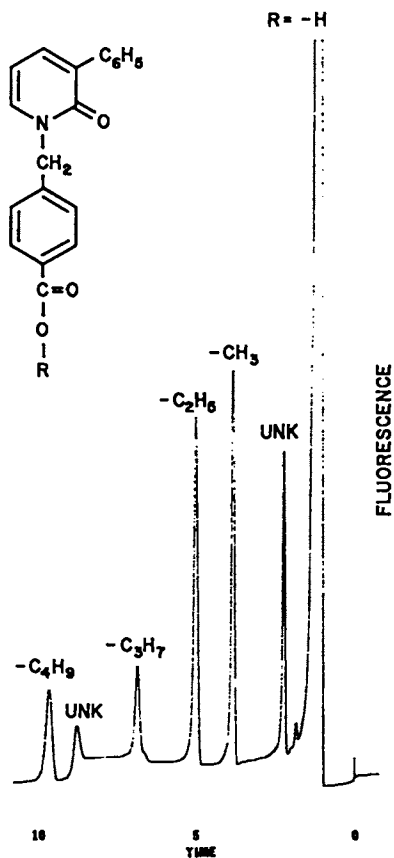


Figure 3. Chromatogram showing separation of alcohol derivatives of Reagent V. Conditions as described in the text under "HPLC Separation Conditions."

stability toward photochemical decay, since their maximum absorbance, 315-324 nm, is outside the normal range of sunlight. Their fluorescence intensity, as mentioned above, is essentially constant over a range of pH from 2 to 12.

A preliminary test for the biodegradability of the 3-phenyl- and 3-carbamoyl-2(1H)pyridones was conducted in a barnyard humus suspension. The analysis by HPLC showed some loss, and the fluorescent compounds seemed to be adsorbed onto the solid. The 3-carbamoyl-2(1H)pyridone (II) also hydrolyzed to 3-carboxylic acid-2(1H)pyridone both in the slurry test and in water solutions that had been left standing 1-2 weeks. In preliminary tests both the 3-phenyl- and the 3-carbamoyl-2(1H)pyridones apparently adsorbed to some extent on silica sand columns. In addition, the solubility of both 1-H compounds was somewhat low,  $1.3 \times 10^{-3} M$  for II, and  $1.0 \times 10^{-2} M$  for IV.

Since sulfonate groups have been used in other ground-water tracers, the goal of this work was to synthesize several *N*-substituted pyridone alkyl sulfonates which might be less susceptible to adsorption as well as more soluble. Alkyl sulfonates of varying chain lengths would be unique in a water system and separately identifiable by HPLC analysis. Two series of compounds were synthesized (VIa-c and VIIa-c). These compounds could be prepared by treating compounds III and IV with the appropriate  $\omega$ -bromoalkyl sulfonate.

A series of bromoalkyl sulfonates was therefore needed to form the *N*-alkyl sulfonated 2-pyridones. Formation of bromoalkyl sulfonates has not been described extensively in the literature (19). Alkyl halides react with sulfite ion to form alkyl sulfonates, a reaction known as the Strecker reaction (20). "Organic Syntheses" (21) gives a brief description of the synthesis of 2-bromoethane with sodium sulfite. A more general synthetic method was developed using alkyl dihalides to form  $\alpha,\omega$ -bromoalkyl sulfonates.

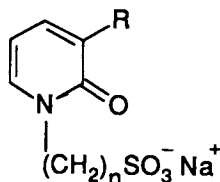
The formation of 2-bromoethylsulfonate followed the method described in "Organic Syntheses" (21). In the attempt to generalize this reaction, we noted that neither 1,3-dibromopropane nor 1,4-dibromobutane was miscible in the ethanol-water reaction solvent. Directly following the described procedure did produce both the 3-bromopropylsulfonate and 4-bromobutylsulfonate, but in low yields of roughly 20%. Improved procedures for alkylation were developed using acetonitrile as the solvent. The yields of the reactions for both III and IV with the ethyl, propyl, and butyl bromosulfonates are given in the "Experimental" section.

These reactions are useful because they run under mild conditions, use inexpensive or easily recoverable starting materials, and have short reaction times. The major problem in purification is the separation of the sodium pyridone sulfonate from excess sodium sulfite, sodium bromide, and sodium bromoalkyl sulfonate. However, these latter compounds usually would not interfere with the use of the pyridone sulfonate as a water tracer. From a practical point of view, the pyridone sulfonates need not be purified, but can be used directly. A modified synthetic procedure involves the treatment of the pyridone sodium salt with a tenfold excess of  $\alpha,\omega$ -dibromoalkane in acetonitrile, followed by removal of the excess dibromide by vacuum distillation. The resulting product is treated with an excess of sodium sulfite in aqueous ethanol. Evaporation of the solvent yields a useful tracer. Procedures given in the experimental section were



those used for isolation of pure compounds. The molar absorptivities and fluorescence quantum yields of the 1-alkyl-3-phenyl- and 3-carbamoyl-2(1H)pyridone sulfonates are shown in Table II.

Table II Relative Fluorescence and Spectroscopic Data for Pyridone Sulfonates



R	n	Compound Number	Molar Absorptivity, $\epsilon \times 10^3$	Fluorescence Quantum Yield, $\phi^a$	Wavelength of Maximum Absorbance, $\lambda_{\max}$ (nm)
C <sub>6</sub> H <sub>5</sub>	2	VIIa	8.6	0.29	315
C <sub>6</sub> H <sub>5</sub>	3	VIIb	5.9	0.34	315
C <sub>6</sub> H <sub>5</sub>	4	VIIc	2.3	0.38	315
CONH <sub>2</sub>	2	VIa	6.1	0.95	325
CONH <sub>2</sub>	3	VIb	6.4	0.95	325
CONH <sub>2</sub>	4	VIc	2.3	0.98	325

<sup>a</sup>Relative to compound I.

Analytical HPLC separations of the homologous alkyl sulfonate series of the 3-phenyl- and 3-carbamoyl-2(1H)pyridones were developed using ion-pairing reagents. These separations, shown in Figures 4 and 5, demonstrate that these compounds would be separately identifiable from the same sample if they were to be used as site-specific water tracers. For example, several locations at the same waste disposal site could be marked. Since the syntheses we have developed are general, additional members of a series could be synthesized if needed. Levels of detection of the compounds are in the parts-per-trillion range. Adsorption studies using sand, sawdust, peat moss, barnyard soil, kaolinite, and bentonite showed essentially no adsorption from 100- $\mu$ g/L solution of pyridone VIb over a period of 24 hr (22). These compounds are currently undergoing some field tests.

**Quantum Yields of Fluorescence.** Table III lists the relative quantum yields of fluorescence of 24 3-substituted 2(1H)-pyridones. Pyridone I has the highest yield measured, which is set at 1.00. An attempt was made to measure the 'absolute' quantum yield  $\phi_{Fl}^I$  of I relative to rhodamine B using ferrioxalate actinometry. A  $\phi_{Fl}^I$  value of  $0.98 \pm 0.02$  was obtained. However, the determination of 'absolute'

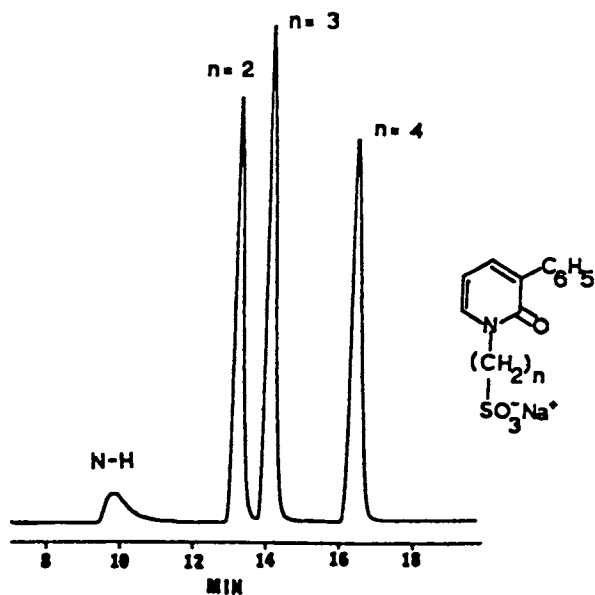


Figure 4. Chromatogram showing separation of the 3-phenyl-2(1H)pyridone alkylsulfonate sodium salts. Conditions as described in the text under "HPLC Separation Conditions."

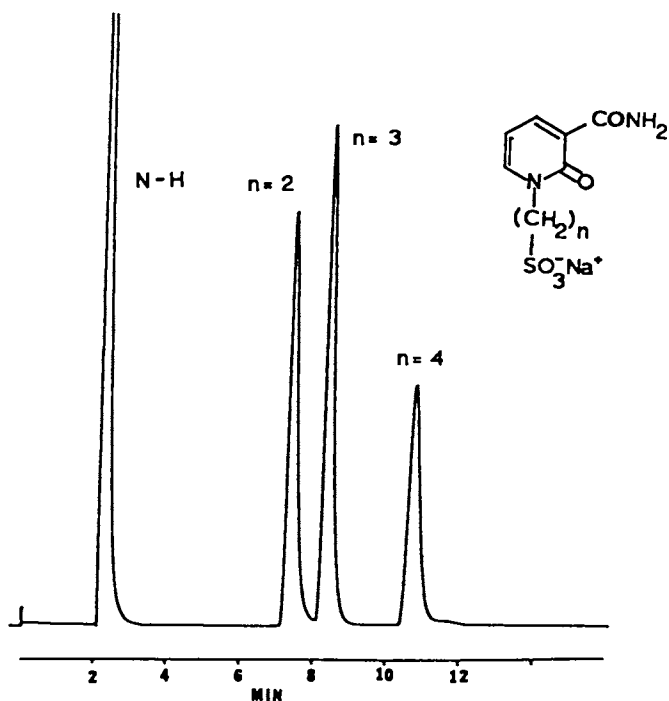


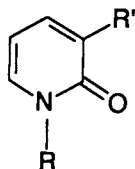
Figure 5. Chromatogram showing separation of the 3-carbamoyl-2(1H)pyridone alkylsulfonate sodium salts. Conditions as described in the text under "HPLC Separation Conditions."

quantum yields of fluorescence presents many problems. For this reason, all values of quantum yields reported here are values relative to I. The 3-CONH<sub>2</sub>, COOH, COOCH<sub>3</sub>, and CN pyridones in Table IIIA are all highly fluorescent. The 3-phenyl pyridones have relative fluorescence in the range 0.2-0.3. Some less fluorescent pyridones are included in Table IIIB. In general, substitution at the 1-position does not have a significant effect on the fluorescence yield. The alcohol derivatives of compound V are unusual in this regard, giving fluorescence yields an order of magnitude less than that of the corresponding acid.

*Limits of Detection.* A signal-to-noise ratio of 2 could be obtained from 5 $\mu$ L of a 10<sup>-8</sup> M solution of pyridone I, under the conditions described in the "Experimental" section. This amount of the solution

Table III Relative Fluorescence and Spectroscopic Data for 3-Substituted 2(1H)Pyridones

Table IIIA

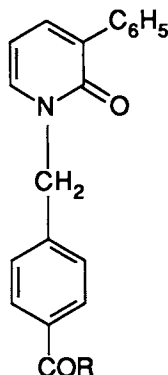


R	R' ( <sup>a</sup> )	Fluorescence Quantum Yield, $\phi^b$	Molar Absorptivity, $\epsilon \times 10^3$	Wavelength (nm)	
				Maximum Absorbance, $\lambda_{max}$	Emission, $\lambda_{em}$
CH <sub>3</sub>	CONH <sub>2</sub> (I)	1.00	8.77	324	384
H	CONH <sub>2</sub> (II)	0.93	7.50	321	382
CH <sub>2</sub> CH <sub>3</sub>	CONH <sub>2</sub>	0.93	8.59	324	382
CH <sub>2</sub> CH <sub>2</sub> CH <sub>3</sub>	CONH <sub>2</sub>	0.92	8.44	325	382
CH(CH <sub>3</sub> ) <sub>2</sub>	CONH <sub>2</sub>	0.83	8.57	324	384
CH <sub>2</sub> (CH <sub>2</sub> ) <sub>2</sub> CH <sub>3</sub>	CONH <sub>2</sub>	0.93	8.56	326	390
C <sub>10</sub> H <sub>5</sub> Cl <sub>6</sub>	CONH <sub>2</sub>	0.68	10.3	331	386
H	C <sub>6</sub> H <sub>5</sub> (IV)	0.24	9.95	311	392
CH <sub>3</sub>	C <sub>6</sub> H <sub>5</sub>	0.33	9.83	313	394
H	Cl	0.012	7.79	304	369
CH <sub>3</sub>	Cl	0.0083	6.83	308	368
CH <sub>3</sub>	CN	0.88	8.84	327	380
CH <sub>3</sub>	COOH	0.65	6.50	308	380
CH <sub>2</sub> C <sub>6</sub> H <sub>4</sub> COOCH <sub>3</sub>	CONH <sub>2</sub>	0.68	5.11	326	384
CH <sub>3</sub>	COOCH <sub>3</sub>	0.58	9.95	327	389
CH <sub>3</sub>	NO <sub>2</sub>	0.0	6.68	365	---

<sup>a</sup>Roman numerals in parentheses denote compounds discussed in text.

<sup>b</sup>Relative to compound I.

Table IIIB



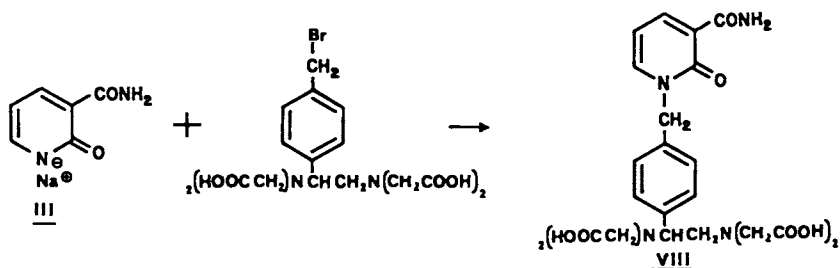
R ( <sup>a</sup> )	Fluorescence Quantum Yield, $\phi^b$	Molar Absorptivity, $\epsilon \times 10^3$	Wavelength (nm)	
			Maximum Absorbance, $\lambda_{\max}$	Emission, $\lambda_{\text{em}}$
OH (Va)	0.28	10.1	317	400
OCH <sub>3</sub>	0.023	10.5	317	390
OC <sub>2</sub> H <sub>5</sub>	0.016	9.69	318	390
OCH <sub>2</sub> CH <sub>2</sub> CH <sub>3</sub>	0.015	10.6	325	390
O(CH <sub>2</sub> ) <sub>3</sub> CH <sub>3</sub>	0.014	9.85	325	392
NH <sub>2</sub>	0.066	9.54	319	398
N(CH <sub>3</sub> ) <sub>2</sub>	0.31	9.41	319	398
OC <sub>6</sub> H <sub>5</sub>	0.088	9.27	319	400

<sup>a</sup>Roman numerals in parentheses denote compounds discussed in text.

<sup>b</sup>Relative to compound I.

contains  $5 \times 10^{-14}$  moles, or  $6.9 \times 10^{-12}$  g, of I. Since the regions of absorption and emission of the other pyridones reported here are essentially the same as for I, other detection limits can be estimated by dividing the values for I by the relative quantum yields, assuming the same chromatographic  $k'$  value of 2. In an attempt to lower the detection limits, the Schoeffel detector was modified to use a zinc metal lamp, which has a resonance line of 308 nm, and a cadmium resonance lamp, which has an intense line at 326 nm. The latter was very close to the wavelength of maximum absorbance ( $\lambda_{\max}$ ) of the pyridones. Each change lowered the detection limit an order of magnitude. Thus, using the cadmium lamp, 5  $\mu\text{L}$  of a  $10^{-10}$  M solution of I was detected. This is  $5 \times 10^{-16}$  moles (0.5 femtomoles) or  $7 \times 10^{-14}$  g (70 femtograms).

**Metal Ion Analysis.** We have reported a sensitive trace-metal analysis based upon HPLC separation of *p*-aminophenyl EDTA chelates and fluorescence detection by postcolumn reaction with fluorescamine (23). An application of the pyridone chemistry already discussed leads to a fluorescent-labeled EDTA (VIII).



We have developed reverse-phase ion-pairing HPLC separations of substituted EDTA metal chelates of several transition metals (including Cd, Zn, Pb, and Hg) and several lanthanides (La, Ce, Eu, Dy, Er, Yb, Lu). Detection levels of these chelates are currently being assessed. A sensitive metal ion analysis employing an inherently fluorescent EDTA seems feasible.

#### Experimental

**Apparatus.** HPLC separations were accomplished using a system consisting of two Waters Associates Model 6000-A Liquid Chromatography pumps, a Model 660 solvent programmer, a Model 440 absorbance detector set at 313 nm, and a Schoeffel FS 970 fluorometer with excitation at 320 nm using a Schoeffel 7-54 excitation filter and a Schoeffel KV 370 emission filter. NMR spectra were obtained on a JEOL FX-270 spectrometer and are referenced either to tetramethylsilane in chloroform-*d*, to *t*-butyl-OD in deuterium oxide, or to dimethyl-*d*<sub>6</sub> sulfoxide as an internal standard. Ultraviolet absorbance data were obtained on a Hitachi 100-80 spectrophotometer. Fluorescence spectra and quantum yields were determined using a Perkin-Elmer Hitachi MPF-2A spectrophotometer. Melting points were determined using a Thomas-Hoover Unimelt, and are uncorrected. Elemental analyses were obtained from Atlantic Microlabs, Atlanta, GA, or Huffman Laboratories, Wheat Ridge, CO.

**Chemicals.** All chemicals were obtained from Aldrich Chemical Company unless otherwise indicated. All other reagents were ACS certified or equivalent.

**HPLC Separation Conditions.** Separations of alkyl bromide and alcohol derivatives were performed using an Altex Ultrasphere C<sub>18</sub> 5- $\mu$ m, 4.6  $\times$  150 mm column. The derivatives of methanol, ethanol, 1-propanol, and 1-butanol were separated using a mobile phase of 65% acetonitrile and 35% water, with a flow rate of 1 mL/min. The derivatives of the alkyl bromides were separated using a linear program from 10% acetonitrile and 90% water to 50% acetonitrile and 50% water in 20 min. The flow rate was 1 mL/min.

Separations of pyridone sulfonates were performed using an Altex Ultrasphere I.P. C<sub>18</sub> 5- $\mu$ m, 4.6  $\times$  150 mm column. The 3-carbamoyl-2(1H)pyridone series was separated using a mobile phase of 89% 0.005-M tetrabutylammonium phosphate (Waters Associates PIC-A

ion-pairing reagent) and 11% acetonitrile with a flow rate of 1 mL/min. The 3-phenyl-2(1H)pyridone series was separated using a mobile phase of 75% 0.005-M tetrabutylammonium phosphate and 25% acetonitrile with a flow rate of 1 mL/min.

**Quantum Yields of Fluorescence Measurements.** All of the quantum yields of fluorescence were measured by the relative fluorescence measurement technique of Parker and Rees (24). This method compares the fluorescence of the compound of interest to the fluorescence of some known compound. All of the fluorescence quantum yields were measured using I as a reference. Compound I had previously been measured by this same method using rhodamine B as a standard.

$$\phi_2 = \frac{(I_f)_2 \epsilon_1 c_1}{(I_f)_1 \epsilon_2 c_2} \phi_1$$

In the equation, the subscripts 1 and 2 refer to the reference compound and the compound of interest, respectively,  $I_f$  is the intensity of the fluorescent signal of each compound measured as peak height in centimeters,  $\epsilon$  is the molar absorptivity,  $c$  is the concentration in moles per liter, and  $\phi$  is the fluorescence quantum yield. In this application,  $\phi_1$  is set at 1.00. The concentrations of the solutions that were tested ranged from  $10^{-4}$  to  $10^{-7}$  M. The solutions run at the higher concentrations were all checked for self-quenching, but none was found. All measurements, except the fluorescence-versus-solvent study, were made in 0.1-M phosphate buffer, pH 7.4. Slit settings on the Perkin-Elmer MPF-2A were 10 m $\mu$  (nm) for both emission and excitation monochromators.

**Limits of Detection Study.** The limits of detection were measured by injecting successively smaller samples (defined as volume times concentration) of compound I, at the most sensitive setting of the Schoeffel 970 until the peak height of the signal from the sample was twice that of the noise. The chromatographic conditions were adjusted so that  $k' = 2$  for the peak. The standard deuterium lamp was used for initial measurements. A modified lamp housing was constructed to accommodate a zinc lamp and a cadmium lamp, both from Ultraviolet Products, San Gabriel, CA. The cadmium lamp was used with an AL3261-1 isolation filter from Corion Corp., Holliston, MA. In using the metal lamps, the monochromator setting on the Schoeffel 970 was adjusted to give a maximum signal when a  $10^{-6}$  M solution of compound I was in the detector cell.

**In Situ Derivatization.** To demonstrate that a group of alcohols could be derivatized at low alcohol concentration, the following experiment was performed. First,  $6 \times 10^{-5}$  mole of each of the alcohols used to form derivatives was dissolved in 100 mL of acetonitrile. Then  $2 \times 10^{-4}$  mole of compound V was added, and the solution was heated at 70°C. This solution was then diluted by taking 1.0 mL of the reaction mixture and diluting to 10 mL with water and acetonitrile, and the diluted solution was analyzed. After 4 h the methanol and ethanol were completely derivatized, but it took 6 h for the *n*-propanol and *n*-butanol derivatives to form.

To demonstrate that a group of alkyl bromides could be derivatized at low alkyl bromide concentration, a similar experiment

was performed with reagent III. In this experiment,  $5 \times 10^{-6}$  mole of each alkyl bromide was dissolved in dimethylformamide. To this solution was added  $1.8 \times 10^{-4}$  mole of reagent III, and the mixture was heated at 70°C. After 3 h the primary alkyl bromides were completely derivatized, but the secondary alkyl bromides took 40 h to be completely derivatized.

**Synthesis of Derivatizing Reagent III.** We placed 50 mL of methanol, which had been previously dried over 4-Å molecular sieves, in a 100-mL round-bottom flask and added 6.0 g of 2-hydroxynicotinic acid and 3 mL of boron trifluoride etherate. The solution was heated to reflux for 24 h and the solvent was removed under reduced pressure. The residue was dissolved in 50 mL of 0.1-N sodium hydroxide and extracted with 60 mL of chloroform. The chloroform extract was concentrated under reduced pressure and the residue crystallized from isopropyl alcohol. The yield of 3-carbomethoxy-2(1H)pyridone was 5.0 g; mp 152.5-154°C; NMR (CDCl<sub>3</sub>) δ 3.85 (s, 3, -CH<sub>3</sub>), 6.34 (t, 1,  $J_{4,5} = J_{5,6} = 7$  Hz, H-5), 7.74 (dd, 1,  $J_{4,5} = 2$  Hz,  $J_{5,6} = 7$  Hz, H-6), 8.21 (dd,  $J_{4,6} = 2$  Hz,  $J_{4,5} = 7$  Hz, H-4); mass spectrum,  $m/e$  153, M<sup>+</sup>.

This product was placed in a 100-mL round-bottom flask, and 50 mL of concentrated ammonium hydroxide was added. The mixture was stirred overnight at room temperature. After 18 h the solution was cooled and the crystals of compound II were collected. No recrystallization was required. The yield was 4.20 g (93%) of II, mp 268-269°C; NMR (DMSO-*d*<sub>6</sub>) δ 6.33 (t, 1,  $J_{4,5} = J_{5,6} = 7$  Hz, H-5), 7.41 (s, 1, -NH), 7.59 (dd, 1,  $J_{5,6} = 7$  Hz,  $J_{4,6} = 2.6$  Hz, H-6), 8.23 (dd, 1,  $J_{5,6} = 7$  Hz,  $J_{4,6} = 2.5$  Hz, H-4), 9.00 (s, 1, -NH), 12.30 (s, 1, H-1); mass spectrum,  $m/e$  138, M<sup>+</sup>. Anal. Calcd for C<sub>6</sub>H<sub>6</sub>N<sub>2</sub>O<sub>2</sub>: C, 52.15; H, 4.38; N, 20.29. Found: C, 51.85; H, 4.46; N, 20.34.

Reagent III was formed by dissolving 0.50 g (3.5 mmol) of II in 25 mL of water in a 50-mL round-bottom flask. To this solution was added 0.15 g (3.61 mmol) of sodium hydroxide, and the mixture was heated on a steam bath for 30 min. The water was removed and the residue suspended in hot toluene. The toluene suspension was filtered and the remaining solid dried in an Abderhalden drying pistol with phosphorus pentoxide. This procedure gave 0.55 g (99%) yield of Reagent III.

**General Method for Forming Derivatives with Reagent III.** To make the derivatives, III was dissolved in 5 mL dimethylformamide, and the alkyl halide was added to the salt solution. The mixture was allowed to stand at room temperature for 24 h, and the dimethylformamide was removed under reduced pressure. The residue was dissolved in water, and the derivative was extracted with 25 mL of chloroform. The derivative was then precipitated from the chloroform with ether-hexane.

**Heptachlor Derivative of III.** Addition of 0.11 g (0.68 mmol) of III and 0.25 g (0.68 mmol) of heptachlor (1,4,5,6,7,8,8-heptachloro-3a,4,7,7a-tetrahydro-4,7-methanoindene) to dimethylformamide gave 0.17 g (50%) of the derivative: mp 280-281°C (dec.); NMR (CDCl<sub>3</sub>) δ 3.19 (dd, 1), 3.96-4.18 (m, 1), 5.62-6.81 (m, 3), 6.39 (t, 1,  $J_{4,5} = J_{5,6} = 7$  Hz, H-5), 7.16 (dd, 1,  $J_{4,6} = 2$  Hz,  $J_{5,6} = 7$  Hz, H-6), 8.38 (dd, 1,  $J_{4,6} = 2$  Hz,  $J_{4,5} = 7$  Hz, H-4); mass spectrum,  $m/e$  472, M<sup>+</sup>.



Anal. Calcd for  $C_{16}H_{10}Cl_6N_2O_2$ : C, 40.46; H, 2.12; N, 5.90. Found: C, 40.67; H, 2.25; N, 5.69.

**Synthesis of Derivatizing Reagent V.** 25.3 g (163 mmol) of 3-phenylpyridine was heated to reflux with 60 mL of 30% hydrogen peroxide for 5 h in 100 mL of glacial acetic acid (25). The glacial acetic acid and excess hydrogen peroxide were removed under reduced pressure. To the residue 150 mL of acetic anhydride was added, and the mixture was heated to reflux for 24 h. The acetic anhydride was removed under reduced pressure, and 10% hydrochloric acid was added to the dark residue. This mixture was allowed to stand for 10 h, and the acid was removed under reduced pressure. The residue was extracted with hot benzene. The solid that formed on cooling was recrystallized from benzene to give crude IV. Purification of the product was obtained by column chromatography of the crude product on silica gel using chloroform as the mobile phase. A total of 13.2 g (47%) of material was collected: mp 222-223.5°C; NMR ( $CDCl_3$ )  $\delta$  6.18 (t, 1,  $J_{4,5} = J_{5,6} = 7$  Hz, H-5), 7.24 (m, 4, aromatic), 7.58 (m, 3, H-4 + H-6 + aromatic); mass spectrum,  $m/e$  171,  $M^+$ . Anal. Calcd for  $C_{11}H_8NO$ : C, 77.17; H, 5.30; N, 8.18. Found: C, 76.92; H, 5.23; N, 8.27.

Pyridone IV was converted to its sodium salt by treatment with an equimolar amount of sodium methoxide in methanol (see procedure below under formation of the 3-phenyl-2(1H)pyridone sulfonates). The sodium salt was next treated with the methyl ester of  $\alpha$ -bromo-*p*-toluic acid, obtained by treatment of the acid with  $BF_3$  etherate. For the formation of V, 3.67 g (16.0 mmol) of the methyl ester of  $\alpha$ -bromo-*p*-toluic acid and 20 mL of dimethylformamide were placed in a 50-mL round-bottom flask. To this was added 3.04 g (15.7 mmol) of the sodium salt of IV. The reaction took place rapidly. After 30 min the solvent was removed under reduced pressure. Crystallization from isopropyl alcohol gave 3.71 g (74%) of 1-(*p*-carboxymethylphenyl)methyl-3-phenyl-2(1H)pyridone. To 0.43 g (1.36 mmol) of this ester was added 0.055 g (1.38 mmol) of sodium hydroxide in 35 mL of water, and the mixture was heated on a steam bath until all the ester dissolved. Concentrated hydrochloric acid was added to protonate the carboxylate anion, and the acid related to V precipitated. Recrystallization from isopropyl alcohol gave 3.42 g (94%) of the product: mp 197-199°C; NMR ( $DMSO-d_6$ )  $\delta$  5.25 (s, 2,  $-CH_2-$ ), 6.36 (t, 1,  $J_{4,5} = J_{5,6} = 7$  Hz, H-5), 7.20 to 7.80 (m, 11, aromatic); mass spectrum,  $m/e$  305,  $M^+$ . Anal. Calcd for  $C_{19}H_{15}NO_3$ : C, 74.75; H, 4.95; N, 4.59. Found: C, 74.53; H, 4.99; N, 4.32.

To 25 mL of dimethylformamide in a 50-mL round-bottom flask was added 0.25 mL (3.42 mmol) of thionyl chloride. After several minutes, 1.00 g (3.28 mmol) of the acid of V was added. The reaction mixture was allowed to stand at room temperature for 18 h, and the solvent was removed under reduced pressure. The residue was then crystallized from chloroform to give 0.97 g (91%) of Reagent V: mp 150-151°C; NMR ( $DMSO-d_6$ )  $\delta$  5.19 (s, 2,  $-CH_2-$ ), 6.23 (t, 1,  $J_{4,5} = J_{5,6} = 7$  Hz, H-5), 7.16-8.08 (m, 11, aromatic); mass spectrum,  $m/e$  339,  $M^+$ .

**General Methods of Forming Derivatives with V.** The preparation of all of the derivatives of V followed one of three general methods:

**Method A.** In this procedure, V was dissolved in 5 mL of the liquid to be derivatized, and the mixture was heated for 30 min at 60°C. The solvent was removed under reduced pressure, and the residue was crystallized from a methanol-water solution.

**Method B.** In this procedure, V was dissolved in 20 mL of acetonitrile, and the compound to be derivatized was bubbled in as a gas. The solvent was removed under reduced pressure, and the residue was crystallized from a methanol-water solution.

**Method C.** In this procedure, V was dissolved in 10 mL of pyridine, and the compound to be derivatized was then added. The mixture was heated at 60°C for 1 h, and the solvent was removed under reduced pressure. The residue was then crystallized from a methanol-water solution.

**Methanol Derivative of V.** Method A. Addition of 0.10 g (0.31 mmol) of V to methanol gave 0.06 g (59%) of XXV: mp 133-134°C; NMR (CDCl<sub>3</sub>) δ 3.79 (s, 3, -OCH<sub>3</sub>), 5.10 (s, 2, -CH<sub>2</sub>-) 6.10 (t,  $J_{4,5} = J_{5,6} = 7$  Hz, H-5), 7.10-7.92 (m, 11, aromatic); mass spectrum,  $m/e$  319, M<sup>+</sup>. Anal. Calcd for C<sub>20</sub>H<sub>17</sub>NO<sub>3</sub>: C, 75.22; H, 5.37; N, 4.39. Found: C, 74.94; H, 5.48; N, 4.22.

**Ethanol Derivative of V.** Method A. Addition of 0.10 g (0.31 mmol) of V to ethanol gave 0.07 g (64%) of XXVI: mp 87.5-89.5°C; NMR (CDCl<sub>3</sub>) δ 1.32 (t, 3, -CH<sub>3</sub>), 4.26 (q, 2, -OCH<sub>2</sub>-), 5.14 (s, 2, -CH<sub>2</sub>-), 6.12 (t, 1,  $J_{4,5} = J_{5,6} = 7$  Hz, H-5), 7.08-7.96 (m, 11, aromatic); mass spectrum,  $m/e$  333, M<sup>+</sup>. Anal. Calcd for C<sub>21</sub>H<sub>19</sub>NO<sub>3</sub>: C, 75.66; H, 5.75; N, 4.20. Found: C, 75.44; H, 5.63; N, 3.95.

**1-Propanol-Derivative of V.** Method A. Addition of 0.30 g (0.98 mmol) of V to *n*-propyl alcohol gave 0.18 g (56%) of XXVII: mp 68-70°C; NMR (CDCl<sub>3</sub>) δ 0.97 (t, 3, -CH<sub>3</sub>), 1.72, (sex., 2, -CH<sub>2</sub>-), 4.21 (t, 2, -OCH<sub>2</sub>-), 5.18 (s, 2, -CH<sub>2</sub>-), 6.18 (t, 1,  $J_{4,5} = J_{5,6} = 8$  Hz, H-5), 7.14-8.00 (m, 11, aromatic); mass spectrum,  $m/e$  347, M<sup>+</sup>. Anal. Calcd for C<sub>22</sub>H<sub>21</sub>NO<sub>3</sub>: C, 76.06; H, 6.09; N, 4.03. Found: C, 75.73; H, 6.11; N, 4.01.

**1-Butanol Derivative of V.** Method A. Addition of 0.30 g (0.98 mmol) of V in *n*-butyl alcohol gave 0.20 g (60%) of XVIII: mp 58-60°C; NMR (CDCl<sub>3</sub>) δ 0.94 (t, 3, -CH<sub>3</sub>), 1.22-1.79 (m, 4, -(CH<sub>2</sub>)<sub>2</sub>-), 4.25 (t, 2, -OCH<sub>2</sub>-), 6.18 (t, 1,  $J_{4,5} = J_{5,6} = 7$  Hz), 7.17-8.02 (m, 11, aromatic); mass spectrum,  $m/e$  361, M<sup>+</sup>. Anal. Calcd for C<sub>23</sub>H<sub>23</sub>NO<sub>3</sub>: C, 76.43; H, 6.41; N, 3.88. Found: C, 76.58; H, 6.16; N, 4.25.

**Ammonia Derivative of V.** Method B. Addition of 0.30 g (0.98 mmol) of V to acetonitrile and addition of ammonia gave 0.20 g (71%) of XXIX: mp 211-212°C; NMR (DMSO-*d*<sub>6</sub>, *t*-BuOD lock) δ 5.16 (s, 2, -CH<sub>2</sub>-), 6.27 (t, 1,  $J_{4,5} = J_{5,6} = 7$  Hz, H-5), 7.05-7.80 (m, 11, aromatic); mass spectrum,  $m/e$  304, M<sup>+</sup>. Anal. Calcd for C<sub>19</sub>H<sub>16</sub>N<sub>2</sub>O<sub>2</sub>: C, 74.98; H, 5.30; N, 9.20. Found: C, 74.79; H, 5.12; N, 9.19.

**Dimethylamine Derivative of V.** Method B. Addition of 0.30 g (0.98 mmol) of V to acetonitrile and addition of dimethylamine gave 0.19 g of XXX: mp 119-120°C; NMR (CDCl<sub>3</sub>) δ 2.98 (s, 6, N(CH<sub>3</sub>)<sub>2</sub>), 5.16 (s, 2, -CH<sub>2</sub>-), 6.19 (t, 1,  $J_{4,5} = J_{5,6} = 7$  Hz, H-5), 7.17-7.66 (m, 11,

aromatic); mass spectrum,  $m/e$  332,  $M^+$ . Anal. Calcd for  $C_{21}H_{20}N_2O_2$ : C, 75.88; H, 6.06; N, 10.25. Found: C, 75.71; H, 5.99; N, 8.28.

**Phenol Derivative of V.** Method C. Addition of 0.49 g (1.44 mmol) of V and 0.14 g (1.49 mmol) of phenol to 10 mL of pyridine gave 0.33 g (58%) of XXXI: mp 126-128°C; NMR ( $CDCl_3$ )  $\delta$  5.22 (s, 2,  $-CH_2-$ ), 6.21 (t, 1,  $J_{4,5} = J_{5,6} = 7$  Hz, H-5), 7.04-8.02 (m, 16, aromatic); mass spectrum,  $m/e$  381,  $M^+$ . Anal. Calcd for  $C_{25}H_{19}NO_3$ : C, 78.72; H, 5.02; N, 3.67. Found: C, 78.86; H, 5.03; N, 3.92.

**2-Bromoethylsulfonate Sodium Salt.** A solution of 1,2-dibromoethane (Caution: toxic) (307.5 g, 1.65 mol) in water (225 mL) and 95% ethanol (625 mL) was heated to reflux and stirred while a solution of sodium sulfate (62.5 g, 0.496 mol) in water (225 mL) was slowly added over a period of 2 h and then refluxed for an additional 2 h. The excess 1,2-dibromoethane was then distilled off with the ethanol and the resultant aqueous solution was allowed to dry. The residue was recrystallized from 95% ethanol (2 L) and dried in an Abderhalden drying apparatus under vacuum because it was hygroscopic. The yield was 67.7 g (68%).  $^1H$  NMR ( $D_2O$ )  $\delta$  3.43 (t, 2, H-1), 3.67 (t, 2, H-2);  $^{13}C$  NMR ( $D_2O$ )  $\delta$  25.61, 54.66.

**3-Bromopropylsulfonate Sodium Salt.** A solution of 1,3-dibromopropane (Caution: irritant) (10.9 mL, 20 g, 99 mmol) in 95% ethanol (37.5 mL) and water (13.5 mL) was stirred vigorously and brought to reflux. A solution of sodium sulfite (3.75 g, 29 mmol) dissolved in water (13.5 mL) was slowly added to the refluxing mixture over a period of 2 h and then refluxed for an additional 2 h. The mixture was poured into a separatory funnel and allowed to cool, whereupon it separated into a two-phase system. The excess 1,3-dibromopropane was drawn off, and the remaining solution was evaporated to dryness. The residue was recrystallized from 95% ethanol 3 times. The yield was 1.15 g (17.7%): mp 279-285°C (-HBr), 306°C (dec.);  $^1H$  NMR ( $D_2O$ )  $\delta$  2.29 (p, 2, H-2), 3.07 (t, 2, H-1), 3.60 (t, 2, H-3);  $^{13}C$  NMR ( $D_2O$ )  $\delta$  29.10, 33.20, 51.02.

**4-Bromobutylsulfonate Sodium Salt.** A solution of 1,4-dibromobutane (Caution: lachrymator, irritant) (12.0 mL, 21.4 g, 99 mmol) in 95% ethanol (37.5 mL) and water (13.5 mL) was vigorously stirred and brought to reflux. A solution of sodium sulfite (3.75 g, 29 mmol) in water (13.5 mL) was slowly added to the refluxing mixture over a period of 2 h and then refluxed for an additional 2 h. The mixture was poured in a separatory funnel and allowed to cool and separate into a two-phase system. The excess 1,4-dibromobutane was drawn off, and the remaining solution was evaporated to dryness. The residue was recrystallized from 95% ethanol 3 times. The yield was 2.08 g (29.3%).  $^1H$  NMR ( $D_2O$ )  $\delta$  1.88 (m, 2), 1.97 (m, 2), 2.89 (m, 2, H-1), 3.45 (m, 2, H-4).

**General Procedures for the Synthesis of the Pyridone Sulfonates VIa,b,c and VIIa,b,c (25).** A solution of 1.25 mmol of the sodium salt of 3-carbamoyl-2(1H)pyridone(III) or 3-phenyl-2(1H)pyridone and 1.25 mmol of the corresponding bromosulfonate sodium salt in 50 mL of acetonitrile was brought to reflux and stirred for 24 h. The reaction mixture was cooled and filtered through a sintered glass

funnel. The remaining solid was triturated with three portions of hot acetonitrile, adding the filtrates to the original filtrate. The acetonitrile was evaporated. Some of the products were contaminated with sodium bromide. Good analyses were difficult to obtain because of this contamination and because the sulfonates were hygroscopic. Structures were supported by NMR data. In one case, a good analysis was obtained. An example is given below.

**3-Phenyl-2(1H)Pyridone Sodium Salt.** A solution of sodium metal (0.25 g, 11.3 mmol) and anhydrous methanol (10 mL) was allowed to react to form sodium methoxide. Pyridone IV (1.88 g, 11 mmol) was added to the solution and allowed to stand at room temperature for 24 h. The methanol was removed under reduced pressure and the residue was extracted with hot benzene 3 times and dried in the Abderhalden drying pistol for 30 min. The yield was 1.7 g (82%).

**3-Phenyl-2(1H)Pyridone-Propylsulfonate Sodium Salt VIIb.** A solution of 3-phenyl-2(1H)pyridone sodium salt (0.264 g, 1.25 mmol) and 3-bromopropylsulfonate sodium salt (0.241 g, 1.25 mmol) in acetonitrile (650 mL) was brought to reflux with stirring for 24 h. The yield was 41%, as determined by HPLC. An analytical sample was obtained from the filtered residue of reaction by preparative HPLC. Anal. Calcd for  $C_{14}H_{14}NSO_4Na \cdot H_2O$ : C, 50.45; H, 4.8; N, 4.2. Found: C, 50.38; H, 4.83; N, 4.19.

Analytical samples of 1-alkyl-3-substituted 2(1H)pyridone sulfonates were obtained by using a Whatman Partisil M-9 10/50 ODS-2 C18 column. The 3-carbamoyl series compounds were obtained using a mobile phase of 90% water and 10% acetonitrile with a flow rate of 3.3 mL per minute. The 3-phenyl series compounds were obtained using a mobile phase of 85% water and 15% acetonitrile with a flow rate of 3.3 mL per minute. Any 3-substituted 2(1H)pyridone was retained at the head of the column.

#### Literature Cited

1. Diebold, G. J.; Zare, R. N. *Science* 1977, 1439.
2. Furata, N.; Otsuki, A. *Anal. Chem.* 1983, 55, 2407.
3. Skoropinski, D. B.; Callis, J. B.; Danielson, J. D. S.; Christian, G. D. *Anal. Chem.* 1986, 58, 2831.
4. Pfeffer, W. D.; Yeung, E. S. *Anal. Chem.* 1986, 58, 2103.
5. Lawrence, J. F.; Frei, R. W. *Chemical Derivatization in Liquid Chromatography*; Elsevier Scientific: New York, 1976.
6. Grushka, E.; Lam, S.; Chassin, J. *Anal. Chem.* 1978, 50, 1398.
7. Frei, R. W.; Lawrence, J. F. *J. Chromatogr.* 1973, 83, 231.
8. Cassidy, R. M.; Le Gay, D. S.; Frei, R. W. *J. Chromatogr. Sci.* 1974, 12, 85.
9. Blau, K.; King, G. S., Eds. *Handbook of Derivatives for Chromatography*; Heyden: Philadelphia, PA, 1978, p 351-384.
10. Chen, R. F. *Nature* 1966, 209, 69.
11. Chen, R. F. *Arch. Biochem. Biophys.* 1967, 120, 609.
12. Seiler, N.; Wiechmann, M. Z. *Anal. Chem.* 1966, 220, 109.
13. Lawrence, J. F. *J. Chromatogr. Sci.* 1979, 17, 147.
14. Holman, W. I. M.; Weigand, C. *Biochem. J.* 1948, 43, 423.
15. Veda, K. J. *Jpn. Biochem. Soc.* 1950, 22, 196; *Chem. Abstr.* 1952, 46, 4541.

16. Robenson, T.; Cepurneck, C. *Phytochemistry* 1965, 4, 75.
17. Chung, N. M.; Tieckelmann, H. *J. Org. Chem.* 1970, 35, 2517.
18. Smart, P. L.; Laidlaw, I. M. S. *Water Resour. Res.* 1977, 13, 15.
19. Yoneda, G. S.; Griffin, M. T.; Carlyle, D. W. *J. Org. Chem.* 1975, 40, 375.
20. Gilbert, E. E. *Sulfonation and Related Reactions*; Robert E. Krieger Publishing: Huntington, NY, 1977, p 137.
21. Marvel, C. S.; Sparberg, M. S. *Org. Synth., Coll.* 1943, 2, 558.
22. Nelson, D. A.; Lenz, D. M. *Gov. Rep. Announce. Index (U.S.)* 1984, 85(5), 130, NTIS No. PB84-132489.
23. Beckett, J. R.; Nelson, D. A. *Anal. Chem.* 1981, 53, 910.
24. Parker, C. A.; Rees, W. T. *Analyst (London)* 1960, 85, 587.
25. Boekelheide, V.; Linn, W. J. *J. Am. Chem. Soc.* 1954, 76, 1286.

RECEIVED September 26, 1988

## Chapter 13

# Room-Temperature Fluorescence and the Remote Detection of Solar-Stimulated Luminescence

Arnold F. Theisen

U.S. Geological Survey, Box 25046, Denver Federal Center,  
MS-964, Denver, CO 80225

Room-temperature fluorescence (RTF) has been used to determine the emission characteristics of a wide variety of materials relative to the wavelengths of selected Fraunhofer lines in support of the Fraunhofer luminescence detector remote-sensing instrument. RTF techniques are now used in the compilation of excitation-emission-matrix (EEM) fluorescence "signatures" of materials. The spectral data are collected with a Perkin-Elmer MPF-44B Fluorescence Spectrometer interfaced to an Apple II+ personal computer. EEM fluorescence data can be displayed as 3-D perspective plots, contour plots, or "color-contour" images. The integrated intensity for selected Fraunhofer lines can also be directly extracted from the EEM data rather than being collected with a separate procedure. Fluorescence, chemical, and mineralogical data will be statistically analyzed to determine the probable physical and/or chemical causes of the fluorescence.

Room-temperature fluorescence (RTF) has been used to determine the emission characteristics of a wide variety of materials relative to the wavelengths of several Fraunhofer lines. Fraunhofer lines are bands of reduced intensity in the solar spectrum caused by the selective absorption of light by gaseous elements in the solar atmosphere. RTF studies have recently included the search for the causes of the luminescence of materials and a compilation of information that will lead to "luminescence signatures" for these materials. For this purpose, excitation-emission matrix (EEM) data are now being collected.

A laboratory spectrometer, Perkin-Elmer MPF-44B<sup>1</sup>, is being used to acquire RTF data. Cyborg Corporation's Integrated System for Automatic Acquisition and Control and an Apple II+ computer have been

This chapter not subject to U.S. copyright  
Published 1989 American Chemical Society

interfaced to the spectrometer to simplify data collection, reduce drudge work, and provide an environment for data analysis. Fully unattended data collection has not yet been achieved, but complete instructions for an operator to accomplish complex procedures are included in software written specifically for required tasks.

Luminescence data for EEM files are produced by stepping the excitation monochromator from 240 to 540 nm or from 300 to 600 nm and scanning the emission monochromator from 300 to 600 nm or from 400 to 830 nm for each excitation step. Intensities are read at 10-nm intervals. To match bandwidth to sampling interval the excitation slitwidth is set at 10 nm. The emission slitwidth is set at 7.5 nm, the scan speed is set to 480 nm/min, and the detector response to 0.3 seconds to produce an effective bandwidth of 10 nm. EEM data are displayed on a computer screen or plotter in 3-D perspective. By treating the EEM data as an image, "color-contour" representations are produced using density slicing.

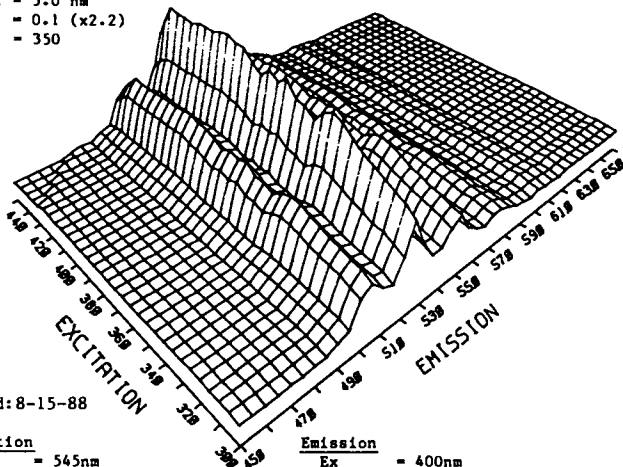
To evaluate the emission characteristics of materials with respect to Fraunhofer lines, the emission monochromator is set at the wavelength of a Fraunhofer line and the excitation monochromator is scanned from 300 nm to 20 nm short of the emission wavelength. Intensity measurements, taken at 10-nm excitation intervals, are intended to be analogous to those that might be taken with the material exposed to sunlight. Therefore, each measurement is convolved with solar spectrum data (1,2) and summed. The integrated intensities are ratioed with the integrated intensity of a known concentration of rhodamine WT dye which, because of its long-term stability, has been chosen as a luminescence standard. The intensities for the material are, therefore, expressed in terms of rhodamine WT dye equivalency (RhWTeq) for a given Fraunhofer-line wavelength. The RhWTeq for a material provides the means by which to gauge its possible detectability in the field, with the Fraunhofer luminescence detector (FLD).

The FLD is a remote-sensing instrument that uses a technique called the "Fraunhofer line-depth method" to detect luminescence emissions from natural and manmade materials stimulated by solar radiation. The Fraunhofer line-depth method requires that four measurements be made for each Fraunhofer line, with all measurements centered at the wavelength of the line minimum. The solar spectrum is measured from a diffuse, reflective, nonluminescent surface so as to include both direct sunlight and diffuse skylight. Measurements with a bandwidth of approximately 10 angstroms are labeled, in the formulas shown below, a for solar continuum and  $d$  for target continuum. Measurements with a bandwidth of approximately 0.7 angstroms are labeled  $b$  for solar line-center and  $c$  for target line-center. If the target material is nonluminescent, then the intensities  $c$  and  $d$  will be equal to the intensities  $b$  and  $a$  times the reflectivity of the material, and the ratio  $b/a$  will equal the ratio  $c/d$ . The luminescence emission bandwidths of materials investigated to date exceed the 10-angstrom continuum measurement bandwidth.

Where the emission wavelength(s) correspond to a Fraunhofer line, then that radiation will increase both the  $c$  and  $d$  intensities and the  $c/d$  ratio will be greater than the  $b/a$  ratio, indicating the presence of a luminescent material. Algebraically, the problem can

Meta-autunite

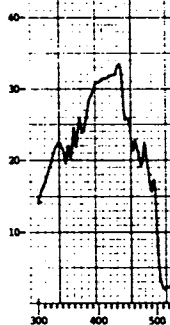
Em slit = 2.5 nm  
 Ex slit = 5.0 nm  
 Gain = 0.1 (x2.2)  
 Filter = 350



revised: 8-15-88

Excitation

Em = 545nm  
 Em slit = 2.5nm  
 Ex slit = 2.5nm  
 Ex scan = 300-530nm  
 Gain = 1.0  
 Filter = 350



Fraun line(nm)	: 423	486	518	589	656
Rho WT equiv(ppb):	0.1	14.8	159	16.1	3.6

Emission

Ex = 400nm  
 Ex slit = 2.5nm  
 Em slit = 2.5nm  
 Em scan = 410-700nm  
 Gain = 1.0  
 Filter = 350

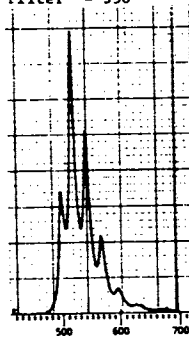


Figure 1. Catalog page of meta-autunite, including 3-D perspective excitation-emission plot, maximum excitation and emission spectra, and rhodamine dye equivalencies.



be stated in the following manner: if  $R$  = reflectivity and  $L$  = luminescence, then

$$c = Rb + La \quad (1)$$

and 
$$d = Ra + La. \quad (2)$$

Subtracting Equation 1 from Equation 2 gives

$$R = (d-c) / (a-b), \quad (3)$$

the reflectivity of the material derived from the measured intensities. Rewriting Equation 2 and substituting Equation 3 into it gives

$$L = (d/a) - R \quad (4)$$

or 
$$L = (d/a) - [(d-c) / (a-b)], \quad (5)$$

the luminescence derived from the measured intensities. For a more complete discussion, see Plascyk (3).

The FLD has been operated in a variety of configurations from both helicopters and fixed-wing aircraft (4,5). Although originally designed to function as a nonimaging radiometer, the FLD has been modified to collect luminescence image data (6). The FLD has successfully detected luminescence from a wide range of materials, including phosphate rock, uranium-bearing sandstone, marine oil slicks, and vegetation stressed geochemically and by drought (7-10).

Both RhWTeq information and EEM file data are being combined with analog plots of maximum excitation and emission spectra to make a catalog of luminescent materials. Figure 1 is one such catalog page. The catalog information provides for quick reference and comparisons of materials. Statistical analyses of RhWTeq values and of chemical and mineralogical data have been used to investigate the probable physical and/or chemical causes of the luminescence. When "luminescence signatures" from EEM data become available, they too will be included in these investigations.

#### Literature Cited

1. Kondrat'ev, K. Y. *Radiation Characteristics of the Atmosphere and Earth's Surface*; Amerind Publishing Co.: New Delhi, 1973. Also National Aeronautics and Space Administration (NASA) TT F-678.
2. Luckiesh, M. *Applications of Germicidal, Erythemat, and Infrared Energy*; D. Van Nostrand: New York, 1946.
3. Plascyk, J. A. *Opt. Eng.* 1975, 14, 339-346.
4. Watson, R. D.; Hemphill, W. R. *U.S. Geol. Surv. Open-File Rep.* 76-202, 1977.
5. Hemphill, W. R.; Settle, M., Eds. *LPI Tech. Rep. 81-031*, 1981.
6. Watson, R. D.; Theisen, A. F. *U.S. Geol. Surv. Open-File Rep.* 77-743, 1977.
7. Watson, R. D.; Henry, M. E.; Theisen, A. F.; Donovan, T. J.; Hemphill, W. R. *Proc. 4th Joint Conf. Sensing of Environmental Pollutants*; American Chemical Society: Washington, D.C., 1978, p 176, 668-671.

8. Watson, R. D.; Theisen, A. F.; Prezelin, B. B. *Int. J. Rem. Sensing* 1981, 2, 61-70.
9. Hemphill, W. R.; Theisen, A. F.; Watson, R. D. In *Optical and Laser Remote Sensing*; Killinger, D. K.; Mooradian, A., Eds.; Springer-Verlag: Berlin, Heidelberg, New York, 1983, p 213-222.
10. Hemphill, W. R.; Theisen, A. F.; Tyson, R. M. *J. Lumin.* 1984, 724-726.

RECEIVED August 15, 1988

## Chapter 14

# Ground-Water Monitoring Using Remote Laser-Induced Fluorescence

Jonathan E. Kenny<sup>1</sup>, George B. Jarvis<sup>1</sup>, Wayne A. Chudyk<sup>2</sup>,  
and Kenneth O. Pohlig<sup>2</sup>

<sup>1</sup>Department of Chemistry, Tufts University, Medford, MA 02155

<sup>2</sup>Department of Civil Engineering, Tufts University, Medford, MA 02155

Field tests of a prototype mobile ground-water contaminant detector are discussed and compared to laboratory tests of similar instrumental apparatus. The prototype field instrument, based on a frequency-quadrupled neodymium:YAG laser and fused-silica fiber optics, has been shown to have parts-per-billion detection limits for several important aromatic pollutants, e.g., phenol and gasoline. Field tests have included monitoring of both surface waters and fuel-oil-contaminated ground water. Compared to the conventional bailing method of ground-water sampling, remote laser-induced fluorescence has the advantage of being a rapid, *in situ* technique that is an excellent early-warning method at a low cost per well.

Various applications of remote sensing have been reported in the recent literature; among them are fiber-optic-based sensors (1-7). Important analytical parameters, such as fluorescence intensity and pH, can be characterized using fiber-optic sensors. The remote-sensing technique that we are currently developing combines fiber optics and laser-induced fluorescence in an instrument capable of detecting and monitoring aromatic compounds in ground and surface waters.

Recently, Hirschfeld et al. (1,2) have reported the feasibility of remote monitoring of ground water using lasers and fiber optics. Their work involved using tracers (organic laser dyes) and excitation with visible continuous-wave lasers to record the movement of ground water. Our work centers on the *in situ* detection and monitoring of small aromatic compounds in ground-water aquifers. Several problems associated with this application of remote monitoring of ground water have been discussed elsewhere (3). Briefly, these include the weaker molar absorptivity and fluorescence quantum yields of small aromatic compounds compared to laser dyes, and the occurrence of the aromatic compounds' absorption peaks in the ultraviolet rather than the visible. The use of ultraviolet excitation sources is problematic because the transmission of the optical fibers in the ultraviolet is much poorer than in the visible, and because the only practical

0097-6156/89/0383-0233\$06.00/0

© 1989 American Chemical Society

ultraviolet lasers are pulsed lasers, which have poorer beam quality than continuous-wave lasers and are more likely to damage the fibers at a given average power, because of their high peak power. However, because most ground water is within 15 m of the surface, calculations indicated the feasibility of the technique, and laboratory and field experiments have been successfully conducted. This report presents the basic design of the instrumentation, its adaptation to a field-portable unit, and a discussion of laboratory and field results.

### *Instrument Design*

The principles of and instrumentation for absorption and fluorescence spectroscopy have been discussed in detail in standard texts (8).

Recent reports have described the laboratory (3) and field (9) versions of the fiber-optic-based Remote Laser-Induced Fluorescence instrument. The basic design of the optical apparatus is shown in block diagram form in Figure 1. A pulsed neodymium:YAG laser with two stages of frequency doubling is used as a source. Several optical elements are used to separate the laser harmonics and focus the ultraviolet (266 nm) onto the tip of a 600- $\mu\text{m}$  fused-silica optical fiber. The laser light travels the length of this excitation fiber by total internal reflection. At the sample, one end of a second 600- $\mu\text{m}$  fused-silica optical fiber, the detection fiber, is held at an angle to the first to improve the fluorescence collection efficiency. The other end of the detection fiber enters the detection module located on the optical table, where it is positioned one focal length from a fused-silica lens that collimates the collected light. The fluorescence is spectrally filtered from interferences and transmitted onto the detection photomultiplier tube (Hamamatsu R928). A beamsplitter deflects approximately 10% of the collected light onto a second photomultiplier tube (Hamamatsu 1P28) to monitor laser power. A 266-nm interference filter blocking all but the laser light is placed before this photomultiplier tube. The fluorescence signal is then corrected for laser intensity fluctuations. In the current system, total fluorescence is collected and related to concentration; the detection system does not analyze the fluorescence according to wavelength. Both photomultiplier signals are processed through gated integrators (EG&G/PAR 162/165). Experimental control and data analysis are accomplished through an interactive BASIC routine run on an IBM portable personal computer.

Adapting the system to a mobile unit involved redesigning the instrumentation for portability and mounting it into a 3  $\times$  4  $\times$  5-ft steel cart. A major requirement for this unit was containment of the Line-Lite laser, optical elements, and detection module in a clean laboratory environment. Other requirements included high ground clearance, accessibility to electricity within 100 ft, and durable construction. The entire mobile unit can be powered by a 5-kW gasoline generator.

### *Experimental*

Laboratory work involved making calibration curves which show the response of the system for various concentrations of pollutant, e.g., phenol. Typically, remote laser-induced fluorescence measurements from both the laboratory apparatus and the mobile unit are made on

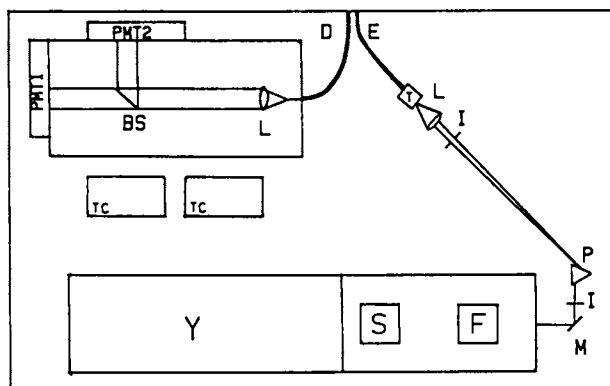


Figure 1. Block diagram showing component layout for both the laboratory apparatus and the mobile unit: Y, Nd:YAG laser; S and F, second and fourth harmonic generation crystals, respectively; M, dichroic mirror; P, dispersive prism; I, iris; L, lens; T, 5-axis fiber positioner; PMT 1, detection photomultiplier tube; PMT 2, power normalization photomultiplier tube; BS, beamsplitter; D, detection optical fiber; E, excitation fiber; TC, oven temperature controller for harmonic generation.

serial dilutions of pollutant in pH=7 buffered water; these are plotted versus log of concentration.

A typical field test involves several steps: (a) transporting the mobile unit to the site; (b) instrument warmup; (c) system check out, consisting of mobile unit measurements of distilled water and a 1-ppm stock phenol solution; and (d) *in situ* measurements of the well water, repeated three times for statistical analysis. Signal levels recorded at a field site may be reported as equivalents of phenol (or other calibrant) using the calibration curves. Therefore, this method allows us to report the upper bounds of pollution levels.

### *Results and Discussion*

**Laboratory Experiments.** An initial experiment involved examining the laser-induced fluorescence for interferences. Such an experiment required the detection fiber to be mounted onto a monochromator for spectral analysis of the collected light. The monochromator scan produced when the optical fiber probe was placed in a sample of pH=7 phosphate-buffered distilled water is shown in Figure 2. The signal at 266 nm is the Rayleigh scattered laser light, and that at 294 nm is the water Raman line. To relate total fluorescence signal to concentration of pollutant, these signals must be removed; removal is accomplished by placing a long-wave-pass colored glass filter before the detection photomultiplier. This decreases the fluorescence emission intensity only slightly (3).

The calibration curves relate the total fluorescence signal collected (not analyzed by wavelength) to the concentration. Shown in Figure 3 are the results of total fluorescence measurements from a serial gasoline dilution at an instrument-to-analyte distance of 25 m, using a high-power laser (Quanta-Ray DCR-1) in the laboratory. Shown in Figure 4 are the results of a similar experiment with phenol at a distance of 10 m using the portable field system. The limits of detection are parts per trillion for the laboratory apparatus and parts per billion for the mobile unit. The instrument-to-analyte distances are limited by the laser pulse energy, but high-energy pulses eventually damage the optical fiber (3). For the mobile unit, maintaining a stable source of ultraviolet light from a portable laser has been our greatest problem; improving the light source will permit increasing the instrument-to-analyte distances or lowering the detection limits. The two calibration curves have similar shapes, as do those for other compounds analyzed with both experimental setups.

**Field Tests.** Recently we conducted a field test at a site contaminated with fuel oil. Our measurements were  $0.0625 \pm 0.0212$  mA for the well water and  $0.0189 \pm 0.0119$  mA for distilled water (showing errors of one standard deviation). From calibration curves, these numbers can be reported as equivalent to 50 ppb phenol or 34 ppb xylenes. Nine-month-old laboratory results (EPA method 624 and GC/FID) for this site indicated concentrations of 25 ppb for benzene, toluene, and xylenes combined and 100 ppb for fuel oil. The important result is the significant difference between the distilled-water and well-water measurements. We are very encouraged by these results and are planning future field tests.

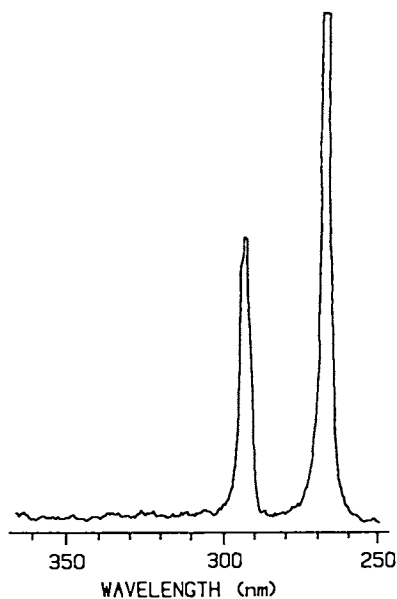


Figure 2. The spectral analysis of light collected by the fiber placed in a pH=7 phosphate-buffered distilled water sample. The spectrum shows the important interferences which must be eliminated to relate the fluorescence intensity to concentration.

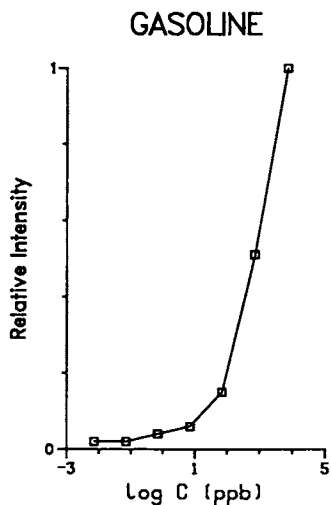


Figure 3. Calibration curve for serial dilution of gasoline in pH=7 buffered water at an instrument-to-analyte distance of 25 m, using laboratory apparatus.

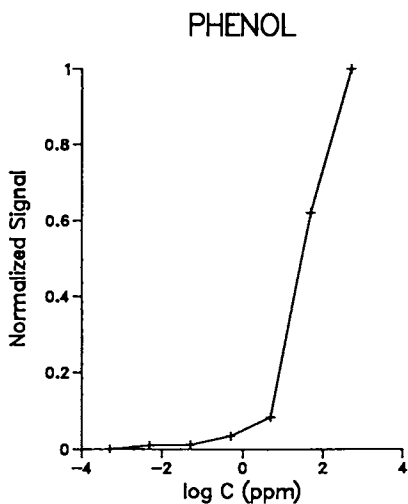


Figure 4. Calibration curve for serial dilution of phenol in pH=7 buffered water at an instrument-to-analyte distance of 10 m, using the portable field system.



### Conclusions

In conclusion, the excellent sensitivity of laser-induced fluorescence has been combined with optical fibers in an *in situ* method of analysis of aromatic compounds. Our device, analogous to conductance probes for ionic solutions, is a generic detector (i.e., not species-specific), but is sensitive and useful for rapid *in situ* monitoring of changes in pollutant concentration at a low cost per well. Measurement times of  $\sim\frac{1}{2}$  hour make it possible that one unit (our approximate cost \$40,000) could service many monitoring wells. We expect that future work on this project will proceed along two lines: the chemists will seek more powerful methods of fluorescence analysis directed at molecule-specific detection, and the civil engineers will develop the methodology of field measurement.

### Acknowledgments

We are grateful for the support of the National Science Foundation, the Environmental Protection Agency, the Center for Environmental Management at Tufts University, and the Alexander Host Foundation.

### Literature Cited

1. Hirschfeld, T.; Deaton, T.; Milanovich, F.; Klainer, S.; Fitzsimmons, C. *Project Summary--Feasibility of Using Fiber Optics for Monitoring Groundwater Contaminants*; U.S. Environmental Protection Agency, Environmental Monitoring Systems Lab.: Las Vegas, NV, January 1984.
2. Hirschfeld, T.; Deaton, T.; Milanovich, F.; Klainer, S. *Opt. Eng.* 1983, 22(5), 527-531.
3. Chudyk, W.A.; Carrabba, M.M.; Kenny, J.E. *Anal. Chem.* 1985, 57, 1242-1252.
4. Schwab, S.; McCreery, R. *Anal. Chem.* 1984, 56, 2199-2204.
5. Schirmer, R.; Gargus, G. *Am. Lab.* 1986, 18(12), 30-39.
6. Angel, S. *Spectroscopy* 1987, 2(4), 38-47.
7. Newby, K.; Reichert, W.; Andrade, J.; Benner, R. *Appl. Opt.*, 1984, 23(11), 1812.
8. Parker, C.A. *Photoluminescence of Solutions*; Elsevier: Amsterdam, 1968.
9. Kenny, J.E.; Jarvis, G.B.; Chudyk, W.A.; Pohlig, K.O. *Anal. Instrum.* 1987, 16(4), 423-445.

RECEIVED September 2, 1988

## Author Index

- Alvarez, Francisco, 127  
Beckett, James R., 206  
Bellama, Jon M., 84  
Bello, Job M., 155  
Blyshak, Lisa A., 167  
Bokoch, Gary M., 52  
Brinckman, Frederick E., 84  
Burrell, Greg J., 155  
Bush, James H., 206  
Chandler, Douglas E., 70  
Chokshi, Hitesh, 127  
Chudyk, Wayne A., 233  
Citta, Linda A., 155  
Comstock, Christopher, 52  
Epstein, Michael S., 98  
Faltynek, Robert A., 84  
Givens, Richard S., 127  
Goldberg, Marvin C., 1,180  
Holl, Walter W., 45  
Hurtubise, Robert J., 155  
Jarvis, George B., 233  
Kawasaki, Takao, 127  
Kazilek, Charles J., 70  
Kenny, Jonathan E., 233  
Kuwana, Theodore, 127  
Lenz, Douglas M., 206  
Matuszewski, Bogdan, 127  
Merkle, Carrie J., 70  
Mueller, Heinz, 52  
Nakashima, Kenichiro, 127  
Negomir, Patricia M., 180  
Nelson, David A., 206  
Olson, Gregory J., 84  
Omann, Geneva M., 23,52  
Orlovic, Mirko, 127  
Parekh, Nikhil, 127  
Patonay, Gabor, 167  
Pohlig, Kenneth O., 233  
Ramasamy, S. M., 155  
Rowe, David W., 206  
Schowen, Richard L., 127  
Sklar, Larry A., 23,52  
Stobaugh, John, 127  
Swann, William N., 52  
Theisen, Arnold F., 228  
Trout, Todd K., 84  
Velapoldi, Rance A., 98  
Warner, Isiah M., 167  
Webb, R. Lee, 45  
Weiner, Eugene R., 1  
Wong, Osborne, 127

## Affiliation Index

- Arizona State University, 70  
Emory University, 167  
National Bureau of Standards, 84,98  
Scripps Clinic and Research Foundation, 23,  
Smith Kline Beckman Corporation, 45,52  
Tufts University, 233  
University of Kansas, 127  
University of Maryland, 84  
University of Wyoming, 155,206  
U.S. Geological Survey, 1,180,228

## Subject Index

## A

- Absorption characteristics,
  - 2-cyanobenz[*f*]isoindole, 129,130*f*
- Absorption spectroscopy, compared to luminescence techniques, 4,6
- Acetonitrile, chemiluminescence, 143,145*f*
- Actin polymerization, correlated with right-angle light scatter, 32,33*f*
- Alcohols
  - derivatization, 221
  - fluorescent derivatives, 212,213*f*,223–224
- Alkyl bromides, derivatives, 209,210*f*
- Alkyl sulfonate series, HPLC separations, 215–217*f*
- Amines, fluorescent derivatives, 212,213*f*
- Amino acids
  - derivatized, fluorescence detection limits, 133*r*
  - primary, chromatogram, 131,132*f*
  - substituted benz[*f*]isoindoles, fluorescence efficiencies, 151*r*
- p*-Aminobenzoic acid, phosphorescence lifetime values, 163
- Analytical probes, fiber optic fluorescent sensors, 16
- Analytical procedure, for concentration of nucleic acids, 49,50*f*
- Analytical utility, cyclodextrins, 167
- Applications
  - macrospectrofluorometric standards, 115–122
  - remote sensing, 233
- Aquatic humic fractions, characterized by fluorescence depolarization spectroscopy, 180
- Aromatic compounds, in ground-water aquifers, 233
- Aromatic molecules, fluorescence spectra, 10
- Atomic absorbance
  - butyltin moieties, 92*r*
  - zinc-treated bacteria, 94,95*f*
- Autunite, luminescence characteristics, 230,231*f*

## B

- Bacon, observations on luminescence, 2
- Bacteria
  - estuarine, image accumulation of BuSn<sup>3+</sup>, 94,95*f*
  - in zinc analysis, 88, 94–96
  - metabolic cycles, 84

- Becquerel, investigation of photoluminescence, 4
- Benzo[*a*]pyrene, room-temperature fluorescence spectra, 157,158*f*,160,161*f*
- Benzo[*e*]pyrene, room-temperature phosphorescence spectrum, 157,159*f*,160,161*f*
- Binary PAH mixtures
  - extraction efficiencies, 175*r*
  - total-luminescence contour plots, 175–177
- Binding and functional data, to relate function to receptor occupancy, 37
- Binding of FLPEP, intact neutrophils, 57,58*f*,60*f*
- Biochemical assays, use of luminescent methods, 14
- Biodegradability, pyridones, 214
- Biofilm, image accumulation of BuSn<sup>3+</sup>, 94,95*f*
- Bioluminescence
  - definition, 5*r*
  - fireflies, 10
  - history, 3
  - See also* Molecular luminescence
- Bioprocessing, elemental uptake and disposition, 84
- Bolognian stone, 2
- Butyltin, bacterial affinity, 92

## C

- Calcium
  - effect on exocytosis, 71
  - redistribution in neutrophils, 71
- Calcium ion, intracellular
  - effect of hexachlorocyclohexanes, 37–41
  - simultaneous measurements, 32,38*f*
- Calcium signal
  - dependence on extracellular calcium, 74,77*f*
  - effect of hyperosmolality, 78,79*f*
- Calcium transients, effect of hyperosmolality, 74,77*f*
- Calibration, standards, 100
- Catecholamines, cyanobenz[*f*]isoindole derivatives, chromatogram, 151,152*f*
- Cations, in living cells, epifluorescence microscopy imaging system, 85,86*f*
- Cell activation, and receptor states, 63
- Cell responses, spectrofluorometric analyses, 23–42

- Cellular communication, by ligand-receptor interaction, 52
- Chemiluminescence
- acetonitrile, 143,145*f*
  - definition, 5*r*
  - detection limits, 139*r*
  - dioxetanes, 140,141*f*
  - dipeptides, 137*r*
  - diphenylanthracene, 140,142*f*
  - efficiencies, amino acids, 151*r*
  - efficiency, peroxyoxalate reaction, 140,141*f*
  - emission spectra, 143,144*f*
  - kinetic analysis, 143,145*f*
  - sensitivity, studies with oxalate esters, 139*r*
- Chemiluminescence-based HPLC detection system, 137,138*f*
- Chemiluminescent reactions, efficiency, 137
- Chemoattractants, activation of neutrophils, 23-42
- Chlorophyll, fluorescent lifetime first measured, 9
- probe, 71,72*f*
- Chromatogram
- 2-cyanobenz[*f*]isoindole derivatives of catecholamines, 151,152*f*
  - neurotensin, 131,134*f*
  - 18 primary amino acids, 131,132*f*
- Complexation, cyclodextrins, 169,174
- Contaminants, remote laser-induced fluorescence analysis, 236
- Cooling, effect on luminescent spectra, 6
- Correction factors, excitation and emission spectra, 102
- Crystalloluminescence, definition, 5*r*
- 2-Cyanobenz[*f*]isoindole
- absorption characteristics, 129,130*f*
  - derivatives of catecholamines, chromatogram, 151,152*f*
- Cyclodextrins
- analytical utility, 167
  - formation of complexes, 169,174
  - functional structure, 167,168*f*
  - physical data, 169*r*
  - use in solid-surface luminescence, 157
  - use in solvent extraction, 170
- D
- Dansyl chloride, as fluorescent derivatizing reagent, 206
- Davy, observations on luminescence, 3
- Decay curves, analyzed with pulsed excitation light source, 189
- Decay time, standards, 106
- Degranulation, simultaneous measurements, 32,36*f*
- Depolarization
- first demonstrated, 7
  - intrinsic causes, 182
  - measurements
    - effect of multicomponent signals, 184
    - principles, 181-183
- Derivatization
- alcohols, 221
  - fluorescent pyridones, general method, 222
- Derivatizing reagent, fluorescent pyridones, synthesis, 222
- Detection limits
- chemiluminescence, 139*r*
  - fluorescence, 133,137,139*r*
  - fluorescent pyridones, 221
- Dioxetanes, chemiluminescence, 140,141*f*
- Dipeptides, chemiluminescence detection, 137*r*
- Diphenylanthracene, chemiluminescence, 140,142*f*
- Dissociation of FLPEP, intact neutrophils, 57,58*f*,60*f*
- DNA from various sources, relative fluorescence intensities, 48
- Dopamine, standard curves, 151,152*f*
- Dose-response curves, HCH and cytosolic Ca ion, 39,40*f*,41*f*
- Dubois, observations on luminescence, 3
- Dye-calcium complex, dissociation, 71,73*f*
- Dyes, to detect trace levels of nucleic acids, 46,47*f*
- Dynamic depolarization spectroscopy, 189
- E
- EDTA-metal chelates, HPLC separations, 220
- Elastase release, to study neutrophil activation, 26,27*r*
- Electroluminescence, definition, 5*r*
- Elemental analysis, epifluorescence microscopy imaging system, 85
- Emission characteristics, with respect to Fraunhofer lines, 229
- Emission phase-angle shift, interpretation, 190
- Emission spectra
- corrected, 103, 104*f*
  - correction factors, 102
  - humic fractions, 195-199
  - Energy levels, Jablonski diagram, 9
  - leu*-Enkephalin, fluorescence detection, 133,136*f*
  - met*-Enkephalin, enzymatic hydrolysis, 133,135*f*
  - Environmental analysis, using fluorescent pyridones, 206-226
  - Environmental probe, use of luminescence, 11
  - Environmental studies, use of luminescent methods, 15

- Enzymatic hydrolysis, *met-enkephalin*, 133,135f
- Enzyme release, effect on osmolality, 74,75f,76f
- Epifluorescence microscopy imaging system, description, 85,86f
- Estuarine bacteria, image accumulation of  $\text{BuSn}^{3+}$ , 94,95f
- Ethidium bromide, in fluorescence studies, 46
- Excimer, first observed, 8
- Exciplex, first observed, 8
- Excitation–emission matrix data, luminescence signatures, 228
- Excitation spectra  
corrected, 103,104f  
correction factors, 102  
humic fractions, 195–199
- Excited states, studied by luminescence, 16
- Exocytosis, osmotic effects, 71
- Extraction, organic examples, with cyclodextrins, 170,172
- Extraction efficiencies  
binary PAH mixtures, 175r  
several PAHs, 173r
- F
- Fiber optic fluorescent sensors, as analytical probe, 16
- Filter paper, as a matrix to obtain RTP, 156
- Fireflies, bioluminescence, 10
- Flavonol, interaction with tin, 89,90f,91f
- Flow cytometry  
analysis of ligand binding, 67  
basic principles, 29,31f  
correlated with right-angle light scatter, 32,34f  
histograms, 29,31f
- Fluorescein absorbance, to study neutrophil activation, 26,27r
- Fluorescein isothiocyanate, fluorescence intensity, 107,109f
- Fluorescence  
as function of solvent composition, 209r  
definition, 5r  
depolarization, 182  
excitation and emission maxima, humic fractions, 199r  
from animal matter, 9  
history, 2  
humic materials, 180  
polarized, first demonstrated, 7  
proteins, 10  
quantum yield values, 160,162r  
quantum yields of pyridone, 215,218  
room temperature, description, 155
- Fluorescence analytical procedure, for concentration of nucleic acids, 49,50f
- Fluorescence assays for neutrophil activation, advantages, 23
- Fluorescence decay time, standards, 106r
- Fluorescence depolarization, time-resolved, 189
- Fluorescence depolarization spectroscopy, 183
- Fluorescence detection  
*leu-enkephalin*, 133,136f  
laser-induced, 18 primary amino acids, 131,133r  
limits, 133,137,139r
- Fluorescence efficiencies, amino acids, 151r
- Fluorescence flux density, ion-doped glass spheres, 111,112f
- Fluorescence intensity, fluorescein isothiocyanate, 107,109f
- Fluorescence measurements  
cyclodextrin–PAH extraction, 171  
information obtained, 180
- Fluorescence methods  
ligand–receptor binding, 53  
nucleic acids, 46  
sensitivity, 46
- Fluorescence polarization  
analysis of ligand binding, 66  
binding of FLPEP, 59,60f
- Fluorescence quantum efficiencies, effect of peptide substituents, 129,131r
- Fluorescence quantum yield  
*p*-aminobenzoic acid, 163,164f  
pyridone sulfonates, 215r  
substituted pyridones, 218r
- Fluorescence spectra  
aromatic molecules, 10  
2-cyanobenz[*f*]isoindole, 129,130f  
effect of pH, 8
- Fluorescent derivatives, limitations, 207
- Fluorescent derivatizing reagents  
development, 206  
pyridone acid chlorides, 212
- Fluorescent lifetime of chlorophyll, first measured, 9
- Fluorescent probes, to detect Ca redistribution, 71
- Fluorescent pyridones  
detection limits, 221  
for environmental analysis, 206–226
- Fluorescent water-tracing compounds, development, 212
- Fluorogenic reagents, drawbacks, 128
- Fluorometer configuration, 29,30f
- Fluorometry, correlated with right-angle light scatter, 32,34f
- Fluorophore composition, humic acid fractions, 199

- Fluorophores in humic fractions, Perrin plots, 184–188
- Fraunhofer, observations on luminescence, 3
- Fraunhofer lines, definition, 228
- Fraunhofer luminescence detector, description, 229
- G
- G protein, ligand, and receptor interaction, 52–69
- G protein families, signaling for receptors, 52–56
- Galileo, observations on luminescence, 2
- Galvanoluminescence, definition, 5r
- Gasoline, total fluorescence measurements, 236,238f
- Gaviola, construction of phase fluorometer, 8
- $\beta$ -Glucuronidase, release from neutrophils, 74,75f
- Gradient elution profile, 18 primary amino acids, 131,132f
- Ground-water contaminants, remote laser-induced fluorescence analysis, 236
- Ground-water monitoring, using remote laser-induced fluorescence, 233–239
- Ground-water tracers, development, 212
- Guanine-nucleotide-binding proteins, *See* G proteins
- Guanine nucleotide dependent receptor interconversion, 61,62f
- H
- Harvey, observations on luminescence, 2
- Heptachlor  
 reaction with pyridone sodium salts, 209,211f  
 pyridone sodium salt derivative, formation, 222
- Hexachlorocyclohexanes, effects on neutrophil function, 37–41
- High-performance liquid chromatographic detection system, chemiluminescence-based, 137,138f
- High-performance liquid chromatographic separation conditions, alkyl bromide and alcohol derivatives, 220
- High-performance liquid chromatographic separations  
 alkyl sulfonate series, 215–217f  
 substituted EDTA–metal chelates, 220
- High-performance liquid chromatography, fluorescent derivatizing reagents, 206
- Histograms, flow cytometry, 29,31f
- Hooke, theory of light origins, 3
- HPLC, *See* High-performance liquid chromatographic or High-performance liquid chromatography
- Humic acid fractions, fluorophore composition, 199
- Humic fractions  
 excitation and emission spectra, 195–199  
 fluorescence excitation and emission maxima, 199r  
 molar volume and shape, 188–189  
 Perrin plots of fluorophores, 184–188  
 Stokes–Einstein and Perrin volumes compared, 191,195r
- Humic materials  
 fluorescence, 180  
 phase-resolved spectra, 201–204f
- Hydrogen peroxide concentration, effect on fluorescence reaction, 146
- Hyperosmolality  
 effect on calcium signal, 78,79f  
 effect on calcium transients, 74,77f  
 effect on intracellular calcium release, 78,79f  
 effect on lysosomal enzyme release, 74,75f
- I
- Immunoassay techniques, based on fluorescence, 14
- Indo-1, as fluorescent probe, 71,72f
- Inorganic ion-doped glasses, characteristics of luminescence, 111r
- Instrumentation, use in luminescence methods, 1,3
- Intensity correlation method, lifetime measurement, 16
- Interaction, ligand, receptor, and G protein, 52–69
- Interconverting receptor model, 63,64f
- Internalization of fluorescent ligands, 52–65
- Intracellular calcium elevation, to study neutrophil activation, 26,27t
- Intracellular calcium release, effect of hyperosmolality, 78,79f
- Intracellular signaling pathways, 52–56
- Ion-doped glass beads, relative luminescence flux, 111,112f,113f
- Ion-doped glasses  
 as standards, 115  
 characteristics of luminescence, 111r
- Irradiation  
 resulting in photobleaching, 108  
 uranyl glass microspheres, 109f

## J

Jablonski, diagram of energy levels, 9

## K

Kinetic analysis, chemiluminescence, 143,145f

Kircher, studies of luminescence, 2

## L

Laser-induced fluorescence detection, 18  
primary amino acids, 131,133r

Lead-doped glasses, corrected spectra, 111,114f

Lifetime difference, measurable, 11

Ligand-receptor-G protein  
interaction, 52-69  
mechanisms, 53  
states, 53,54f

Ligand-receptor dynamics, model, 63,64f

Ligand-receptor interaction, cellular  
communication, 52

Ligand binding  
in intact cell, 63  
real-time analytical methods, 63

Ligand design, for EMI technique, 96

Light, historical theories, 3

Light-scattering assays, of neutrophil  
functions, 28

Light emission, from chemically generated  
fluorescent molecule, 139

Light modulation method, interpretation of  
emission phase-angle shifts, 190

Linearity, instrument, 107

Luciferase, discovery, 4

Luciferin, discovery, 4

Luminescence

causes, 5r  
characteristics, inorganic ion-doped  
glasses, 111r  
classification into six kinds, 4,5r  
definition, 99  
definitions of types, 5r  
*See also* Molecular luminescence,  
Bioluminescence

Luminescence analysis, solid-surface,  
description, 155

Luminescence detection, sensitivity, 6

Luminescence intensities, butyltin  
moieties, 92r

Luminescence intensity, zinc-treated  
bacteria, 94,95f

Luminescence lifetime spectroscopy, 16

Luminescence measurements, reliance on  
standards, 98

Luminescence methods, growth and expansion, 1

Luminescence parameters  
calculated, 160

combined for selectivity enhancement, 12r

Luminescence signatures, excitation-emission  
matrix data, 228

Luminescence standards, requirements, 99

Luminescence techniques, compared to  
absorption spectroscopy, 4,6

Luminescence variables, measurable, 6

Luminescence wavelength standards, 101r

Luminescent catalog, sample page, 230,231f

Luminescent emission and quantum theory, 6

Luminescent methods

use in biochemical assays, 14

use in environmental studies, 15

Luminescent spectra, effect of cooling, 6

Lysosomal enzyme release, effect of  
hyperosmolality, 74,75f

## M

Macrospectrofluorometric standards  
applications, 115-122

descriptions, 99-107

Macrostandards, use, 110

Malaria vaccine proteins, nucleic acid  
content, 48

Mathematical model, time-dependent  
emission, 143

Matrix standards, uses, 117

Membrane depolarization, to study neutrophil  
activation, 26,27r

Membrane fusion  
effect of osmotic gradient, 78  
promotion, 70

Metabolic cycles, bacteria, 84

Metal biotransformations in environmental  
matrices, 84-97

Metal ion analysis, fluorescent-labeled  
EDTA, 219

Microscopy, coupled with spectro-  
fluorometry, 85

Microspectrofluorometric standards, 107-115

Microstandards, use, 110

Molar absorptivity  
pyridone sulfonates, 215r  
substituted pyridones, 218r

Molar volume, of humic fractions, 188-189

Molecular luminescence, history, 1

Molecular rotational diffusion, 183

Monochromator wavelength calibration,  
spectral lines, 101

Multicomponent signals, effect on  
depolarization measurements, 184

Multicomponent systems, analysis with  
phase-sensitive detection, 10

American Chemical Society

Library

1155 16th St., N.W.

Washington, D.C. 20036

- Multidimensional fluorescence analysis, cyclodextrin solvent-extraction systems, 167–179
- Multidimensional measurements, as probe of environment, 11
- N
- Naphthalene-2,3-dicarboxaldehyde, as fluorogenic reagent, 128
- Neurotensin, chromatogram, 131,134f
- Neutrophil activation
- advantages of fluorescence assays, 23
  - spectrofluorometric assays, 26,27t
- Neutrophil functions, spectroscopic assays, 28t
- Neutrophils
- detection of calcium signals, 70–82
  - interactions, 56
  - intact, dissociation of FLPEP, 57,58f,60f
  - reasons for use in assays, 24
  - receptor-mediated signal transduction, 25f
  - receptor states, 56
  - release of  $\beta$ -glucuronidase, 74,75f
- Newton, theory of light origins, 3
- Norepinephrine, standard curve, 151,152f
- Nucleic acids
- fluorescence analytical procedure, 49,50f
  - fluorescence methods, 46
  - in malaria vaccine proteins, 48
  - in pharmaceutical preparations, 45
  - limitations of assays, 45
  - relative fluorescence intensities, 48
- Nucleophilic fluorescent derivatizing reagents, pyridone sodium salts, 209
- O
- Organic fluorophore, irradiation, 108
- Organic samples, extraction with cyclodextrins, 170
- Organic trace analysis, by solid-surface luminescence, 156
- Organic tracing compounds, properties, 212
- Osmolality, effect on enzyme release, 74,75f,76f
- Osmotic effects, exocytosis, 71
- Osmotic gradient, effect on membrane fusion, 78
- Oxalate esters
- chemiluminescence efficiencies, 148
  - chemiluminescence sensitivity, 139t
- Oxidant production, to study neutrophil activation, 26,27t
- P
- Pasteur, observations on luminescence, 3
- Peptide substituents, effect on fluorescence quantum efficiencies, 129,131t
- Peptides, assay, 131–136
- Permeabilized cell, use in transduction mechanisms, 61,62f
- Peroxyoxalate method, efficiency, 137
- Peroxyoxalate reaction, chemiluminescence efficiency, 140,141f
- Perrin, observation of depolarization, 7
- Perrin equation, 183
- Perrin plots, fluorophores in humic fractions, 184–188
- Perrin volume, compared to Stokes–Einstein volume, 191,195t
- pH, effect on fluorescence spectrum, 8
- Phase fluorometer, first constructed, 8
- Phase-resolved emission maxima, humic fractions, 199t
- Phase-resolved emission spectra, theory, 199
- Phase-resolved spectra, humic materials, 201–204f
- Phase-sensitive detection, to analyze multicomponent systems, 10
- Phenol
- fluorescent derivatives, 212,213f
  - pyridone acid chloride derivative, formation, 225
  - total fluorescence measurements, 236,238f
- Phosphorescence
- definition, 5t
  - history, 2
  - quantum yield values, 160,162t
- Phosphorescence lifetime values, sodium acetate–sodium chloride mixtures, 163
- Phosphorescence quantum yield, *p*-aminobenzoic acid, 163,164f
- Phosphorimetry, use in analysis, 9
- Phosphoroscope, first built, 4
- Photobleaching
- organic species when irradiated, 107,109f
  - techniques to reduce, 108
- o*-Phthalaldehyde, as fluorogenic reagent, 128
- Polarized fluorescence, first demonstrated, 7
- Pollutant polynuclear aromatic hydrocarbons, standard, 117,118f
- Polynuclear aromatic hydrocarbons
- extraction efficiencies, 173
  - extraction with cyclodextrins, 170
  - pollutant, standard, 117,118f
  - standard reference materials, 115,117t
- Porosity measurements, geologic thin section, 108,109f
- Proteins, fluorescence, 10
- Pseudomonas fluorescens*, culture conditions, 87



- Pseudosimultaneous measurement, right-angle light scatter, 32,35f
- Pulse fluorometry, use in analysis, 9
- Pulsed excitation light source, analysis of decay curves, 189
- Pyridone acid chloride derivatives, formation, 223–224
- phenol derivative, formation, 225
- Pyridone acid chlorides as fluorescent derivatizing reagents, 212
- synthesis, 223
- Pyridone alkyl sulfonates, as ground-water tracers, 214
- Pyridone compounds absorption–emission, 207
- derivatizing reagents, 207–209
- fluorescence as function of solvent composition, 209
- Pyridone sodium salts as fluorescent derivatizing reagents, 209
- heptachlor derivative, formation, 222
- Pyridone sulfonates HPLC separation conditions, 220
- relative fluorescence, 215r
- spectroscopic data, 215r
- synthesis, 225
- Pyridones biodegradability, 214
- fluorescence quantum yields, 215,218
- relative fluorescence and spectroscopic data, 218r
- Q**
- Quantum efficiencies, fluorescence, effect of peptide substituents, 129,131r
- Quantum theory, and luminescent emission, 6
- Quantum yield definition, 8
- fluorescence pyridone sulfonates, 215r
- substituted pyridones, 218r
- fluorescence measurements, technique, 221
- solid-surface fluorescence and phosphorescence, 160,162r
- standards, 103
- Quantum-counter standards, 103
- Quenching effects, oxalates, 148r
- Quinine sulfate, corrected excitation and emission spectra, 103,104f
- R**
- Radioligand methods, limits, 53
- Rare earth ion probes, use, 14
- Rate constants, chemiluminescence intensity, 146,147f
- Raw fluorescence signal, during SRM certification process, 115
- Real-time methods, analysis of ligand binding, 65
- Receptor fast and slowly dissociating assignments, 59
- association rate constants, 59,60f
- ligand–G protein, interaction, 52–69
- rapidly dissociating, related to LRG interaction, 57
- Receptor binding characteristics, to initiate responses, 37
- Receptor interconversion, guanine nucleotide dependent, 61,62f
- Receptor states and cell activation, 63
- in neutrophils, 56
- Receptors, and neutrophil function, 56
- Receptor-mediated signal transduction, in neutrophils, 25f
- Relative fluorescence, pyridone sulfonates, 215r
- Relative fluorescence data, pyridones, 218r
- Relative fluorescence intensities DNAs from various sources, 48r
- various nucleic acids, 48r
- Relative luminescence flux, ion-doped glass beads, 111,112f,113f
- Remote detection, solar-stimulated luminescence, 228–231
- Remote laser-induced fluorescence instrument, design, 234,235f
- Remote sensing, applications, 233
- Requirements, standards, 107
- Resonance radiation, first demonstrated, 7
- Reversed-phase HPLC analysis, SRMs, 117–122
- Right-angle light scatter correlated with concentration, 32,33f
- correlated with side scatter, 32,34f
- pseudosimultaneous measurement, 32,35f
- Room-temperature fluorescence description, 155
- to determine emission characteristics, 228
- Room-temperature fluorescence spectrum, benzo[a]pyrene, 157,158f,160,161f
- Room-temperature phosphorescence spectrum, benzo[e]pyrene, 157,159f,160,161f
- Rotational relaxation time, related to molecular volume, 184
- S**
- Secretion, effect of Ca, 71
- Secretory cells, functions, 70
- Selectivity, enhancement by combining parameters, 12r

- Sensitivity  
 fluorescence methods, 46  
 instrument, 107  
 luminescence detection, 6
- Sensitized fluorescence, first demonstrated, 7
- Shape, humic fractions, 188–189
- Silica gel chromatoplates, in solid-surface luminescence work, 157
- Simultaneous measurements  
 degranulation, 32,36f  
 intracellular Ca ion, 32,38f
- Size and shape, standards, 110
- Sodium acetate, in solid-surface luminescence work, 157
- Sodium acetate–sodium chloride mixtures, phosphorescence lifetime values, 163
- Solar-stimulated luminescence, remote detection, 228–231
- Solid-surface fluorescence techniques  
 historical survey, 156  
 trace organic analysis, 156
- Solid-surface luminescence  
 effect of temperature, 160  
 interactions, 160  
 with  $\alpha$ -cyclodextrin–NaCl mixtures, 157
- Solid-surface luminescence analysis  
 description, 155  
 for trace organic compounds, 156  
 in environmental analysis, 157
- Solvent, effect on extraction, PAHs, 174
- Solvent composition, effect on fluorescence, 209
- Solvent extraction, and use of cyclodextrins, 170
- Sonoluminescence, definition, 5r
- Spectral analysis, collected light, 236,237f
- Spectral line narrowing techniques, usefulness, 13
- Spectral lines, for monochromator wavelength calibration, 101r
- Spectral responsivity, standards, 100
- Spectrofluorometric assays, to study neutrophil activation, 26,27r
- Spectrofluorometric method, analysis of ligand binding, 65
- Spectrofluorometry  
 coupled with microscopy, 85  
 wide use, 98
- Spectroscope, development, 3
- Spectroscopic assays, of neutrophil functions, 28
- Spectroscopic data  
 pyridone sulfonates, 215r  
 pyridones, 218r
- SRM, See Standard reference materials
- Stability  
 instrument, 107  
 standards, 107
- Standard reference materials  
 for PAHs, 115,117r  
 reversed-phase HPLC analysis, 117–122
- Standards  
 calibration, 100  
 corrected excitation and emission spectra, 103r  
 decay time, 106  
 definition and uses, 99  
 fluorescence decay time, 106r  
 functions, 100  
 quantum-counter, 103  
 quantum-yield, 103  
 requirements, 99,107  
 size and shape, 110  
 spectral responsivity, 100  
 stability, 107  
 wavelength calibration, 100
- Stokes–Einstein volume  
 compared to Perrin volume, 191,195r  
 equation to calculate, 191
- Stokes, investigation of photoluminescence, 4
- Stokes' law, 4
- Synthesis  
 derivatizing reagent, fluorescent pyridones, 222,223  
 pyridone sulfonates, 225
- T
- Tangent  $\Delta$   
 as function of temperature, 191–194f  
 equation to calculate, 190
- Temperature  
 effect on extraction, PAHs, 174  
 effect on solid-surface luminescence, 160
- Thermoluminescence  
 definition, 5r  
 definition and use, 15
- Time-resolved fluorescence  
 depolarization, 189
- Tin–flavonol complex, variation of molar ratio of ligand to metal, 89,92r
- Tin accumulation, bacteria, 92,93f
- Tin analysis, in bacteria, 87,89–94
- Total-luminescence contour plots, binary PAH mixtures, 175
- Trace organic analysis, solid-surface fluorescence techniques, 156
- Transduction mechanisms, using permeabilized cell, 61,62f
- Transmittance, used to monitor aggregation, 28
- Triboluminescence, definition, 5r

## U

- Uranium-doped glass microspheres
  - luminescence intensity, 111,112*f*
  - See also* Uranyl glass microspheres
- Uranium-doped glasses, as standards, 115
- Uranyl glass microspheres
  - irradiation, 109*f*
  - See also* Uranium-doped glass microspheres

## V

- Vavilov, explanation of quantum yield, 8

## W

- Water-tracing compounds, development, 212
- Wavelength calibration, standards, 100
- Weber, effect of pH on fluorescence spectrum, 8
- Wiedemann, investigation of photoluminescence, 4
- Wood, demonstration of resonance radiation, 7

## Z

- Zinc analysis, in bacteria, 88,94–96
- Zinc bromide, treatment of bacteria, 94

*Production by Joyce A. Jones  
Indexing by Janet S. Dodd*

*Elements typeset by Hot Type Ltd., Washington, DC  
Printed and bound by Maple Press, York, PA*